



January 2014

# Determining The Origin And Possible Mechanisms Of QPOS In X-Ray Emissions Of Neutron Stars And Black Holes

Brent Thomson

Follow this and additional works at: <https://commons.und.edu/theses>

---

## Recommended Citation

Thomson, Brent, "Determining The Origin And Possible Mechanisms Of QPOS In X-Ray Emissions Of Neutron Stars And Black Holes" (2014). *Theses and Dissertations*. 1721.  
<https://commons.und.edu/theses/1721>

This Dissertation is brought to you for free and open access by the Theses, Dissertations, and Senior Projects at UND Scholarly Commons. It has been accepted for inclusion in Theses and Dissertations by an authorized administrator of UND Scholarly Commons. For more information, please contact [zeinebyousif@library.und.edu](mailto:zeinebyousif@library.und.edu).

DETERMINING THE ORIGIN AND POSSIBLE MECHANISMS OF QPOS  
IN X-RAY EMISSIONS OF NEUTRON STARS AND BLACK HOLES

by

Brent Wayne Thomson  
Bachelor of Science, University of North Dakota, 2003  
Bachelor of Arts, University of North Dakota, 2003

A Dissertation  
Submitted to the Graduate Faculty

of the

University of North Dakota

In partial fulfillment of the requirements

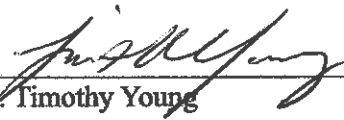
for the degree of

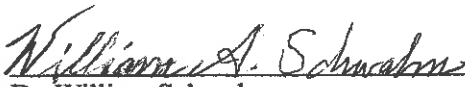
Doctor of Philosophy

Grand Forks, North Dakota  
December  
2014

Copyright 2014 Brent Thomson

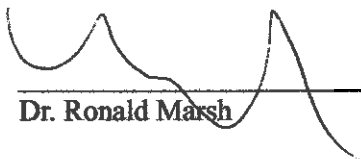
This dissertation, submitted by Brent Thomson in partial fulfillment of the requirements for the Degree of Doctor of Philosophy from the University of North Dakota, has been read by the Faculty Advisory Committee under whom the work has been done, and is hereby approved.

  
\_\_\_\_\_  
Dr. Timothy Young

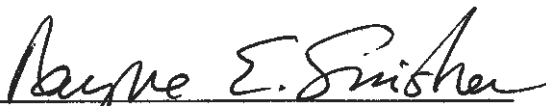
  
\_\_\_\_\_  
Dr. William Schwalm

  
\_\_\_\_\_  
Dr. Graeme Dewar

  
\_\_\_\_\_  
Dr. Ju Kim

  
\_\_\_\_\_  
Dr. Ronald Marsh

This dissertation is being submitted by the appointed advisory committee as having met all of the requirements of the Graduate School at the University of North Dakota and is hereby approved.

  
\_\_\_\_\_  
Dr. Wayne Swisher

  
\_\_\_\_\_  
Date

Title            Determining the Origin and Possible Mechanisms of QPOs in x-ray emissions of  
neutron stars and black holes

Department    Physics and Astrophysics

Degree         Doctor of Philosophy

In presenting this dissertation in partial fulfillment of the requirements for a graduate degree from the University of North Dakota, I agree that the library of this University shall make it freely available for inspection. I further agree that permission for extensive copying for scholarly purposes may be granted by the professor who supervised my dissertation work or, in his absence, by the Chairperson of the department or the dean of the Graduate School. It is understood that any copying or publication or other use of this dissertation or part thereof for financial gain shall not be allowed without my written permission. It is also understood that due recognition shall be given to me and to the University of North Dakota in any scholarly use which may be made of any material in my Dissertation.

Brent Thomson  
December 10, 2014

## TABLE OF CONTENTS

LIST OF FIGURES.....	vii
ACKNOWLEDGMENTS.....	x
ABSTRACT.....	xi
CHAPTER.	
I. INTRODUCTION.....	1
Ia. Detection Method of QPOs.....	11
Ib. General Methods in Asteroseismology.....	13
Ic. Optical Solar Oscillation.....	16
Id. Determining the Periodicity of X-Ray Light Curves.....	23
Ie. Quality Factor $Q_0$ .....	28
II. QPO MODELS.....	30
IIa. Criteria for QPO Models.....	30
IIb. Relativistic Precession Models.....	31
IIc. Relativistic Resonance Models.....	32
IId. Beat-Frequency Models.....	33
IIe. Beat Frequency Interaction.....	35
IIf. Radii of Interest.....	38
IIg. Boundary Layer of the Inner Disk.....	40
IIh. Coupling between the Vertical and Radial Epicyclic Oscillations.....	46
III. KERR GEOMETRY.....	49
IIIa. Dimensionality of the Kerr Metric Terms.....	49
IIIb. The Kerr Metric.....	52
IIIc. Orbital Radii.....	62
IIId. Frequencies and Radii Relevant to the QPO Models.....	69
IIIe. The Gravitational Potential of a Kerr Black Hole.....	73
IV. ALFVEN RADII OF ACCRETION DISKS.....	80
IVa. Blandford-Znajek Mechanism.....	83
V. GENERAL PRINCIPLES OF ACCRETION DISKS.....	96
Va. Angular Momentum Transport.....	100
Vb. Hydrodynamics.....	105
Vc. Magnetohydrodynamics.....	106

	Vd. Magnetorotational Instability (MRI).....	108
	Ve. Vertical Pressure Balance.....	117
	Vf. Viscous Processes.....	118
	Vg. Radiative Transport.....	120
	Vh. Conservation Equations.....	121
	Vi. Thick Disks and Tori.....	122
	Vj. Papaloizou-Pringle Modes.....	125
	Vk. Equation of State.....	125
VI.	ACCRETION RATE.....	131
	VIa. Magnetic Influence on the Disk.....	141
	VIb. Accretion onto a Kerr Black Hole.....	143
	VIc. Luminosity of an Accretion Disk.....	146
	VId. Conservation of Rest-Mass.....	149
	VIe. Conservation of Angular Momentum.....	149
	VI f. Energy Conservation.....	150
	VIg. Thin Disks, Slim Disks, and ADAFs.....	152
VII.	DISKOSEISMOLOGY.....	156
	VIIa. Vibration modes.....	158
	VIIb. Basic Oscillation properties.....	161
	VIIc. Properties of the Nodes.....	162
	VII d. Variations from Spherical Symmetry.....	165
	VII e. Oscillations and Instabilities in rotating fields.....	168
	VII f. Rayleigh Instability for differential rotation.....	170
	VII g. Magnetorotational (Balbus-Hawley) Instability.....	171
	VII h. Global Instabilities.....	177
	VII i. Non-radial Stellar Pulsation.....	178
	VII j. Oscillation motion for g-modes.....	179
	VII k. Standing Wave Characteristics.....	183
	VIII. Classification and Coupling of Radial and Vertical oscillations.....	186
	VII m. Trapped Oscillations.....	194
VIII.	RADIAL PULSATION (HELIOSEISMOLOGY).....	198
	VIIIa. Helioseismology in a Cylindrical Reference Frame.....	199
	VIIIb. Adiabatic Index Relation for a Disk.....	203
IX.	DISKOSEISMOLOGICAL APPROACH.....	208
	IXa. Physical context of the Radial Potential Energy Expression.....	213
	IXb. Context of the Orbital Frequencies.....	219
	IXc. Physical Context of the Fractional Displacements.....	223
	IXd. Thermodynamics and Internal Energy Transport.....	225

IXe. Determining the Adiabatic Index in the Corona of a star.....	234
X. PULSATION ACTIVITY.....	239
Xa. The Fractional Displacement Solutions per the Simple Harmonic Oscillation Equation.....	243
Xb. The Radial Displacement Solutions per the Elliptic Equation.....	254
XI. CONCLUSIONS.....	260
REFERENCES.....	274



## LIST OF FIGURES

Figure	Page
1. X-ray light curves of GRS 1915+105 on day 152 with finer time resolution.....	12
2. A detailed view of the kilohertz QPO in Sco X-1.....	25
3. Anatomy of the Boundary/Cusp Layer model in an Accretion Disk.....	45
4. The Length of the Event Horizon versus the ISCO.....	78
5. Comparison of the Magnetic Fields of the Black Hole and Disk.....	90
6. Alfven Radius for $n = 2$ versus ISCO for 6 M BH.....	90
7. Alfven Radius for $n = 3$ versus ISCO for 6 M BH.....	91
8. Alfven Radius for $n = 4$ versus ISCO for 6 M BH.....	91
9. Alfven Radius for $n = 2$ versus ISCO for 8 M BH.....	92
10. Alfven Radius for $n = 3$ versus ISCO for 8 M BH.....	92
11. Alfven Radius for $n = 4$ versus ISCO for 8 M BH.....	93
12. Alfven Radius for $n = 2$ versus ISCO for 10 M BH.....	93
13. Alfven Radius for $n = 3$ versus ISCO for 10 M BH.....	94
14. Alfven Radius for $n = 4$ versus ISCO for 10 M BH.....	94
15. Alpha coefficient per adiabatic index.....	137
16. Radius of Influence per adiabatic index.....	138
17. Density coefficient per adiabatic index.....	139
18. Diagram of the Radial Potential Energy Curve with the roots shown for each case of $q$ .....	215
19. Lengths of Event Horizon versus ISCO (Marginally Stable Circular Orbit) versus spin.....	241
20. First solution of the radial fractional displacement versus spin for fixed $r$ .....	243
21. First solution of the vertical fractional displacement versus spin for fixed $r$ .....	244

22. First Radial Displacement for fixed index = $5/3$ .....	245
23. First Radial Displacement for fixed index = $3/2$ .....	246
24. First Radial Displacement for fixed index = $4/3$ .....	246
25. First solution of radial fractional displacement versus spin for fixed $r = \text{ISCO}$ .....	248
26. First solution of radial fractional displacement versus spin for fixed $r = \text{ISCO}$ .....	249
27. First Vertical Displacement for fixed index = $5/3$ .....	250
28. First Vertical Displacement for fixed index = $3/2$ .....	250
29. First Vertical Displacement for fixed index = $4/3$ .....	251
30. Parameter space for adiabatic index versus $a$ (First Vertical Displacement Solution).....	252
31. Parameter space for adiabatic index versus $a$ (First Vertical Displacement Solution).....	253
32. Radial Displacement per elliptic solution for fixed index = $5/3$ .....	254
33. Radial Displacement per elliptic solution for fixed index = 1.6.....	255
34. Radial Displacement per elliptic solution for fixed index = $3/2$ .....	255
35. Radial Displacement per elliptic solution for fixed index = 1.4.....	256
36. Radial Displacement per elliptic solution for fixed index = $4/3$ .....	257

## ACKNOWLEDGMENTS

I wish to express my sincere appreciation to the members of my advisory committee for their guidance and support during my time in the doctoral program at the University of North Dakota, as well as their patience.

## ABSTRACT

QPOs (Quasi-Periodic Oscillations) are time oscillations that appear in the light curve of observational data in x-ray bands. They are of mysterious origin although they are believed to be a result of the intense gravity around neutron stars and black holes and emit x-rays from accretion disks. I investigate a derived ratio between two periods has been found in the QPO data. The two periods, which appear as peaks in the power density spectrum have been found to be in a 3:2 ratio and can possibly distinguish theoretical models. In the work presented here, two physical approaches are developed that can explain the integer resonance ratio.

One is a cusp layer model, which is based on a boundary layer model that uses the physical conditions at opposite sides of said layer to explore the magnitude of the vertical versus radial epicyclic frequencies and confirm the anticipated scales of the observed frequencies. It also happens to recreate a 3:2 resonance ratio for the Keplerian angular frequencies at the ISCO, taken as the preferred radius for the boundary layer model.

A toy model was recreated and utilized to emulate the Alfvén radius due to the accretion disk's innate magnetic field and explore how it serves as a disruption radius and impacts the accretion of mass and the effective inner edge of the disk. The simulations show that there is no significance deviation from the ISCO as an effective inner edge for the accretion disk due to the magnetospheric influence of the disk alone.

I also invoke a parameter to handle the coupling between the vertical and radial epicyclic frequencies and relate it to the pressure within the disk. I show the coupling is strongest at the

equatorial plane where pressure is at its maximum value.

A model I utilize is a relativistic resonance model, combined with a helioseismological approach to explore the pulsation of the inner edge of the accretion disk that imparts the resonance of the accreting matter moving along the Kerr space-time orbits. The helioseismological model gives a characteristic frequency for small perturbations in the stellar matter within the atmosphere of a star. The diskoseismological model extends that principle to material within an accretion disk. I take it to the same extent that the QPO frequencies are due to small perturbations along the marginally stable circular orbit, in the vertical and radial directions and use it as a probe into the inner disk and what information it yields. The inner disk edge, per the model, is treated as a vibrating surface that yields the radial and vertical epicyclic frequencies as characteristic features of the vibration. The epicyclic frequencies found using the physical parameters of the model within the cusp layer inside the disk could explain the physical context of the phenomenon responsible for the creation of the QPOs. An approach within the diskoseismological model uses the cylindrical reference frame of a disk in terms of the distribution of mass in combination with the strong gravity of the central object and the Keplerian velocity and sonic speed to yield a natural resonance ratio of  $3/2$  as well.

The model can be used as a diagnostic tool to explore the physical phenomena of the material orbits and the disk itself. Most importantly, the model can be used to determine and constrain the ratio of spin to mass of the compact object itself. It yields new information as previously undetermined by any earlier model; the adiabatic index at a specific radius within the accretion disk, which serves to lend insight into the innate phenomena of accretion disks at large. It establishes what were previously unknown information, such as the mass density distribution at a specific radius and outward, the radius of influence in terms of the sonic radius, the accretion

rate, and the temperature distribution at the same radius for the accretion disk, as all are dependent on the adiabatic index. In all previous literature, the adiabatic index is taken as an assumptive estimate, and the models build on that assumed value of the adiabatic index. This model allows us to obtain an actual value of the adiabatic index at the ISCO and use it as an establishing feature to refine models on for more physically realistic observations.

# CHAPTER I

## INTRODUCTION

X-ray observations of compact objects have been shown to have a quasi-periodic feature in the detected signals. These features are called QPOs or Quasi-Periodic Oscillations. There is no standard model to explain the nature of the oscillations. A QPO (Quasi-periodic Oscillation) is a particular signal that appears in the emitted radiation from stellar objects (black holes, neutron stars, and white dwarfs). It manifests itself as a repeated brightening in the x-ray radiation at specific beats in time. The repetition in brightness is thought to occur when gas spirals inward towards the compact object and heats up as it piles up near the stellar surface within an accretion disk, in a localized region, to the point it emits x-rays. The analysis of the brightening in the x-ray radiation do not come in exact time intervals and thus called quasi periodic and the frequency in time is very high on the order of ten to a thousand cycles per second (10 Hz to 1 KHz). The importance of QPOs is in their ability to diagnose both the region around strong gravity and to test theories of General Relativity. They originate from regions of intense gravity and stand as informative tests of general relativity. The fundamental source of QPOs must be located near the compact objects, so it is necessary to explore the phenomena occurring in the vicinity of the stellar objects and pinpoint the causes of the QPOs.

Different models have been proposed to explain the origin of the QPO signals. I will outline the current models in the literature and in this dissertation I will present two models that I have developed to describe these quasi-periodic oscillations.

Observations of the QPO signals started in 1996 with the Rossi X-ray Timing Explorer and QPO frequencies up to 1000 Hz were detected. Twin-peak QPOs were also found, consisting of two peaks of roughly same power at high amplitudes, at particular frequencies in an energy range, although not exactly equal (Yi, 2007). A peculiar feature came into notice with multiple observations from numerous sources: a persistent 3:2 ratio between double QPO frequencies found in certain spectra measurements. This is particularly prominent for black hole candidates although neutron stars do manifest the same 3:2 frequency ratio with the QPO peaks wandering about a particular frequency.

There are three distinct types of QPOs: LFQPO (Low Frequency QPO, 1 to 100 Hz), Hecto-hertz QPO (100 to 200 Hz), and HFQPO (High Frequency QPO, 200-1500 Hz). The individual peaks are associated with a set of oscillators and the time evolution of the oscillator. The HFQPO is thought to originate from orbital motion in the inner part of accretion disks around compact objects, while LFQPOs are thought to originate from a point farther out in the disk.

There have been a small number of HFQPOs detected for black holes and many detected for neutron stars. A unique feature of the black hole HFQPOs is that they have a distinctive 3:2 ratio signature, based on persistent frequency values where the higher frequency will be 1.5 times the value of the lower frequency. Neutron star HFQPOs also show the 3:2 ratio-clustering feature, albeit due to two correlating peaks for both frequencies which switch amplitudes when passing the 3:2 ratio. This may be attributed to the neutron star's strong magnetic field interacting with the inner disk and affecting the phenomenon responsible for the QPO signals. The most likely effect of the magnetic field would be to cause vertical and radial oscillations to



switch in magnitude.

A unifying approach to the model would be to establish a connection, between the HFQPOs and the strong gravity of the compact object in question. This would then be used to infer object properties using the QPO measurements. The constant 3:2 integer ratio frequencies' stability implies a strong dependence primarily on the Kerr geometry and less so on the physics of the accreted plasma (where the magnetic field controls the overall advection). The Kerr geometry determines the strength of the gravity and determines the conditions in the accretion disk.

There are a large variety of ideas and models to explain QPOs. Some cases are applied to both neutron stars and black holes to explain common features between both, and some are limited to one and not the other, to explain the differences in the signal features. Some models also accommodate resonances and some do not.

There are two general classes for the QPO models: Hotspot models and Disk Oscillation Models. They both relate the QPOs to a specific radius in the accretion disk, albeit with further qualifying characteristics.

The Hotspot Models are: Relativistic Precession, proposed by Stella (1999), and discussed (Morsink, Stella, 1999), (Stella and Vietri, 2012), and Tidal Disruption, proposed and discussed by Cadez (2008), Kostic (2009), and Germana (2009).

The Disk Oscillation Models are: Warped Disk Resonance, proposed and discussed by Kato (2000, 2001, 2004, 2005, 2008), both the Epicyclic and Keplerian Resonance Models by Abramowicz and Kluzniak (2000, 2001, 2004, 2005), and two models focusing on resonances

between non-axisymmetric oscillating modes of a torus, by Bursa (2005), and Torok (2010). These models are discussed later in this dissertation along with their strengths and weaknesses. There is no universally accepted model that satisfactorily explains all the features of QPOs and pinpoints a single mechanism.

The distinction between the two models comes down to dealing with the localization of the region responsible for the QPO signal. A hotspot model focuses on an angular section at a specific radius that co-rotates with the disk, whereas a disk oscillation model shifts the focus to a boundary region that extends from a specific radius outward in a full annular region, with no angular section preference. A crucial element that may determine the validity of one model over the other is the hydrodynamical or magnetohydrodynamical shear that occurs in the vicinity of the inner disk that aids or inhibits the coagulation of plasma into blobs or hotspots that congregate in angular sections or disperses outward into annular sections.

A criterion for exploring variations in the QPO frequency is to explore candidates responsible for the change in frequency. The frequency cannot be associated with the star or the Kerr space-time alone, so it is necessary to focus on the gas within the accretion disk. Some possibilities depend on the radius of the disk from where the signals are generated, so the search for a frequency reverts to a search for a specific radius. The radius has to be sharp enough to show dramatic changes over a small radial distance.

There are three particular locations that qualify for the sharp radius: the boundary layer between the disk plasma and the star; the ISCO (Innermost Stable Circular Orbit); and the transition region where the flow becomes the most affected by the star's magnetic field.

The first two candidates fit the criteria for the HFQPOs (High Frequency Quasi-Periodic Oscillations) since the Kerr geometry is the dominant influence over the frequency characteristics. The third is an intriguing option for the LFQPOs (Low Frequency Quasi-Periodic Oscillations) since they are thought at a radius further out in the disk.

Miller, Lamb and Psaltis proposed a good candidate for a region where the flow goes from subsonic to supersonic, known as the sonic point. The inward radial velocity increases sharply with decreasing radius and this is thought to be a crucial criterion for the sharp radius where drastic changes in the accretion properties occur such as plasma falling rapidly towards the compact object (Miller M. L., 1998).

There are many kinds of matter waves in astronomy. They range from geological quakes (solid shock waves), to stellar explosive waves (gas shock waves), to stellar pulsations and stellar convection waves (gas shock waves), to space-time perturbations (gravity waves). In my dissertation I will concentrate on waves created in accretion disks, which are thought to include pressure waves (p-waves and s-waves) and gravity waves (g-waves). As of currently, varying models have offered different mechanisms, which have possible explanations but require more precise data. I use several models to investigate outcomes that can be tested.

In Chapter I, I will go over the calculation of the periodic nature of QPO in the x-ray data. In the introduction I discuss the nature of oscillations in stars. I discuss how the x-ray data is collected and processed and the QPO signal is detected.

In Chapter II I continue the discussion of QPO models and go through the anatomy of an

accretion disk for a deeper look at the parameters needed in analyzing the QPO models. Then I go into detail about the varying models that discuss the possible origin and mechanisms behind the generation of the QPO signal. I also then explore a cusp layer model that serves as an informative source of the signal based on physical parameters. The physics of the accretion disk and the geometry will be explored to determine the conditions for boundary layer dimensions and any further implications for the radial distribution of matter to test out the peculiar requirements for the production of the QPO signal, such as the scaling of the double QPO frequencies.

In chapter III, I discuss the physical and mathematical vocabulary of the Kerr metric terms and how it defines the geometry of space-time around a rotating compact object.

For chapter IV, I begin to look at the Alfvén radius (where magnetic forces start to influence the motion) and compare that to the ISCO (the inner most stable circular orbit). My objective is to utilize the Blandford-Znajek mechanism as a model to explain, and determine the Alfvén radii as prospective determining radii for the generation of the LF (Low Frequency) QPO. The radius at which the magnetic field of the compact object starts to affect the accreted plasma is the Alfvén radius. The Blandford-Znajek mechanism focuses on two contributing magnetic influences, the disk and the compact object (black hole in particular). As the plasma falls through the event horizon, the magnetic field lines carried in with the plasma becomes frozen into the flow outside the event horizon and gets twisted along with the space-time, by the rotation of the black hole, frame dragging, in Kerr geometry.

The disk is endowed with its own electric current and as it rotates, it generates a poloidal

magnetic field. Each source (the black hole's ergospheric plasma, or the disk's) would have a corresponding Alfvén radius, and since the disk tends to be the dominant influence in most cases, its Alfvén radius is the definitive radius for the system. This means that the effects of the magnetic field become reduced as one moves out from the Alfvén radius. However, in cases of high spin, the black hole's magnetic field becomes comparable to that of the disk, and dominates it.

Matter passing from the disk Alfvén radius (due to the disk magnetic field) to the black hole Alfvén radius (due to the ergospheric plasma, projected from the event horizon) would change magnetic field strength and cause a change in velocity in the plasma stream. This is important because it would cause a magnetohydrodynamical feedback in the plasma stream, which indicates physical information can travel back out into the disk. I determine the location of the Alfvén radius due to the accretion disk's magnetic field and how it impacts the shape and nature of the accretion disk.

Chapter V expands on the basics of accretion disks and the physics that govern them. Chapter VI deals with the accretion rate and reveals the basics of the accumulation of matter by compact objects and important parameters involved in accretion. This chapter bears information which importance that will become apparent in Chapter VII.

Chapter VII explores the phenomenon of diskoseismology and the physical phenomena that accompany it. I now move to a description of the oscillations in the disk using a model that is similar to that for a star. The disk is a massive body with its own self-gravity (that is neglected

in contrast to that of the central object in terms of the pulsations) that constrains its boundaries, and is endowed with plasma, much like a star. The disk differs from a star in the geometrical setting: the star is spherically symmetric and the disk is an axisymmetrical torus that is preferably described with a cylindrical reference frame. The ISCO (Innermost Stable Circular Orbit) or marginally stable radius is the last radius where infalling particles' angular velocities remain Keplerian inside a radius. The warped space-time starts to change the particles' trajectories. This is done via a precession process inside that radius in closer proximity to the compact object. For most models, the disk inner edge is set at the ISCO. In the disk's reference frame, it behaves as a gravitationally bound body of heated, charged mass that behaves like a section of gas in a pulsating star. The disk has a pulsating surface, driven by convection and radiation processes in its interior.

I also create a classical diskoseismological approach for the HF (High Frequency) QPOs and show that the natural motion of infalling gas along Kerr space-time produces a unique relativistic beat that determines the HF QPO frequency signature. The ISCO (Innermost Stable Circular Orbit), also known as the marginally stable circular orbit, serves as a natural boundary for the inner edge of the disk and the inner edge as a result of the moving plasma, the radius of the inner edge oscillates to a beat imparted by the unique Kerr geometry in its proximity. The diskoseismological approach also yields a previously unknown quantity, the adiabatic index, which was taken as an assumed value in previous papers. The adiabatic index is the ratio of specific heats of a gas and speaks to the nature of the advecting gas within the accretion disk. Accretion disk models almost always invoke a polytropic equation of state to describe the gas. Disk oscillations are incumbent on the speed of sound, in terms of the pressure, which relies on

the adiabatic index.

The diskoseismological model developed in this dissertation invokes two equations being equivalent to each other, one derived via the hydrostatic equilibrium condition that yields an acoustic-based equation pertaining to the pressure involved in the plasma, and the other from the epicyclic frequency equations derived from Abramowicz's paper (Abramowicz M. A., 2002).

Chapter VIII delves into the helioseismological expressions, and modifies it for the accretion disk setting. It then uses the QPO frequency in that context as a probe into the inner disk of the accretion disk and reveals the nature of the gas in that region. By connecting the QPO frequency to the adiabatic index affirmatively, it yields more information about the composition of the accretion disk than one would expect. This adiabatic index value also serves as a parameter that serves to constrain the ratio of the angular momentum to the mass of the compact object as to align with the radial and vertical epicyclic frequency expressions.

This is expected to happen because the frequencies are equal and when the Keplerian frequencies are factored out, the remaining expressions are left equivalent to each other and the three factors in the expressions (adiabatic index, mass, and angular momentum parameter,  $a$ ) act as a constraint so the net value is zero. Knowing two of these factors yields the third value to satisfy the expression. At the marginally stable radius, the disk has its closest approach to the compact object (black hole) and it is at that point the compact object has its strongest influence in contrast to the rest of the disk where plasma motion reduces to the Newtonian values. Material inside the ISCO radius, called the plunging region, will be moving at relativistic speeds as it approaches the horizon. No stable orbits are supported inside the ISCO radius, and the

particles' orbits start to precess and lead to increased collisions between each other. Their angular momentum is dissipated and their paths become one of a free-fall towards the central object. The plasma will have an adiabatic index of  $4/3$  at the event horizon, which is the value for relativistic gas.

The value of the adiabatic index also gives us the radius of influence in terms of the sonic radius, and the density, radial velocity, and temperature distributions as stated in Novikov and Thorne's classic paper (Novikov I. a., 1973), which took the adiabatic index as a presumed value,  $\gamma = 1.4$ . In the dissertation presented here I calculate the adiabatic index value. The listed quantities are derived algebraically and are used to describe the general accretion traits of general-relativistic disks. I will determine the value of the adiabatic index within the range of ideal gas,  $5/3$ , to relativistic gas,  $4/3$ . Using the Abramowicz QPO frequency expression to yield the value of the adiabatic index sets the location of the accreting gas at the ISCO and tells us about the nature of the gas advecting across that radius. For a higher spin, the ISCO moves inward to an orbit at a radius that becomes increasingly closer to the event horizon until at maximal spin, the ISCO coincide at the same radius as the event horizon. For an inwardly moving ISCO, the adiabatic index would shift towards a relativistic gas value.

The quantities discussed in Chapter VI is loosely dependent on the adiabatic index so by confirming the value of the adiabatic index in Chapter VII and Chapter VIII, which was previously taken as an estimated value in models, it can confirm a key feature observationally.

Chapter IX delves into the nature of the pulsations and what it reveals about the



mechanisms of the inner disk, and focuses on particular features of the diskoseismological equations. It also reveals trends about the frequency of the pulsations and the significance in terms of the properties of the compact object.

In the Conclusions, I summarize the important implications of the equations and their solutions and what it means in terms of the accretion disk and the QPO signal in general.

### **Detection Process of QPO Signals**

The process of obtaining the stellar QPO observations begins with the following steps: a x-ray telescope with a detector focuses on a point source and three regions in space are defined; two source regions (the compact object under observation, and a star for reference) and one background region, which will be used to create light curves. An extraction range (area of capture, usually circular) is centered on the star of concern, with a position and radius selected to focus on the capture region to extract the background region. The data is recorded over a time range (from minutes to hours), with the option of excluding a particular block of time, giving the option of refining the duration. The raw data is counts of x-ray particles and can be converted into intensity and plotted against time, this is the x-ray light curve.

A separate background-subtracted light curve is created for contrasting with the source light curves. The light curve is created using the count rate, which is the counts per bin per total observational good time, or counts per time bin, merged with intersecting good time intervals, depending on observational conditions and is expressed in terms of intensity (or number of

photon strikes onto the detector chip) over an time interval.

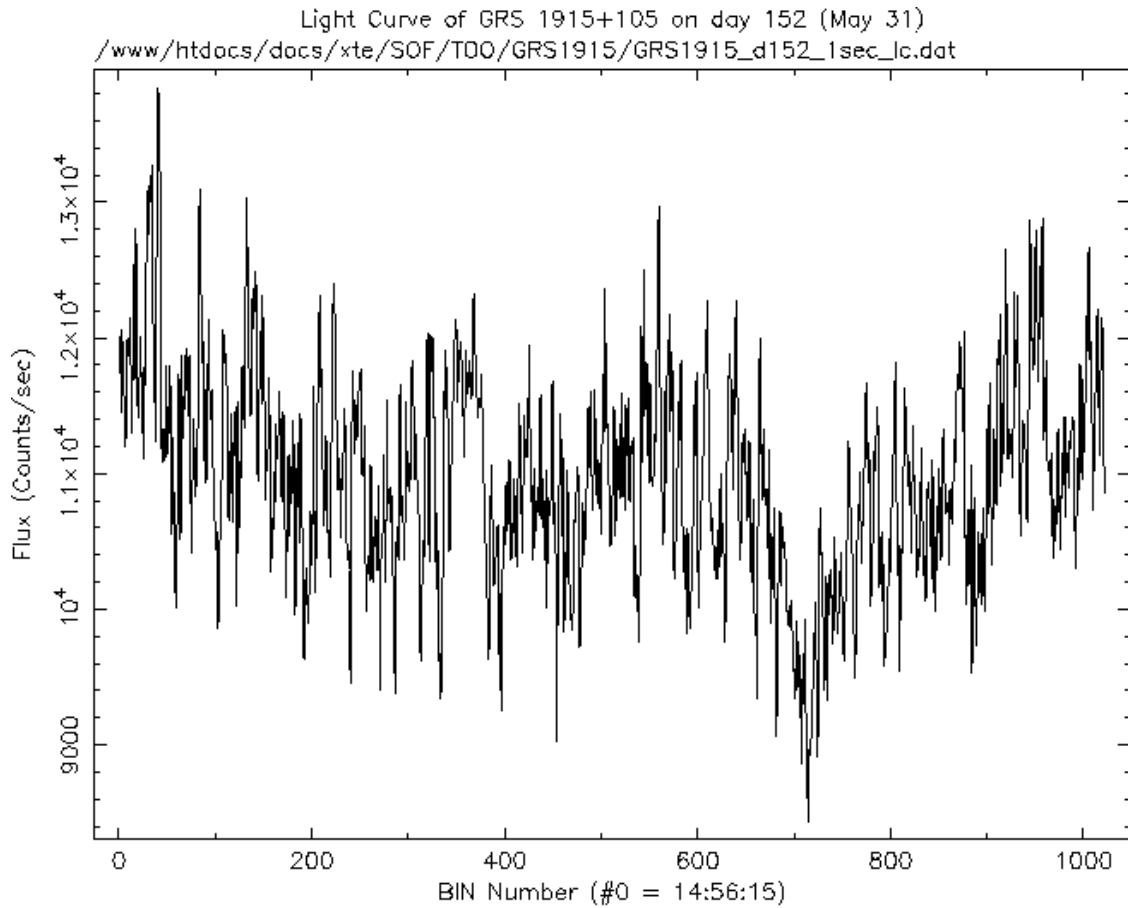


Figure 1. X-ray light curves of GRS 1915+105 on day 152 with finer time resolution. This light curve covers from 14:56:15 to 15:13:18. (Corbet, 2004)

A filter can be used to limit an energy range, for example, 0.3-10 keV. Each channel for the filter is set in one unit of 10 eV. A count bin is a snapshot in duration, or time period for capture. A binsize is set in terms of seconds (binsize 10 = 10 seconds). The light curves are created for the two source regions, including the background counts to check for data artifacts. The light curve is corrected for bad columns (gaps in data) and the loss of counts due to the use

of an annulus, and the background light curve data subtracted. If an instrumental feature appears in both sources, it would appear in both curves. If the feature is present in both the background subtracted and unsubtracted light curves, it is not a background feature. If the feature does not appear in both sources, the dip in the count rate is taken as an indication of a variable star.

In the case of QPO's, gamma ray burst light curves (which also emits in x-rays), or any variable x-ray source, where the count rate changes dramatically over time, a light curve can be produced with a fixed number of counts per bin, as opposed to a constant binsize. Power-laws, broken power-laws models can be fit to the light curve to process the data and reveal its context. Timing analysis can also be used to search for structure in the data (Meringa, 2013).

### **General methods in Asteroseismology**

Asteroseismology is the study of the inner dynamics and characteristics of stars, including their variability and periodicities. I will now make the connection between periods found in oscillating stars to the possible variability found in the movement of gas in the accretion disks around compact objects. The variability can be used to connect the QPO x-ray observations to the inner dynamics and characteristics of accretion disks and treat it as a diagnostic probe into their interior. I now discuss the basics of variable stars and then apply the theory to a disk scenario.

Variable stars with periods have been known to exist since the 17<sup>th</sup> century, when the astronomer Jan Fokkens Holwarda discovered the magnitude of the star Mira had a period of

eleven months (Hoffleit, 1977). The astronomer Harold Shapley didn't establish the relation between variability and stellar pulsations concretely until almost three centuries later in 1914 after Henrietta Leavitt discovered the relation between distance and luminosity in her Periodic-Luminosity relation in 1908, which helped clarify the relationship between the two concepts (Leavitt, 1908).

A solar oscillation reveals inner dynamics and characteristics of stars (such as the Sun, for one), and is the basis of research in the field of helioseismology. Expanding such ideas to other stars leads to the field of asteroseismology.

Pulsation frequencies are sensitive to the internal structure characteristics of the star and each frequency serves as a distinct probe into different regions of the inner structure. Current knowledge of the stars is limited by assuming spherical symmetry. In general, rotation and magnetic fields are excluded in interior stellar models. In this dissertation, I invoke Keplerian rotation for my accretion disk models and model the magnetic field of the accretion disk as well. Departures from sphericity have been found through the process of interferometry, due to improved technology and tools (Domiciano de Souza, 2003).

A variable star can belong to different pulsating classes if detected modes of different origin are excited. They are classified into types, according to their amplitudes, periods, temperatures, light curve shapes, and other parameters. Stars exhibit a broad range of pulsations; the largest pulsations are the radial pulsations in spherical symmetry.

In distant stars, only the large-scale structure can be resolved since the small-scale structure details are averaged out in the observations. The sensitivity of brightness variations are limited to modes with less than 3 to 4 node lines at the surface of the star.

The general measure of stellar pulsation periods is the dynamical timescale, given as:

$$t_{dyn} = \left(\frac{R^3}{GM}\right)^{\frac{1}{2}} \propto \frac{1}{\rho^{\frac{1}{2}}} \quad (1.1)$$

where  $R$  is the surface radius of the star,  $M$  being the mass of the star,  $G$  the gravitational constant, and  $\rho$  the mean density of the star. It is also proportional to the inverse of the Keplerian frequency. The pulsation period of the star can give an indication of the general properties of the star itself.

Modes are either standing acoustic waves (known as pressure modes, or p-modes), or internal gravity waves (known as g-modes), which involve departure from the spherical symmetry and are non-radial by definition.

Waves or oscillations can be intrinsically stable, or intrinsically unstable. Intrinsically unstable oscillations emanate from amplification of small disturbances through the heat-engine mechanism (cooling plasma sinking and compressing and becoming more opaque to radiation, then becoming heated again and rising against increased pressure underneath the pocket of plasma, expanding in the process and becoming more transparent to radiation, releasing pent-up radiation and energy in the process) in a particular region of the star. The perturbation grows in amplitude until an amplitude-limiting mechanism kicks in (the limits set by the opacity mechanism which serves as a valve in releasing or retaining radiation within a layer in the star), locking in the final amplitude of the oscillation.

The pulsation mechanism, the process of producing a wave or oscillation, depends on the details of the type of mode (g-mode, s-mode, or p-mode), so the amplitudes will vary over the range of unstable modes. It depends on the location in the star that describes the physical conditions of the gas (opacity) within the stellar structure. An example is the Cepheid instability strip, which is indicated as dotted lines that cuts almost vertically across the diagram and serves

as dividing lines between pulsation classes. The type of radial pulsation found in Cepheids is referred to as Classical pulsations. Observationally this can be plotted in certain specific regions in the Hertzsprung-Russell diagram, called the instability strip, which displays an array of stars with different pulsation classifications.

Intrinsically unstable oscillations or pulsations are stochastically excited, by external forcing (such as near-surface convection). Amplitudes are determined by the balance between the energy input by both forcing and damping. The forcing and the damping vary relatively slowly with frequency, so the excitation of modes result in a substantial frequency range. These kinds of pulsations are known as solar-like pulsations. The final amplitude is determined by the gravity of the star, which we will later see is important in the oscillations of the material in an accretion disk.

### **Optical Stellar Oscillation**

The first step in understanding disk dynamics is to look at stellar pulsations. Photometry and spectroscopy are used as asteroseismology techniques. Information on stellar oscillations or pulsations comes from optical photons. Oscillations affect the amount of light emitted or flux (in units  $\frac{ergs}{s*cm^2}$ ) emanating from pulsating stars. The physics of why this occurs can be understood because the material oscillating at the surface, under influence of gravity, will change the amount of radiation emerging due to changes in temperature, pressure and density. In the case of QPOs (quasi-periodic oscillations), this can apply to accretion disks, as I will show later. The flux of

light is calculated by integrating over a source function (a term in the radiation transfer equation that accounts for the emission of light from material,  $S_\nu$ ) along the line of sight from the star. The flux is determined by the emission of light from the full surface of the star and can be related to the luminosity. For the geometry in a disk the flux is still an integration over the material that is producing photons. The furthest seen into a gas in any geometry is given by the optical depth and the last scattering photon at an optical depth of  $\tau = 2/3$ . The intensity variations due to intrinsic pulsation of the star can be derived from photometry time series. It is from the variation of the light from stars that are pulsating star that we know a mechanism exists inside the star that makes it increase and decrease its radius. It is this mechanism that I will use to explain the movement of gas in the accretion disks around compact objects.

To explore the pulsation mechanism and how it affects the flux of light, there needs to be a discussion of the events that transpire during the pulsation cycle.

The physicist, Sir Arthur Eddington, proposed the concept that pulsating stars are thermodynamic heat engines; the gases within the layers of the star do work as they expand and contract during the pulsation cycle. If a layer does positive work on its surroundings, it contributes to driving the oscillations. If a layer does negative work on its surroundings, it dampens the oscillations. If the total work of the layers is positive, the oscillations will grow in amplitude and if the total work is negative, the oscillations will decay as a result. So it continues until equilibrium is attained and the total work is zero.

A driving process entails heat flowing into a layer during a high-temperature part of the cycle and leaving during a low-temperature part of the cycle. The driving layers absorb heat at

the time of their maximal compression, and maximal pressure will be attained after maximal compression. The oscillations will be amplified at this point. At the center of the star, the matter is compressed and the temperature rises as a consequence and thermonuclear energy is generated. The energy mechanism ( $\epsilon$ -mechanism) operates in the core of the star although it is not enough to drive the pulsations.

Eddington proposed a valve mechanism; if a layer became more opaque during compression, the energy flowing towards the surface gets stored up and dammed, pushing the surface layers up. When the expanding layer becomes more transparent, the trapped heat escapes and the layer collapses back to its original position. In the remainder of the star, the opacity decreases with compression. The opacity  $\kappa$  depends on density and the temperature of the stellar gases:

$$\kappa \propto \frac{\rho}{T^2} \quad (1.2)$$

In compressing the layers of a star, the density and temperature increases. Although the opacity is more sensitive to temperature changes, the opacity decreases with compression as a result. It requires special conditions for stellar pulsations. These special conditions were identified by S.A. Zhevakin, and verified by Rudolph Kippenhahn, Norman Baker, and John Cox.

They determined the regions within a star where the valve mechanism can operate successfully are the partial ionization zones, layers of the star where gases are partially ionized. Part of the work done on the gases while compressed gets directed into ionizing the matter rather than heating the gas itself. With a smaller temperature rise, the opacity increases with the increase in density. The ions recombine with electrons and release energy during expansion and



the opacity decreases with the decrease in density.

This opacity mechanism is referred to as the  $\kappa$ -mechanism. In the partial ionization zone, the  $\kappa$ -mechanism is supported by the tendency of heat flow, during compression, into the zone (due to its temperature being lower than that of its surroundings). The heat flow effect is referred to as the  $\gamma$ -mechanism, due to the smaller ratio of specific heats,  $C_V$  and  $C_P$ , having larger values each. The partial ionization zones serve as the pistons that drive the pulsations of the star. Convection is the thermal process that determines the efficiency of the pulsation. The pulsations will affect the variability in the emitted radiation during each pulsation cycle in terms of modulating the released photons as the opacity varies in time and controls the release of the radiation from the partial ionization zones. Spectroscopic time-series give direct measures of change in the surface velocity. Observations in light curve and spectra give pulsation properties such as luminosity, period, frequency, and velocity values and then through analytic and computer models used to determine the amplitude of the pulsation at the surface of stars and the physical processes occurring in the interior that power the pulsations.

It is at this point it becomes relevant to understand the physics behind pulsations that occur in stellar interiors, such as that of the Sun. The physical equations described below show how physical perturbations travel through the interior gas in stars, and I extend this to accretion disks with some modifications in Chapter VIII. First, we start with the Sun, for example. In the basic helioseismological setting, we start with the basic physical properties and work from there.

Starting with Newton's second law:

$$m \frac{d^2 R}{dt^2} = -\frac{GMm}{R^2} + 4 \pi R^2 P \quad (1.3)$$

In the equilibrium model,

$$\frac{GMm}{R_0^2} = 4\pi R_0^2 P_0 \qquad m \frac{d^2 R}{dt^2} = 0 \qquad (1.4)$$

The quantities,  $R$  (radius) and  $P$  (pressure), can be linearized by writing them as:

$$R = R_0 + \delta R \qquad P = P_0 + \delta P \qquad (1.5a,b)$$

Inserting equations (8.3a,b) into equation (8.1) yields the following expression:

$$m \frac{d^2(R_0 + \delta R)}{dt^2} = -\frac{GMm}{(R_0 + \delta R)^2} + 4\pi(R_0 + \delta R)^2(P_0 + \delta P) \qquad (1.6)$$

Taking the first order approximation:

$$\frac{1}{(R_0 + \delta R)^2} \approx \frac{1}{R_0^2} \left(1 - 2 \frac{\delta R}{R_0}\right) \qquad (1.7)$$

And focusing only on the terms up to the first power of the delta gives us:

$$m \frac{d^2(\delta R)}{dt^2} = -\frac{GMm}{R_0^2} + \frac{2GMm}{R_0^3} \delta R + 4\pi R_0^2 P_0 + 8\pi R_0 P_0 \delta R + 4\pi R_0^2 \delta P \qquad (1.8)$$

Since from the equilibrium model, the hydrostatic equilibrium condition requires that the following equation is true:

$$\frac{GMm}{R_0^2} = 4\pi R_0^2 P_0 \qquad (1.9)$$

With this condition, two of the terms cancel and gives us:

$$m \frac{d^2(\delta R)}{dt^2} = \frac{2GMm}{R_0^3} \delta R + 8\pi R_0 P_0 \delta R + 4\pi R_0^2 \delta P \qquad (1.10)$$

To reduce  $\delta R$  and  $\delta P$  to one, the oscillations are presumed to be adiabatic. The adiabatic relation relates the pressure and the volume,

$$PV^\gamma = \text{constant} \quad (1.11)$$

Where  $\gamma$  is the ratio of specific heats of the gases. The volume of the model is  $\frac{4}{3}\pi R^3$ ,

(1.12)

so the adiabatic relation can be modified as:

$$PR^{3\gamma} = \text{constant} \quad (1.13)$$

The linearized version of this relation is stated as:

$$\frac{\delta P}{P_0} = -3\gamma \frac{\delta R}{R_0} \quad (1.14)$$

Inserting this into Newton's second law expression (linearized version) gives us:

$$m \frac{d^2(\delta R)}{dt^2} = \frac{2GMm}{R_0^3} \delta R + 8\pi R_0^2 P_0 \delta R + 4\pi R_0^2 \delta P \quad (1.15)$$

Recalling the hydrostatic equilibrium condition (equation 1.9),  $\frac{GMm}{R_0^2} = 4\pi R_0^2 P_0$

and rewriting (1.15) in terms of (1.9) adjusts the following equation in a way:

$$\frac{2}{R_0} (4\pi R_0^2 P_0) \delta R = \frac{2}{R_0} \left( \frac{GMm}{R_0^2} \right) \delta R \quad (1.16)$$

And the equation (1.15) becomes:

$$m \frac{d^2(\delta R)}{dt^2} = \frac{2GMm}{R_0^3} \delta R + \frac{2GMm}{R_0^3} \delta R + 4\pi R_0^2 \left( \frac{P_0}{P_0} \right) \delta P \quad (1.17a)$$

$$= \frac{4GMm}{R_0^3} \delta R + 4\pi R_0^2 P_0 \left( \frac{\delta P}{P_0} \right) \quad (1.17b)$$

Inserting the adiabatic relation (eq. 1.14) into the last term of (1.17b) gives us:

$$= \frac{4GMm}{R_0^3} \delta R + \left( \frac{GMm}{R_0^2} \right) \left( -3\gamma \frac{\delta R}{R_0} \right) \quad (1.17c)$$

$$m \frac{d^2(\delta R)}{dt^2} = (4 - 3\gamma) \left( \frac{GMm}{R_0^3} \delta R \right) \quad (1.17d)$$

This yields a harmonic oscillator expression:

$$\frac{d^2(\delta R)}{dt^2} + (3\gamma - 4) \left( \frac{GM}{R_0^3} \delta R \right) = 0 \quad (1.18)$$

Let  $\delta R = e^{\lambda t}$ ; and inserting it in eq. (8.17) gives the following:

$$(1.19) \quad \left( \lambda^2 + \frac{(3\gamma-4)GMm}{R_0^3} \right) e^{\lambda t} = 0$$

(1.20)

$$(\lambda^2 + \omega^2) e^{\omega t} = 0 \quad (1.21)$$

Which means the roots of equation (1.21) are:

$$\lambda = \pm i\omega \quad (1.22)$$

So the radial relation becomes:

$$\delta R = A e^{i\omega t} = A e^{\frac{i(3\gamma-4)GMm}{R_0^3} t} \quad (1.23)$$

The adiabatic index determines the dynamical stability of the stellar object. If the adiabatic index  $\gamma < \frac{4}{3}$ , the exponent becomes negative and the stellar object collapses. In this context, matter would be succumbing to the force of gravity in a free-fall. If the adiabatic index  $\gamma > \frac{4}{3}$ , the exponent is positive and the equation expresses simple harmonic motion of the matter within the stellar object and summarizes the harmonic behavior as pulsations in the matter.

The angular frequency is obtained thusly:

$$\omega^2 = \frac{(3\gamma-4)GMm}{R_0^3} \quad \text{and for an ideal gas, } \gamma = \frac{5}{3} \quad (1.24a,b)$$

$$\omega^2 = \left(3 \left(\frac{5}{3}\right) - 4\right) \frac{GMm}{R_0^3} = \frac{GM}{R_0^3} \quad (1.25)$$

$$\omega = \left(\frac{GM}{R_0^3}\right)^{\frac{1}{2}} \quad (1.26)$$

The frequency of the pulsations is also same as the Keplerian frequency. The period, or the dynamical timescale for the pulsations can be expressed by the following equation (Carroll B. W., An Introduction to Modern Astrophysics, 1996):

$$\Pi = \frac{2\pi}{\sqrt{\frac{4\pi G \rho (3\gamma - 4)}{3}}} = \frac{2\pi}{\omega} \quad (1.27)$$

The pulsations manifest a periodicity that is determined by the frequency of the simple harmonic oscillator equation derived from the helioseismological model. In Chapter VIII these equations will be adapted for an accretion disk in a cylindrical reference frame in order to assess the QPO problem. I will show that (1) the QPO periodicity is a direct consequence of pulsations at a specific radius in the accretion disk and (2) the diskoseismological equations in the cylindrical reference frame can describe the oscillations.

### **Determining the Periodicity of X-Ray Light Curves**

Oscillating matter will have a periodicity to its motion. To find the periodicity of an x-ray emission that originated from a compact object, we have to find periodic emissions in the x-ray light curve. In order to find a distinctive period it is common to take the Fourier Transform of

the time series data (light curve) and produce a power spectrum. The plasma is heated to the point that it emits x-rays. The observed radiation is recorded by satellite telescopes that detect the time of arrival of each photon that hits the detector with an accuracy of microseconds. This provides a count rate time series  $c(t)$ , which is inserted in a Fourier transform and squared to provide a power density. Timing analysis is used here.

A mathematical approach is utilized to single out the peaks of the signal from the noise. A Fourier integral is applied to find the amplitude in the frequency domain for a known function of time,  $f(t)$ , the amplitude being represented by  $F(\omega)$ :

$$F(\omega) = \int_{-\infty}^{\infty} f(t)e^{-i\omega t} dt \quad (1.28)$$

A Fast Fourier Transform (FFT) is generally the algorithm used to process the data and find the discrete Fourier transform and its inverse. Fourier analysis converts time to frequency and vice versa. The transform will take the data over a time domain and convert it to data over a frequency domain, resulting in peaks at particular frequencies. If the signal was represented by a single-frequency harmonic function,

$$f(t) = A \cos(\omega_0 t + \delta_0) \quad (1.29)$$

where  $A$  signifies the amplitude,  $\omega_0$  the angular frequency, and  $\delta_0$  the phase shift,  $F(\omega)$  would have delta-function peaks at  $\omega = \omega_0$  and  $\omega = -\omega_0$ .

A Leahy normalization is used where  $N$  is the total of counts and  $T$  is the duration of the observation (van der Klis, Quasi-periodic oscillations and noise in low mass x-ray binaries, 1989). The pure Poisson noise has a chi-squared distribution with the probability of a power

greater than  $P$  in a given bin being  $e^{-i\omega t}$ .

It makes it possible to determine the chance probability of a peak in a greater density spectrum.

$$P(\omega) = \frac{2}{N} \left[ \int_0^T |c(t) e^{-i\omega t}|^2 dt \right] \quad (1.30)$$

The fractional root mean squared variability at frequency,  $\omega$ , is  $\left[ \frac{P(\omega)}{N} \right]^{\frac{1}{2}}$ .

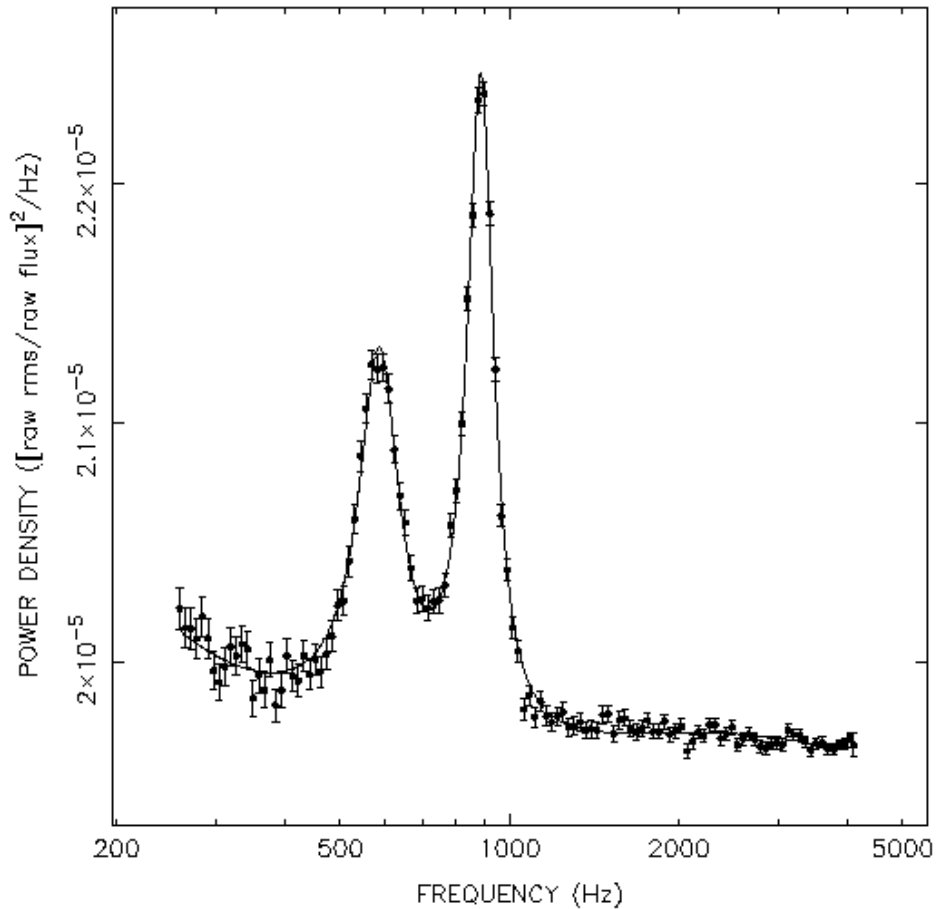


Figure 2. A detailed view of the kilohertz QPO in Sco X-1. (RXTE Guest Observer Facility, 2001)

The black holes' power density spectra have features comparable to an energy spectrum.

Power laws describe long stretches (akin to a continuum spectrum) with gradual changes in the slope and sharper features (spectral lines). In the power density spectra, the frequencies are the time between flux increases in the x-ray energy bands, set by the filter. The fast Fourier Transform converts the time domain into a frequency domain and gives us the characteristic frequency associated with a significant periodicity. A periodic variation in luminosity would manifest itself as a delta function for a long observation. There are a number of broad-peaked features that emerge in the power density spectra with a Gaussian distribution in the peaks, and those are identified as the quasi-periodic oscillations (QPOs). A pronounced peak would signify a definite period, but a wider peak indicates an overlap of periods that reinforce each other at a particular frequency, hence the ‘quasi-periodic’ quality of the QPO.

Photometry and spectroscopic time series obtained during observations can give frequency spectra. If the signal-to-noise ratio is high enough, the oscillations will produce peaks in the power spectra above the ambient noise at particular corresponding oscillation frequencies. In an ideal case, a perfect time series would show all frequencies of global oscillations of a star, given that the signal is dominant above the noise. Such is rarely the case.

The collection of data occurs over a finite time of integration in which a detector is triggered by incoming radiation and then no data is collected in an interval in which the data is read out and stored digitally. The integration time is brief and the time series is not continuous, but rather, discrete. The detection process occurs at a rate such that the time series are sampled at the same time intervals, and at a high enough rate to resolve the time scales of variation. As the data is discretely sampled at a constant rate, a discrete Fourier transform is used to single out the signal as a function of frequency within a band. The highest frequency, the Nyquist



frequency ( $\omega_{Nyq}$ ), limits the highest frequency resolved.

With evenly spaced data, and a sampling interval  $\Delta t$ ,

$$\omega_{Nyq} = \frac{\pi}{\Delta t} \quad (1.31)$$

For unevenly spaced data, the Nyquist frequency differs, especially with large gaps and undersampling in the data. Since the data has a finite length  $T$ , there also corresponds a finite frequency resolution  $\Delta\omega$  in the Fourier domain:

$$\Delta\omega \propto \frac{1}{T} \quad (1.32)$$

If two or more signals manifest in a time series, more closely spaced than the frequency resolution, the signals will not be apparent as a pair of separate peaks in the Fourier domain but rather be discerned as single or deformed peaks instead. A limiting feature for the data would be such that any signals with a frequency below this resolution would not be detected affirmatively. Missing or incomplete data can complicate things further in that the gaps can lead to additional peaks in the Fourier domain, which skews the interpretation of the data, particularly in the case of multi-periodic pulsating sources. Regular gaps occur, due to the inability of observers to maintain a constant direct line of sight with the star due to the rotation of the earth during times such as the daytime and the period in the year when the star in question drops below the observable horizon.

These blank features, or gaps, in the data are known as the window function, (for example the durations that the Earth is not in direct line of sight with the compact object in question, such as the daytime) in the time domain and the spectral window is the equivalent for the Fourier domain. The spectral window exhibits multiple peaks even in the case of a monochromatic signal. A time series containing multiple signals obtained in the same sample yields a complex Fourier spectrum. Despite any data sampling problems, the Fourier transform was determined to

be the optimal approach in deducing the frequencies from any star and providing necessary frequency information (Schwarzenberg-Czerny, 1997).

### Quality Factor Q

A way to determine the quasi-periodicity of any distinct features, in the frequency spectrum of x-ray luminosities from the background noise, is the quality factor. The quality factor is used to detect the presence of a QPO signal in the frequency spectrum. The variability quality factor  $Q_0$  is defined by observers with a constructed Fourier variability power spectra,  $I(\nu)$ . It is derived by the detection of a peak at a frequency  $\nu_0$  in  $I(\nu)$  which is the square of the observed amplitude, and the full width of the peak at half maximum,  $\Delta\nu$ . The relation for  $Q_0$  is given:

$$Q_0 = \frac{\nu_0}{\Delta\nu} \quad (1.33)$$

QPOs with quasi-periodic variability in the kHz frequency range are observed from low mass black holes and neutron stars. And for a strong QPO signal, the quality factor is high ( $Q \sim 200$  in case of one source, 4U 1608-52 as measured by Barret (Barret, 2005)). The quality factor  $Q$  increases with decreasing accretion rate, and the lowest values of the accretion rate  $\dot{m}$  has a rapid drop in the quality due to a change in the nature of the gas as it enters the plunging region (the gas crosses the sonic point where the speed becomes transonic). As the frequency is larger in magnitude than the peak width, the peak contrast approximates a Dirac delta function.

If the peak width increases but the frequency is still significantly constant, the peak broadens, approximating a Gaussian function. It also indicates a quasi-periodic behavior in the

luminosity. If the peak width widens further and approaches the frequency in magnitude, the periodicity or quasi-periodicity vanishes and the overall periodicity is zero. Abramowicz (M.A. Abramowicz, 2010) inferred that since the QPO quality factor was high, kinematic effects of orbiting hotspots or clumps were disqualified as the cause of the QPO phenomenon due to the differential rotation of the disk creating a severe shear in the gas and disrupting the local coherence of any aggregate clumps. The significance of this quality factor points towards a disk oscillation model as an appropriate descriptive model for QPOs, especially in the case of black holes.

## **CHAPTER II**

### **QPO MODELS**

#### **Criteria for QPO Models**

I am going to discuss a range of models that attempt to explain the mechanism behind the production of the QPO feature in x-ray emissions from compact objects. There are three classes of models; the Relativistic Resonance models, Relativistic Precession models, and Beat Frequency models. Each class of models has their own strengths and weaknesses. The models do have commonalities that can be described in detail.

I will now discuss general characteristics of any model that would attempt to describe a QPO. As I have mentioned before, a QPO signal is theorized to come from the gas in the accretion disk orbiting at a particular radius where the gas undergoes a change where it forms a shock wave where it goes from subsonic to sonic. QPO models explore possible types of processes, such as hotspot-forming or oscillations, thought to produce frequencies in an observed range from 0.001 to 10 kHz frequencies. Due to the fundamental time scales (in range of milliseconds), QPOs are speculated to be very close to compact objects with intense gravity.

## Relativistic Precession Models

Relativistic precession models are a class of models that match identified frequencies (orbital, radial, vertical, precession) to predicted frequencies. Further physics is required to single out one or more radii in the disk that correlate to the observed frequencies. Stella and Vietri (Stella L. V., Lense-Thirring Precession and Quasi-Periodic Oscillations in Low-Mass X-Ray Binaries, 1998) (Stella L. V., kHz Quasiperiodic Oscillations in Low-Mass X-Ray Binaries as Probes of General Relativity in the Strong Field Regime, 1999) identified the upper kHz QPO frequency with the orbital frequency  $\nu_\phi$  at the inner edge and related  $\nu_l$  and  $\nu_h$  with the periastron and nodal precession of the orbit.

The frequency  $\nu_h$  is predicted to be proportional to  $\nu_u^2$ , which matches observation and the QPO peak separation  $\Delta\nu = \nu_r$ . The oblateness of the compact object skews the precession rates and requires further correction (Morsink, 1999) (Stella L. V., kHz Quasiperiodic Oscillations in Low-Mass X-Ray Binaries as Probes of General Relativity in the Strong Field Regime, 1999).

Their strengths are predictive and rely only on the compact object characteristics as parameters and General Relativity.

Their weaknesses are their unmodified form; they do not conform exactly to observations (Homan, 2002) (van Straaten, 2005). The observed quadratic dependences between  $\nu_u$  and  $\nu_h$  imply Lense-Thirring precession. Blobs orbiting in the disk in epicyclic motions in sideband patterns can be used as a testing feature in these models (Karas, 1999) (Schnittman, 2004). Disk

oscillation models predict frequencies close to the actual frequencies and may require hydrodynamical effects to modify the frequencies to produce combinations between them to match the observed frequencies better.

### **Relativistic Resonance Models**

Relativistic resonance models focus on the fact that specific radii are responsible for specific epicyclic frequencies and the frequencies have simple integer ratios with each other or the spin frequency. General Relativity singles out the frequencies from the disk and imparts resonances onto the disk as it moves along space-time (Abramowicz M. K., 2001). A particular kind of resonance may occur in these models in which an eigenfrequency  $\nu_0$  is perturbed at  $\nu_1$  commensurate with  $\nu_\theta$ , and resonances occur when

$$\frac{\nu_0}{\nu_1} = \frac{2}{n}, \quad n = 1, 2, 3 \dots \quad (2.1)$$

this type of resonance is the parametric resonance. Radii have been singled out where  $\nu_\theta/\nu_r$  is  $1/2$  or  $\nu_r/\nu_\theta = 2/3$ . Resonances with  $n = 3$  which would be the lowest value allowable for  $\nu_r < \nu_\theta$ , and where  $\nu_\theta = 2$  or  $\nu_\theta = 3$ , can be explanations for the observed ratios for the HF QPOs of black holes (Abramowicz M. K., 2004).

As for the ISCO frequencies, the resonance frequencies also scale with the inverse mass of the compact object, and the resonance can be used to constrain the mass and angular momentum of the compact object.

Resonances can emerge in the interaction between the spin of the compact object and the disk (Psaltis, 2001) (van der Klis, 2002). Different models approach how different frequencies

emerge and interact, such as Wijnands (Wijnands, 2003), who suggested  $\nu_0 - \nu_r = \nu_{spin}$ , or  $\nu_{spin}/2$ , or Kluzniak, who suggested a number of ways that the epicyclic frequencies could resonate with  $\nu_{spin}$  or  $\nu_{spin}/2$ , and the disk g-modes resonate in a frequency ratio of  $\sqrt{2}$ , which would match the twin kHz QPO observation of SAZJ1808.4-3658.

Another model invokes the relation  $\nu_\theta - \nu_r = \nu_{spin}/2$  (Lee, 2004); where the spin-orbit beat frequency equals the vertical epicyclic frequency. The radius at which the frequency emerges is far enough out such that  $\nu_0 \approx \nu_\theta$ ,  $\nu_0 \approx \nu_{spin}$  and would account for the fact that sometimes the frequency separation is sometimes  $\nu_{spin}$ , and sometimes  $\nu_{spin}/2$ .

The radii required for a resonance are fixed so the frequencies are constant, which suit HF QPO models for black holes.

### **Beat-frequency models**

When orbital frequencies beat with the spin frequency of a compact object, more frequencies can be produced as a result (Alpar, 1985) (Lamb F. S., 1985) (Miller M. L., 1998). This requires a non-aligned magnetic field reaching out to a relevant orbital radius, which may disqualify black holes since they do not have an intrinsic magnetic field of their own. Unless the Blandford-Znajek mechanism comes in play and uses the twisting of magnetic field lines of the plasma outside the black hole horizon to create a secondary magnetic field influence due to the black hole spinning in space-time.

Spin-orbit interaction occurs at the difference frequency between the orbital and spin

frequencies. This is the interaction frequency for the disk/star system; the frequency in which an orbiting particle surpasses a specific point on the spinning compact object. A blob moving at  $v_{orb}$  overtakes the magnetic field lines moving at  $v_{spin}$ . This occurs at a rate of  $v_{beat}$  times per unit time where  $v_{beat}$  is the beat frequency.

If the beat interaction happens at the magnetospheric radius of an accreting compact object, for a close radius,  $v_{spin} < v_{orb}$ , and for a farther radius,  $v_{spin} > v_{orb}$ . If there exists an  $n$ -fold symmetric azimuthal pattern associated with the spin, then frequency multiples would emerge: (for two pulsar beams)

$$v_{beat} = 2(v_{orb} - v_{spin}) \quad (2.23)$$

Other azimuthal motions such as periastron or nodal precession would beat with the spin. In the magnetospheric beat-frequency model, blobs orbiting near the magnetospheric radius interact with the spin (Alpar, 1985). The sonic point beat-frequency model for kHz QPOs has  $v_u$  and  $v_l$  correlating to  $v_\phi$  and  $v_{beat}$  at the sonic radius (Miller M. L., 1998). The beat happens when a pulse hits blobs orbiting at  $r_{sonic}$  once per beat period, modulating the accretion rate. The model predicts a constant frequency separation of  $v_{spin}$ , despite observations.

If an azimuthal influence at the spin-resonance radius is in play, a frequency interaction occurs between the orbital motions at  $r_{sonic}$  and the azimuthal influence. It would explain  $v_l$  and set  $v_u = v_\phi(r_{sonic})$ . The beat would be occurring between two radii within the disk.



## Beat Frequency Interaction

A particular feature for QPOs (in the neutron star case but not in the black hole case) is the frequency separation between a pair of QPOs for a source is approximately  $\nu_{\text{spin}}$  or  $\nu_{\text{spin}}/2$ , with the spin frequency inferred from persistent pulsations or brightness oscillations during x-ray bursts.

To understand the connection between the frequency separation and the accretion disk kinematics causing it, we turn to an analogy of a clock. In this analogy, a clock has a minute hand and an hour hand. Each time the two hands line up, a bell rings out. The frequency of the minute hand is  $\nu_{\text{minute}}$ , and the frequency of the hour hand is  $\nu_{\text{hour}}$ . The frequency of the bell, or signal is  $\nu_{\text{bell}} = \nu_{\text{minute}} - \nu_{\text{hour}}$ . (2.2)

The negative sign is due to both hands rotating in the same direction. The opposite of the situation would have the hands' frequencies added. Within an accretion disk, the torque applied by accretion would align the rotation axes of the star and disk, so all spins should be in the same direction. A notable feature of beat frequency models is the fact that they generate only one sideband frequency as opposed to two.

Consider a model consisting of two frequencies,  $\nu_1$  and  $\nu_2$ , producing an amplitude:

$$A = \cos(2\pi\nu_1) \cos(2\pi\nu_2) = \frac{1}{2} \cos[2\pi(\nu_1 + \nu_2)] + \frac{1}{2} \cos[2\pi(\nu_1 - \nu_2)] \quad (2.3)$$

The modulation mechanism creates two oscillations at  $\nu_1 + \nu_2$  and  $\nu_1 - \nu_2$ .

Since both oscillations in a pair of QPOs are not equivalent, it is surmised that one frequency is a fundamental frequency and the second frequency is a modulation of that

fundamental frequency (van der Klis, Millisecond oscillations in X-ray Binaries, 2000). As far as the clock analogy goes, it would be as if the bell rings out every time the hands line up and when the minute hand passes 12.

Stella and Vietra proposed that QPOs were direct reflections of epicyclic frequencies of particles on geodesic paths (Stella L. a., 1998). D. Psaltis and C. Norman contend that the QPOs are due to oscillation modes of a thin annulus in a disk, and that the radius of the annulus could be the sonic point radius.

Miller shows that the observed frequency of a localized hotspot is the orbital frequency at the sonic point and not the stellar rotational frequency (Miller M. L., 1998). Miller surmised that the orbital frequency at the sonic point is converted into the upper QPO due to fluctuations in density.

The lower QPO frequency's existence entails interaction with a second frequency in beat frequency models. If the separation is  $\Delta\nu = \nu_{spin}$ , several possibilities exist. (2.4)

Miller contended that the stellar magnetic field would be the causative factor for the second frequency. When the gas passes the magnetic maximum, it loses angular momentum at an increased rate and cause a fluctuation in its density, causing a modulation in the accretion rate and the flux. The modulation occurs at the frequency  $\nu \sim \nu_{sonic} - \nu_{spin}$  (Lamb F. a., 2001). But further observations indicate this is not the case. (2.5)

Returning to the clock analogy to understand the half spin frequency, the clock has two hour hands set at 180 degrees from each other, moving at an angular frequency  $\nu_{hour}$ , and the observed frequency is  $2(\nu_{min} + \nu_{hour})$ . A resonance would be responsible for the half-spin

frequency. Gas is orbiting in a circle at frequency,  $\nu_{orb}$ . It is subjected to a vertical forcing term with frequency,  $\nu_{force,rest}$ , (as measured in the rest frame of an observer). For most forcing frequencies, with many orbits, the phases will add incoherently and the vertical motion will not be large. If the vertical motion has a natural frequency, forcing of that frequency will result in a resonance and drive substantial motion. This frequency is the vertical epicyclic frequency.

If the forcing frequency measured in the orbital frame is equal to the vertical epicyclic frequency, a resonance results:

$$\nu_{vert} = \nu_{force,rest} . \quad (2.6)$$

The forcing frequency  $\nu_{force,rest}$ , measured in a non-rotating frame, becomes a new frequency in the orbital frame:

$$\nu_{force,rest} = \nu_{force} - \nu_{orb} . \quad (2.7)$$

Taking both equations (2.6) and (2.7) as such:

$$\nu_{force,rest} = \nu_{force} - \nu_{orb}, \quad \nu_{vert} + \nu_{orb} = \nu_{force} \quad (2.8a,b)$$

Since the vertical epicyclic frequency is very close to the spin frequency for all radii, the two frequencies can be set equal to each other:

$$\nu_{force} \approx \nu_{spin} . \quad (2.9)$$

and the forcing frequency in the non-rotating frame is the stellar spin frequency:

$$2\nu_{orb} \approx \nu_{spin}, \quad (2.10)$$

$$\nu_{orb} \approx \frac{\nu_{spin}}{2} . \quad (2.11)$$

The vertical movement of gas in the accretion disk happens the most strongly at the radius where  $\nu_{orb} \approx \frac{\nu_{spin}}{2}$ ; it is not always the case that the frequency separation  $\Delta\nu$  is equal to the half spin frequency. There have been observations that  $\nu_{orb} \approx \nu_{spin}$ . The spin resonance scenario can also explain the spin frequency separation.

$$(2.12a,b)$$

Assume there are very few blobs of gas at the spin resonance radius, for a comparatively smooth flow. A single blob of gas orbits at  $\frac{v_{spin}}{2}$ . Assume the driving force is magnetic in origin. When the magnetic maximum is aligned with the orbital phase of the blob, there is a downward push. When a periodic force drives a system, the system aligns into phase with the driving force. The blob of gas will be at a vertical maximum when the orbital phase lines up with the magnetic maximum. Due to the isolated blob of gas, the main modulation in play for the beat frequency model is the orbital motion, which leads to the frequency difference  $\frac{v_{spin}}{2}$ . All of the blobs are in phase with the driving force and reaches a vertical maximum at the moment the orbital phase lines up with the magnetic maximum. The largest vertical extent at the radius is at the location of the magnetic maximum. The vertical maximum follows the magnetic maximum as a result and has a frequency equal to  $v_{spin}$ .

The group speed moves at  $v_{spin}$  despite the individual speeds of the blobs around  $\frac{v_{spin}}{2}$ . The pattern speed becomes the prominent feature in the beat frequency mechanism. This analogy reconciles the observation of frequency separations of  $\frac{v_{spin}}{2}$  and  $v_{spin}$ .

### **Radii of Interest**

I now comment on the specific locations in the accretion disk so we can pinpoint the location of the production of the QPO signal. The QPO signal is speculated to come from a particular radius and we will search for it. Relativistic Resonance and Precession models focus on the orbital and epicyclic frequencies that depend strongly on preferred radii to create them.

Constant frequencies emanate from constant radii. Variable radii depend on accretion mass rate  $\dot{m}$  in disk physics. Constant radii rely only on the compact object's parameters only, particularly the strong-field gravitational effects such as in the case of the ISCO radius or resonant radii. The inner disk edge sits at the inner radius  $r_{in}$ , where the flow starts to veer from the Keplerian speeds and the radial velocity becomes comparable to that of the azimuthal velocity and serves as a natural radius. It also serves as a demarcation line between the Newtonian case and the Schwarzschild or Kerr case, depending on the spin of the compact object.

Due to the gravitational effect of the difference in orbital angular momentum between radii, the density contrast at  $r_{in}$  is sharp and the change in radial velocity is abrupt (Paczynski, 1987). Without magnetic stresses,  $r_{ms}$  establishes a lower limit for the flow, and the scenario for magnetic stress inclusion remains unknown (Abramowicz M. J., 1978) (Liang, 1980) (Lai, 1998) (Krolik, 2002) (Watarai, 2003).

A possible effect on the flow would be the radiation drag by photons emitted within  $r_{in}$ , which removes angular momentum from the flow via the Poynting-Robertson effect and limit the flow at  $r_{rad}$  (Miller M. L., 1998). The accretion flow carrying the radiation that generates the drag that hinders the flow sets the radius at a fixed point but the flow details and geometries can make the flow variable. As stated in Miller,  $r_{rad}$  cannot exceed  $r \sim \frac{15GM}{c^2}$  and decreases for increasing  $\dot{M}$ . With a powerful magnetic field, electromagnetic stresses truncate the disk outside the ISCO and the  $r_{rad}$ , at the magnetospheric radius  $r_{mag}$ , which decreases in length as  $\dot{M}$  increases.

Orbital motion may still occur as far up as  $r_{rad}$  within  $r_{mag}$  (Miller M. L., 1998). These disk truncation mechanisms may not apply for black holes if no magnetic field is present

(especially if the black hole has zero to minimal spin and the Blandford-Znajek mechanism cannot activate). Some pick the radius of maximum flux from the disk (Gruzinov, 1999) or the radius of maximal pressure in toroidal flow (Kluźniak W. A., 2004) as a preferred radius. In such cases, the function which such extremum would be located would be localized to such an extent and narrow enough to create the QPO signal.

### **Boundary Layer of the Inner Disk**

Different models focus on a localized region within the accretion disk that is responsible for the emergence of the QPO signal in the x-ray emissions. So I will focus on the inner disk and determine the criteria for the conditions that could create the QPO in a bounded region, which is an undefined section of the disk. I will modify a model for a boundary layer for neutron stars to determine the scale of the luminosity layer (Ryden). The boundary layer is where the accretion disk meets the neutron star, and is the dominant source of high-energy radiation in low mass x-ray binaries. I derive an algebraic expression that constrains the radial portion of the boundary layer to a radius  $R_*$ , and the boundary layer width,  $b$ . The radius  $R_*$  can be chosen anywhere within the accretion disk, and in this particular case, will be set at the ISCO and used to find the ratio of Keplerian frequencies at both that radius and the other boundary layer end radius, to detect a resonance between the two frequencies. A boundary layer near the compact object emits a significant amount of the luminosity, even more than the remainder of the accretion disk; of which the boundary layer consists of a very thin region. This region would be set at the inner edge of the accretion disk for the disk luminosity. Since the boundary layer would contribute to

the overall x-ray luminosity, and the QPO signal cannot come from a radius below the ISCO, the boundary layer will be set at that radius and I will use it to explore how the boundary layer modulates the QPO signal.

Consider the boundary layer of a non-magnetic compact object, of mass  $M$  and radius  $R_{Surf}$ . The boundary layer consists of the region  $R_* < R < R_* + b$ , with  $R_*$  denoting the inner radius of the boundary layer,  $R$  a radial distance along the equatorial plane, and  $b$  as the width of the boundary layer. In this case, the star surface is selected as the generic radius for the boundary layer in this case, ( $R_{Surf} = R_*$ ), where the angular velocity decreases from the Keplerian value (Ryden):

$$\Omega(R_{Surf} + b) = \left( \frac{GM_*}{(R_{Surf} + b)^3} \right)^{\frac{1}{2}} \quad (2.13)$$

To the angular velocity at the neutron star's surface:

$$\Omega_{Surf} = \left( \frac{GM_*}{R_{Surf}^3} \right)^{\frac{1}{2}} \quad (2.14)$$

The radial extent of the boundary layer is less than the disk thickness  $H$  just outside the boundary layer, which is also less than the selected radius  $R_*$ . To show how the scaling  $b < H < R_*$  is determined, we start with the equation of conservation of radial momentum:

$$u_R \frac{\partial u_R}{\partial t} - \frac{u_\Phi^2}{R} + \frac{1}{\rho} \frac{\partial P}{\partial R} + \frac{GM_*}{R_*^2} = 0, \quad (2.15)$$

which contains the centrifugal term and the gravity terms. For a Keplerian disk, the centrifugal and gravity terms balance each other out. In the boundary layer, the gravitational term is balanced by the pressure gradient term. The magnitude of the pressure gradient is:

$$\frac{1}{\rho} \frac{\partial P}{\partial R} \sim \frac{v_K^2}{b} = \left( \frac{v_K}{v_s} \right)^2 \frac{c_s^2}{b} = M_\Phi \frac{v_s^2}{b} \quad (2.16)$$

Where  $c_s$  is the speed of sound at the outer edge of the boundary layer and  $b$  is the thickness of the same layer. From the balance of the forces,

$$\frac{c_s^2}{b} \sim \frac{GM_*}{(R_* + b)^2} \quad (2.17)$$

So 
$$b \sim \frac{R_* + b}{M_\Phi^2} \quad (2.18)$$

with  $M_\Phi$  as the rotational Mach number at the outer edge of the boundary layer (Ryden).  $R_*$  can be any radius of interest, whether it be the radius of the compact object, or a preferred radius at a distance from the compact object. A cusp layer can be characterized as a boundary layer set at a further radius out in the accretion disk.

In a thin disk,  $M_\Phi \gg 1$ , and  $H \sim \frac{R}{M_\Phi}$ , so

$$b \sim \frac{H}{M_\Phi} \sim \frac{R}{M_\Phi^2} \quad (2.19)$$

$$M_\Phi \sim \frac{R}{H}; \quad (2.20)$$

$$M_\Phi \gg 1 \quad \rightarrow \quad R_* > H > b \quad (2.21)$$

The blackbody temperature of the boundary layer is (Ryden):

$$T_{BL} = M_\Phi^2 T_* = \left( \frac{R_*}{H} \right)^{\frac{1}{4}} T_* \quad (2.22)$$

In the disk at a radius  $r$  from the center of the star at a distance  $z$  from the mid-plane, the pressure of the gas, due to the vertical balance against gravity, is given by:

$$\frac{dP}{P} = \frac{-\Omega_K^2}{c_s^2} z dz \quad (2.23)$$

Where  $c_s$  is the speed sound, and  $\Omega_K$  is the Keplerian angular velocity. The scale height of the



disk is given as stated in Kenyon and Hartmann 1987:

$$\frac{H}{R} = \frac{1}{R} \left( \frac{c_s^2 R^3}{GM_*} \right)^{\frac{1}{2}} \rightarrow \left( \frac{H}{R} \right) = \frac{c_s}{R\Omega_K} = \frac{c_s}{v_K} \quad (2.24)$$

Since  $R$  is greater than  $H$  for a thin disk ( $R \gg H$ ), it follows that the Keplerian velocity is greater than the sound of speed, or, in other words, is supersonic at radii of all values for  $R > H$  in the inner disk ( $v_K > c_s$ ).

If the internal temperature of the disk,  $T_{inc}(r)$ , which scales to the square of the sound speed ( $T_{inc}(r) \propto c_s^2$ ), falls off more slowly than  $1/r$ , then the relative thickness of the disk will increase outwards and the surface of the disk will be concave.

Going back to the expression (2.17) and expanding on it:

$$M_\Phi^2 \frac{c_s^2}{b} \sim \frac{GM_*}{(R_* + b)^2} \quad (2.25)$$

$$M_\Phi \sim \frac{R_*}{H} \sim \sqrt{\frac{R_*}{b}} \quad (2.26)$$

Inserting the equation (2.26) into the centrifugal force expression (2.25):

$$\left( \frac{R_*}{H} \right)^2 \frac{c_s^2}{b} = \left( \frac{R_*}{b} \right) \frac{c_s^2}{b} = \frac{GM_*}{(R_* + b)^2} \quad (2.27)$$

We multiply both sides of the equation (2.27) by  $\left( \frac{b^2}{R_* c_s^2} \right) (R_* + b)^2$  to get the equation in the form of a quadratic equation in terms of  $R_*$  and  $b$ :

$$\begin{aligned} (R_* + b)^2 &= \frac{GM_*}{R_* c_s^2} b^2 = \frac{GM_*}{R_* c_s^2} \left( \frac{R_*^2}{R_*^2} \right) b^2 \\ &= \frac{GM_* R_*^2}{R_*^3 c_s^2} b^2 = \frac{(R_* \Omega_K)^2}{c_s^2} b^2 = \frac{v_K^2}{c_s^2} b^2 \end{aligned} \quad (2.28)$$

The Keplerian angular velocity is inserted into the equation and multiplied with the radius to give the Keplerian velocity. We get a simple quadratic equation in terms of  $R_*$  and  $b$  now:

$$R_*^2 + 2R_*b + b^2 = \left(\frac{v_K^2}{c_s^2}\right) b^2 \quad (2.29)$$

$$R_*^2 + 2R_*b + \left(1 - \frac{v_K^2}{c_s^2}\right) b^2 = 0 \quad (2.30)$$

Using the quadratic formula to find the roots of  $b$  from (2.41):

$$R_* = \frac{2b \pm \sqrt{(2b)^2 - 4b^2 \left(\frac{v_K^2}{c_s^2} - 1\right)}}{2} = b \pm \sqrt{b^2 \left(1 - \left(\frac{v_K^2}{c_s^2} - 1\right)\right)} \quad (2.31)$$

In the case where the radius  $R_*$  is set at the ISCO ( $R_* = r_{ms}$ ), and the Keplerian velocity is equal to the sonic velocity,

$$v_K = v_s; \quad R_* = b \pm b = 0, \text{ or } 2b. \quad (2.32)$$

The variable  $b$  is the radial width of the cusp layer, and  $c_s$  is the speed of sound at the outer edge of the boundary layer, and  $H$  is the disk thickness or height, and  $R_*$  is the generic radius, and  $M_*$  is the mass of same compact object. The scaling of the boundary or cusp layer goes as:

$$b < H < R_* \text{ for a thin disk.} \quad (2.33a)$$

The Keplerian frequency at the far end of the boundary layer is given as:

$$\Omega(R_* + b) = \left(\frac{GM_*}{(R_* + b)^3}\right)^{\frac{1}{2}} \quad (2.34)$$

We compare the Keplerian frequencies at both ends of the boundary layer:

$$v_{R_*} = R_* \Omega_{R_*} \quad v_{R_*+b} = (R_* + b) \Omega_{R_*+b} \quad (2.35a,b)$$

The ratio of angular frequencies at either side of the boundary layer can be found given as:

$$\frac{\Omega_{R_*}}{\Omega_{R_*+b}} = \frac{(R_*+b)}{R_*} = \frac{R_*}{R_*} + \frac{b}{R_*} = 1 + \frac{b}{R_*} \quad (2.36)$$

Given that  $R_*$  is either 0 or  $2b$  for the ISCO for the cusp layer, we take the latter result as it is the

only physically realistic value in Kerr space-time (only existing for massive, rotating bodies), so the ratio of the frequencies is:

$$\frac{\Omega_{R^*}}{\Omega_{R^*+b}} = 1 + \frac{b}{2R^*} = 1 + \frac{1}{2} = \frac{3}{2} \quad (2.37)$$

That is how I obtain the unique ratio of 3:2 as recovered via the cusp layer model, which matches the QPO frequency resonance.

The fact that the scaling of the dimensions of the boundary layer (or cusp layer) would jibe with the epicyclic resonance model - recall that  $\omega_\theta \geq \omega_K > \omega_R$ . The cusp layer would contribute a significant amount of the disk luminosity and contain the QPO signal within the overall x-ray light curve.

## Anatomy of an Accretion Disk

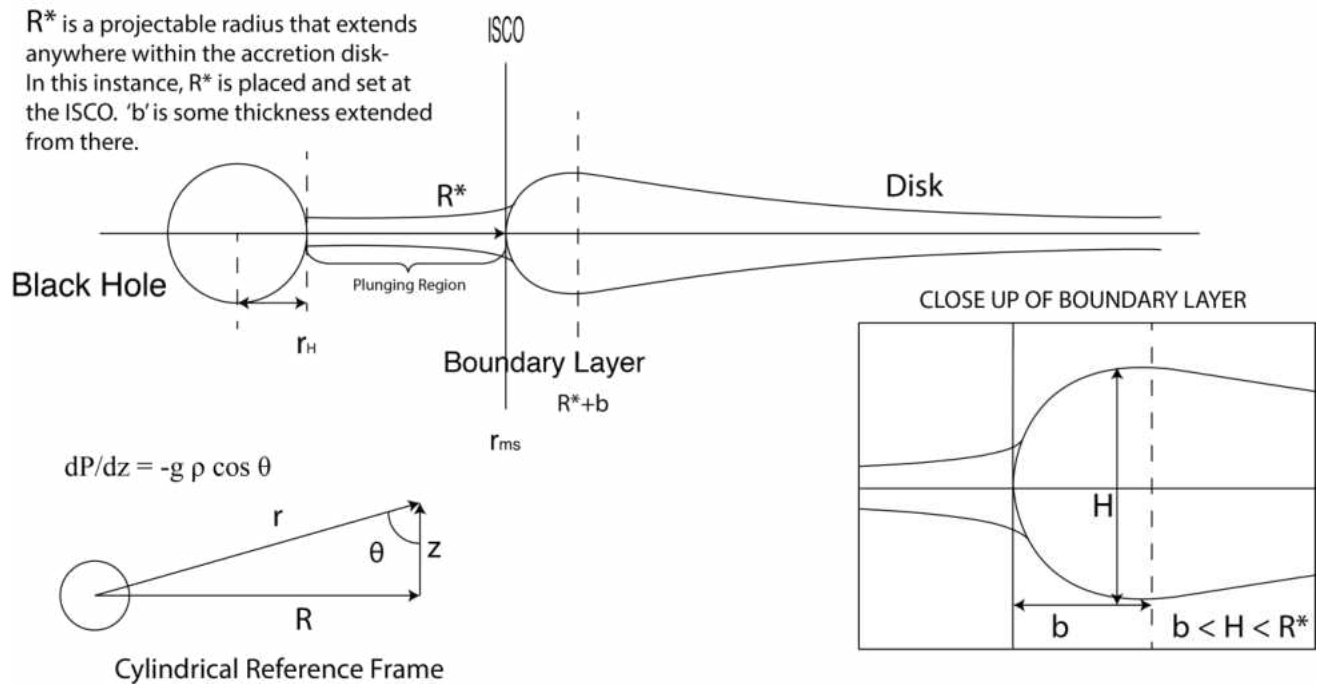


Figure 3. Anatomy of the Boundary/Cusp Layer model in an Accretion Disk.

## The Coupling between the Vertical and Radial Oscillations

We now discuss the relativistic epicyclic resonance model as dictated in Abramowicz 2005, which is defined by the following equations:

$$\delta\ddot{r} + \omega_r^2 \delta r = 0 \quad \delta\ddot{z} + \omega_z^2 \delta z = 0 \quad \text{where } \omega_z \geq \omega_K > \omega_r \quad (2.38)$$

At the ISCO,  $\omega_r(r_{\text{ms}}) = 0$ ,  $\omega_r^2 < 0$  for  $r < r_{\text{ms}}$ .

For a nearly Keplerian fluid (Shakura-Sunyaev disk) with a sound speed  $c_s^2/(w_K^2 r^2) = \beta \ll 1$ , the frequencies of the fluid's epicyclic oscillations,  $\varpi_r, \varpi_z$ , are modified by the pressure:

$$\varpi_r = \omega_r - \chi_r \beta \quad \varpi_z = \omega_z - \chi_z \beta \quad (2.39a,b)$$

A modification is introduced that is very small but crucial in that it provides a weak pressure coupling between the epicyclic modes of the fluid oscillations that lead to a 3/2 resonance.

In Mathieu's form:

$$\delta\ddot{z} + \omega_z^2 [1 + \chi \cos(\varpi_r t)] \delta z = 0 \quad \delta\ddot{r} + \varpi_r^2 \delta r = 0 \quad (2.40a,b)$$

A parametric resonance occurs when:

$$\varpi_r = \frac{2\omega_z}{n}; \quad n = 1, 2, 3, \dots \quad (2.41)$$

In strong gravity,  $\omega_r < \omega_z$ , so  $n = 3$  is the lowest possible integer value, corresponding to the strongest resonance. The ratio of  $\frac{\omega_z}{\omega_r} = \frac{v_{\text{upper}}}{v_{\text{lower}}} = 3/2$  is the most often observed.

The epicyclic resonance model mirrors the expected properties of the boundary layer:

$$b < H < R_* \rightarrow \omega_r < \omega_z \text{ (or } \omega_\theta) \quad (2.42b)$$

Where  $\omega_r$  is the radial epicyclic frequency and  $\omega_z$  is the vertical epicyclic frequency.

I can relate the coupling factor to the pressure, and in turn, locate the strongest value of the coupling factor to find where the epicyclic frequencies would be the most tightly coupled.

Going back to the resonance model equations:

$$\delta\ddot{z} + \omega_z^2[1 + \chi \cos(\varpi_r t)]\delta z = 0 \quad \delta\ddot{r} + \varpi_r^2 \delta r = 0 \quad (2.43)$$

Recall that:

$$\frac{dP}{P} = -\frac{\Omega_K^2}{c_s^2} z dz \quad (2.44)$$

$$P = P_0 e^{-\frac{\Omega_K^2 z^2}{2 v_s^2}} \quad \text{Let } z = R \cos \theta \quad (2.45)$$

$$P = P_0 e^{-\frac{\Omega_K^2 R^2}{2 c_s^2} \cos^2 \theta} \rightarrow \ln\left(\frac{P}{P_0}\right) = -\frac{\Omega_K^2 R^2}{2 c_s^2} \cos^2 \theta = -\frac{v_K^2}{2 c_s^2} \cos^2 \theta \quad (2.46)$$

$$\text{Since } \frac{H}{R} = \frac{c_s}{v_K} \rightarrow \frac{1}{\sqrt{2}} \left(\frac{R}{H}\right) = \sqrt{-\ln\left(\frac{P}{P_0}\right)} = \sqrt{\ln\left(\frac{P_0}{P}\right)} \quad (2.47)$$

Let  $\chi$  be defined in the following way:

$$\frac{c_s}{v_K} = \chi; \quad \text{where } \chi \text{ is a scalar multiple value of } v_K$$

(2.48)

$$\left(\frac{H}{R}\right) = \frac{c_s}{v_K} = \chi \quad (2.49)$$

$$\chi = \frac{H}{R} \quad \chi < 1 \quad (2.50)$$

Which leads to:

$$\frac{1}{\sqrt{2}} \left(\frac{R}{H}\right) = \sqrt{\ln\left(\frac{P_0}{P}\right)} = \frac{1}{\sqrt{2}\chi} = \sqrt{\ln\left(\frac{P_0}{P}\right)} \quad (2.51)$$

$$\chi = \sqrt{\frac{1}{2 \ln\left(\frac{P_0}{P}\right)}} \quad (2.52)$$

That is how the coefficient would depend on the pressure in the accretion disk in the coupling relation, as we would determine through the calculations. From equation (2.62), the pressure maximum is at  $P_0$ , and the coupling factor decreases in value as the pressure drops at increasing vertical distance from the equatorial plane and the value of the denominator increases. For a thin disk,  $H \ll R$ , which means  $c_s \ll v_K$ , and  $\chi \ll 1$ , which implies a weak coupling between the vertical and radial modes where pressure is concerned, and the pressure would be strongest near the equatorial plane and where the disk would be the thinnest, so the ideal radius for the strongest coupling between the vertical and radial oscillations would be at the very edge of the inner disk, namely, the ISCO.

CHAPTER III  
KERR GEOMETRY

**Dimensionality of the General Relativity metric terms**

I will now start explaining the physical and mathematical vocabulary of the Kerr and Schwarzschild metrics and how it determines the curvature of space-time in the proximity of a non-rotating or rotating compact object. For black holes and accretion disks, black holes generally are uncharged and the dominant source of gravity (the Kerr-Newman metric is a further-modified metric that takes electric charge in account) and by comparison, the accretion disk self-gravity is negligible. The black hole or neutron star's gravitational influence is the dominating factor and determines the local curvature of the space-time fabric around it and the trajectories of the falling particles moving through the space-time, towards the central massive object. For a rotating black hole, this is defined by the Kerr metric, which takes on two parameters: the mass of the central body (black hole or neutron star) and its angular momentum (signified by  $J$ ). The terms include the gravitational constant,  $G$ , and the speed of light,  $c$ , which are set to one for simplification purposes (Press, 1972):

$$M = \frac{GM}{c^2} \qquad J = \frac{GMa}{c} \qquad (3.1a,b)$$

$$a = \frac{Jc}{GM} \qquad a = \frac{J}{M} \text{ with } (G = c = 1) \qquad (3.1c,d)$$

Exploring the dimensionality of the Kerr metric terms to understand them in a physical context, we focus on them:  $M$  as the mass of the compact object, whether it be a neutron star or black hole, and  $a$  as the angular momentum parameter.

How  $M$  gives us the physical parameter of length is simple-for example, the Schwarzschild radius is:

$$r_S = \frac{2GM}{c^2} = 2 \left( \frac{G}{c^2} \right) M = \frac{2 \left( \frac{\frac{m^3}{kg}}{s^2} \right) M}{\left( \frac{m}{s} \right)^2} = 2 \left( \frac{m}{kg} \right) M = 2 M. \qquad (3.2)$$

So in this equation (3.2), the units meters and kilograms are convertible by multiplying the mass in terms of  $(kg)$  with the geometricized constant  $(G/c^2)$  in terms of  $(m/kg)$  to yield a measure of distance  $(m)$ .

The Schwarzschild solution for the General relativity metric is obtained this way:

$$\frac{1}{2} m v^2 = \frac{GMm}{r} \rightarrow v^2 = \frac{2GM}{r}, \text{ and since } v = c \qquad (3.3)$$

The radius  $r$  is rearranged and we get the Schwarzschild solution:  $r = r_S = \frac{2GM}{c^2}$

(3.4)

$G$  and  $c$  is usually geometricized (set to one) since they are constants so the radius of the neutron star or black hole is written in terms of the mass due to its being the only changing quantity:

$$r_S = r = 2M \qquad (3.5a)$$

The geometricized term  $(G/c^2)$  is equivalent to the physical terms of meter/kilogram  $(m/kg)$ .

The gravitational constant is so small and the speed of light so large, that the geometricized terms reduce to a very small quantity. It requires a large amount of mass (usually expressed in solar



masses) to turn it into a discernible quantity as the Schwarzschild radius can show in physical terms:

$$r_S = \frac{2GM}{c^2} = 2.95 \text{ km} \left( \frac{M}{M_\odot} \right) \quad (3.5b)$$

The Kerr metric terms are more complicated than the Schwarzschild metric in that it figures in the angular momentum of the compact object,  $J$ , and deals with the angular momentum parameter,  $a$ .

The relation between  $J$  and  $a$  is as follows:

$$J = M a = \left( \frac{G}{c} \right) M a \quad (3.6)$$

The classical expression for the angular momentum for a star is;

$$L = \frac{GM^2}{c} \quad (3.7)$$

We can draw an analogous relationship between the Kerr and the classical expressions (equations 3.6 and 3.7):

$$J = \frac{GMa}{c} = \frac{GMa}{c} \left( \frac{M}{M} \right) = \frac{GM^2}{c} \left( \frac{a}{M} \right) = L \left( \frac{a}{M} \right) \quad (3.8)$$

The dimensionless parameter  $(a/M)$  acts as a coefficient of the classical angular momentum of the compact object. When  $a = 0$ , the compact object resides in a metric that reverts to the Schwarzschild metric, and when  $a = M$ , the angular momentum is at its maximum value and tweaks the metric significantly. The dimensionless parameter  $(a/M)$  is also denoted in scientific literature as the parameter  $a_*$ , or the lower case  $j$ . The dimensionality of the angular momentum parameter can be inferred through the relation:

$$J = \frac{G}{c} M a \rightarrow a = \frac{cJ}{GM} = \frac{\left( \frac{m}{s} \right) \left( kg \frac{m^2}{s} \right)}{\left( \frac{m^3}{s^2} \right) (kg)} = kg \quad (3.9)$$

The physical parameter  $a$  is in terms of the mass equivalent of the angular momentum of the compact object, that when multiplied with  $G/c^2$ , yields a measure in terms of radial distance.

The event horizon relation is written as:

$$r_H = M \pm \sqrt{M^2 - a^2} = \left(\frac{G}{c^2}\right) [M \pm \sqrt{M^2 - a^2}] = \left(\frac{GM}{c^2}\right) \left[1 \pm \sqrt{1 - \left(\frac{a}{M}\right)^2}\right] \quad (3.10)$$

When  $J$  reaches a maximum for  $a = M$ , the black hole event horizon is:  $r_H = \left(\frac{GM}{c^2}\right) = \frac{1}{2} r_S$   
(3.11)

And when  $J = 0$  for  $a = 0$ , the event horizon is:  $r_H = \left(\frac{GM}{c^2}\right) (1 + 1) = \frac{2GM}{c^2}$ , or the Schwarzschild radius.

### The Kerr metric

We can get the terms for the Kerr metric, which would describe the space-time around a rotating black hole. I will be using it to determine the location of the event horizon (given by the solution to the Kerr metric with the angular momentum parameter  $a$  included). Starting with Boyer-Lindquist coordinates from the Kerr metric for a rotating Black Hole:

$$d\tau^2 = \left(1 - \frac{2M}{r}\right) dt^2 + \frac{4Ma}{r} dt d\phi - \frac{1}{1 - \frac{2M}{r} + \frac{a^2}{r^2}} dr^2 - \left(1 + \frac{a^2}{r^2} + \frac{2Ma^2}{r^3}\right) r^2 d\phi^2 \quad (3.12)$$

The specific angular momentum,  $a$ :

$$a = J/M \text{ where } 0 \leq M \leq 1;$$

For some physical context, the physical value of  $J$  for a star like the sun is

$$J = 1.63 \times 10^{48} \text{ g cm}^2 / \text{s} \rightarrow a = 0.185 M;$$

If  $a = 0$ , then the metric for the Black hole reverts to that of a non-rotating black hole (Schwarzschild).

Focusing on the radial component of the metric,

$$\frac{1}{1 - \frac{2M}{r} + \frac{a^2}{r^2}} dr^2 \quad (3.13)$$

This component blows up if the denominator approaches zero, implying a singularity exists:

$$1 - \frac{2M}{r} + \frac{a^2}{r^2} = 0 \quad (3.14)$$

Multiplying equation (3.14) by  $r^2$ , yields equation (3.15):

$$r^2 \left( 1 - \frac{2GM}{rc^2} + \frac{a^2}{r^2} \right) = 0 \quad (3.15)$$

Assuming  $G$  and  $c^2$  has been set to equal to one:

$$r^2 - 2Mr + a^2 = 0 \quad (3.16)$$

Using the quadratic formula to find the roots for this equation:

$$r = \left( M \pm \frac{\sqrt{4M^2 - 4a^2}}{2} \right) \quad (3.17)$$

which simplifies as:

$$r = M \pm \sqrt{M^2 - a^2} \quad (3.18)$$

If the equation is reevaluated with  $G$  and  $c^2$  included, the context of the roots become clearer in terms of distance:

$$1 - \frac{2GM}{rc^2} + \frac{a^2}{r^2} = 0 = 1 - \frac{R_s}{r} + \frac{a^2}{r^2} \quad (3.19)$$

Where  $R_s$  is the Schwarzschild radius ( $R_s = \frac{2GM}{c^2}$ )

$$r^2 \left( 1 - \frac{2GM}{c^2 r} + \frac{a^2}{r^2} \right) = r^2 - \frac{2GM}{c^2} r + a^2 = 0 \quad (3.20)$$

The roots comes out as such since  $a = 1$ ,  $b = 2GM/c^2$  and  $c = a^2$ ;

$$r = \frac{\frac{2GM}{c^2} \pm \sqrt{\frac{4G^2 M^2}{c^4} - 4a^2}}{2} = \frac{GM}{c^2} \pm \sqrt{\frac{G^2 M^2}{c^4} - a^2} \quad (3.21)$$

Expressing it in terms of the Schwarzschild radius ( $R_s$ ),

$$r = \frac{1}{2} R_s \pm \sqrt{\frac{1}{4} R_s^2 - a^2} \quad (3.22a)$$

As  $a \rightarrow 0$ ,  $r = \frac{1}{2} R_s \pm \frac{1}{2} R_s$ ; which gives us two possible answers:  $0$ , or  $R_s$ . (3.22b)

The unit  $a$  can only exists between values of zero and  $M$ , because if it exceeds either value, it goes outside the domain contained within the square root and a takes on an imaginary value. Thus,  $a^2 \leq M^2$ .

Resetting  $G$  and  $c^2$  to one,  $r$  reverts to:

$$r = M \pm \sqrt{M^2 - a^2} \quad (3.23)$$

The unit 'a' can also be expressed into terms of  $R_s$ .

The Kerr Metric's two horizons:

$$R_{mn} = M - \sqrt{M^2 - a^2} \quad (\text{inner horizon}) \quad (3.24)$$

$$R_{mx} = M + \sqrt{M^2 - a^2} \quad (\text{outer horizon}) \quad (3.25)$$

In the static case:

$$R_{static} = M + \sqrt{M^2 - a^2 \cos^2 \theta} \quad (3.26)$$

$$\text{For } \theta = \frac{\pi}{2}, a \rightarrow 0;$$

$$R_{static} = M + \sqrt{M^2} = 2M = \frac{2GM}{c^2} = R_s \quad (3.27)$$

The volume between  $R_h$  and  $R_{static}$  is defined as the black hole's ergosphere. When the black hole is rotating, three radii come into play:  $R_{max}$ ,  $R_{min}$ , and  $R_{static}$ .

At  $R_{static}$ , no force can keep anything static. Spacetime rotates around the black hole at the speed of light; this is frame-dragging, or the Lense-Thirring Effect. Within the ergosphere, frame-dragging dominates. At  $R_{min}$ , matter flows out and at  $R_{max}$ , matter flows in. As the black hole rotates faster,  $R_{min}$  and  $R_{max}$ , or  $R_{inner}$  and  $R_{outer}$ , respectively, moves in towards each other

where they meet for the value of  $a = M$ . The event horizons would effectively be destroyed and a naked singularity would become exposed.

To find the angular velocity  $\Omega_H$ :

$$g_{\phi\phi} = r_H^2 + a^2 + \frac{2Ma^2}{r_H} \quad \Delta = r^2 - 2Mr + a^2 \quad (3.28a,b)$$

$$g_{tt} = 0 = \frac{\Delta - a^2 \sin^2 \theta}{\zeta^2} \quad \zeta^2 = r^2 + a^2 \cos^2 \theta \quad (3.28c,d)$$

$$g_{t\phi} \dot{t} + g_{\phi\phi} \dot{\phi} = 0 \quad (3.28e)$$

$$\frac{d\phi}{dt} = -\frac{g_{t\phi}}{g_{\phi\phi}} = \frac{2Mar}{(r^2 + a^2) - a^2 \sin^2 \theta} \quad (3.29)$$

Multiply equation (3.28e) by  $2\dot{\phi}$  :

$$2 g_{t\phi} \dot{t} \dot{\phi} = -2 g_{\phi\phi} \dot{\phi}^2 \quad (3.30)$$

$$g_{tt} \dot{t}^2 + 2 g_{t\phi} \dot{t} \dot{\phi} + g_{\phi\phi} \dot{\phi}^2 = 0 \quad (3.31)$$

Divide equation (3.31) by  $\dot{t}^2$ :

$$\frac{g_{tt} \dot{t}^2 + 2 g_{t\phi} \dot{t} \dot{\phi} + g_{\phi\phi} \dot{\phi}^2}{\dot{t}^2} = 0 \quad (3.32)$$

I get:

$$g_{tt} + 2g_{t\phi} \left(\frac{\dot{\phi}}{\dot{t}}\right) + g_{\phi\phi} \left(\frac{\dot{\phi}}{\dot{t}}\right)^2 = 0 \quad (3.33)$$

Notice that  $\left(\frac{\dot{t}}{\dot{\phi}}\right) = \frac{\frac{d\phi}{d\tau}}{\frac{dt}{d\tau}} = \frac{d\phi}{dt}$  (3.34)

And inserting the equation (3.34) into equation (3.33) yields:

$$g_{\phi\phi} \left(\frac{d\phi}{dt}\right)^2 + 2g_{t\phi} \left(\frac{d\phi}{dt}\right) + g_{tt} = 0 \quad (3.35)$$

Using the quadratic formula again for equation (3.35):

$$\frac{d\phi}{dt} = \frac{-2g_{t\phi} \pm \sqrt{4g_{t\phi}^2 - 4g_{tt}g_{\phi\phi}}}{2g_{\phi\phi}} \quad (3.36)$$

$$\frac{d\phi}{dt} = -2 \left(\frac{g_{t\phi}}{g_{\phi\phi}}\right) \pm \sqrt{\left(\frac{g_{t\phi}}{g_{\phi\phi}}\right)^2 - \left(\frac{g_{tt}}{g_{\phi\phi}}\right)} \quad (3.37)$$

For a non-rotating black hole,  $g_{t\phi} = 0$  (3.38)

$$g_{tt} = -\left(1 - \frac{2M}{r}\right) \quad (3.40)$$

$$g_{\phi\phi} = r^2 \sin^2 \theta = r^2 \quad (\theta = \pi/2) \quad (3.41)$$

$$\frac{d\phi}{dt} = \sqrt{-\frac{g_{tt}}{g_{\phi\phi}}} = \frac{1}{r} \sqrt{1 - \frac{2M}{r}} \quad (3.42)$$

For a rotating black hole,

$$\frac{d\phi}{dt} = -\frac{g_{t\phi}}{g_{\phi\phi}} = \frac{2Mar}{((r^2+a^2)^2 - a^2 \delta \sin^2 \theta)} \quad (3.43)$$

$$\frac{d\phi}{dt} = -\frac{g_{t\phi}}{g_{\phi\phi}} \pm \frac{g_{t\phi}}{g_{\phi\phi}} = 0 \vee -2 \frac{g_{t\phi}}{g_{\phi\phi}} \quad (3.44)$$

For a maximally rotating black hole,  $\theta = \pi/2$  and  $a = M$ ,

So the angular velocity becomes:

$$\frac{d\Phi}{dt} = \frac{2M^2}{r^3 + rM^2 + 2M^3} \quad (3.45)$$

At the horizon,  $\Delta = 0$  and  $r^2 + a^2 = 2Mr_H$ , which gives us: (3.46)

$$g_{tt} = \frac{a^2 \sin^2 \theta}{\zeta^2} \quad (3.47)$$

$$g_{t\Phi} = \frac{-2Mar_H \sin^2 \theta}{\zeta^2} \quad (3.48)$$

$$g_{\Phi\Phi} = \frac{(2Mr_H)^2 \sin^2 \theta}{\zeta^2} \quad (3.49)$$

$$\left[ \left( \frac{g_{t\Phi}}{g_{\Phi\Phi}} \right)^2 - \left( \frac{g_{tt}}{g_{\Phi\Phi}} \right)^2 \right]^{1/2} = \left[ \frac{a^2}{(2Mr_H)^2} - \frac{a^2}{(2Mr_H)^2} \right]^{1/2} = 0 \quad (3.50)$$

$$\frac{d\Phi}{dt} = \Omega_H = \frac{g_{t\Phi}}{g_{\Phi\Phi}} = \frac{a}{2Mr_H} = \frac{a}{r_H^2 + a^2} \quad (3.51)$$

The space-time metric  $g_{\mu\nu}$  is given by the Kerr metric in the form of spherical Boyer-Lindquist coordinates (Press, 1972):

$$g_{tt} = \left( 1 - \frac{2Mr}{\Sigma} \right) \quad g^{tt} = -(r^2 + a^2)^2 - a^2 \Delta \sin^2 \theta \quad (3.52a,b)$$

$$g_{t\Phi} = -\frac{4Mar \sin^2 \theta}{\Sigma} \quad g^{t\Phi} = -\frac{2Mar}{\Sigma \Delta} \quad (3.52c,d)$$

$$g_{\Phi\Phi} = \left( r^2 + a^2 + 2Ma^2 r \frac{\sin^2 \theta}{\Sigma} \right) \sin^2 \theta \quad g^{\Phi\Phi} = \frac{\Delta - a^2 \sin^2 \theta}{\Delta \Sigma \sin^2 \theta} \quad (3.52e,f)$$



$$g_{rr} = \frac{\Sigma}{\Delta} \qquad g_{\theta\theta} = \Sigma \qquad (3.52g,h)$$

$$g^{rr} = \frac{\Delta}{\Sigma} \qquad g^{\theta\theta} = \frac{1}{\Sigma} \qquad (3.52i,j)$$

$$\Delta = r^2 - 2Mr + a^2 \qquad \Sigma = r^2 + a^2 \cos^2 \theta \qquad (3.53a,b)$$

The Kerr metric is time-independent and azimuthal angle ( $\phi$ ) independent, around the symmetry axis. The two symmetries are expressed in a coordinate independent way, by Killing vectors (Press, 1972):

$$\eta^\mu = \delta^\mu t \qquad \xi^\mu = \delta^\mu \phi \qquad (3.54a,b)$$

and the covariant derivative,  $\nabla_\mu$  ;

$$\nabla_{(\mu} \eta_{\nu)} = 0 \qquad \nabla_{(\mu} \xi_{\nu)} = 0 \qquad (3.55a,b)$$

$$\eta^\mu \nabla_\mu \xi_\nu = \xi^\mu \nabla_\mu \eta_\nu \qquad (3.55c)$$

In Boyer-Lindquist coordinates, the metric now becomes:

$$g_{tt} = (\eta\eta) \qquad g^{tt} = -\frac{\xi\xi}{(\eta\xi)^2 - (\eta\eta)(\xi\xi)} = -e^{2\phi} \qquad (3.56a,b)$$

$$g_{t\phi} = (\eta\xi) \qquad g^{t\phi} = -\frac{\eta\xi}{(\eta\xi)^2 - (\eta\eta)(\xi\xi)} = +\omega e^{2\phi} \qquad (3.56c,d)$$

$$g_{\phi\phi} = (\xi\xi) \qquad g^{\phi\phi} = -\frac{\eta\xi}{(\eta\xi)^2 - (\eta\eta)(\xi\xi)} = -\tilde{r}^2 e^{2\phi} \qquad (3.56e,f)$$

The quantities are:

$$\omega = \frac{(\eta\xi)}{\xi\xi} \qquad \text{the frame dragging angular velocity,} \qquad (3.57)$$

$$\phi = \frac{1}{2} \ln((\eta\eta) + \omega(\eta\xi)) \quad \text{the gravitational potential} \quad (3.58)$$

$$-\tilde{r}^2 = -\frac{\xi\xi}{\eta\eta} \quad \text{the square of the gyration radius} \quad (3.59)$$

In classical Newtonian gravity, the angular momentum  $\ell$  is equal to  $r^2\Omega$ . (3.60)

In Kerr geometry, the modified angular momentum is  $\ell = \tilde{r}^2(\Omega - \omega)$ , (3.61)

containing two terms: the angular velocity,  $\Omega$ , and the angular velocity of the frame dragging (known as the Lenses-Thirring effect),  $\omega$ . This creates two different physical frames of reference; the stationary frame with respect to other stars apart from the rotating object in question ( $\Omega = 0$ ), and the zero angular momentum observer (ZAMO) frame of reference that doesn't rotate locally ( $\ell = 0$ ).

Two sets of observers are considered:

$$\text{Stationary observer at infinity: } N^i = \eta^i \quad (3.62)$$

$$\text{ZAMO: } n^i = e^\phi(\eta^i + \omega \xi^i) \quad (3.63)$$

where  $N^i$  and  $n^i$  are projected onto the space normal to the plane of the observer's perspective (Press, 1972). The two frames co-rotate with each other at the frame-dragging velocity,

$$\omega = -\frac{g_{t\phi}}{g_{\phi\phi}} \quad (3.64)$$

Circular geodesic motion generally occurs along the equatorial plane where  $\theta = \frac{\pi}{2}$  in the Kerr geometry and the accretion disk is set along the equatorial plane in the black hole's reference frame. The equation that defines the circular motion is:

$$u_i = A(\eta^i + \Omega \xi^i), \quad u_i \nabla_i u_k = 0 \quad (3.65a,b)$$

$\Omega$  is the angular velocity as observed by a stationary observer, and  $A$  is the red-shift factor ( $A=-$

$u_t$ );

$$-A^{-2} = g_{tt} + 2 \Omega g_{t\phi} + \Omega^2 g_{\phi\phi} \quad (3.66)$$

$$\Omega = \frac{u_\phi}{u_t} = \frac{d\phi}{dt} \quad (3.67)$$

Due to the Killing symmetries, the energy  $\varepsilon$  and specific angular momentum  $\mathcal{L}$  are constant along the particle trajectory (Press, 1972):

$$\mathcal{E} = -\mu_\eta = -u_t \quad \mathcal{L} = -\frac{\mu_\xi}{\mu_\eta} = -\frac{u_\phi}{u_t} \quad (3.68a,b)$$

the other quantities are cast in these terms accordingly;

$$\Omega = \frac{\mathcal{L} g_{tt} + g_{t\phi}}{\mathcal{L} g_{t\phi} + g_{\phi\phi}} \quad \mathcal{L} = \frac{\Omega g_{tt} + g_{t\phi}}{\Omega g_{t\phi} + g_{\phi\phi}} \quad (3.69a,b)$$

$$\mathcal{E} = -A(g_{tt} + \Omega g_{t\phi}) \quad (3.69c)$$

The effective potential also is expressed as:

$$U_{eff} = \frac{1}{2} \ln(g^{tt} - 2 \mathcal{L} g^{t\phi} + \mathcal{L}^2 g^{\phi\phi}) \quad (3.70)$$

As determined in terms of the effective potential and the rescaled energy  $\varepsilon^* = \ln \varepsilon$ , a slightly perturbed non-circular motion under the condition,

$$V^2 = u_r u_r g_{rr} \ll u_\phi u_\phi g_{\phi\phi}, \quad (3.71a,b)$$

$$= u_\theta u_\theta g_{\theta\theta} \ll u_\phi u_\phi g_{\phi\phi} \quad (3.71c,d)$$

is expressed by the following equation:

$$\frac{1}{2} V^2 = \varepsilon^* - U_{eff} \quad (3.72)$$

This is the same equation that applies in the Newtonian case. As well as for Newtonian theory as for the general relativistic case, unperturbed circular orbits are given by the condition of the extrema of the effective potential:

$$\left(\frac{\delta U_{eff}}{dr}\right) = 0 \quad (3.73)$$

The unperturbed orbits follow simple harmonic oscillator equations (for  $V$  being either in the radial or vertical direction:  $(\delta\dot{r},$  and  $\delta\dot{\theta},$  respectively).

$$\delta\ddot{r} + \omega_r^2 \delta r = 0 \quad d\ddot{\theta} + \omega_\theta^2 \delta\theta = 0 \quad (3.74a,b)$$

This is where the radial and vertical epicyclic frequencies come from: perturbed orbits of infalling matter and their motion along the Kerr metric. The epicyclic frequencies are defined as the second derivatives of the effective potential,

$$\omega_r^2 = \left(\frac{\delta^2 U_{eff}}{\delta r^2}\right) \quad \omega_\theta^2 = \left(\frac{\delta^2 U_{eff}}{\delta \theta^2}\right) \quad (3.75a,b)$$

where  $dx^{*2} = -g_{xx} dx^2$ .

The formulae in the Kerr metric (with  $x = r/M$ ) are as follows:

$$\Omega_K^2 = \left(\frac{GM}{R^3}\right) \left(1 + a \left(\frac{M}{R^3}\right)^2\right)^{-1} \quad (3.76)$$

$$(\omega_r^*)^2 = \Omega_K^2 (1 - 6x^{-1} + 8ax^{-3/2} - 3a^2x^{-2}) \quad (3.77)$$

$$(\omega_\theta^*)^2 = \Omega_K^2 (1 - 4ax^{-3/2} + 3a^2x^{-2}) \quad (3.78)$$

## Orbital radii

Circular orbits in the Kerr metric exist in the region  $r > r_{ph}$ ,  $r_{ph}$  being the photon orbit. Bound orbits are found in the region  $r > r_{mb}$ ,  $r_{mb}$  being the marginally bound orbit, and stable orbits belong to the region  $r > r_{ms}$ ,  $r_{ms}$  being the marginally stable orbit, and also known as the Innermost Stable Circular Orbit (ISCO). Out of the listed radii, the last one is usually at the radius the inner disk edge is set at, for most accretion disk models.

The radii are determined by the formulae:

$$\text{Photon orbit: } r_{ph} = r_G [1 + \cos[2/3 \cos^{-1}(a)]] \quad (3.79)$$

$$\text{Bound orbit: } r_{mb} = r_G [1 - a/2 + [1 - a^2]^{1/2}] \quad (3.80)$$

$$\text{Stable orbit: } r_{ms} = r_G [3 + Z_2 - [(3 - Z_1)(3 + Z_1 - 2Z_2)]^{1/2}] \quad (3.81)$$

$$\text{with } Z_1 = 1 + (1 - a^2)^{1/3} [(1 + a)^{1/3} + (1 - a)^{1/3}], \quad Z_2 = (3a^2 + Z_1^2)^{1/2}. \quad (3.82a,b)$$

The Keplerian angular momentum is expressed as:

$$\ell_k = \ell_k(r, a) = \frac{r^2 - 2ar^{\frac{1}{2}} + a^2}{r^{\frac{3}{2}} - 2r^{\frac{1}{2}} + a} \quad (3.83)$$

The black hole event horizon is defined by the following equation:

$$r_H = r_G/2 (1 + [1 - a^2]^{1/2}) = M + (M^2 - a^2)^{1/2}; \quad (3.84)$$

and the ergosphere:

$$r_G = M + (M^2 - a^2 \cos^2 \theta)^{1/2}; \quad (3.85)$$

The ergosphere is thickest at the equator where  $\theta = \frac{\pi}{2}$  and thinnest at the poles where  $\theta = 0$  or  $\pi$ . The ergosphere bulges at the equator and as the spin increases, it flattens until at the

maximal rate of spin, the ergosphere is flat and the singularity is exposed.

In the non-rotating case the metric terms  $g_{t\phi} = g^{t\phi} = 0$  vanish and the Kerr metric becomes the Schwarzschild metric instead.

Going back to the Kerr metric expressed in Boyer-Lindquist coordinates:

$$ds^2 = -\frac{\Delta}{\Sigma}(dt - a \sin^2 \theta d\phi)^2 + \Sigma \left( \frac{dr^2}{\Delta} + d\theta^2 \right) + \frac{\sin^2 \theta}{2} (a dt - (r^2 + a^2)d\phi)^2 \quad (3.86)$$

$$\Delta = r^2 - 2Mr + a^2 \quad \Sigma = r^2 + a^2 \cos^2 \theta \quad (3.87a,b)$$

where  $M$  is mass,  $a$  is the angular momentum per unit mass ( $a = J/M$ ). This equation yields roots that are the solutions for the black hole's event horizons.

The Kerr space-time metric is also a separable partial differential equation that enables separation of variables in a Hamilton-Jacobi equation for geodesics. The equation contains symmetries (time-translational and rotational) that render it integrable.

The equatorial plane is the setting for the orbiting particles within the accretion disk so the angle  $\theta$  is set at  $\theta = \frac{\pi}{2}$ . The motions are purely circular and the circular motions as well as ensuing perturbations in the circular motion can be expressed by approximations in the geodesic equation:

$$\frac{d^2 x^\mu}{ds^2} + \Gamma_{\alpha\beta}^\mu \frac{dx^\alpha}{ds} \frac{dx^\beta}{ds} = 0 \quad (3.88)$$

with  $s$  being the proper time along geodesic paths, and  $\Gamma$  as the Christoffel symbols of the space-time metric.

With the circular motion in the equatorial plane,  $r = r_0$ ,  $\theta = \frac{\pi}{2}$ , a position vector  $z^\mu(s) =$

$\{t(s), r_0, \frac{\pi}{2}, \Omega_0 * t(s)\}$ , is introduced, with  $\Omega_0$  being the orbital frequency.

The Christoffel symbols for the Kerr metric show for the circular motion,  $\mu = 0, 2, 3$  components of the geodesic equation are trivial and the  $\mu = 1$  component gives us:

$$\Omega_0 = \pm \frac{\Omega_s}{1 \pm a\Omega_s} \quad (3.89)$$

with  $\Omega_s$  being the Keplerian frequency, and the plus sign denoting a direct orbit and the minus sign denoting a retrograde orbit. Using the angular velocity solution to the geodesic equation in the normalization condition for the 4-velocity,  $g_{\mu\nu}u^\mu u^\nu = -1$ , an expression for the particle's energy per unit mass can be found:

$$\frac{E}{m} = \frac{r^2 - 2Mr \pm a\sqrt{Mr}}{r(r^2 - 3Mr \pm 2a\sqrt{Mr})^{\frac{1}{2}}} \quad (3.90)$$

where  $E = mu_0$ . The denominator gives the photon orbit  $r_{ph}$  if set to zero and its roots are found.

The circular motion is only possible for regions beyond the value  $r > r_{ph}$ . A deviation vector is introduced to determine the epicyclic motion:

$$\xi^\mu(s) = x^\mu(s) - z^\mu(s)$$

The geodesic equation is expanded in powers of  $\xi^\mu$  about the circular orbits. A linear approximation gives two decoupled oscillations in the radial and vertical directions.

The frequencies of the oscillations are:

$$\Omega_r^2 = \Omega_0^2 \left( 1 - \frac{6M}{r} - \frac{3a^2}{r^2} \pm 8a\Omega_s \right) \quad (3.91)$$

$$\Omega_\theta^2 = \Omega_0^2 \left( 1 + \frac{3a^2}{r^2} \mp 4a\Omega_s \right) \quad (3.92)$$

The condition for stability of circular motions against oscillations require that  $\Omega_r^2, \Omega_\theta^2 >$

0. The radii for the innermost stable circular orbit (ISCO) can be determined from this

condition.

The vertical oscillation is always non-negative in the region of existence and radial stability of the circular motion. The motion is stable with respect to the oscillations in the vertical direction.

The perturbations in the circular motion, as well as the circular motion itself, yields three frequencies:  $\Omega_0, \Omega_r, \Omega_\theta$ .

In Newtonian gravity, all three frequencies would be the same and equal to the Keplerian frequency,  $\Omega_K$ . In an Schwarzschild field, the vertical epicyclic frequency and the orbital frequency would be equal to the Keplerian frequency while the radial epicyclic frequency would not be. The Kerr field with strong rotational dynamics skews the frequencies from the standard Newtonian and Schwarzschild expressions. The scale at which the Kerr metric affects the frequencies is important for understanding the astrophysical significance of the phenomena in question.

The characteristic frequency scale is:

$$\Omega \rightarrow \nu_l = \frac{c^3}{2\pi GM} = \frac{1}{\pi} \left( \frac{c^2}{2GM} \right) * c = \frac{1}{\pi} \frac{c}{r_s} \quad (3.93)$$

$$\cong 3.2 \times 10^4 \left( \frac{M}{M_\odot} \right)^{-1} \text{ Hz} \quad (3.94)$$

Using the orbital angular velocity expression, the orbital frequency around a maximally rotating black hole is:

$$\nu_0 = \frac{1}{2} \nu_l \cong 1.6 \times 10^4 \left( \frac{M}{M_\odot} \right)^{-1} \text{ Hz, at the direct ISCO} \quad (3.95)$$

$$\nu_0 = \frac{1}{26} \nu_l \cong 1.2 \times 10^3 \left( \frac{M}{M_\odot} \right)^{-1} \text{ Hz, at the retrograde ISCO} \quad (3.96)$$



As the value of  $a$  (angular momentum parameter per unit mass) increases, the ISCO radius moves towards the black hole horizon and the corresponding orbital frequency increases and approaches a maximum value. The vertical epicyclic frequency reaches its maximum then declines in value where  $\nu_\theta = 0$  at  $r = M$ , for  $a = M$ .

Both frequencies decrease with increasing values of  $a$  for the retrograde ISCO radius and their ratio lingers about unity. For particular orbits near the black hole horizon, the predicted values of the epicyclic frequencies are close to the detected frequencies for the twin peak QPOs, in a 3:2 ratio for some black hole binaries (J1550-564, H1743-322, and GRS1915+105, for example, with corresponding frequency pairs of 184, 276 Hz, 165, 241 Hz, and 113, 168 Hz, respectively). The highest epicyclic frequencies of small oscillations are found about circular orbits in the Kerr field. The highest epicyclic frequencies can be found for specific values of the direct and the retrograde ISCO radii.

Taking the first derivative of the expression with respect to  $r$ , we get:

$$r^3(8M - r) + a^2(5r - 4Mr) \pm 2a\sqrt{Mr} (a^2 + r(M - 6r)) = 0 \quad (3.97)$$

This gives the radii for the highest epicyclic frequencies.

$$\text{At } a = 0, r_{max} = 8M, \text{ and } \nu_{r_{MAX}} \approx 707.1 \left(\frac{M}{M_\odot}\right)^{-1} \text{ Hz} \quad (3.98)$$

For non-zero values of  $a$ , the equation has to be solved numerically to find the radii.

At  $a = M$ , for the direct orbit,  $r_{max} \approx 2.4 M$ ,

$$\nu_{r_{MAX}} \approx 2453 \left(\frac{M}{M_\odot}\right)^{-1} \text{ Hz} \quad (3.99)$$

At  $a = M$  for the retrograde orbit,  $r_{max} \approx 11.8 M$ ,

$$\nu_{r_{MAX}} \approx 422.6 \left( \frac{M}{M_{\odot}} \right)^{-1} \text{ Hz} \quad (3.100)$$

At the characteristic ISCO radii, when the radial epicyclic frequency reaches its highest value, the ratio of the frequencies  $\frac{\nu_{\theta}}{\nu_r} = 2:1$  remains the same even as  $a$  approaches the maximal value of  $M$ . This matches observed twin QPO frequencies in the X-ray spectrum of black hole binaries. For example, GRS1915+105 exhibited a pair of QPOs that fall in the expected range of epicyclic frequencies (164, 328 Hz) for a black hole of spin  $a \sim 0.8-0.9 M$ .

The frequencies show consistent ratios of  $\frac{\nu_{\theta}}{\nu_{r_{MAX}}} = 2 : 1$ ,  $\frac{\nu_0}{\nu_{r_{MAX}}} = 2 : 1$ , and  $\frac{\nu_0}{\nu_{\theta}} = 1 : 1$ .

Going back to the vertical epicyclic frequency, the expression also gives the highest values for high  $a$ . The maxima of the following equation give the characteristic orbital radii that yield the highest vertical epicyclic frequency:

$$r(r^3 + a^2(5r - 2M)) + 2a\sqrt{Mr}(a^2 - 3r^2) = 0 \quad (3.101)$$

This also is to be solved numerically as well.

For  $a = M$ ,  $r_{max} \approx 1.86 M$  and the highest vertical epicyclic frequency is:

$$\nu_{\theta_{MAX}} \approx 4875 \left( \frac{M}{M_{\odot}} \right)^{-1} \text{ Hz} \quad (3.102)$$

$$\nu_{r_{MAX}} \approx 2236 \left( \frac{M}{M_{\odot}} \right)^{-1} \text{ Hz} \quad \text{at the same radius} \quad (3.103)$$

The ratio of the two frequencies is  $2 : 1$  as well.

## Frequencies and Radii Relevant to the QPO Models

I return to the QPO models and now start referring to the specific radii associated with the disk in terms of the Kerr metric, so they will have a physical context. The plasma in the disk at specific radii will have Keplerian frequencies associated with their motion or orbits. The QPO frequencies can be taken as being associated with an interaction at a radius. For example, a particle moving in circular motion, under the influence of gravity in the equatorial plane of a spinning object, is perturbed from its original path. It will then have an orbital frequency, a radial epicyclic frequency (frequency to go through a full cycle in radial motion), and a vertical epicyclic frequency (frequency to go through a full cycle in latitudinal motion).

To use an analogy, the radial motion of a particle would be akin to a snake weaving side to side on the equatorial plane, and the vertical motion would be comparable to a dolphin weaving up and down through the equatorial plane.

In the case of Newtonian gravity, these frequencies are degenerate but due to the deviation from the  $1/r^2$  power law and frame dragging, the frequencies separate in close proximity to the rotating compact object. For a black hole, the general relativistic modification requires invoking Kerr space-time geometry. The Keplerian frequency is the largest of the three frequencies in play and at the ISCO in general-relativistic geometry,

$$\nu_K = 2200 \text{ Hz} \left( \frac{M_\odot}{M} \right) \text{ for } j \ll 1 \quad (3.104)$$

Where the dimensionless angular momentum parameter is  $j = (a/M)^{1/2}$ . These formulae are exact for black holes in Schwarzschild geometry but at order  $j^2$  veers towards Kerr geometry for a rotating black hole (Hartle J. a., 1968). The radial epicyclic frequency vanishes at the ISCO so

it is surmised that there must be no restoring acceleration at that radius if the particle moves past that radius. It should be noted that the quality factor also drops off sharply at that point, indicating the QPO can only occur at the ISCO as a minimally possible radius.

There is no established exact source of the QPO phenomenon, but the source most focused on in accretion disk phenomena is the disk due to its size and established anatomy, particularly the event horizon and the ISCO and orbital radii beyond, where the Keplerian orbital motion at any and all radii and oscillation modes produce a range of variable frequencies. Structures such as the corona, magnetosphere, compact object/disk boundary, or jets can serve to contribute to frequency variables as well. It is orbital motion, particularly general-relativistic epicyclic motions and disk oscillations that are invoked in most cases for QPO phenomenon studies.

Free-particle orbits around a spherically symmetric massive object are closed in Newtonian space-time and have a Keplerian frequency in Kerr metric and physical terms:

$$\nu_k = \sqrt{\frac{GM}{r^3}} * \frac{1}{2\pi} \approx 1184 \text{ Hz} \left(\frac{r}{\text{km}}\right)^{-\frac{3}{2}} m_{1.4}^{\frac{1}{2}} \quad (3.105a)$$

$$\approx 184 \text{ Hz} \left(\frac{r}{100 \text{ km}}\right)^{-\frac{3}{2}} m_{10}^{\frac{1}{2}} \quad (3.105b)$$

where  $m_{1.4}$  and  $m_{10}$  are the compact object's mass in solar mass units of 1.4 and 10  $\left(\frac{M}{M_{\odot}}\right)$ , respectively and  $r$  is the orbital radius in km.

In General Relativity, the orbits are not closed and a precession effect emerges that leads to overlapping open orbits of the falling particles. The azimuthal, radial, and vertical motion

veers from the Newtonian motion (Merloni, 1999). As a result, eccentric orbits veer about the periastron precession frequency,  $\nu_{peri}$ , and the orbits tilted relative to the equatorial plane of the spinning compact object wobble at the nodal precession frequency,  $\nu_{peri} = \nu_{\phi} - \nu_r$ .

General Relativity predicts for a region beyond a particular radius, no stable orbital motion is possible so Newtonian expressions are only viable beyond that radius towards infinity. This radius is the ISCO (Bardeen, 1972). Inside this radius is the plunging region. An precession effect occurs with particles' orbits that lead to increased collisions and further dissipation of their angular momentum that result in a free-fall towards the compact object.

The equation that determines the ISCO radius comes from the condition,  $r^2 - 6 r_g r + 8r_g^2 r^{\frac{3}{2}} - 3 r_g^2 \geq 0$  (Bardeen, 1972), for stable orbits and can be solved analytically for the values of  $a = 0$ , and  $a = M$ .

(3.106)

For the values in between, the marginally stable circular radius has to be determined numerically. For Schwarzschild geometry ( $a = 0$ ),  $r_{ms}$  (ISCO) is:

$$r_{ms} = 6 r_g = \frac{6GM}{c^2} \approx 12.5 km * m_{1.4} \approx 8.9 m_{10} km, \quad (3.107)$$

and the (highest stable) orbital frequency is:

$$\nu_{ms} = \frac{c^3}{2\pi 6^{\frac{3}{2}} GM} \approx \frac{1156}{m_{1.4}} Hz \approx \frac{219}{m_{10}} Hz \quad (3.108)$$

For prograde orbital motion in the equatorial plane due to the Kerr geometry, the ISCO is:

$$\text{for } j \rightarrow 1, r_{ms} \rightarrow r_g = \frac{GM}{c^2} \quad \text{and} \quad \nu_{ms} = \frac{c^3}{4\pi GM} \approx \frac{1611}{m_{10}} Hz \quad (3.109)$$

The corresponding frequency also increases with the value of  $j$ , and the orbital frequency can be used to infer the compact object's spin (Sunyaev, 1973).

To first order in  $j$  (Kluźniak W. M., 1990) (Miller M. L., 1998) (Miller M. L., 1998),

$$r_{ms} = \left( \frac{6GM}{c^2} \right) (1 - 0.54 j) \quad (3.110)$$

$$v_{ms} = \left( \frac{c^3}{2\pi 6^{\frac{3}{2}} GM} \right) (1 + 0.75 j) \quad (3.111)$$

Disk flows can penetrate further than the ISCO, provided they do not surpass the marginally bound orbit radius  $r_{mb} = r_g(2 - j) + 2 r_g (1 - j)^{1/2}$ , which is inside the ISCO, before the plasma plunges through the event horizon (Abramowicz M. K., 2004).

(3.112)

A Schwarzschild metric describes the space-time outside a spherically symmetric stationary star. The Kerr metric describes the space-time outside a spinning star to first order in  $j$ , and the precise frequencies, depending on the distribution of mass (Hartle J. T., 1968) (Miller M. L., 1998) (Shibata, 1998) (Morsink, 1999) (Markovic) (Sibgatullin, 2002) (Abramowicz M. A., 2002).

Periastron and nodal precession are prograde since  $v_r$  and  $v_\theta < v_\phi$ . Periastron precession is due to the non- $1/r^2$  nature of gravity as defined by General Relativity.

Nodal precession is due to the frame dragging or Lense-Thirring precession (Lense, 1918) caused by the compact object's spin. In the case of a neutron star, a frequency  $v_\phi$  for stable orbital motion constrains its mass and its radius (Miller M. L., 1998), in which  $R$  must be smaller than the orbital radius  $r$  and the ISCO has to be less than  $r$  for Keplerian orbits. This ( $R < r$ ) condition leads to the frequency  $v_\phi$  putting a mass-dependent upper limit on  $R$  and the ISCO condition puts a upper limit on the neutron star's mass,

$$\frac{6GM}{c^2} < \left( \frac{GM}{4\pi^2 v^2} \right)^{\frac{1}{3}} \rightarrow M < \frac{c^3}{2\pi 6^{\frac{2}{3}} G v} \quad (3.113)$$

Confirmation through detection of the ISCO would serve as proof of strong-field general-relativistic effects and prove the compact object is smaller than the ISCO (Kluźniak W. W., 1985) (Paczynski, 1987) (Biehle, 1993). When the accretion disk inner edge reaches the ISCO, the QPO frequency would reach an upper limit while the accretion rate  $\dot{M}$  increases (Miller M. L., 1998).

### The Gravitational Potential of a Kerr Black Hole

The Paczynski-Witta pseudo-Newtonian potential for a black hole is written as:

$$\Phi = \frac{GM}{r-r_G} \quad r_G = \frac{2GM}{c^2} \quad (3.114a,b)$$

This pseudo-Newtonian potential is usually invoked in a number of astrophysical models for simplification purposes and approximates the gravity of a compact object in simulations.

But a more appropriate expression for a pseudo-Newtonian potential for a Kerr black hole or neutron star would be:

$$\Phi = \frac{GM}{r-r_H} \quad r_H = M + \sqrt{M^2 - a^2} \quad (3.115a,b)$$

$$\Phi = \frac{GM}{r\left(1-\frac{r_H}{r}\right)} = \frac{GM}{r\left(1-\frac{1}{r}\left(\frac{G}{c^2}\right)[M+\sqrt{M^2-a^2}]\right)} = \frac{GM}{r\left(1-\frac{r_G}{2r}\left(1+\sqrt{1-\left(\frac{a}{M}\right)^2}\right)\right)} \quad (3.116)$$

When  $a = 0$ , it reverts to the same expression for the Paczynski-Witta potential.

$$\Phi = \frac{GM}{r\left(1 - \frac{1}{r}\left(\frac{2GM}{c^2}\right)\right)} = \frac{GM}{r\left(1 - \frac{r_g}{r}\right)} \quad (3.117)$$

This would be an appropriate expression for cases of significant compact object spin for astrophysical settings.

The Paczynski-Witta potential can be derived in steps. First, beginning in Newtonian theory, with the parameters  $E$  for energy and  $L$  for angular momentum,  $\Phi(r)$  for the gravitational potential, and  $V$  for the radial velocity. The orbital motion is described in terms of the effective potential:

$$U(r, L) = \Phi(r) + \frac{L^2}{2r^2} \quad (3.118)$$

$$\frac{1}{2}V^2 = E - U(r, L) \quad (3.119)$$

Circular orbits' locations are determined by the extrema of the potential as stated by equation (3.110):

$$\left(\frac{dU}{dr}\right)_L = 0 \quad (3.120)$$

or to restate it in terms of the effective potential;

$$\left(\frac{d\Phi}{dr}\right) - L^2 \left(\frac{1}{r^3}\right) = 0 \quad (3.121)$$

The particles are moving in circular orbits confined to the equatorial plane ( $\theta = \frac{\pi}{2}$ ) in Schwarzschild space-time, and I can construct a positive small quantity from the radial component of the four-velocity  $u^r$ ,

$$V^2 = (u^r)^2 g^{rr} \ll 1 \quad (3.122)$$



Since  $u_\phi$  and  $u_t$  are constants of the motion, the angular momentum of the particle,  $L$ , becomes:

$$L = -\frac{u_\phi}{u_t}; \quad (3.123)$$

Which is also a constant of the motion. The condition  $1 = u_i u_k g^{ik} = (u_t)^2 g^{tt} + (u_\phi)^2 g^{\phi\phi} + (u_r)^2 g^{rr}$  can be restated as:

$$\frac{1}{2} \ln[1 + V^2] = \ln u^t + \frac{1}{2} \ln[g^{tt} + L^2 g^{\phi\phi}] \quad (3.125)$$

The left hand side of the equation can be expanded to give the result of  $\frac{1}{2} V^2$ , and setting the definition of  $E = \ln u_t$ , the effective potential becomes:

$$U(r, L) = -\frac{1}{2} \ln[g^{tt} + L^2 g^{\phi\phi}]; \quad (3.126)$$

The condition is restated in a form that mirrors that of the Newtonian formula. The Newtonian condition for the vanishing derivative of the effective potential can be applied to the relativistic effective potential:

$$\left(\frac{dg^{tt}}{dr}\right) + L^2 \left(\frac{\partial g^{\phi\phi}}{\partial r}\right) = 0 \quad (3.127)$$

On the equatorial plane,  $g^{\phi\phi} = -\frac{1}{r^2}$ ,  $g^{tt} = \frac{r}{r-r_G}$ , or  $g^{tt} = \frac{r}{r-r_H}$ , for a rotating black hole.

$$(3.128a,b,c)$$

The equation becomes:

$$\frac{d}{dr} \left(-\frac{GM}{r-r_G}\right) - L^2 \left(\frac{1}{r^3}\right) = 0 \quad \frac{d}{dr} \left(-\frac{GM}{r-r_H}\right) - L^2 \left(\frac{1}{r^3}\right) = 0 \quad (3.129a,b)$$

Comparing Newton's and Einstein's equations, the gravitational potential should have the same Paczynski-Witta form.

To derive the previous equation, the following relation is invoked:

$$g^{tt} = \frac{r}{r-r_G} = \frac{r_G}{r-r_G} + 1 = 2\Phi(r) + 1 \quad (3.130a)$$

$$g^{tt} = \frac{r}{r-r_H} = \frac{r_H}{r-r_H} + 1 = 2\Phi(r) + 1 \quad (3.130b)$$

The Keplerian angular momentum in Schwarzschild space-time, or Kerr space-time, can be derived, along with the Paczynski-Witta potential with the same formula:

$$L_K^2 = \frac{GMr^3}{(r-r_G)^2} \quad \text{or for a rotating black hole,} \quad L_K^2 = \frac{GMr^3}{(r-r_H)^2} \quad (3.131a,b)$$

The Newtonian angular momentum is expressed as:  $L = r^2\Omega$  (3.132)

But the Schwarzschild angular momentum is expressed as:  $L = \frac{r^2\Omega}{1-\frac{r_G}{r}}$  (3.133)

And the Kerr analog of the angular momentum would be:  $L = \frac{r^2\Omega}{1-\frac{r_H}{r}}$  (3.134)

The Keplerian angular velocity as calculated in Schwarzschild geometry and in the Paczynski-Witta potential are not equal:

$$\Omega_{SCH} = \left(\frac{GM}{r^3}\right)^{\frac{1}{2}} \quad \Omega_{PW} = \left(\frac{GM}{r^3}\right)^{\frac{1}{2}} \left(\frac{r}{(r-r_G)}\right) \quad (3.135a,b)$$

The Keplerian angular velocity for Kerr space-time would be:

$$\Omega_{KERR} = \left(\frac{GM}{r^3}\right)^{\frac{1}{2}} \left(\frac{r}{(r-r_H)}\right) \quad (3.136)$$

The distinction between a Schwarzschild event horizon and a Kerr event horizon is that the angular momentum of the black hole acts as a disguising factor that obscures the contribution of the mass to the size of the event horizon. A black hole with a high spin would cause the event horizon to shrink inward as well as the ISCO, causing those dimensions to be commensurate to that of a smaller stationary black hole.

To use an analogy, if I was a black hole and I started spinning, I would appear to become smaller, due to the bending of light around me caused by the warping of space-time around me. As I hit the maximal rate of spin, I would appear to be approximately twice as thin as I was before, or appear to have just half of the mass I had when I was not spinning (in the Schwarzschild case).

In nature, most if not all black holes will have some degree of spin so the Schwarzschild metric will have a limited degree of accuracy in describing the geometry and scale of the space-time metric in its proximity.

There could be a way to constrain the ratio of spin over mass, and together with a high resolution observation of the event horizon with a large telescope and using the equation (3.317):

$$r_H = M + \sqrt{M^2 - a^2}; \quad (3.137)$$

The dimensionless ratio of  $a$  to  $M$  can be determined by comparing the measurement of the event horizon to the ISCO, which can be determined by finding where the drop-off in the quality factor is in radial terms from the center of the accretion disk. For example, the ratio of the ISCO radius to the event horizon (Figure 3) for zero spin is  $6 r_S$  to  $2 r_S$ , or 3 to 1. For

maximal spin, the ratio of  $r_{ms}$  (or ISCO), to  $r_H$  is  $1 r_S$  to  $1 r_S$ , or 1 to 1.

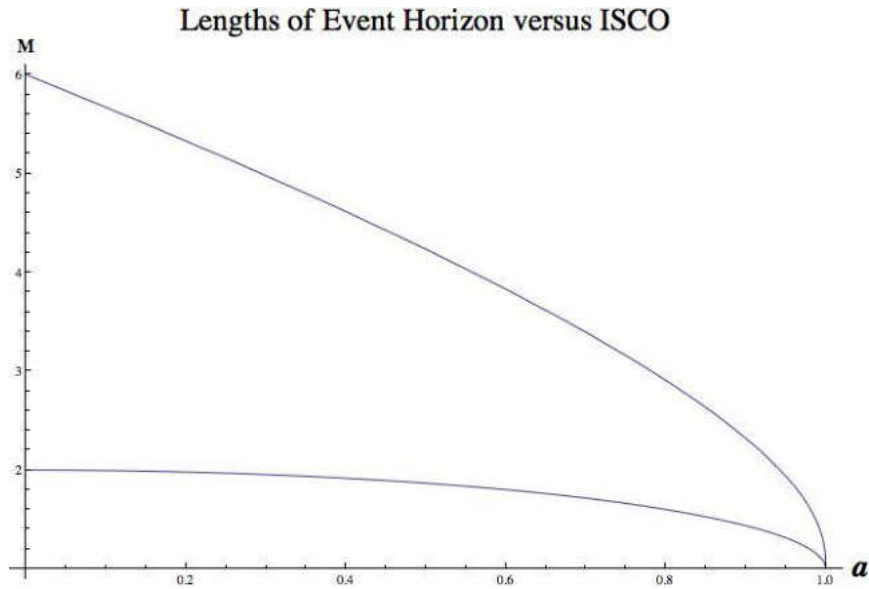


Figure 4. The Length of the Event Horizon versus the ISCO in terms of geometricized mass versus angular momentum parameter  $a$ .

As depicted in Figure 4, in the Schwarzschild metric, the ISCO is approximately 3 times the length of the event horizon, projected out from the center of the black hole. In the Kerr metric, spin modifies the metric such that the radius of the event horizon and the marginally stable circular orbit simultaneously shrinks in length until they both reach the same radius at maximal spin.

Establishing the location of the ISCO and then measuring the width of the event horizon observationally can give the precise ratio of the angular momentum parameter,  $a$ , to  $M$ . This method would be the best way to determine the dimensionless ratio  $a^*$  (or  $j$ ) of the angular momentum parameter  $a$  to the mass  $M$ . Determining the drop-off in the quality factor gives the location of the ISCO, and then locating the event horizon with a telescope with a large enough

resolution, would accomplish this.

One such telescope project, EHT, would take on such an approach using a collection of telescopes to take observations of a galaxy with a black hole event horizon large enough to be measured at a distance (EventHorizonTelescope, 2014). It uses a VLBI (Very Long Baseline Interferometry) approach to effectively create an Earth-sized telescope to obtain a high enough resolution to resolve the size of a galaxy's black hole. That, combined with finding the ISCO, would give the ratio of the angular momentum and the mass of the black hole at the center of the galaxy being observed.

## CHAPTER IV

### Alfven Radii of Accretion Disks

I now start discussing the Alfven radius as determined by modelling an accretion disk's magnetic field. This can show how the magnetic field can affect the advection of gas within the inner disk. I will use it to explore how the magnetic field of the disk will have such an effect on the advection in the disk itself. The determination of the Alfven radius starts with finding the strength of a magnetic field due to a source. For example, a star will possess its own magnetic field, and depending on the nature of the star, the magnetic field will be sufficiently magnetic to deflect the infalling material. The strength of the magnetic field is proportional to  $1/r^3$ , so the field will increase rapidly for incoming plasma. When the magnetic energy density is comparable to the kinetic energy density:

$$u_K = \frac{1}{2} \rho v^2 \quad (4.1)$$

$$u_M = \frac{B^2}{8\pi} \quad (4.2)$$

The magnetic field will start channeling the matter towards the poles of the star. The location where this begins to happen is the Alfven radius,  $r_A$ , where this condition is satisfied:

$$\frac{1}{2} \rho v^2 = \frac{B^2}{8\pi} \quad (4.3)$$

For gases falling in from a large distance, the free-fall velocity is:  $v = \sqrt{\frac{2GM}{r}}$  (4.4)

The relation between density, velocity, and the mass accretion rate is:

$$\dot{M} = 4\pi r^2 \rho v = A * \rho v \quad (4.5)$$

The equation analogous to Kerr geometry for the mass conservation rate is (Sadowski, 2009):

$$\dot{M} = -2\pi \Sigma \Delta^{\frac{1}{2}} \frac{V}{\sqrt{1-V^2}} \quad (4.6)$$

where  $V$  is the gas radial infall velocity measured by an observer co-rotating with the fluid at

$$\text{fixed } r, \text{ and} \quad \Delta = r^2 - 2Mr + a^2 \quad \text{and} \quad \Sigma = r^2 + a^2 \cos^2 \theta \quad (4.7a,b)$$

The radial dependence of the magnetic dipole field strength is:

$$B(r) = B_s \left(\frac{R}{r}\right)^3 \quad (4.8)$$

where  $B_s$  is the surface value of the magnetic field. Inserting equations (4.5 and 4.8) into the energy density equation (4.3), I can derive:

$$r_A = \left(\frac{B_s^4 R^{12}}{2GM\dot{M}^2}\right)^{\frac{1}{7}} \quad (\text{for the disk}) \quad (4.9)$$

Putting in the Kerr geometry terms from equations (4.6, and 4.7a,b) gives us:

$$r_A = \left(\frac{B_s^4 R^{12}}{2GM \left(-2\pi \Sigma \Delta^{\frac{1}{2}} \frac{V}{\sqrt{1-V^2}}\right)^2}\right)^{\frac{1}{7}} \quad (4.10)$$

And taking, at the compact object radius,  $V = R_{BH} \Omega_{BH} = R_{BH} * \frac{a}{2MR_{BH}} = \frac{a}{2M}$

$$r_A = \left(\frac{B_s^4 R^{12}}{2GM \left(-2\pi \Sigma \Delta^{\frac{1}{2}} \frac{V}{\sqrt{1-V^2}}\right)^2}\right)^{\frac{1}{7}} = \left(\frac{B_s^4 R^{12}}{2GM \left(4\pi^2 \Sigma^2 \Delta \frac{V^2}{(1-V^2)}\right)}\right)^{\frac{1}{7}} \quad (4.11)$$

$$= \left( \frac{B_S^4 R^{12}}{2GM \left( 4\pi^2 \Sigma^2 (R^2 + 2MR + a^2) \frac{\left(\frac{a}{2M}\right)^2}{\left(1 - \left(\frac{a}{2M}\right)^2\right)} \right)} \right)^{\frac{1}{7}} \quad (4.12)$$

$$r_A = \left( \frac{B_S^4 R^{12} \left(1 - \frac{a^2}{4M^2}\right)}{2GM \left( 4\pi^2 \Sigma^2 (R^2 + 2MR + a^2) \left(\frac{a^2}{4M^2}\right) \right)} \right)^{\frac{1}{7}} \quad (4.13)$$

$$r_A = \left( \frac{B_S^4 R^{12} \left(1 - \frac{a^2}{4M^2}\right)}{2GM \left( 4\pi^2 \Sigma^2 R^2 \left(1 + \frac{2M}{R} + \frac{a^2}{R^2}\right) \left(\frac{a^2}{4M^2}\right) \right)} \right)^{\frac{1}{7}} \quad (4.14)$$

$$r_A = \left( \frac{B_S^4 R^{10} \left(1 - \frac{a^2}{4M^2}\right)}{2GM \left( 4\pi^2 \Sigma^2 \left(1 + \frac{2M}{R} + \frac{a^2}{R^2}\right) \left(\frac{a^2}{4M^2}\right) \right)} \right)^{\frac{1}{7}} \quad (3.15)$$

This gives the Alfvén radius generated by the Blandford-Znajek mechanism. There are two effective Alfvén radii in the accretion disk system; that of the disk, and that due to the spiraling magnetic field lines frozen into the flow within the black hole ergosphere, with an additional angular velocity imparted onto the plasma by the precession in Kerr space-time.

There are two competing magnetic fields within the accretion disk system as defined by the Blandford-Znajek mechanism. In most cases, the disk magnetic field is the overwhelming factor. In the case of extremely high black hole spin ( $a \rightarrow M$ ), the black hole magnetic field overwhelms that of the disk and its Alfvén radius extends farther out into the accretion disk system, exceeding even that of the Alfvén radius of the disk, and serves as the disruptive influence.



## **Blandford-Znajek Mechanism**

I utilize a toy model developed by Li-Xin Li to determine how the magnetic field of the accretion disk affects its own anatomy, particularly the advection of the infalling charged matter (Li, 2000). The toy model uses a Kerr black hole with a toroidal electric current set in a geometrically thin disk staged around the black hole. The toroidal electric current generates a poloidal magnetic field with its motion, with the field lines threading through the black hole and the disk.

The magnetic field interacts with the plasma and the rotation of the black hole and disk induces an electromotive force on the black hole's event horizon and disk. The EMF can be the source of power imparted onto astrophysical loads at a distance.

The rotation of the charged matter within the accretion disk and rotation of the black hole induces an electromotive force, which can be used to power an astrophysical load at a distance (Li, 2000).

The toy model explores a range of parameters relating to the rotation of the black hole and the distribution of electric current within the disk and determines the amount of power generated by the black hole and the disk and the ratio of the power to determine the dominant influence on the charged matter. It also determines the torque created by both sources.

Inside the disk, matter loses its angular momentum, and it drifts towards the compact object where it eventually will be gravitationally captured. The power is derived from the gravitational binding energy between the black hole and the disk as opposed to the rotational energy of the black hole itself.

The implications are that the Blandford-Znajek mechanism is not efficient in deriving

energy from the rotating black hole versus its disk. The Blandford-Znajek mechanism is a process of energy generation derived from a rotating black hole and was thought to be the source powering radio jets and researched as a source for GRBs (Gamma-ray bursts).

Blandford and Znajek developed the Blandford-Znajek mechanism in 1977. In their description, the black hole is neutral although it has a rotating accretion disk (Blandford, 1977). The distribution of mass rises in density near the event horizon and the mass will have become magnetized over time and be carrying magnetic field lines inward with it. As the black hole consumes the accretion disk, the field lines of the magnetic field will persist and linger, becoming threaded out through the horizon, essentially becoming frozen into the fluid. The frame of the magnetic field lines is dragged along with the rotating black hole. The rotating field lines will induce an electromotive force that serves to accelerate plasma towards relativistic speeds along the axis of rotation. The matter gets swept up in the magnetic field and spirals upwards towards the poles (Perepelitsa).

The rotation of the plasma caught inside the ergosphere (the ellipsoidal region between the outer event horizon and the static limit radius) forces the magnetic lines to rotate as well, and the magnetic twist propagates away from the black hole, culminating in a Poynting flux. A feedback action results, when the magnetic field forces plasma in orbits with negative mechanical energy at infinity before capture by the black hole. There is an outflux of mechanical energy yet the overall energy flux is conserved. The energy is converted from mechanical to purely electromagnetic at a distance. In this context, the ergospheric plasma and magnetic field take on roles of negative and positive energy particles in the Penrose process (Komissarov, 2009).

This process is favored as an explanation and studied for exploration of black hole phenomena, since relativistic Lorentz factors are required for jet emissions in AGNs and GRBs and provides a clean way of energy extraction.

Not much is known about the distribution or generation of the magnetic field inside the disk, the energy extracted from the black hole versus the disk or what comparable factor the black hole contributes to the overall system's extracted energy.

For a wide variety of parameters, the disk's power dominates that of the black hole's power. Only in cases of high black hole spin does the black hole's power start to dominate over that of the disk's power.

The model uses a physical coordinate system that utilizes the Kerr metric. The Kerr black hole has an accompanying thin disk in the equatorial plane endowed with a distribution of electric current. The Kerr black hole has mass  $M$ , angular momentum  $J = M*a$  (geometric units  $G, c$  set to one), and Boyer-Lindquist coordinates  $(t, r, \theta, \phi)$  for the black hole (Li, 2000).

The radius of the black hole's outer horizon is:

$$r_H = M + \sqrt{M^2 - a^2} \quad (4.16)$$

Angular velocity:

$$\Omega_H = \frac{a}{2Mr_H} \quad (4.17)$$

Keplerian angular velocity:

$$\Omega_K = \left(\frac{M}{R^3}\right)^{\frac{1}{2}} \frac{1}{1+a\left(\frac{M}{R^3}\right)^{\frac{1}{2}}} \quad (4.18)$$

The outer edge of the disk is set at  $r = r_b$ , and the inner edge of the disk is at the ISCO (Innermost Stable Circular Orbit, or “marginally stable” orbit) on the equatorial plane.

$$r_{ms} = M \left[ 3 + z_2 - ((3 - z_1)(3 + z_1 + 2z_2))^{\frac{1}{2}} \right] \quad (4.19)$$

$$z_1 = 1 + \left( 1 - \frac{a^2}{M^2} \right)^{\frac{1}{3}} \left[ \left( 1 + \frac{a}{M} \right)^{\frac{1}{3}} + \left( 1 - \frac{a}{M} \right)^{\frac{1}{3}} \right] \quad (4.20a)$$

$$z_2 = \left( \frac{3a^2}{M^2} + z_1^2 \right)^{\frac{1}{2}} \quad (4.20b)$$

The toroidal electric current within the disk has a surface density, distributed between  $r_{ms}$  and  $r_b$ . The magnetic field generated by the current at a fixed radius is determined by the following equations.

The toroidal component of the electromagnetic vector potential is signified by  $A_\phi$ . The magnetic flux through the surface of a bounded circular area with constant radius and constant angle  $\theta$  is represented by the following equation:

$$\psi(r, \theta) = 2\pi A_\phi(r, \theta) = 2\pi \int_{r_{ms}}^{r_b} J(r') (dA_\phi/dr') dr' \quad (4.21)$$

In which the circular area is multiplied by  $2\pi$  and rotated through all angles to give the volume. The limits of the radial component of the volume extend from  $r_{ms}$ , the innermost stable orbit in the equatorial plane, and the inner edge of the disk, to  $r_b$ , a particular selected radius encapsulating the magnetic field of the region of concern.

The magnetic flux potential inside the integral,  $\frac{dA_\phi}{dr'}$ , is given as an equation with a mix of sums of coefficients multiplied with coordinates and Legendre functions (Li, 2000):

$$\begin{aligned}
\frac{dA_\phi}{dr'} &= 2 \sum_{l=1} [\alpha_r^l (r * a \sin^2 \theta \left(\frac{\Delta}{\Sigma}\right) \frac{1}{(M^2 - a^2)^{\frac{1}{2}}} P_l'(u)P_l(\cos \theta) \\
&\quad - a \sin^2 \theta \cos \theta \frac{r^2 + a^2}{\Sigma} * P_l(u)P_l''(\cos \theta)] \\
+ 2 \sum_{l=1} [\alpha_i^l (-a^2 \sin^2 \theta \left(\frac{\Delta}{\Sigma}\right) \frac{1}{(M^2 - a^2)^{\frac{1}{2}}} P_l'(u)P_l(\cos \theta) - r \sin^2 \theta \cos \theta \frac{r^2 + a^2}{\Sigma} \\
&\quad * P_l(u)P_l'(\cos \theta) + \Delta \left(\frac{\sin^2 \theta}{l(l+1)}\right) \frac{1}{(M^2 - a^2)^{\frac{1}{2}}} P_l'(u)P_l''(\cos \theta)] \\
+ 2 \sum_{l=1} [\beta_r^l (r * a \sin^2 \theta \left(\frac{\Delta}{\Sigma}\right) \frac{1}{(M^2 - a^2)^{\frac{1}{2}}} Q_l'(u)P_l(\cos \theta) - a \sin^2 \theta \cos \theta \frac{r^2 + a^2}{\Sigma} \\
&\quad * Q_l(u)P_l''(\cos \theta)] \\
+ 2 \sum_{l=1} [\beta_i^l (-a^2 \sin^2 \theta \left(\frac{\Delta}{\Sigma}\right) \frac{1}{(M^2 - a^2)^{\frac{1}{2}}} Q_l'(u)P_l(\cos \theta) - \\
&\quad r \sin^2 \theta \cos \theta \frac{r^2 + a^2}{\Sigma} * Q_l(u)P_l'(\cos \theta) + \Delta \left(\frac{\sin^2 \theta}{l(l+1)}\right) \frac{1}{(M^2 - a^2)^{\frac{1}{2}}} Q_l'(u)P_l''(\cos \theta)]
\end{aligned} \tag{4.22}$$

The special variables in the equation above are signified as such:

$$\Delta = r^2 - 2Mr + a^2 \quad \Sigma = r^2 + a^2 \cos \theta \tag{4.23a,b}$$

$$A = (r^2 + a^2)^2 - \Delta a^2 \sin^2 \theta \quad u = (r-M)/(M^2 - a^2)^{1/2} \tag{4.23c,d}$$

and  $P_l(z)$  and  $Q_l(z)$  are Legendre functions, and  $P_l'(z) = \frac{dP_l(z)}{dz}$  and  $Q_l'(z) = \frac{dQ_l(z)}{dz}$ , and the

coefficients  $\alpha_r^l$ ,  $\alpha_i^l$ ,  $\beta_r^l$ ,  $\beta_i^l$  are given as:

$$\alpha_r^l = \frac{(2l+1)\pi}{l(l+1)(M^2 - a^2)} \left(\frac{\Sigma'}{A'}\right)^{\frac{1}{2}} \Delta' a P_l(0)Q_l'(u') \tag{4.24}$$

$$\alpha_i^l = \frac{(2l+1)\pi}{l(l+1)(M^2 - a^2)^{\frac{1}{2}}} \left(\frac{\Sigma'}{A'}\right)^{\frac{1}{2}} [-(r'^2 + a'^2)P_l(0)Q_l'(u') + \left(\frac{\frac{\Sigma'}{A'}}{r'^{l(l+1)}}\right) * \left(\frac{1}{(M^2 - a^2)^{\frac{1}{2}}}\right) P_l'(0)Q_l'(u')] \quad (4.25)$$

$$\beta_r^l = \frac{(2l+1)\pi}{l(l+1)(M^2 - a^2)} \left(\frac{\Sigma'}{A'}\right)^{\frac{1}{2}} \Delta' a P_l(0)Q_l'(u') \quad (4.26)$$

$$\beta_i^l = \frac{(2l+1)\pi}{l(l+1)(M^2 - a^2)^{\frac{1}{2}}} \left(\frac{\Sigma'}{A'}\right)^{\frac{1}{2}} [-(r'^2 + a'^2)P_l(0)P_l'(u') + \left(\frac{\frac{\Sigma'}{A'}}{r'^{l(l+1)}}\right) * \left(\frac{1}{(M^2 - a^2)^{\frac{1}{2}}}\right) P_l'(0)P_l'(u')] \quad (4.27)$$

The inset variables in the coefficients are specified as such:

$$\Delta' = \Delta(r = r') \quad \Sigma' = \Sigma(r = r', \theta = \pi/2) \quad A' = A(r = r', \theta = \pi/2) \quad (4.28a,b,c)$$

The Legendre polynomial expressions are composed of two components: one radial and one angular. The radial component is dependent on distance because it comprises of a broken power law function.

$$P_l(r) = A_l r^l + \left(\frac{B_l}{r^{l+1}}\right) \quad (4.29)$$

If the radius extends to infinity, the positive exponent variable will blow up towards infinity so  $A_l$  has to be set at zero to neutralize it. If the radius goes back to zero, the negative exponent variable will tend towards zero, which in its form, its value will tend towards infinity as well so  $B_l$  has to be set to zero. Either conditional case is dependent on where the radius is, so

the radius has to be defined so either case or coefficient can be preset as zero so the other part of the function can do its work.

Which is why if  $r > r'$  ( $r'$  being the critical distance),  $\alpha^r_l, \alpha^i_l = 0$  for all  $l$ , and  $\beta^r_l, \beta^i_l$  will retain their values.

If  $r < r'$ ,  $\beta^r_l, \beta^i_l = 0$  for all  $l$  and  $\alpha^r_l, \alpha^i_l$  will retain their values as well.

The normal component of the magnetic field in the disk is given in the equation:

$$B_D = \frac{1}{2\pi} \left( \frac{\Delta}{A} \right)_{\theta=\frac{\pi}{2}}^{\frac{1}{2}} \frac{d\psi(r_H, \frac{\pi}{2})}{dr} \quad (4.30)$$

The poloidal component of the magnetic field in the disk is given in the equation:

$$B_H = \frac{1}{2\pi (r_H^2 + a^2) \sin \theta} \frac{d\psi(r_H, \theta)}{d\theta} \quad (4.31)$$

As the disk rotates with the black hole, the magnetic field within interacts with charged particles and induces electromagnetic fields. The net EMF on the black hole is given by the equation:

$$\varepsilon_H = \frac{1}{2\pi} \Omega_H \psi(r_H) \quad (4.32)$$

The symbol  $\psi(r_H)$  signifies the magnetic flux through the northern hemisphere of the black hole's horizon, ( $\psi(r_H) = \psi(r_H, \pi/2)$ ).

I find that the magnetic field of the disk dominates over that of the black hole for the majority of values of the angular momentum parameter,  $a$ , until the magnetic field of the black hole due to the Blandford-Znajek mechanism dominates for sufficiently high enough spin. The magnetic field contributions would have a corresponding Alfven radius for each, where the

magnetic energy density becomes comparable to the kinetic energy density of the advecting plasma and begin to divert the plasma towards the poles. The Alfvén radius would be the magnetospheric radius and serve as a boundary for a transition layer where a major disruption in the advection would occur.

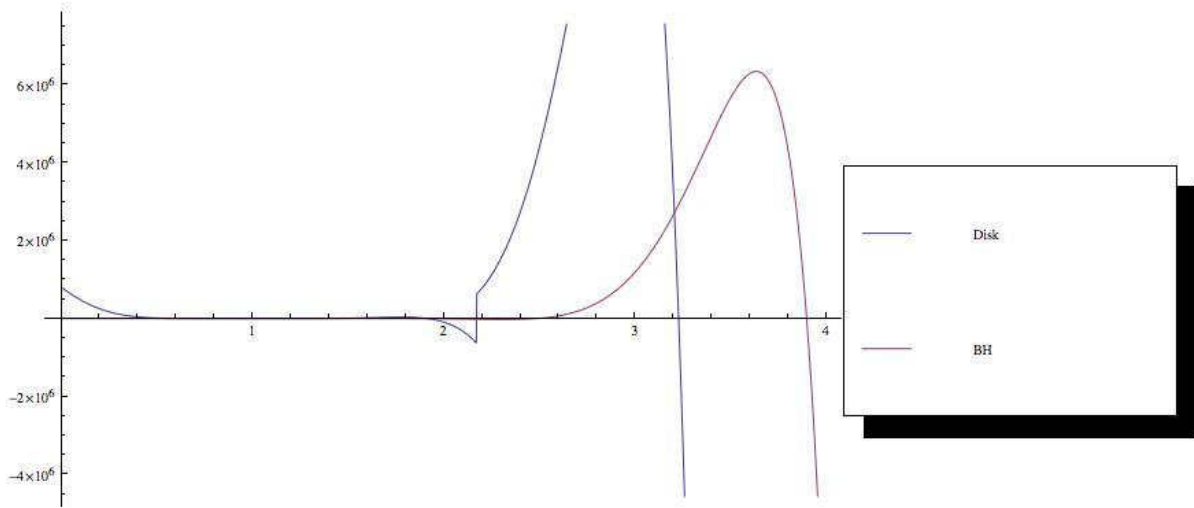


Figure 5. Comparison of the Magnetic Fields of the Black Hole and Disk.

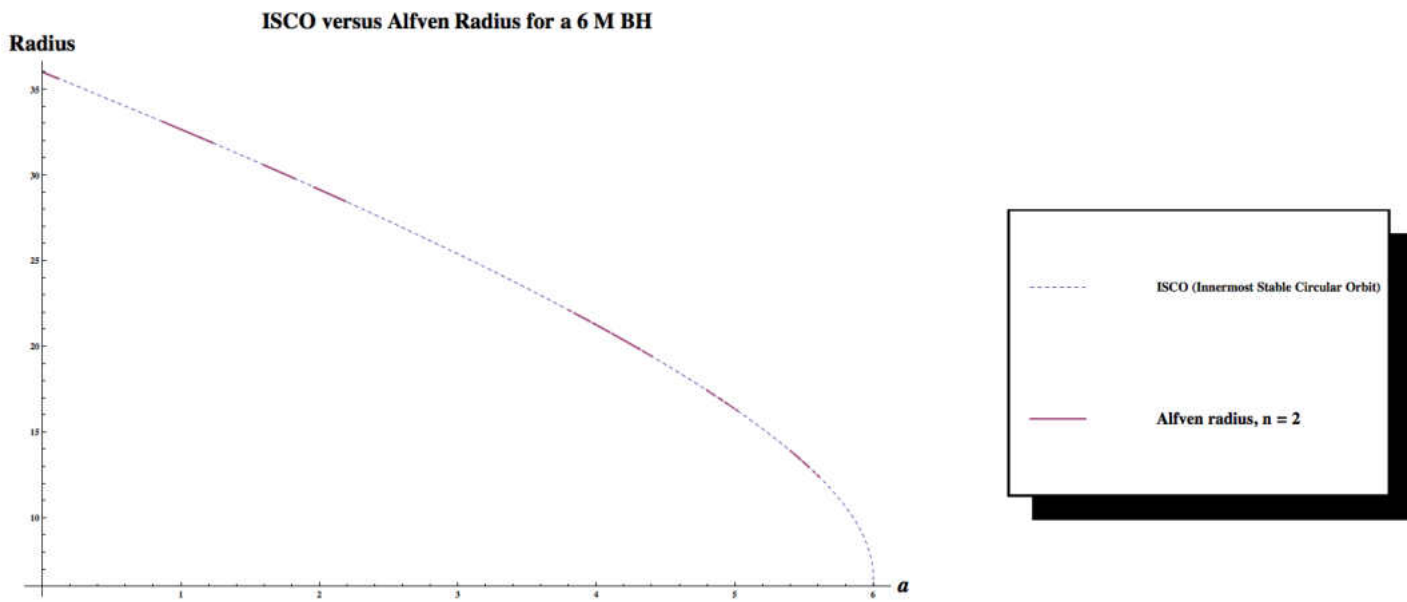


Figure 6. Alfvén Radius for  $n = 2$  versus ISCO for 6 M BH.



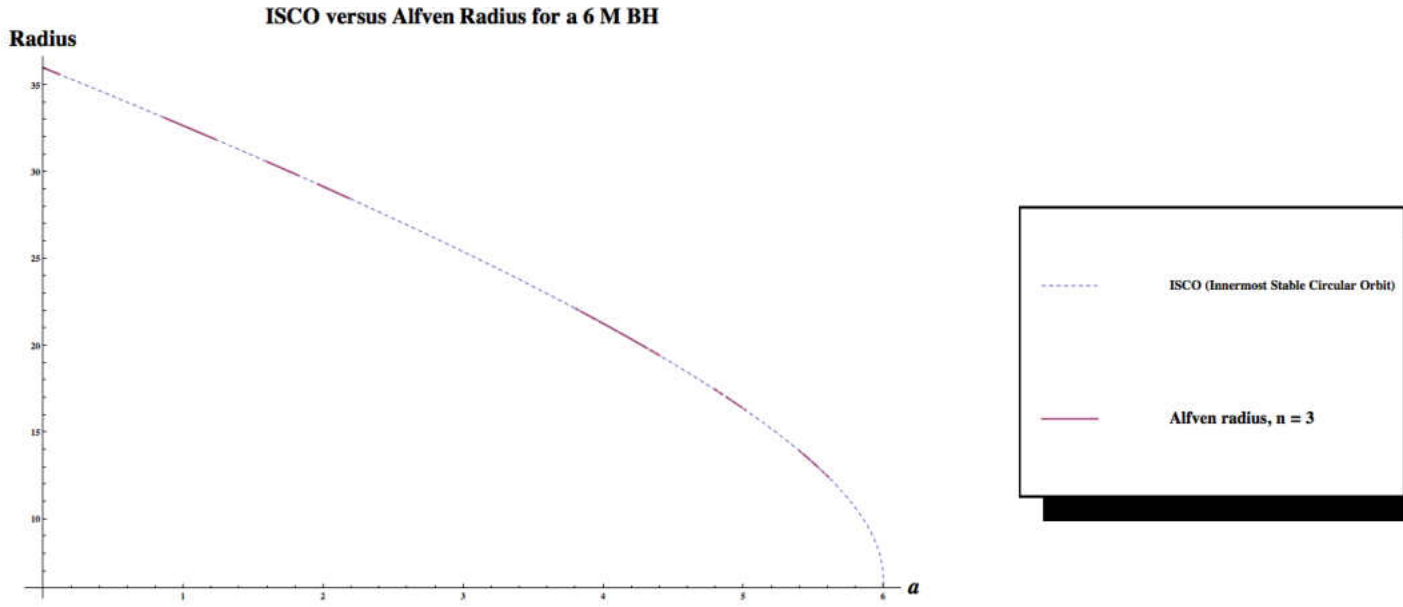


Figure 7. Alfven Radius for  $n = 3$  versus ISCO for 6 M BH.

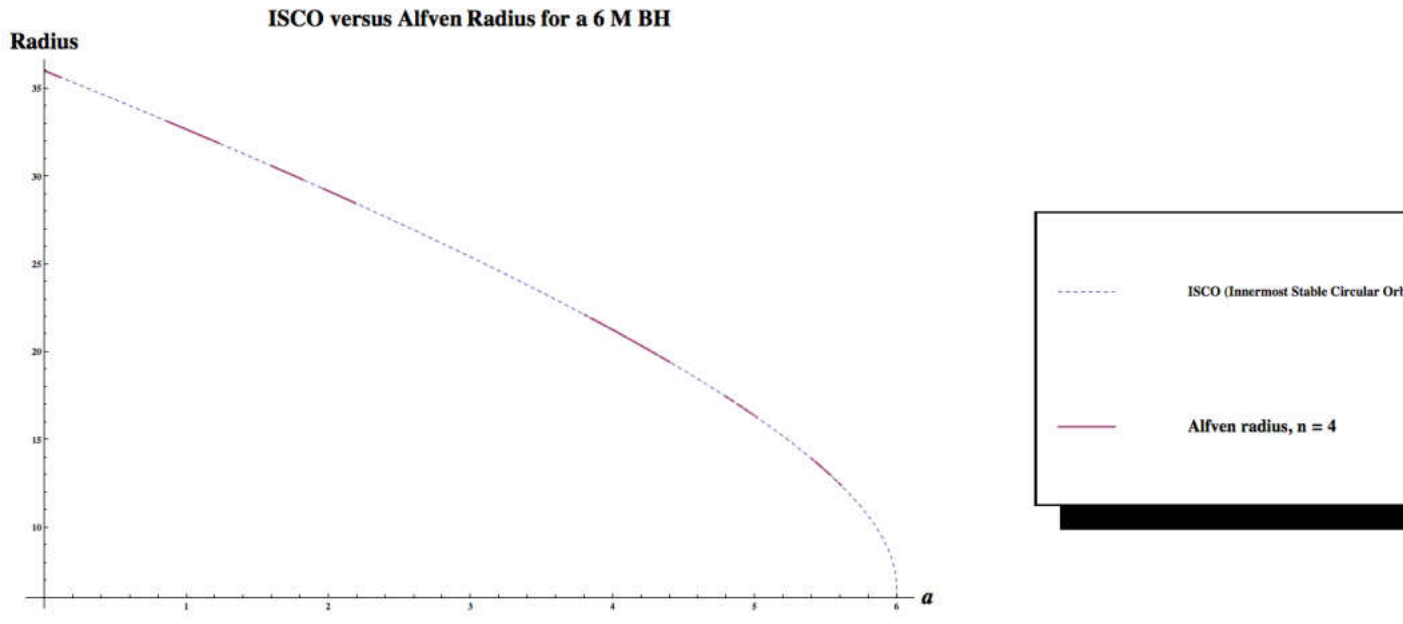


Figure 8. Alfven Radius for  $n = 4$  versus ISCO for 6 M BH.

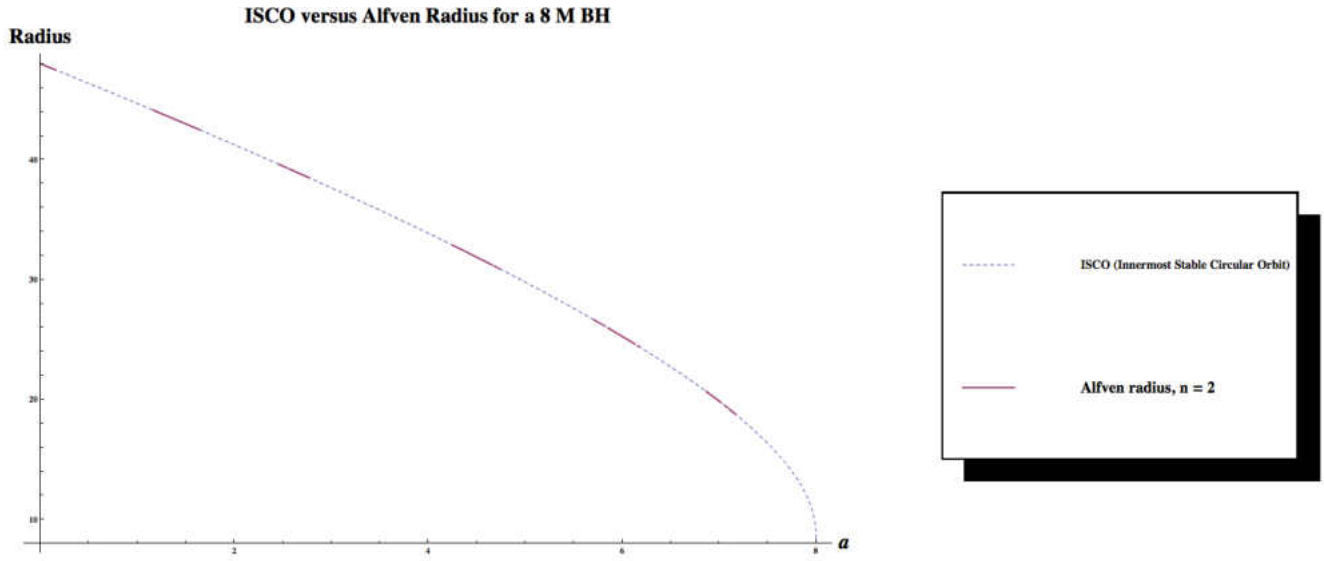


Figure 9. Alfvén Radius for  $n = 2$  versus ISCO for 8 M BH.

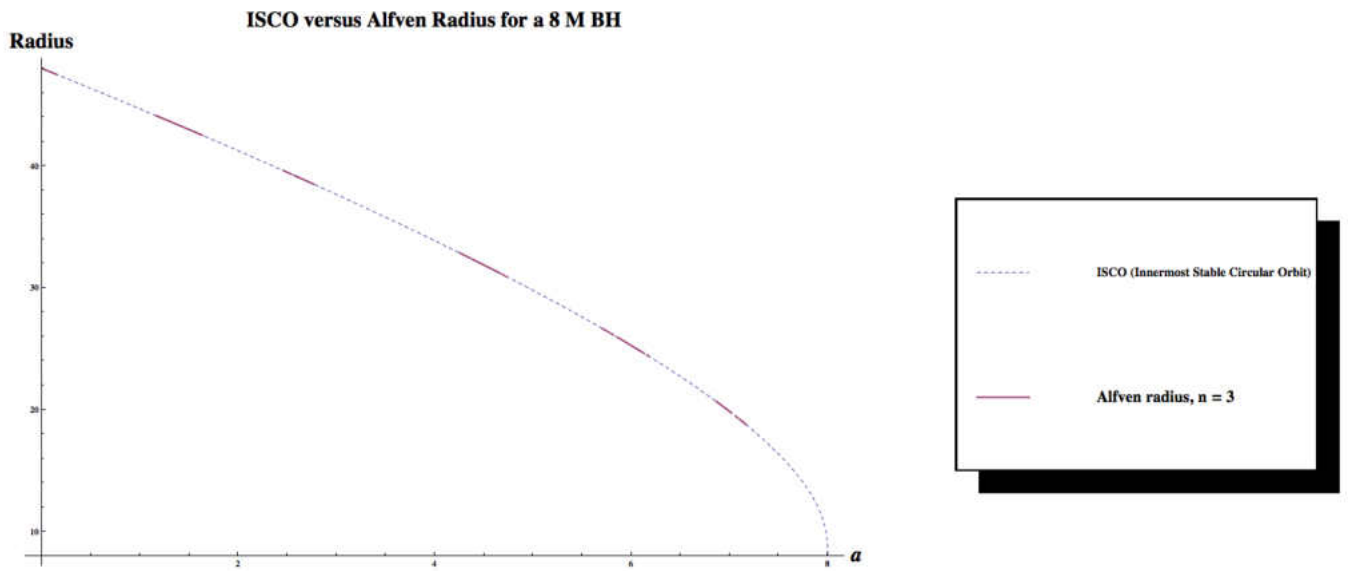


Figure 10. Alfvén Radius for  $n = 3$  versus ISCO for 8 M BH.

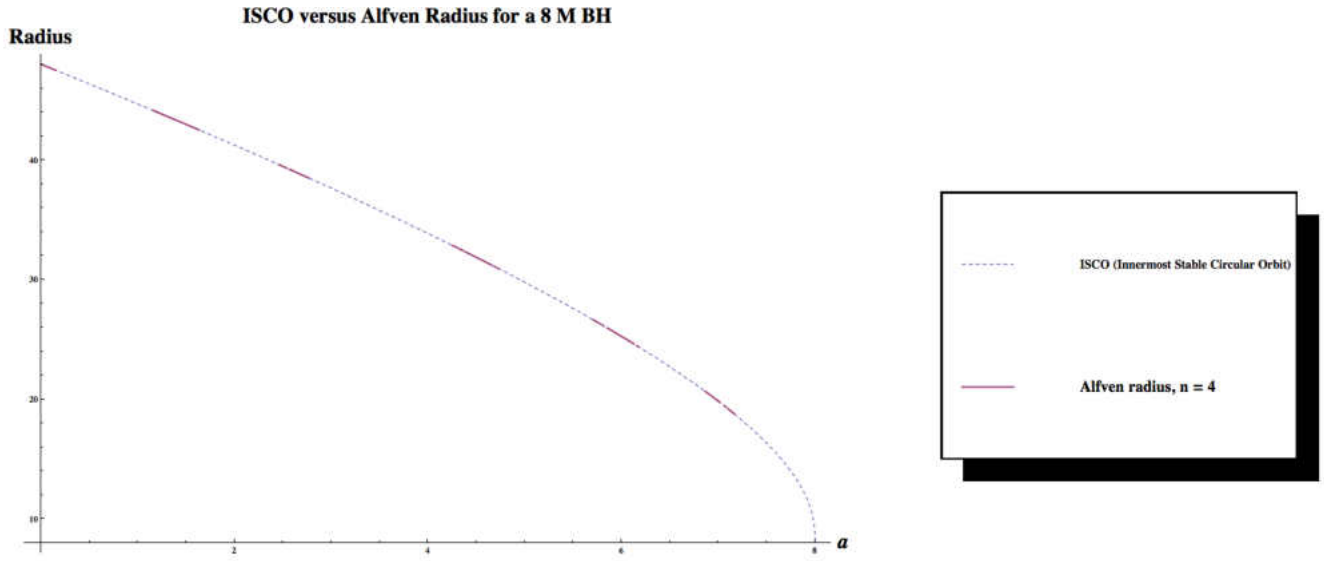


Figure 11. Alfvén Radius for  $n = 4$  versus ISCO for 8 M BH.

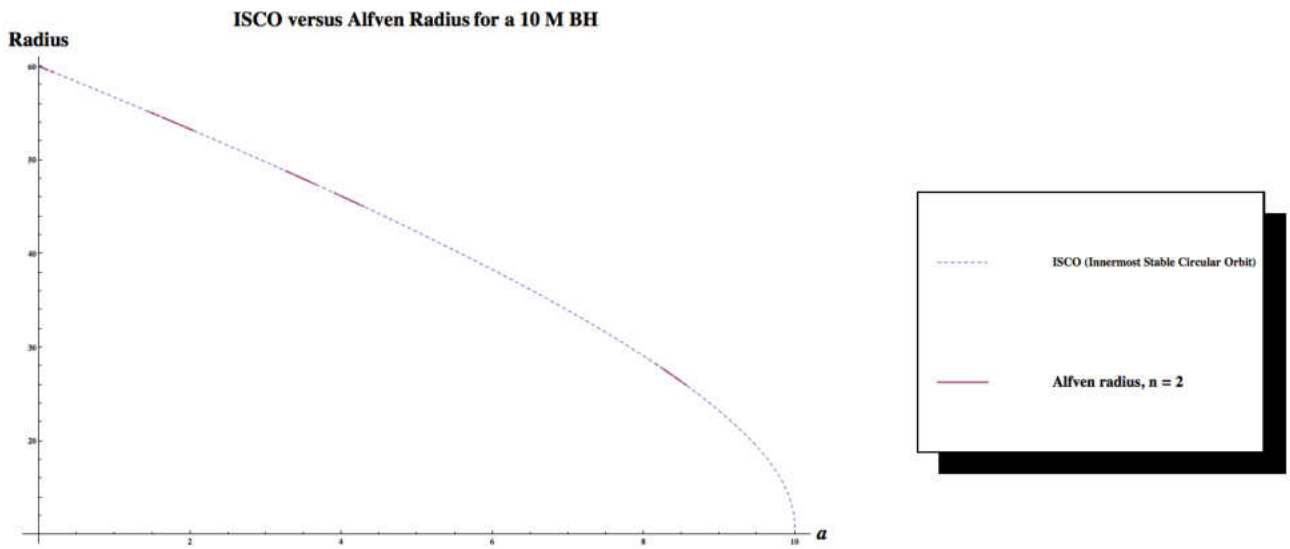


Figure 12. Alfvén Radius for  $n = 2$  versus ISCO for 10 M BH.

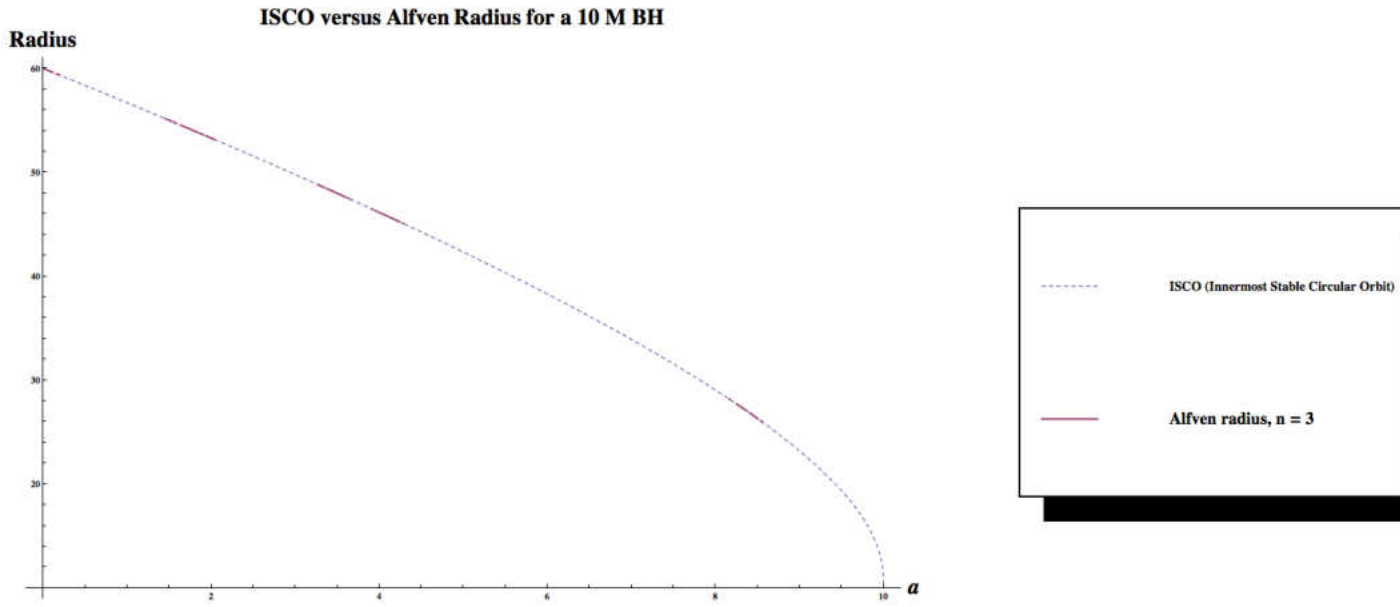


Figure 13. Alfvén Radius for  $n = 3$  versus ISCO for 10 M BH.

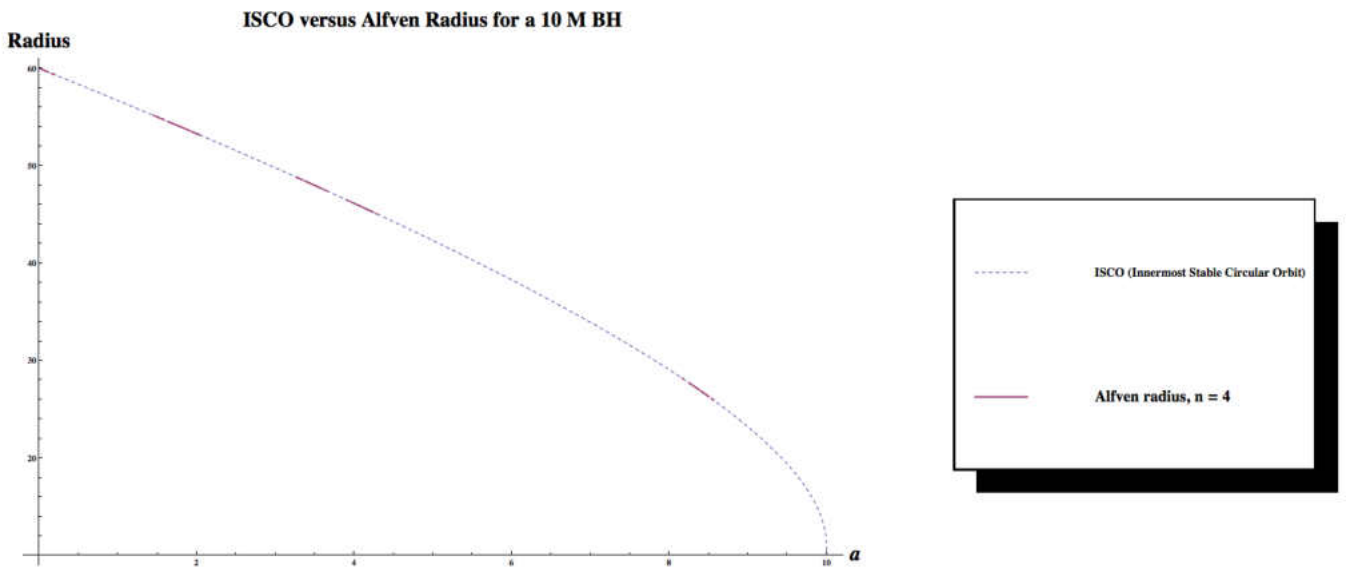


Figure 14. Alfvén Radius for  $n = 4$  versus ISCO for 10 M BH.

Using the toy model to determine the magnetic field strength and using it to determine the Alfvén radius, the plotted radius is projected from the inner edge into the disk. The ISCO is

plotted along with the Alfvén radius for a set of  $n$  values for the current distribution in the inner disk, with  $n = 2$  for a dipole configuration (Figures 6, 9, and 12),  $n = 3$  for a quadrupole configuration (Figures 7, 10, and 11), and  $n = 4$  for a multipole configuration (Figures 8, 11, and 14). A range of masses are plotted for each set of  $n$ , to see how the Alfvén radius varies as it follows from the parameters of the Li-Zin model. It coincides with the ISCO in every case including for each current distribution configuration.

The boundary layer radius is also plotted in each graph and shown in dashed lines. I determined the magnetic field by integrating the magnetic potential over a radial range, from the marginally stable circular orbit radius out to a pre-determined radius. I then determined the Alfvén radius using the value of the magnetic field, and projected outward from the ISCO, which is the inner disk edge. It is plotted as a thin line while the ISCO is plotted as a dashed line for each graph. In each graph, the dotted line and straight line overlap since they sit almost right on top of the other and the graphing function in Mathematica will show the dotted line where it overlaps the straight line by default as not to lose visual track of the data. I found that the magnetospheric radius does not extend very far out from the ISCO and influence the advection to a degree where the overall anatomy or rate of the accretion would be modified significantly. The marginally stable circular orbit is effectively the inner disk edge even when the strength of the disk magnetic field is taken in consideration in terms of a disruptive influence in the advection of the plasma.

## CHAPTER V

### GENERAL PRINCIPLES OF ACCRETION DISKS

I delve into the basic principles that govern accretion disks in this chapter. By understanding these basic principles, we can predict the intrinsic behavior of the gas in accretion disks and how they form and persist in nature. All accretion disk models can be described by these physical principles.

Accretion disks play a large role in the evolution of large-scale structures of stars, protoplanetary systems, and galaxies. Galaxies are the most extreme examples of accretion in which they have all kinds of stellar bodies orbiting around a supermassive black hole.

An accretion disk is an accumulation of matter captured by gravitational attraction and composed of gas and dust particles moving in an orbit around a central massive body. The central body is the origin of the gravitational field that captures the material and generally can be a star or degenerate object. The orbits of the material can be determined by the angular momentum of the material orbiting around the central object. The orbits can vary from the circular, to the elliptical, and in extremely rare cases, parabolic and hyperbolic. The force of gravity of the central object, which causes the infalling material with an angular (lateral) momentum sufficiently high enough to escape and overshoot the central body, and end up spiraling around the attractive central body as a consequence. When the material's angular momentum decrease due to dissipative processes, it will no longer be able to continually orbit the

central object and will spiral down into its gravitational well. In general relativistic terms, the central body curves space time to the point that all moving matter, in its inertial frame, is moving in a straight line, but due to the curvature induced by the massive body, the straight line is curved, to an outside observer, by the presence of gravity and the matter follows the modified path accordingly.

Gravity acts upon the accreting matter and causes it to collect into a quasi-stable disk and the accreting particles start to collide, which leads to collisional heating. In most cases the disk is opaque (optically thick) and thus emits blackbody radiation as a result. The blackbody spectrum is integrated over all radii for the accretion disk. In general, in a blackbody matter with a particular temperature will emit light corresponding to the Planck function, and in the case of accretion disks with massive central objects, the temperature will be approximately around 100,000 - 1,000,000 K. The blackbody spectrum peaks at a specific wavelength,  $\lambda_{Max}$ , which through Wien's law shortens with increased temperature of the matter (*Carroll B. W., An Introduction to Modern Astrophysics, 1996*). This is important here comes in the temperature of accretion disks can be related to the amount of material collected by the central object. With a high mass central object, the material accretion rate in the accretion disk will be higher and moving at higher speeds as well. The particle and gas collisions in the disk give rise to the state of the temperature of the disk, in this case the peak wavelength will fall in the x-ray spectrum.

The weaker the gravity within the accretion disk, the fewer collisions, the lower the temperature, and the redder the blackbody peak will be for the radiation emanating from the disk. Stars with lower masses attract less matter which result in smaller accretion disks. Those accretion disks will emit radiation in the infrared band of the electromagnetic spectrum. More massive stars with accompanying accretion disks will show disk emission at higher energies,

extending through visual and ultraviolet, and cumulating in the x-ray spectrum for the most powerful objects, namely neutron stars and black holes. For such a large accretion disk with a supermassive central body, the peak of the blackbody Planck function for electromagnetic radiation would fall in the x-ray spectrum.

For large accretion disks, the influx of falling and spiraling material means a large quantity of moving ionized particles, which in turn generates a moving magnetic field that migrates inward towards the black hole. The generated magnetic fields are, for the most extreme cases, extremely powerful and cause material to be swept up towards the magnetic poles along a line perpendicular to the accretion disk.

The jets, which I do not investigate in this dissertation, serve as a mechanism that serves to dissipate some angular momentum with a minimal loss of mass in the process. As the mass falls towards the black hole, the sharper gravitational gradient causes the material to collide in a Brownian manner, causing intense frictional heating as a result. The accretion disk closest to the event horizon of a black hole is heated enough to the point where x-rays are emitted from that region.

The high luminosity of galactical accretion disks is due to the influx of an extremely large quantity of gas accreted by their central bodies, the supermassive black holes.

The process of energy production is capable of converting approximately 10 percent of the infalling mass into energy. It also stands as one of the most efficient methods of energy production. Black hole accretion, in the case of quasars, is the most powerful and most efficient sustained energy source known in the universe. The black holes in the centers of galaxies are classified as “supermassive,” or, falling in the range of about  $\sim 10^6$  to  $\sim 10^9$  solar masses.



In closed binary systems, the primary star will be the more massive partner and start capturing mass from the secondary star, which would lead to the primary star evolving at an accelerated rate in contrast to the secondary star, and will become either a white dwarf, a neutron star (minimal mass of 1.44 solar masses or above), or a black hole (minimal mass of 3 solar masses or above), depending on its final mass (*Carroll B. W., An Introduction to Modern Astrophysics, 1996*). The secondary star will likely evolve into a red giant and expand beyond its original size and overflow its Roche lobe. At which point, the primary star will start gravitationally capturing the secondary star's mass and accumulate and absorb it as its own. The captured gas flows through the Roche lobe and angular momentum prevents it from falling directly towards the primary star and instead serves to form an accretion disk. Binary systems that have characteristic x-ray emissions typically have a black hole, or a neutron star, serving as the engine powering the emission and can be considered as a scaled-down version of quasars.

The physics behind accretion disks rest on two main schools of scientific thought: the established Kerr metric fields derived from General Relativity for a rotating massive body and the strong gravity associated with close proximity to the black hole's or neutron star's gravitational field, particularly the event horizon of a black hole, and a developing description of matter's inherent properties that serve as a counter to the strong gravity of the black hole or neutron star (McClintock, 2006).

The stress energy tensor  $T_{uv}$  and other material equations serve to summarize the behavior of the material within the accretion disk, such as radiation transport, convection, turbulence, viscosity, and magnetic fields that serve as a means of transporting angular momentum.

## Angular Momentum Transport

The angular momentum transport deals with how spiraling plasma can linger in an accretion disk and how angular momentum can be dissipated resulting in accreting the advected plasma. Starting with the assumption that total angular momentum of the disk is conserved, the angular momentum loss of the mass towards the center has to have been compensated by the difference (gain) in the angular momentum farther from the center. Thus, there has to be a method of angular momentum transfer from inward to outward for which an accretion disk can exist (Weizsacker, 1948).

As the Rayleigh stability criterion states, there must be a laminar flow per unit mass where

$$\frac{\partial(R^2\Omega)}{\partial R} > 0, \quad (5.1)$$

with  $\Omega$  representing the angular velocity of a fluid element, and  $R$ , the radial distance from the center for an accretion disk. The laminar flow indicates a smooth, disparate parallel flow of multiple elements that do not interact with each other. This de-emphasizes a possible role and existence of a hydrodynamic mechanism for the angular mechanism transport.

In the description by Sunyaev-Shakura (1973), viscous stresses were assumed to dissipate part of the gravitational energy by way of heating the matter closer to the center of the accretion disk and radiating it away in another form of energy. Viscosity by itself doesn't account as a mechanism for angular momentum transport due to being a phenomenon that occurs on close contact and does not extend to longer distances such as those nearer the exterior of the accretion disk.

Turbulence-driven viscosity accounts for the angular momentum transfer but was not attributed to a specific, well-defined driving phenomenon (*Lynden-Bell, 1974*).

The standard physics approach to viscosity includes an adjustable parameter,  $\alpha$ , which describes the increased viscosity due to arising turbulent eddies inside the disk.

Balbus and Hawley introduced an origin of a means of angular momentum transport within accretion disks in a paper in 1991, which introduced the phenomenon of magnetorotational instability (MRI). In this model the rotating accretion disk would have moving electrically charged particles, which in turn, induces a magnetic field within the accretion disk. A weakly magnetized disk moving around a massive central body would be unstable and provide a possible mechanism for angular momentum redistribution to higher orbits within the accretion disks (*Balbus S. a., 1991*).

In Shakura and Sunyaev's 1973 paper, the authors provided a model for the turbulence in the gas as a source of the viscosity (*Shakura, 1973*). The disk viscosity can be estimated by this equation:

$$\nu = \alpha c_s H \quad (5.2)$$

With  $c_s$  being the sound speed,  $H$  the disk height, and  $\alpha$  being the free parameter, falling between zero (meaning no accretion) and one (full accretion).

Typical values of  $\alpha$  used for magnetohydrodynamical simulations are close to 0.01 but observations indicate a value closer to 0.1.

In all models that depend on stationary and axisymmetric location of the accreted matter, all physical quantities depend only on two coordinates: the radial distance  $r$ , and the vertical distance from the equatorial symmetry plane  $z$ . Most models rely on the assumption that the disk is not vertically thick. For example, in thin disks,  $z/r \ll 1$  everywhere within the matter

distribution, and in “slim” disks,  $z/r \leq 1$ .

Three types of analytic solutions of the black hole accretion flows have been obtained for accretion disks with three ranges of accretion rates  $\dot{m}$  and optical depth  $\tau$ , with the mass

$$\text{accretion rate, } \dot{m} = \frac{\dot{M}}{\dot{M}_{Edd}}, \text{ being scaled to the Eddington rate:} \quad (5.3)$$

$$\text{The thin Shakura-Sunyaev disks: } \quad \dot{m} \ll 1, \tau \gg 1 \quad (5.4)$$

$$\text{The slim disks:} \quad \dot{m} \sim 1, \tau \gg 1 \quad (5.5)$$

$$\text{The ADAF (Advection Dominated Accretion Flow) type disks: } \quad \dot{m} \ll 1, \tau \ll 1 \quad (5.6)$$

For turbulent motion,

$$v = v_{turb} * l_{turb} \quad (5.7)$$

Where  $v_{turb}$  is the velocity of turbulent cells relative to the mean gas motion and  $l_{turb}$  is the size of the largest turbulent cells, estimated by

$$l_{turb} \sim H = c_s / \Omega \quad v_{turb} \sim c_s; \quad (5.8a,b)$$

$$\Omega = \left( \frac{GM}{r^3} \right)^{\frac{1}{2}}; \quad \Omega = \text{orbital angular velocity} \quad (5.9)$$

$r$  = radial distance from central massive object

$M$  = mass of central object

The equations of disk structure include that of hydrostatic equilibrium, and conservation of angular momentum, and operating on the assumption that the disk is thin, the equations can be written in terms of the free parameter  $\alpha$ .

The disk height, mid-plane temperature, and mid-plane density can be determined:

$$H = 1.7 * 10^8 \alpha^{-1/10} \dot{M}^{3/20} M_I^{-3/8} R_{10}^{9/8} f^{3/5} \text{ cm}; \quad (5.10)$$

$$T_c = 1.4 * 10^4 \alpha^{-1/5} M_{16}^{3/10} m_1^{1/4} R_{10}^{-3/4} f^{6/5} \text{ K}; \quad (5.11)$$

$$\rho = 3.1 * 10^{-8} \alpha^{-7/10} \dot{M}_{16}^{11/20} m_1^{5/8} R_{10}^{-15/8} f^{11/5} \text{ g/cm}^3; \quad (5.12)$$

$T_c$  is the mid-plane temperature,  $\rho$  the mid-plane density,  $\dot{M}_{16}$  is the accretion rate in terms of  $10^{16}$  g/s,  $m_1$  is the mass of the central body in solar mass units,  $R_{10}$  is the radius of a point in the disk in units of  $10^{10}$  cm, and

$$f = [1 - (R^*/R)^{1/2}]^{1/4}, \quad (5.13)$$

where  $R^*$  is the radius where angular momentum stops being transported inwardly.

The Shakura-Sunyaev  $\alpha$ -disk model is thermally and viscously unstable (Shakura, 1973).

Another model, the  $\beta$ -disk, in contrast to the  $\alpha$ -disk model, is stable in both senses by taking viscosity to be proportional to the gas pressure:

$$\nu = \alpha * P_{gas} \quad (5.14)$$

In the Shakura-Sunyaev model, viscosity is proportional to the total pressure (Shakura, 1973):

$$P_{total} = P_{rad} + P_{gas} = \rho * c_s^2 \quad (5.15)$$

$$\nu = \alpha * c_s H = \alpha \frac{c_s^2}{\Omega} = \alpha \frac{P_{total}}{\rho * \Omega} \quad (5.16)$$

A key assumption is that the disk is in thermal equilibrium and can radiate the heat efficiently. The viscous heat is radiated away in the vertical direction, cooling the disk in the process and the disk becomes geometrically thin. The ability of the accreting matter to retain the radiation (higher opacity) affects whether the matter expands in response and the disk changes its shape and swells accordingly. The geometrically thin shape of the disk assumption may not apply for the radiatively inefficient case. The disk puffs up into a torus (veering from a thin disk

to a slim disk) or another three-dimensional solution such as an ADAF (advection dominated accretion flow) that describes the accretion. The ADAF solutions require an accretion rate that is smaller than a few percent of the Eddington limit. Another analytical model for accretion disks is referred to as “Polish doughnuts,” referring to the disk’s physical appearance, which would resemble a fat donut with a narrow hole.

All the models operate on the reasonable assumption that the accreted matter is able to maintain a temporary and tentative equilibrium against the gravity in an axisymmetric reference frame, moving in approximately circular orbits. The high angular momentum provides a counterbalance against the compact object’s gravity while viscous stresses dissipate and redistribute the angular momentum, removing the balance against the gravitational pull. The most likely mechanism for angular momentum transport is the Balbus-Hawley magnetorotational instability (MRI) –induced turbulence that appears in weakly magnetized non-rigid rotating fluids (Balbus S. a., 1991).

The induced turbulence produced by the MRI instability dissipates the energy and redirects the angular momentum, which causes the matter to slip through the gravitational potential barrier and culminate in a fatal fall in towards the black hole’s event horizon or the neutron star’s physical surface. The dissipated energy can heat up the accretion disk and it can be cooled via a number of processes, including radiation, convection, and advection.

## Hydrodynamics

This section explains how the plasma moves in the accretion disk. Hydrodynamics is the study of fluids in motion, and pertains to gas and plasmas moving through space under certain conditions. With a mass flow, a set of hydrodynamic equations is solved to describe the flow.

Using the following equation:

$$\frac{d^2r}{dt^2} = \frac{dv}{dt} = \frac{dv}{dr} \frac{dr}{dt} = v \frac{dv}{dr} \quad (5.17)$$

and using equation (5.17) in Newton's 2<sup>nd</sup> law, equation (1.3):

$$\rho v \frac{dv}{dr} = -\frac{dP}{dr} - \frac{GM_r \rho}{r^2} \quad \text{where } v \text{ is velocity of the flow;} \quad (5.18)$$

This requires that another equation be included to solve for the 3 unknowns, r, v and  $\rho$ : that of the conservation of mass;

$$4\pi r^2 \rho v = \text{constant} = \dot{M}_0 \quad (5.19)$$

This implies that  $\frac{d}{dr}(\rho v r^2) = 0$ . (5.20)

The gases and plasmas in a convection zone will adhere to behavior as dictated by hydrodynamical laws and hydrodynamics is invoked to understand how the gases behave during convection where energy transfers occur in the form of heat through direct contact between gas particles.

The rising hot plasma and sinking cooler plasma at the top of a convection zone creates longitudinal waves (p-waves) that travel radially outward through the photosphere into the chromosphere (next layer). The outward energy flux is defined as:

$$F_E = \frac{1}{2} \rho v_w^2 v_s \quad (5.21)$$

Where  $v_s$  is the local sound speed and  $v_w$  is the velocity amplitude of the oscillation wave motion

for particles driven about their equilibrium positions by ‘piston’ mechanism of the convection zone (*Carroll B. W., An Introduction to Modern Astrophysics, 1996*).

$$v_s = \sqrt{\frac{\gamma P}{\rho}} = \sqrt{\frac{\gamma \left( \frac{\rho K T}{\mu m_H} \right)}{\rho}} = \sqrt{\frac{\gamma K T}{\mu m_H}} \propto \sqrt{T} \text{ for fixed } \mu \text{ and } \gamma \quad (5.22)$$

At the top of the convection zone, when the wave starts moving, the sound of speed is less than the velocity amplitude speed:  $v_w < v_s$ . The density of the plasma drops with altitude so the wave speeds up as it passes through the ionized medium, becoming supersonic ( $v_w > v_s$ ) and forms a shock wave. The shock front at the forefront of the shockwave heats the gas via collisions and ramping up the ionization of gas behind the shock. The mechanical energy of the wave is converted to thermal energy and the shock wave subsides. The motions of the convection zone translate to heating of the gas in the chromosphere, or the next outer layer of the atmosphere within the star or disk (*Carroll B. W., An Introduction to Modern Astrophysics, 1996*). This process neglects the influence of magnetic fields. The understanding of the shock wave dynamics is significant when it comes to focusing on the source of heating that leads to the generation and release of energy in the form of radiation, particularly x-ray radiation in the inner disk.

## **Magnetohydrodynamics**

To fully understand the pulsations of stellar surfaces, magnetohydrodynamics is necessary to be brought into play. Magnetohydrodynamics is the study of the interactions between plasmas and magnetic fields. The magnetic field's presence introduces the potential



presence of a second wave motion, akin to transverse waves moving along magnetic field lines and serving as a restoring force due to the tension of the field lines. It is for this reason why it is important to find where the magnetic field becomes significant and the Alfvén radius would start to disrupt the advection of the plasma. A magnetic field contains stored energy and the space of the magnetic field has a magnetic energy density:

$$u_m = \frac{B^2}{8\pi} \quad (5.23)$$

One way to increase the magnetic energy density is to compress a plasma of volume  $V$  containing a number of magnetic field lines, perpendicularly to these lines, and the field lines increase in density as a response. Mechanical work is done during compression, which implies the existence of magnetic pressure.

The magnetic pressure is equal to the magnetic energy density:

$$P_m = \frac{B^2}{8\pi} \quad (5.24)$$

Waves are an important way to import energy; waves can propagate in magnetic fields. As a magnetic field line is displaced perpendicular to the direction of the line's original position by an amount, a magnetic pressure gradient is created and the pressure in direction of the displacement increases due to the increase in number density in field lines, while the magnetic pressure in the opposite direction causes a tendency for the field lines to revert back to their original positions and density. The magnetic pressure gradient is the tension that restores the position of the magnetic field (*Carroll B. W., An Introduction to Modern Astrophysics, 1996*).

A disturbance in the magnetic field line can propagate along the line in the form of an wave, called an Alfvén wave. The speed of an Alfvén wave can be determined:

$$v_s = \sqrt{\frac{\gamma P_g}{\rho}} \rightarrow v_m \sim \sqrt{\frac{P_m}{\rho}} = \frac{B}{8\pi\sqrt{\rho}} \quad (5.25)$$

It turns out that  $v_m = \frac{B}{\sqrt{4\pi\rho}}$ . (5.26)

Thus, Alfvén waves carry energy along magnetic field lines. A magnetic field varying in time induces an electric field that creates currents in plasma and Joule heating will occur as a result. Magnetohydrodynamics also contributes to the heating and overall temperature scheme of the stellar atmosphere.

Motions of gas also contribute to MHD, and a rotating star with a magnetic field will drag along its magnetic field lines and create a torque that serves to slow the star's own rotation. Its solar wind, a large motion of gas away from the surface, serves to transfer angular momentum outward. This can be applied for accretion disks as well, which I will show in Chapter VII (*Carroll B. W., An Introduction to Modern Astrophysics, 1996*).

### **Magnetorotational Instability**

A description for the MRI instability can reveal the physical reason in the Balbus-Hawley model (Balbus S. a., 1991). Two fluid elements within a weakly magnetized disk are connected by magnetic tension, which can be compared to a spring connecting the two mass elements together. The innermost mass element moves faster due to a higher angular velocity than the outermost element. The spring stretches and in response, the innermost element slows down while the outermost element speeds up (Balbus S. A., 2003). The angular momentum is transported by that method and energy is released.

Given the magnetic field  $B_z$  projected in the  $z$  direction, and Alfvén speed  $v_A$ ,

$$v_A = \frac{B_z^2}{4\pi\rho} \quad (5.27)$$

The dispersion relation for perturbations in the magnetic field quantities are expressed in the following equation:

$$dX \sim e^{i(kx - \omega t)} \quad (5.28)$$

Where  $X$  is a preferred displacement in a direction,  $k$  and  $\omega$  are wave number and frequency, respectively, which serves as a solution to the following extended dispersion relation equation that summarizes the contributed angular frequencies by different processes (Alfvén, rotational):

$$\omega^4 - (2k v_A + \omega_r)^2 + k v_A (k v_A + r \frac{d(\Omega)^2}{dr}) = 0 \quad (5.29)$$

$\Omega$  is the angular velocity of the fluid, and  $\omega_r$  is the radial epicyclic frequency of the emitted radiation. The equation yields an unstable result for  $\omega^2 < 0$ , on the condition that

$$k v_A + r \frac{d(\Omega)^2}{dr} < 0. \quad (5.30)$$

This gives the condition for occurrence of the MRI (Magneto-Rotational Instability) in weakly magnetized disks:

$$\frac{d(\Omega)}{dr} < 0. \quad (5.31)$$

This is fulfilled as the angular velocity decreases with radius in accretion disks.

It also can be shown that for the spring-like tension within the disk, that the Rayleigh stability criterion can be replaced with a new condition:

$$\frac{d\Omega^2}{d \ln r} > 0. \quad (5.32)$$

Most astrophysical disks do not satisfy this condition; hence they are prone to the

magnetorotational instability (Balbus S. a., 1991).

The question remains whether MRI simulations validate the Shakura-Sunyaev viscosity prescription. Recent simulations show that variations in the Maxwell stress  $\tau_{MAX}$  due to turbulence by MRI instability are strongly correlated to a variation of  $\sim \alpha * P$ .

The Shakura-Sunyaev prescription may be accurate when averaged over a long duration. For accretion disks the role that angular momentum plays is critically important. There exists a zone within the accretion disk where the specific angular momentum  $L$  of the accreted mass is not smaller than the Keplerian angular momentum in the same area (Shakura, 1973):

$$L(x_i) \geq L_K(x_i). \quad (5.33)$$

$L_K$  refers to the angular momentum of a free particle on a circular geodesic orbit around the central objects, as opposed to Bondi accretion, where the specific angular momentum everywhere is smaller than the Keplerian angular momentum except in the innermost region of the accretion disk. In the thick Shakura-Sunyaev disk case, the specific angular momentum is equal to the Keplerian angular momentum everywhere within the disk.

In their paper, Shakura and Sunyaev made a set of assumptions that reduced the system of thin disk equations to a set of algebraic equations (Shakura, 1973). The vertical and continuity equations are algebraic, and the radial momentum equation becomes a trivial identity with the assumptions that the radial pressure and velocity gradients vanish and the rotation is Keplerian, as in  $\Omega = \Omega_K^+$ . The algebraic angular momentum equation is set with the assumption that  $L_{in} = L_K(ISCO)$ . The assumption fixes the eigenvalue of the system.

Since the rotation is Keplerian,  $\Omega$  is a function of  $r$ . The right hand side of equation (5.29) represents the advective cooling, and is assumed negligible in the Shakura-Sunyaev model. The first term on the left-hand side of the equation (5.29), which represents viscous heating, is algebraic. The second term represents radiative cooling, and is also algebraic. All these algebraic equations are linear in three radial ranges: outer, middle, and inner, in the accretion disk.

The Shakura-Sunyaev model can be set in terms of polynomial formulae. The Shakura-Sunyaev model yielding these equations is a basis of accretion disk theory and remains a foundation in the subject. The Shakura-Sunyaev disk is comprised of cold gas that moves in tight spirals that form Keplerian orbits. The Shakura-Sunyaev thin disk is relatively luminous and has a thermal electromagnetic spectrum, which approximates a blackbody spectrum.

Novikov and Thorne worked out the general relativistic version of the Shakura-Sunyaev disk model, which gave the formulae for the disk characteristic quantities in terms of the mass accretion rate  $\dot{M}_0$  and viscosity parameter alpha (Novikov I. a., 1973).

The characteristic equations are broken up by region:

Outer region:

$$p = p_{gas} \quad K = K_{ff} \quad (\text{free-free electron opacity}) \quad (5.34a,b)$$

$$F = (7.0 \cdot 10^{26} \text{ erg/cm}^2) (M^2 M_{o*}) r_*^{-3} B^{-1} C^{-1/2} Q \quad (5.34c)$$

$$\Sigma = (4.0 \cdot 10^5 \text{ g/cm}^2) (\alpha m^{2/10} \dot{m}^{7/10}) r_*^{3/4} \mathcal{A}_{10}^{1/2} B^{-4/5} C^2 D^{-1/20} \mathcal{E}^{-1/20} Q_{20}^{3/20} \quad (5.34d)$$

$$H = (4.0 \cdot 10^2 \text{ cm}) (\alpha^{-1/10} m^{18/20} \dot{m}^{-3/20}) r_*^{-9/8} \mathcal{A}_{20}^{19/20} B^{-11/10} C^2 D^{-23/40} \mathcal{E}^{-19/40} Q_{20}^{3/20} \quad (5.34e)$$

$$\rho = (4.0 \cdot 10^2 \text{ g/cm}^3) (\alpha^{-7/10} m^{-7/10} \dot{m}^{11/20}) r_*^{-15/8} \mathcal{A}_{20}^{-17/20} B^{3/10} C^2 D^{-1/40} \mathcal{E}^{-17/40} Q_{20}^{11/20} \quad (5.34f)$$

$$T = (2.0 \cdot 10^8 \text{ K}) (\alpha^{-1/5} m^{-1/5} \dot{m}^{3/10}) r_*^{3/4} \mathcal{A}_{10}^{-1/10} B^{-1/5} D^{-3/20} \mathcal{E}^{1/20} Q_{10}^{3/20} \quad (5.34g)$$

$$\beta(1 - \beta) = (3)(\alpha_{10}^{-1} m^{-1/10} \dot{m}^{-7/10}) r_*^{3/8} \mathcal{A}^{-11/20} \mathcal{B}^{9/10} \mathcal{D}^{7/40} \mathcal{E}^1 Q^{-7/20} \quad (5.34h)$$

$$\frac{\tau_{\text{eff}}}{\tau_{\text{es}}} = (2*10^3)(\alpha_{10}^{-1/5} \dot{m}^{-1/2}) r_*^{3/4} \mathcal{A}^{1/2} \mathcal{B}^{2/5} \mathcal{D}^{1/4} \mathcal{E}^1 Q^{-1/2} \quad (5.34i)$$

Middle region:

$$p = p_{\text{gas}} \quad K = K_{\text{es}} \quad (\text{electron scattering opacity}) \quad (5.35a,b)$$

$$F = (7.0*10^{26} \text{ erg/cm}^2/\text{s})(m^{-1} \dot{m}) r_*^{-3} \mathcal{B}^{-1} \mathcal{C}^{-1/2} Q \quad (5.35c)$$

$$\Sigma = (9.0*10^4 \text{ g/cm}^2)(\alpha_{10}^{-4/5} m^{1/5} \dot{m}^{3/5}) r_*^{-3/5} \mathcal{B}^{-4/5} \mathcal{C}^{1/2} \mathcal{D}^{-4/5} Q^{3/5} \quad (5.35d)$$

$$H = (1.0*10^3 \text{ cm})(\alpha_{10}^{-1/10} m^{9/10} \dot{m}^{-1/5}) r_*^{21/20} \mathcal{A}^1 \mathcal{B}^{-6/5} \mathcal{C}^{1/2} \mathcal{D}^{-3/5} \mathcal{E}^{-1/2} Q^{1/5} \quad (5.35e)$$

$$\rho = (4.0*10^1 \text{ g/cm}^3)(\alpha_{10}^{-7/10} m^{-7/10} \dot{m}^{2/5}) r_*^{-33/26} \mathcal{A}^{-1} \mathcal{B}^{3/5} \mathcal{D}^{-1/5} \mathcal{E}^{1/2} Q^{2/5} \quad (5.35f)$$

$$T = (2.0*10^8 \text{ K})(\alpha_{10}^{-1/5} m^{-1/5} \dot{m}^{2/5}) r_*^{-9/10} \mathcal{B}^{-2/5} \mathcal{D}^{-1/5} Q^{2/5} \quad (5.35g)$$

$$\beta(1 - \beta) = (7*10^{-3})(\alpha_{10}^{-1/10} m^{-1/10} \dot{m}^{-4/5}) r_*^{21/20} \mathcal{A}^{-1} \mathcal{B}^{9/5} \mathcal{D}^{2/5} \mathcal{E}^{1/2} Q^{4/5} \quad (5.35h)$$

$$\frac{\tau_{\text{eff}}}{\tau_{\text{es}}} = (2*10^{-6})(\dot{m}^{-1}) r_*^{3/2} \mathcal{A}^{-1} \mathcal{B}^2 \mathcal{D}^{1/2} \mathcal{E}^{1/2} Q^{-1} \quad (5.35i)$$

Inner region:

$$p = p_{\text{rad}} \quad K = K_{\text{es}} \quad (\text{electron scattering opacity}) \quad (5.36a,b)$$

$$F = (7.0*10^{26} \text{ erg/cm}^2/\text{s})(m^{-1} \dot{m}) r_*^{-3} \mathcal{B}^{-1} \mathcal{C}^{-1/2} Q \quad (5.36c)$$

$$\Sigma = (5 \text{ g/cm}^2)(\alpha_{10}^{-1} \dot{m}^{-1}) r_*^{-3/2} \mathcal{A}^{-2} \mathcal{B}^3 \mathcal{C}^{1/2} \mathcal{E} Q \quad (5.36d)$$

$$H = (1.0*10^5 \text{ cm})(\dot{m}) \mathcal{A}^2 \mathcal{B}^{-3} \mathcal{C}^{1/2} \mathcal{D}^{-1} \mathcal{E}^{-1} Q \quad (5.36e)$$

$$\rho = (2.0*10^{-5} \text{ g/cm}^3)(\alpha_{10}^{-1} m^{-1} \dot{m}^{-2}) r_*^{3/2} \mathcal{A}^{-4} \mathcal{B}^6 \mathcal{D} \mathcal{E}^2 Q^{-2} \quad (5.36f)$$

$$T = (5.0*10^7 \text{ K})(\alpha_{10}^{-1/4} m^{-1/4}) r_*^{-3/8} \mathcal{A}^{-1/2} \mathcal{B}^{-1/2} \mathcal{E}^{1/4} \quad (5.36g)$$

$$\beta(1 - \beta) = (4*10^{-6})(\alpha_{10}^{-1/4} m^{-1/4} \dot{m}^{-2}) r_*^{21/8} \mathcal{A}^{-5/2} \mathcal{B}^{9/2} \mathcal{D} \mathcal{E}^{5/4} Q^{-2} \quad (5.36h)$$

$$(\tau_{eff} * \tau_{es})^{\frac{1}{2}} = (I * 10^{-4}) (\alpha^{-\frac{17}{16}} m^{-1/10} \dot{m}^{-2}) r_*^{93/32} \mathcal{A}^{-\frac{25}{8}} \mathcal{B}^{\frac{41}{8}} \mathcal{C}^{\frac{1}{2}} \mathcal{D}^{\frac{1}{2}} \mathcal{E}^{\frac{5}{4}} Q^{-2} \quad (5.36i)$$

The radial functions in the above equations are defined as such:

$$\mathcal{A} = 1 + a_*^2 y^{-4} + 2a_*^2 y^{-6} \quad \mathcal{B} = 1 + a_* y^{-3} \quad (5.37a,b)$$

$$\mathcal{C} = 1 - 3y^{-2} + 2a_* y^{-3} \quad \mathcal{D} = 1 - 2y^{-2} + a_*^2 y^{-4} \quad (5.37c,d)$$

$$\mathcal{E} = 1 + 4a_*^2 y^{-4} - 4a_*^2 y^{-6} + 3a_*^4 y^{-8} \quad Q_o = \frac{1 + a y^{-3}}{y(1 - 3y^{-2} + 2ay^{-3})^{\frac{1}{2}}} \quad (5.37e,f)$$

$$Q = Q_o \left[ y - y_o - \left( \frac{3}{2} \right) a \ln \left( \frac{y}{y_o} \right) - \frac{3(y_1 - a)^2}{y_1(y_1 - y_2)(y_1 - y_3)} \ln \left( \frac{y - y_1}{y_0 - y_1} \right) \right] -$$

$$Q_o \left[ \frac{3(y_2 - a)^2}{y_1(y_2 - y_1)(y_2 - y_3)} \ln \left( \frac{y - y_2}{y_0 - y_2} \right) - \frac{3(y_3 - a)^2}{y_1(y_3 - y_1)(y_3 - y_2)} \ln \left( \frac{y - y_3}{y_0 - y_3} \right) \right] \quad (5.37g,h)$$

Where  $y = \left( \frac{r}{M} \right)^{\frac{1}{2}}$ ,  $a_* = \frac{a}{M}$ ,  $y_o = \left( \frac{r_{ms}}{M} \right)^{\frac{1}{2}}$ , and  $y_1, y_2, y_3$  are roots of the equation: (5.38a,b,c)

$$y^3 - 3y + 2a_* = 0 \quad (5.39a)$$

$$y_1 = 2 \cos \left[ \frac{\cos^{-1} a_* - \pi}{3} \right] \quad (5.39b)$$

$$y_2 = 2 \cos \left[ \frac{\cos^{-1} a_* + \pi}{3} \right] \quad (5.39c)$$

$$y_3 = -2 \cos \left[ \frac{\cos^{-1} a_*}{3} \right] \quad (5.39d)$$

The Shakura-Sunyaev solutions are local solutions, which operate on the assumption that the viscous torque goes to zero at the ISCO. The locations of the pressure maxima are situated at the cusp of the disk ( $r_{cusp}$ ), the sonic radius, the point where the falling material goes supersonic ( $r_{sound}$ ), and the center of the disk ( $r_{center}$ ), for both the Shakura-Sunyaev and Novikov-Thorne

models. The cusp is located at the ISCO and the angular momentum is Keplerian outside the ISCO and constant beyond the ISCO. However, for real flows, the cusp, center of the disk, and sonic radius are not one and same with the position of the ISCO and the angular momentum is super-Keplerian between the cusp and the center of the disk.

The Shakura-Sunyaev and Novikov-Thorne models assume that accretion is efficient at generation of heat via viscous processes at a specific radius, which are radiating the heat away (Shakura, 1973) (Novikov I. a., 1973). The viscous heating is balanced by another factor: radiative cooling, and no other cooling mechanism is necessitated up until a certain luminosity ( $L \sim 0.3 L_{\text{Edd}}$ ), and the accretion rate is small.

At a high enough luminosity ( $0.3 L_{\text{Edd}}$ ), and with the disk being sufficiently thick enough, another cooling mechanism comes into play: advection.

Advection is the horizontal flow of thermal energy and gravitationally captured and falling matter in towards a central object. The viscosity-generated heat doesn't transfer energy into photons and escape the disk fast enough so it gets carried inward by the motion of the gas. As the luminosity increases, the advective cooling increases and for the significantly high luminous cases, is comparable with the radiative cooling process. In these cases, the thin disk models are inapplicable.

In the slim disk case, an additional problem emerges where the equations (5.34-5.36) aren't applicable and instead requires a system of two-dimensional ordinary differential equations with a critical point; one where the gas velocity surpasses the local speed of sound at a particular radius. In the limit of low accretion rates, they converge towards the solutions of the



thin disk cases. Slim disks conform more to the physical world in contrast with thin disks in that they extend all the way to the black hole event horizon as opposed to the ISCO in the thin disk case. I will be using the thin disk model because the accretion rate is approximate enough for the presence of QPO frequencies at the ISCO radius.

Slim disks deviate from the thin disk cases, in that they have different angular momentum profiles where the slim disks rotate with super-Keplerian velocities and for higher accretion rates, the difference increases significantly. The disk thickness also increases with the accretion rate and as the rate approaches the Eddington limit, the height/radius ratio reaches a maximal value of 0.3. The flux becomes modified by the advection and an increasing fraction of the viscous heat is advected inward and released nearer to the event horizon of the black hole.

As advection increases, the conversion of gravitational potential energy into radiative flux due to collision of particles decreases with increased accretion rates. The disk luminosity only becomes slightly super-Eddington to an extent and does so due to the geometry of the flow being constrained to the equatorial plane and not being spherical. The accretion moves inward along the equatorial plane while the radiation can escape vertically.

Advection can fully determine the dynamics as seen in the ADAF, or Advection-Dominated Accretion Flow, case (Narayan R. a., Advection-dominated accretion: A self-similar solution, 1994) (Narayan R. a., Advection-dominated accretion: Self-similarity and bipolar outflows, 1995) (Narayan R. a., Advection-dominated accretion: Underfed Black Holes and Neutron Stars, 1995).

Almost all of the viscous energy is advected into the black hole rather than radiated. In contrast

to the slim disk scenario, which is invoked for high luminosities, ADAF is used when the luminosity and mass accretion rates are low.

Due to the lower radiative energy losses, ADAF objects are significantly less luminous than thin disks or slim disks. They are close to the virial temperature, tend to be optically thin, and quasi-spherical. Their spectra obey a power law and are non-thermal, with a strong Compton component. They usually are used for studies in the Hard (high energy) x-ray case seen in x-ray binaries.

The ADAF solutions were derived similarly to the slim and thin disk cases.

They are:

$$v = \left(3.0 * 10^{10} \frac{cm}{s}\right) \alpha c1 r^{-\frac{1}{2}} \quad (5.40a)$$

$$\Omega = \left(2.03 * \frac{10^5}{s}\right) c2 m^{-1} r^{-\frac{3}{2}} \quad (5.40b)$$

$$c_s^2 = \left(9.0 * \frac{10^{20} cm}{s^2}\right) c3 r^{-\frac{3}{2}} \quad (5.40c)$$

$$\rho = \left(1.07 * \frac{10^{-5} g}{cm^3}\right) \alpha^{-1} c1^{-1} c3^{-\frac{1}{2}} m^{-1} \dot{m} r^{-\frac{3}{2}} \quad (5.40d)$$

$$P = \left(9.67 * \frac{10^{15} \frac{g}{cm}}{s^2}\right) \alpha^{-1} c1^{-1} c3^{\frac{1}{2}} m^{-1} \dot{m} r^{-\frac{5}{2}} \quad (5.40e)$$

$$B = (4.93 * 10^8 G) \alpha^{-\frac{1}{2}} (1 - \beta m)^{\frac{1}{2}} c1^{-\frac{1}{2}} c3^{\frac{1}{4}} m^{-\frac{1}{2}} \dot{m}^{\frac{1}{2}} r^{-\frac{5}{4}} \quad (5.40f)$$

$$q+ = \left(2.94 * \frac{10^{21} erg}{cm^3 s}\right) \epsilon' c3^{\frac{1}{2}} m^{-2} \dot{m} r^{-4} \quad (5.40g)$$

$$\tau_{es} = (1.75) \alpha^{-1} c1^{-1} \dot{m} r^{-\frac{1}{2}} \quad (5.40h)$$

The variable,  $v$ , is the radial infall velocity,  $q+$  is the viscous dissipation of energy per unit volume. The constants  $c1$ ,  $c2$ ,  $c3$  are as follows:

$$c1 = \frac{5+2\epsilon'}{3\alpha^2} g(\alpha, \epsilon') \quad (5.41a)$$

$$c2 = \left( \frac{2\epsilon'(5+2\epsilon')}{9\alpha^2} g(\alpha, \epsilon') \right)^{\frac{1}{2}} \quad (5.41b)$$

$$c3 = \frac{2(5+2\epsilon')}{9\alpha^2} g(\alpha, \epsilon') \quad (5.41c)$$

$$\epsilon' = (1/f_{adv} ((5/3 - \gamma g)/(\gamma g - 1))) \quad (5.41d)$$

$$g(\alpha, \epsilon') = \left[ 1 + \frac{18\alpha^2}{(5+2\epsilon')^2} \right]^{\frac{1}{2}} - 1 \quad (5.41e)$$

$f_{adv}$  is a parameter, which is the fraction of viscously dissipated energy that is advected.  $1 - f_{adv}$  is the fraction that is radiated locally energy.

### Vertical Pressure Balance

This is important because a balance between the vertical pressure force and the tidal gravitational force (difference in gravitational strength at opposite ends of a region) of the compact object determines the thickness of the disk, from the condition of hydrostatic equilibrium as defined by equation (2.23).

$$\frac{dp}{dz} = -\rho_0 g = \frac{-\rho_0 GMz}{r^3} \quad (5.42)$$

This yields a general solution:

$$h \approx \left( \frac{p}{\rho_0} \right)^{\frac{1}{2}} \left( \frac{r^3}{GM} \right)^{\frac{1}{2}} \cong \frac{c_s}{\Omega} \quad (5.43)$$

where  $h$  is the half thickness of the disk,  $c_s$  is the sound speed of the gas, and  $\Omega = \left( \frac{M}{r^3} \right)^{\frac{1}{2}}$ , the

angular velocity of the gas.

Notice that there's a scale between both the height and the radial extent of the disk and the sound speed and the angular velocity, respectfully:

$$h = \frac{c_s}{\Omega} \rightarrow \frac{h}{r} = \frac{c_s}{r\Omega} = \frac{c_s}{v} = c_s \left( \frac{r}{GM} \right)^{\frac{1}{2}} \quad (5.44)$$

The ratio of the sound speed to velocity also scales to the ratio of height over radius of the disk.

For a geometrically thin disk,  $h \ll r$ .

### Viscous Processes

The sources of viscosity as well as turbulence within the plasma flow are thought to be due to chaotic magnetic fields. A typical star will have a magnetic field of  $B_s \sim 100$  gauss. Plasma flowing off a secondary star into the disk will ferry field lines across to it. The deposited magnetic field will be chaotic due to the facet of no preferred direction in the plasma advected to the disk. Disk turbulence will contribute to the overall chaoticity of the magnetic field.

The shear of the gas flow will amplify the magnetic field at a rate:

$$\frac{dB_{\tilde{\varphi}}}{d\tau} = \sigma_{\tilde{\varphi}} B_r \approx \Omega B_r \quad \frac{dB_r}{d\tau} = 0 \quad (5.45a,b)$$

corresponding to an increase of  $B$  by amount  $B_r$  for every electrical current circuit around the compact object. The growing magnetic field will be offset by reconnection of field lines at the interfaces between chaotic cells, pinch-off of field lines, and escape of "magnetic bubbles".

The field can be described by pressure and viscosity:

$$t_{\phi r}^{mag} < p^{mag} = \frac{B^2}{8\pi} \quad (5.46)$$

This becomes important when it comes to examining the magnetic field of the inner disk. The shear stress  $t_{\phi r}$  will generally be smaller than magnetic pressure and the shearing of the field will be projected into the  $\phi$ -direction. The magnetic pressure cannot surpass the thermal pressure:

$$p^{mag} \leq p^{therm} \cong \rho_0 c_s^2 \quad (5.47)$$

The field lines would extend out of the disk, reconnect and escape. The magnetic viscous stress will satisfy the following equation:

$$t_{\phi r}^{mag} \leq p \cong \rho_0 c_s^2 \quad (5.48)$$

where  $c_s$  is the sound speed, and  $p$  is the pressure.

The coefficient of dynamical viscosity associated with the turbulent gas is:

$$\eta \approx \rho_0 v_{turb} \ell_{turb} \quad (5.49)$$

where  $v_{turb}$  is the speed of turbulent motions relative to the mean rest frame of gas, and  $\ell_{turb}$  being the characteristic size of the largest turbulent cells. The size of the turbulent cells define how far a wave can propagate before it is dissipated.

If the turbulent speed exceeds the sound speed, shocks develop and convert the turbulent energy into heat. Thus it is necessary that  $v_{turb} \leq c_s$ . The turbulent scale is limited by the disk thickness (height) :  $\ell_{turb} \leq h$ .

The shear stress due to turbulence is limited by:

$$t_{\phi r}^{turb} \cong \eta \sigma_{\phi r} \leq (\rho_0 c_s h) \Omega \cong \rho_0 c_s^2 \cong p \quad (5.50)$$

The shear stress is important because it can play a significant part in the suppression of any hotspots forming in the inner disk and lend further credence to a relativistic resonance model in terms of describing the inner disk of accretion disks.

## Radiative Transport

Viscosity-generated heat has to be transported to the surfaces of the disk before being radiated. The disk is optically thick, so the energy transport can be calculated by using the diffusion approximation reduced to Newtonian form:

$$\frac{d}{dz} \left[ \frac{1}{3} a T^4 \right] = \bar{K} \rho_0 q^z \quad (5.51)$$

The equation of transport's solution is:

$$a T^4 \cong \bar{K} \Sigma F \quad (5.52)$$

where  $\bar{K}$  is the average opacity,  $\Sigma$  is the surface density, and  $F$  is the flux. The dominant opacity source for the outer disk will be free-free transitions and by a comparable magnitude, bound-free transitions. For the outer regions,

$$\bar{K} \approx \bar{K}_{ff} \approx 0.64 \times 10^{23} \left( \frac{\rho_0}{\frac{g}{cm^3}} \right) \left( \frac{T}{K} \right)^{-\frac{2}{3}} \frac{cm^2}{g} \quad (5.53)$$

For the inner regions, for electron-scattering opacity:

$$\bar{K} \approx \bar{K}_{es} \approx 0.40 \frac{cm^2}{g} \quad (5.54)$$

For the majority of the disk, gas pressure dominates over the radiation pressure:

$$c_s^2 \cong \frac{p}{\rho_0} \cong \frac{p^{gas}}{\rho_0} \cong \frac{T}{m_p} \cong \frac{T}{10^{13} K} \quad (5.55)$$

In the innermost regions of the disk with an escalated temperature, radiation pressure is dominant:

$$c_s^2 \cong \frac{p}{\rho_0} \cong \frac{p^{rad}}{\rho_0} \cong \frac{\frac{1}{3} a T^4}{\rho_0} \quad (5.56)$$

The laws of conservation (rest-mass, angular momentum, radiative transport, energy,

vertical pressure balance, magnitude of viscosity, and magnitude of opacity) govern the steady-state disk structure and are described in the next section. They yield the characteristics and predictive behavior of accretion inside the disk and depict the overall picture of the accretion disk. They serve as the foundation of accretion disk theory.

### Conservation Equations

The conservation of mass and conservation of energy-momentum equations can be used to describe the accretion disk structure:

$$(\rho u^\mu)_{;\mu} = 0 \quad T_\nu^\mu{}_{;\nu} = 0 \quad (5.57a,b)$$

Where  $\rho$  is the rest mass density,  $u^\mu$  is the 4-velocity of the matter, and  $T_\nu^\mu$  is the stress energy tensor. They lead to further definitive equations, for state, prescription of viscosity, opacity, conductivity, etc.

$$(T_\nu^\mu)_{GEN} = (T_\nu^\mu)_{FLU} + (T_\nu^\mu)_{RAD} + (T_\nu^\mu)_{VIS} + (T_\nu^\mu)_{MAX} \quad (5.58a)$$

$$(T_\nu^\mu)_{FLU} = (\rho u^\mu)(W u_\nu) + \delta_\nu^\mu p \quad (5.58b)$$

$$(T_\nu^\mu)_{RAD} = u^\mu F_\nu + u_\nu F^\mu \quad (\text{usually set to 0 in models}) \quad (5.58c)$$

$$(T_\nu^\mu)_{VIS} = \nu_* \sigma_\nu^\mu \quad (\text{usually set to 0 for thick accretion disk models}) \quad (5.58d)$$

$$(T_\nu^\mu)_{MAX} = b^2 \left( u^\mu + \frac{1}{2} \delta_\nu^\mu \right) - b^\mu b_\nu \quad (5.58e)$$

Where  $W$  is the enthalpy,  $p$  is the pressure,  $F^\mu$  is the radiation flux,  $\nu_*$  is the kinematic viscosity,

and  $\sigma_v^\mu$  is the shear, and  $b^\mu$  is the magnetic field, measured in the rest frame.

The fluid part is expressed by:

$$(T_v^\mu)_{FLU} = (\rho u^\mu)(W u_v) + \delta_v^\mu p \quad (5.59)$$

where  $\rho$  is the conserved mass density,  $W$  the enthalpy, and  $p$  the perfect fluid isotropic pressure.

They are linked with other equations by the first law of thermodynamics:

$$dU = TdS - PdV \quad (5.60)$$

which becomes:

$$d\epsilon = Wd\rho + \rho TdS \quad (5.61)$$

where  $T$  is the temperature,  $S$  the entropy per unit mass, and  $\epsilon = \rho c^2 + \Pi$ , being the total energy density and  $\Pi$  the internal energy density;

$$V = \frac{1}{\rho} \quad U = \frac{\Pi}{\rho} \quad W = \frac{p+\epsilon}{\rho} \quad (5.62a,b,c)$$

### Thick disks and Tori

I also discuss thick disks and tori since the conditions for advection will be modified and this would have an effect on the occurrence of quasi-periodic oscillations. Some collaborating physicists, utilizing a set of equations, created a method of recreating perfect fluid equilibriums, for infalling matter revolving around a Kerr black hole in circular orbits. For the stress energy tensor and 4-velocity:

$$T_v^\mu = (\rho u^\mu)(W u_v) - p \delta_v^\mu \quad (6.81)$$

$$u^\mu = A(\eta^\mu + \Omega \xi^\mu) \quad (6.82)$$



and deriving from the condition  $\nabla_{\mu} T_{\nu}^{\mu} = 0$ , (6.83)

$$\nabla_{\nu} \ln A - \frac{L \nabla_{\nu} \Omega}{1-L\Omega} = \frac{1}{\rho} \nabla_{\nu} p; \quad (6.84)$$

For the perfect fluid case where  $S_{\nu}^{\mu} = 0$  and  $\delta u^{\mu} = 0$ , (6.85a,b)

the equilibrium condition takes the case that:

$$\frac{\nabla_{\nu} p}{p+\epsilon} = \nabla_{\nu} \ln A + \frac{l \nabla_{\nu} \Omega}{1+l\Omega} \quad (6.86)$$

For a baryotropic fluid  $p = p(\epsilon)$ , the left-hand side of the equation is a gradient of a scalar function, so the right-hand side must also be a gradient of a scalar, which it only is true if the time scale depends on the angular frequency:

$$l = l(\Omega) \quad (6.87)$$

This condition leads to a set of integrability conditions, known as the von Zeipel theorems, derived by Boyer, Bardeen, Abramowicz, Komissarov among others.

Within real flows, viscous dissipative processes with timescales longer than the dynamical timescale define  $l$ .

Paczynski assumed a result  $l = l(\Omega)$ , as noted above, which bypassed the dilemma of basing it on unsure assumptions about viscosity using a free function. Models based on a selected  $l$  behaves more physically realistic than those based on a free function  $\alpha(r, \theta) = \text{constant}$ .

Solving for  $\Omega$ :

$$l \left( \Omega = - \frac{\Omega g_{\phi\phi}(r,\theta) + g_{t\phi}(r,\theta)}{\Omega g_{t\phi}(r,\theta) + g_{tt}(r,\theta)} \right) \quad (6.88a)$$

$$\Omega = \Omega(r, \theta) \quad A(r, \theta) = (g_{tt} + 2\Omega g_{t\phi} + \Omega^2 g_{\phi\phi})^{\frac{1}{2}} \quad l = l(r, \theta) \quad (6.89b,c,d)$$

In Boyer-Lindquist coordinates, the equipressure surface equations can be recast in terms of

$p = p(r; \theta) = \text{constant}$ ,  $r = r(\theta)$ , and  $r(\theta)$  given by:

$$-\frac{dr}{d\theta} = \frac{\partial_{\theta} p}{\partial_r p} = \frac{(1-l\Omega)\partial_{\theta} \ln A + l\partial_{\theta}\Omega}{(1-l\Omega)\partial_r \ln A + l\partial_r\Omega} \quad (6.90)$$

With  $\Omega(r; \theta)$ ,  $A = A(r; \theta)$ , and  $l(r; \theta)$  given, the right-hand side of the equation takes the form of a known function,  $f(r, \theta)$ :

$$f(r, \theta) = \frac{dr}{d\theta} \quad (6.91)$$

This function can be integrated to obtain the equipressure surfaces  $p = p(r; \theta)$  in the radial form  $r = r(\theta)$ . Surfaces of constant pressure within a thick disk can be found from the relativistic version of the effective potential  $\phi$ :

$$\phi - \phi_{in} = - \int_0^p \frac{dp}{\rho W} \quad (6.92)$$

where  $\phi_{in}$  is the potential at the boundary of the thick disk. With constant angular momentum, the potential reduces to:

$$\phi = \ln(-u_t) \quad (6.93)$$

and given that  $l > l_{ms}$ , the potential  $\phi(r, \theta)$  will contain a saddle point  $\phi_{cusp}$  at  $r = r_{cusp}$ , on the equatorial plane ( $\theta = \frac{\pi}{2}$ ). A parameter can be defined as the potential barrier at the inner edge of the disk:

$$\Delta\phi = \phi_{in} - \phi_{cusp} \quad (6.94)$$

If  $\Delta\phi < 0$ , the disk resides within its Roche lobe. The disk is marginally stable against local axisymmetric perturbations and unstable against low-order non-axisymmetrical perturbations.

This would be significant in descriptions of undulations in the matter flow across the Roche lobe in the inner disk.

### Papaloizou-Pringle modes

If  $\Delta\phi > 0$ , the disk overflows its Roche lobe and accretion occurs across the cusp via pressure-gradient forces. The accretion is not reliant on dissipation of angular momentum, thus viscosity isn't important here. The accretion neutralizes the growth of the Papaloizou-Pringle instability.

### Equation of State

The equation of state is that of an ideal gas plus that of radiation:

$$P = \frac{\rho K T}{\mu m_H} + a T^4 \quad (5.63)$$

where  $K$  is the Boltzmann constant,  $T$  the temperature,  $\rho$  the density,  $\mu$  the average particle mass, and  $m_H$  the atomic mass constant.

There are two different temperatures that are important in a plasma; temperature  $T_i$  and molecular  $\mu_i$  of ions, and  $T_e$  and  $\mu_e$  of electrons. The pressure for the plasma is:

$$p = p_i + p_e = \frac{\rho K T_i}{\mu_i m_H} + \frac{\rho K T_e}{\mu_e m_H} \quad (5.64)$$

The perfect fluid case is described by the fluid part of the stress energy tensor and is the only essential description for the fluid part and all other parts vanish. Since  $\nabla_\mu (T_\nu^\mu \eta^\mu) = 0 =$

$$\nabla_\nu(T_\nu^\mu \xi^\nu); \quad (5.65)$$

The following equations are derived which describe the Bernoulli function and angular momentum of the plasma:

$$\mathcal{B} = -W(\mu\eta) = -Wu^t \quad \mathcal{J} = W(\mu\xi) = u^\phi \quad (5.66a,b)$$

where  $\mathcal{B}$  is the Bernoulli function, and  $\mathcal{J}$  is the angular momentum. Their ratio is a constant of motion:

$$\mathcal{L} = \frac{\mathcal{J}}{\mathcal{B}} = -\frac{u_\phi}{u_t} \quad (5.67)$$

This is analogous to the specific angular momentum, which is also a constant of geodesic motion.

The radiation part is expressed by the equation:

$$(T_\nu^\mu)_{RAD} = u^\mu F_\nu + u_\nu F^\mu \quad (5.68)$$

with  $F^\mu$  being the radiation flux.

With vertically thin disks (height  $H \ll r$ ), radiation is presumed to be emitted from the equatorial plane ( $\theta = \frac{\pi}{2}$ ), and the vertical component of flux expressed as  $F$ . The total radiation flux  $F_{tot}$  (in ergs) is emitted from both the upper and lower surfaces of the disk and expressed as:

$$F_{tot} = 2Hf \quad f \text{ being the radiation emissivity} \quad (5.69)$$

The emissivity is expressed by: (5.70a,b)

$$f = \frac{F}{2H} = \begin{cases} f_{br} + f_{synch} + f_{synch,C} + F_{br,C}; & \text{Optically thin case} \\ \frac{8\sigma T_c^4}{3H\tau}; & \text{Optically thick case} \end{cases}$$

The first case describes the plunging region since it is optically thin while the second case describes the disk since it is optically thick.

In the intermediate case the solution used is (Hubeny, 1990): (5.71)

$$f = \frac{4\sigma T_e^4}{H} \left[ \frac{3\tau}{2} + \sqrt{3} + \frac{4\sigma T_e^4}{H} (f_{br} + f_{synch} + f_{br,C} + f_{synch,C})^{-1} \right]^{-1}$$

The Planck mean opacity and radiation pressure is expressed as: (5.72a,b)

$$\tau_{abs} = \frac{H}{4\sigma T_e^4} (f_{br} + f_{synch} + f_{br,C} + f_{synch,C}) \quad p_r = \frac{fH}{2c} \left( \tau + \frac{2}{\sqrt{3}} \right)$$

The Bremsstrahlung emissivity is caused by ion-electron and electron-electron collisions:

$$f_{br} = f_{ei} + f_{ee} \quad (5.73)$$

The ion-electron part is expressed as (Svenson, 1982): (5.74a,b)

$$f_{ei} = n_e \bar{n} \sigma_T c \alpha_f m_e c^2 \times \begin{cases} 4 \left( \frac{2\theta_e}{\pi^3} \right)^{\frac{1}{2}} (1 + 1.781\theta_e^{1.34}); & \theta_e < 1 \\ \frac{9\theta_e}{2\pi} [\ln(1.123\theta_e + 0.48) + 1.5]; & \theta_e > 1 \end{cases}$$

With  $n_e$  the electron number density,  $\bar{n}$  ion number density averaged over all species,  $\sigma_T$  the Thomson cross section,  $\alpha_f = 1/137$ , the fine structure constant, and  $\theta_e = \frac{KT_e}{mc^2}$ , the dimensionless electron temperature.

The electron-electron part is expressed by (Stepney, 1997): (5.75a,b)

$$f_{ee} = n_e^2 c r_e^2 m_e c^2 \alpha_f \times \begin{cases} \frac{20}{9\sqrt{\pi}} (44 - 3\pi^2) \theta_e^{\frac{3}{2}} \left( 1 + 1.1\theta_e + \theta_e^2 - 1.25\theta_e^{\frac{5}{2}} \right); & \theta_e < 1 \\ 24\theta_e [\ln(2\eta\theta_e) + 1.28]; & \theta_e > 1 \end{cases}$$

With  $r_e = \frac{e^2}{m_e c^2}$  being the classical radius of the electron, and  $\eta = e^{-\gamma_E} = 0.5616$ .

The synchrotron emission of relativistic Maxwellian distribution of electrons is given by

(Narayan R. a., Advection-dominated Accretion. Underfed black holes and neutron stars, 1995):

$$f_{synch} = \frac{2\pi}{3c^2} kT_e \frac{d}{dr} \left[ \frac{3eB\theta_e^2 x_m}{4\pi m_e c} \right]; \text{ only valid for } \theta_e > 1; \quad (5.76)$$

which works for most cases.

$B$  is the equipartion magnetic field strength, and  $x_m$  is the solution of the transcendental equation

(5.77):

$$e^{1.8899x_m^{\frac{1}{3}}} = \frac{(2.49 \times 10^{-10}) \left( \frac{4\pi n_e r}{B} \right) \left( x_m^{-\frac{7}{6}} + 0.40 x_m^{-\frac{17}{12}} + 0.5316 x_m^{-\frac{5}{3}} \right)}{\theta_e^3 K_2 \left( \frac{1}{\theta_e} \right)} \quad (5.77)$$

with  $K_2$  the modified Bessel function of the 2<sup>nd</sup> kind.

Comptonization of bremsstrahlung and synchrotron radiation is expressed by (Esin, 1996):

$$f_{br,C} = f_{br} \left[ \eta_1 - \frac{\eta_1 x_c}{3\theta_e} - \frac{3\eta_1 [3^{-(\eta_3+1)} - 3\theta_e^{-(\eta_3+1)}]}{\eta_3+1} \right] \quad (5.78)$$

$$f_{synch,C} = f_{synch} \left[ \eta_1 - \eta_2 \left( \frac{x_e}{\theta_e} \right)^{\eta_3} \right] \quad (5.79)$$

With  $\eta = 1 + \eta_1 + \eta_2 \left( \frac{x}{\theta_e} \right)^{\eta_3}$ ; Compton energy enhancement factor;

(5.80)

$$x = \frac{h\nu}{m_e c^2} \quad x_c = \frac{h\nu_e}{m_e c^2} \quad \eta_1 = \frac{x_2(x_1-1)}{1-x_1x_2} \quad (5.81a,b,c)$$

$$x_1 = 1 + 4\theta_e + 16\theta_e^2 \quad \eta_2 = \frac{-\eta_1}{3\eta_3} \quad (5.81d,e)$$

$$x_2 = 1 - e^{-\tau_{es}} \quad \eta_3 = -1 - \frac{\ln x_2}{\ln x_1} \quad (5.81f,g)$$

The stress part is described by the equation:  $(T_v^\mu)_{VIS} = v_* \sigma_v^\mu$  (5.82)

The shear tensor is defined as:  $\sigma_{\mu\nu} = (\nabla_{(\mu} u_{\nu)} - \theta g_{\mu\nu})_\perp$  (5.83)

Where  $(X^\mu)_\perp = X^\alpha (\delta_\nu^\mu + u^\mu u_\alpha)$  for objects projected into (5.84)

instantaneous 3-space perpendicular to  $u^\mu$ .

The vorticity is:  $\omega_{\mu\nu} = (\nabla_{[\mu} u_{\nu]})_\perp$  (5.85)

The expansion variable  $\theta$  is:  $\theta = \frac{\nabla_\mu u^\mu}{3}$  (5.86)

In the case of purely circular motion,  $u^i = A(\eta^i + \Omega \xi^i)$  (5.87)

The quantities become:  $\theta = 0$   $\sigma_{\mu\nu} = \frac{1}{2} A^3 \psi^2 \partial_\mu \Omega$   $\omega_{\mu\nu} = \frac{1}{2} A^2 \psi^2 \partial_\mu \ell$

(5.88a,b,c)

$$\psi^2 = g_{t\phi}^2 - g_{tt} g_{\phi\phi}; \quad (X^\mu)_\perp u_\mu = 0; \quad (5.88d,e)$$

So in the case of purely circular motion,  $\sigma_{\mu\nu} \eta^\mu = -\Omega \sigma_{\mu\nu} \xi^\nu$   $\omega_{\mu\nu} \eta^\nu = -\Omega \omega_{\mu\nu} \xi^\mu$  (5.89a,b)

The viscous stress tensor is proportional to the shear (Landau, 1959):  $S_v^\mu = \nu \rho \sigma_v^\mu$  (5.90)

The rate of heat generation by viscous stress in volume  $V$  is expressed as:

$$Q^+ \int S_v^\mu \sigma_v^\mu dV; \quad (5.91)$$

The rate of viscous angular momentum and energy transport across surface  $S$  with unit normal

vector  $N^\mu$  is expressed as:  $\mathcal{J}_s = \int S_v^\mu \xi^\nu \nu N_\mu dS$   $\mathcal{B}_s = \int S_v^\mu \eta^\nu N^\mu dS$  (5.92a,b)

In the case of purely circular motion,

$$\mathcal{B}_s = -\Omega_s \mathcal{J}_s \quad (5.93)$$

Where  $\Omega_s = \Omega$  averaged on the surface  $S$ .

The Maxwell part is expressed by the stress energy tensor for the electromagnetic field:

$$(T_v^\mu)_{MAX} = b^2 \left( u^\mu + \frac{1}{2} \delta_\nu^\mu \right) - b^\mu b_\nu \quad (5.94a)$$

$$b^\mu = u^\nu * F_\nu^\mu \quad \text{magnetic field in fluid rest frame} \quad (5.94b)$$

and  $* F_\nu^\mu$  is the dual of Faraday tensor. Due to the fact  $b^\mu u_\mu = 0$ , (5.94c)

the dual of Faraday tensor becomes:  $* F_\nu^\mu = b^\mu u_\nu - b_\nu u^\mu$  (5.95)

The Faraday tensor satisfies the homogenous Maxwell equation  $* F_\nu^\mu{}_{;\nu} = 0$ . (5.96)

The spatial component yields the induction equation and the time component yields the divergence-free constraint.

With these physical equations, one can recreate the conditions of an accretion disk and obtain relevant physical information about the events that occur in the gas and dust, and the central objects. The accretion disks can also provide information about the conditions of the massive compact objects that harbor the disks, including the strong gravity from the compact objects. The effects of General relativity can be confirmed through signs revealed by the gas within the reach of the zone of influence. In the context of the Relativistic Resonance model, the epicyclic frequencies that are a result of General Relativity and would not exist in a strictly Newtonian framework. The double QPO signal would serve as a great test of unique effects due to the warping of space-time.



## **CHAPTER VI**

### **ACCRETION RATE**

I delve into the accretion rate since it is an important physical parameter that dictates the flow of material in accretion disks. It is also loosely dependent on the value of the adiabatic index whose significance will become apparent when I discuss the diskoseismological approach to link the QPO frequency to the adiabatic index. In this way I can determine the value of the adiabatic index at a specific radius, in Chapter IX. The accretion disk system comprises of a compact object such as a black hole or neutron star and at least one companion star in a binary system. Accretion occurs when the companion star overfills its Roche equipotential lobe and loses mass to its dominant partner through the inner Lagrangian (L1) point. Since the gas has a higher angular momentum, it will not accrete directly to the compact object but fall in narrow streams of gas, forming an accretion disk. The gas moves in Keplerian orbits and slowly loses angular momentum through viscous processes that cause the gas to spiral in at a faster rate.

As the gas nears the compact object, it heats up and the matter becomes ionized. The disk terminates at the ISCO (Innermost Stable Circular Orbit) because the particles can't travel in stable circular orbits behind that point. The orbits of the falling particles become ellipses that precess around the compact object's center and these orbits overlap with each other and result in collisions and dissipating the lateral momentum, causing the particles to fall inward at a faster

rate. The matter also heats up as a result of the collisions. At this point, there is nothing to stall the particles' fatal fall through the event horizon.

For a Schwarzschild black hole, all particles with angular momentum per unit mass less than  $\tilde{L} < 2 r_G c$  will eventually be captured by the black hole (Novikov I. a., 1973):

$$r_G = \frac{2GM}{c^2} \quad \tilde{L} < 2 \left( \frac{2GM}{c^2} \right) c = \frac{4GM}{c} \quad (6.1a,b)$$

Inside the accretion disk, angular momentum has to be transferred away outwardly or otherwise dissipated to maintain the continuous infall flow of matter. The condition for capture can be expressed as such:

$$b = \frac{\tilde{L}}{c} < b_{capture} = 2r_G \left( \frac{c}{v_\infty} \right) = \frac{4GM}{cv_\infty} \quad (6.2)$$

The “capture cross section” of the black hole is:

$$\sigma = \pi b_{capture}^2 = 4\pi r_G^2 \left( \frac{c}{v_\infty} \right)^2 = 4\pi \left( \frac{2GM}{c^2} \right)^2 \left( \frac{c}{v_\infty} \right)^2 = \frac{16\pi G^2 M^2}{c^2 v_\infty^2} \quad (6.3)$$

In case of the Kerr black hole, the capture cross section is of the same order of magnitude. The rate at which the black hole gains rest mass per unit time crossing through a sphere of  $r \gg b_{capture}$  is:

$$\dot{M}_0 = \left( \frac{\rho_\infty v_\infty}{4\pi} \right) 4\pi r^2 \Delta\Omega = \rho_\infty v_\infty \sigma = \frac{4\pi r_G^2 \rho_\infty c^2}{v_\infty} \quad (6.4)$$

Recast in typical astrophysical units (Novikov I. a., 1973):

$$\frac{d \left( \frac{M_0}{M_\odot} \right)}{d \left( \frac{t}{10^{10} \text{yrs}} \right)} = 10^{-13} \left( \frac{\rho_\infty}{10^{-24} \frac{g}{\text{cm}^3}} \right) \left( \frac{M}{M_\odot} \right)^2 \left( \frac{v_\infty}{10 \frac{\text{km}}{\text{s}}} \right)^{-1} \quad (6.5)$$

Gas accreting into a black hole, containing magnetic fields, electrons, and ions, interact strongly which causes it to obey fluid-dynamic laws as opposed to laws of non-interacting particles.

We use a hydrodynamic description to discuss the accretion. The black hole is at rest with respect to the gas, and in this case, is a Schwarzschild black hole, thus it is spherically symmetric. The gravitational field at distances greater than the black hole's radius governs the basic characteristics of the flow, including the accretion rate.

The flow at small distances is supersonic and is causally detached from the flow conditions at large distances. The mass flow and other quantities at large distances can be treated using the Newtonian treatment. The motion of the gas is assumed to be adiabatic. Deviations from adiabatic flow (due to radiative losses and transport) can be compensated by modifying the adiabatic index. The flow is governed by two equations: conservation of rest mass and the Euler equation.

$$\dot{M}_0 = 4\pi r^2 \rho u \quad (6.6)$$

$$u \frac{du}{dr} = -\frac{1}{\rho} \frac{d\rho}{dr} - \frac{GM}{r^2} \quad (6.7)$$

where  $\dot{M}_0$  is the total rate of accretion of rest mass,  $u$  is the radial velocity, and  $M$  is the mass of the black hole. Pressure and density is assumed to follow adiabatic law:  $P = K\rho^\gamma$

(6.8)

and speed of sound:

$$a_s = \sqrt{\frac{\gamma P}{\rho}} \quad (6.9)$$

In order to find the accretion  $\dot{M}_0$  and the distributions of density and velocity ( $\rho(r), u(r)$ ) in the flow, we use the Bernoulli equation in this form:

$$\frac{1}{2}u^2 + \frac{1}{\gamma-1} a_s^2 - \frac{GM}{r} = \text{constant} = \frac{1}{\gamma-1} a_\infty^2 \quad (6.10)$$

(where  $a_s$  is the speed of sound, not  $c_s$  and  $a_\infty$  is the speed of sound at infinity).

The enthalpy is written as:

$$W = \frac{a_s^2}{\gamma-1} \quad (6.11)$$

The law of mass conservation is recast with density written in terms of the sound speed:

$$u = \frac{\dot{M}_0}{4\pi\rho_\infty r^2} \left(\frac{a_\infty}{a}\right)^{\frac{2}{\gamma-1}} \quad (6.12)$$

The accretion rate  $\dot{M}_0$  is unknown at this point but once determined, the radial distributions of density, sound speed, and velocity can be determined as well.

The mass flux is determined by invoking the two equations together. The Bernoulli equation for fixed  $r$  defines an ellipse, and the conservation of mass equation for each value of  $r$  defines a hyperbola of power,  $ua^{\frac{2}{\gamma-1}} = \text{constant}$ . Invoking both equations for every value of  $r$ , with two unknowns,  $u$  and  $a$ , gives us two overlapping functions for  $u$  and  $a$ , for each particular radius. Solving the two equations finds the intersection point between the ellipse and hyperbola for each radial value.

In the  $(u, a)$  plane, the curve  $u(a)$  is found parametrically for the intersections of ellipses and hyperbolae. Each pair either has two intersection points, one point of tangency, or no

intersection. If there is no intersection for either curve, there is no possible value of  $u(a)$  at that radial value and thus there is no possible flow. There are only two possible solutions: both curves intersect twice for all values of  $r$ , corresponding to two families of intersection points, or both curves intersect twice for all values of  $r$ , except for one: at  $r = r_s$ , one point of tangency; the sonic point where the flow goes from subsonic to supersonic.

To understand how the mass accretion rate is arrived at, we need to explore the physical context of the equations. There exists a spherical inflow under the influence of gravity. The flow starts off at rest at infinity and starts falling inward at a subsonic speed. At some point during the free-fall, there will be a sonic transition where the flow breaks the sound speed (goes from subsonic to supersonic speeds).

The conservation of mass and steady momentum equations leads us to the sonic point or the sonic radius. The accretion rate  $\dot{M}_0$  can be calculated by calculating the flow velocity at the sonic radius (transition radius, or sonic point)  $r_s$ . The Euler equation is recast in the form:

$$u \frac{du}{dr} = -\frac{a^2}{\rho} \frac{d\rho}{dr} - \frac{GM}{r^2} \quad (6.13)$$

The conservation of mass equation is differentiated with respect to  $r$  and taking  $\frac{du}{dr}$  from Euler's equation:

$$\dot{M} = 4\pi r^2 \rho u, \quad u \text{ being the sound speed} \quad (6.14)$$

$$\nabla * (\rho u) = 0 \rightarrow (4\pi r^2)(\rho u) = \dot{M} = \text{constant} \quad (6.15)$$

The steady momentum equation gives us:

$$(u * \nabla)u = -\frac{1}{\rho} \nabla p - \nabla \psi \quad (6.16)$$

Which leads to:  $u \frac{du}{dr} = -\frac{1}{\rho} \frac{\partial p}{\partial r} - \frac{GM}{r^2}$  (6.17)

And the pressure gradient gives the following relation:

$$\frac{1}{\rho} \frac{\partial p}{\partial r} = \frac{1}{\rho} \frac{\partial p}{\partial \rho} \frac{\partial \rho}{\partial r} = c_s^2 \frac{1}{\rho} \frac{\partial \rho}{\partial r} \quad (6.18)$$

Returning to the conservation of mass equation,

$$\frac{\partial}{\partial r} (r^2 \rho u) = 0 \rightarrow 2r\rho u + r^2 u \frac{\partial \rho}{\partial r} + r^2 \rho \frac{\partial u}{\partial r} = 0 \quad (6.19)$$

$$-\frac{1}{\rho} \frac{\partial \rho}{\partial r} = \frac{2}{r} + \frac{1}{u} \frac{\partial u}{\partial r} \quad (6.20)$$

This leads to:

$$u \frac{\partial u}{\partial r} = -\frac{1}{\rho} \frac{\partial p}{\partial r} - \frac{GM}{r^2} = c_s^2 \left( \frac{2}{r} + \frac{1}{u} \frac{\partial u}{\partial r} \right) - \frac{GM}{r^2} \quad \text{where } c_s = a_s \quad (6.21)$$

$$\frac{d\rho}{dr} \left( \frac{u^2 - a^2}{\rho} \right) = -\frac{GM}{r^2} + \frac{2u^2}{r} \quad (6.22)$$

The sonic point exists where  $a = u$ , so,

$$\frac{2u_s^2}{r} = \frac{GM}{r_s^2} \rightarrow u_s^2 = a_s^2 = \frac{GM}{2r_s} \quad r_s = \frac{GM}{2a_s^2} \quad (6.23a,b,c)$$

Taking this result with Bernoulli's equation, we get the speed of sound at  $r_s$  in terms of speed of sound at infinity:

$$a_s = u_s = a_\infty \left( \frac{2}{5-3\gamma} \right)^{\frac{1}{2}} \quad (6.24)$$

The sonic radius is found by using the last two equations (6.23c and 6.24) together:

$$r_s = \frac{5-3\gamma}{4} \frac{GM}{a_\infty^2} \quad (6.25)$$

The accretion rate can be calculated now (Novikov I. a., 1973):

$$\dot{M}_0 = 4\pi u_s r^2 \left( \frac{a_s}{a_\infty} \right)^{\gamma-1} \rho_\infty \quad (6.26)$$

$$= \frac{4\gamma^2 \alpha G^2 M^2 \rho_\infty}{a_\infty^3} = \alpha r_G^2 c \rho_\infty \left( \frac{m_p c^2}{KT_\infty} \right)^{\frac{3}{2}} \quad (6.27)$$

With  $\alpha$  a constant of order unity depending on  $\gamma$ ;

$$\alpha = \frac{\pi}{4\gamma^{\frac{3}{2}}} \left( \frac{2}{5-3\gamma} \right)^{\frac{(\frac{1}{2})(5-3\gamma)}{\gamma-1}} \approx \begin{cases} 1.5 \text{ for } \gamma = 1 \\ 1.2 \text{ for } \gamma = 1.4 \\ 0.3 \text{ for } \gamma = \frac{5}{3} \end{cases} \quad (6.28)$$

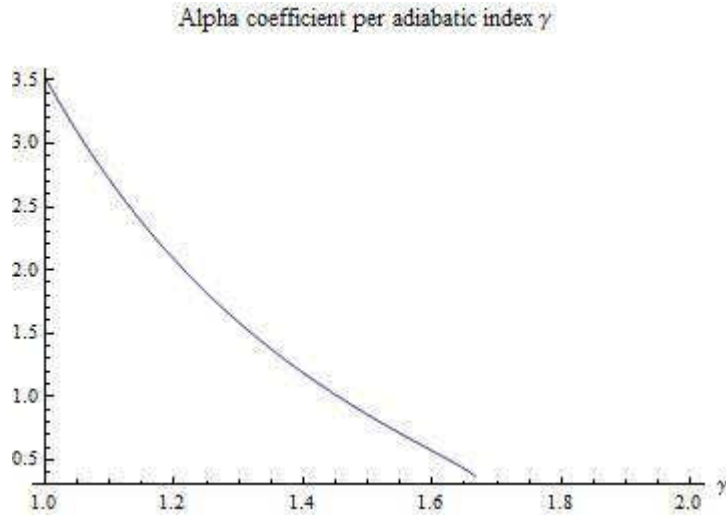


Figure 15. Alpha coefficient versus adiabatic index.

The alpha coefficient is plotted versus value of adiabatic index  $\gamma$ . It decreases with increasing value of  $\gamma$ .

Around a temperature of  $10^4$  K, the gas will be ionized partially so in compression, energy will be diverted into ionization rather than heating the gas itself. The adiabatic index outside and near the sonic point will be below that of ionized gas ( $\gamma < \frac{5}{3}$ ) and  $\gamma = 1.4$  would be more realistic (by Thorne's suggestion, (Novikov I. a., 1973)) for use in future equations.

In the isothermal case, the sound speed  $c_s$  is constant, so the temperature determines  $r_s$ . The density at the sonic point is:

$$\rho_s = \frac{\dot{M}}{4\pi r^2 c_s} \quad (6.29)$$

The Bernoulli equation gives us:

$$\frac{1}{2}u^2 + c_s^2 \ln \rho - \frac{GM}{r} = \frac{1}{2}c_s^2 + c_s^2 \ln \rho_s - \frac{GM}{r_s} \quad \frac{GM}{r_s} = 2c_s^2 \quad (6.30a,b)$$

$$u^2 = 2c_s^2 \left[ \ln \frac{\rho_s}{\rho} - \frac{3}{2} \right] + \frac{2GM}{r} \quad (6.31)$$

For a given density at infinity, we can find the sonic density  $\rho_s$  and with a given black hole mass  $M$  and temperature  $T$ , we can determine the accretion rate. As  $r$  approaches zero, the flow velocity approaches a particular value:  $u^2 \rightarrow \frac{2GM}{r}$ , which is the free-fall velocity for an unit mass element, and as  $r$  approaches infinity, the flow velocity will approach zero, which means that  $\rho_\infty = \rho_s e^{-\frac{3}{2}}$ . (6.32)

The radius of influence is where the black hole's influence diminishes and the density and velocity values approach their values at infinity:

$$r_i = \frac{2GM}{a_\infty^2} = r_g \left( \frac{c}{a_\infty} \right)^2 = \frac{2GM}{c^2} \frac{c^2 r_s}{GM} \left( \frac{4}{5-3\gamma} \right) \quad (6.33a)$$

$$= \left( \frac{8}{5-3\gamma} \right) r_s; \text{ for } \gamma = 1.4, \quad r_i = 10 r_s \quad (6.33b)$$

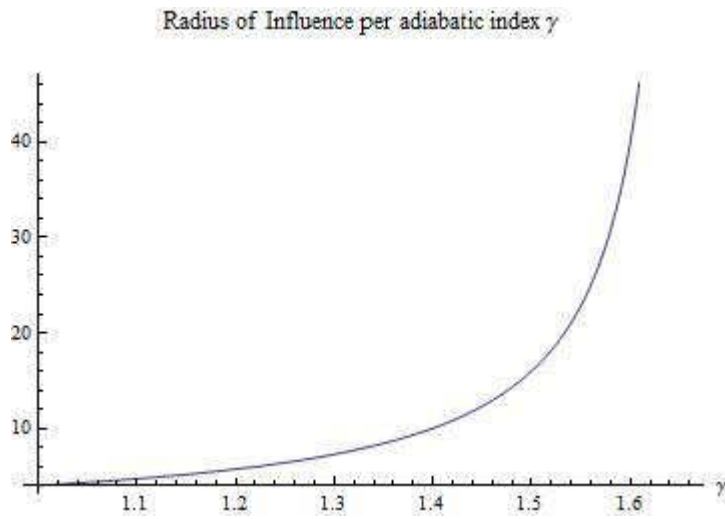


Figure 16. Radius of Influence versus adiabatic index.



The radius of influence is plotted as a function of the adiabatic index,  $\gamma$ , in terms of the sonic radius. The higher the value of  $\gamma$ , the farther out the radius of influence extends out from the central object.

At the radius of influence, the gas falls with a velocity approximately equal to  $a_\infty$  and the density and sound speed increases from that point inward. When it passes the sonic point, the gas is in a near free fall;

$$u = \left(\frac{2GM}{r}\right)^{\frac{1}{2}} = a_\infty \left(\frac{r_i}{r}\right)^{\frac{1}{2}} \text{ for } r < r_s \quad (6.34)$$

So the conservation of mass equation can be written as;

$$\rho = \frac{\dot{M}_0}{4\pi r^2 u} = \frac{\alpha \gamma^{\frac{3}{2}}}{4\pi} \rho_\infty \left(\frac{r_i}{r}\right)^{\frac{3}{2}} \cong 0.2 \rho_\infty \left(\frac{r_i}{r}\right)^{\frac{3}{2}} \quad (6.35)$$

$$\text{for } \gamma = 1.4, \text{ Density coefficient} = \frac{\alpha \gamma^{\frac{3}{2}}}{4\pi} \quad (6.36)$$

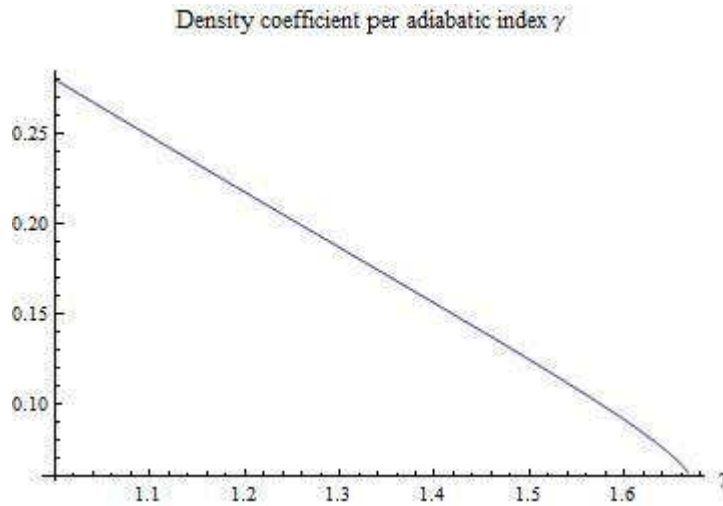


Figure 17. Density coefficient versus adiabatic index.

The value of the density coefficient is plotted as a function of adiabatic index  $\gamma$ . At  $\gamma = 1.4$ , the density coefficient is approximately equal to 0.2. The value of the density coefficient drops with increasing adiabatic index value. The adiabatic index value can give us the distribution of the density in the disk when using the conservation of mass equation (equation 6.6).

With adiabatic compression, the temperature rises as a result (Bondi H. , 1952):

$$\text{at } r < r_s, \quad T = \left( \frac{\alpha \gamma^2}{4\pi} \right)^{\gamma-1} T_\infty \left( \frac{r_i}{r} \right)^{\frac{3}{2}(\gamma-1)} \cong 0.5 T_\infty \left( \frac{r_i}{r} \right)^{\frac{3}{2}(\gamma-1)} \quad (6.37)$$

Knowing the adiabatic index at the sonic point gives the temperature distribution at that radial location. The accretion rate is:

$$\dot{M}_0 = r_G^2 c \rho_\infty \left( \frac{c}{a_\infty} \right)^3 \quad (6.38)$$

$$\cong \left( 1 \times 10^{11} \frac{g}{s} \right) \left( \frac{M}{M_\odot} \right)^2 \left( \frac{\rho_\infty}{10^{-24} \frac{g}{cm^3}} \right) \left( \frac{a_\infty}{10^{-24} \frac{g}{cm^3}} \right) \left( \frac{T_\infty}{10^4 K} \right)^{-\frac{3}{2}} \quad (6.39)$$

$$\text{or } \frac{d \left( \frac{M}{M_\odot} \right)}{d \left( \frac{t}{10^{10} yrs} \right)} \cong (10^{-5}) \left( \frac{M}{M_\odot} \right)^2 \left( \frac{\rho_\infty}{10^{-24} \frac{g}{cm^3}} \right) \left( \frac{a_\infty}{10 \frac{km}{s}} \right)^{-3} \quad (6.40)$$

If in the case of the double QPO signal, the ISCO and the sonic point are coinciding at the same radius, the QPO signal, when using the diskoseismological model discussed in Chapter VIII, yields a value of the adiabatic index value, which also can provide the mass accretion rate at the ISCO as well.

## Magnetic Influence on the Disk

In this section, I discuss the magnetic influence on the disk which is relevant in discussing the rate of accretion in the inner disk. In the disk, for temperatures above  $10^4$  K, the magnetic field lines will be frozen into the gas as it accretes towards the compact object (black hole or neutron star). The strength of the typical intergalactic field is generally about  $10^{-6}$  G, and its energy density generally about  $\sim \frac{B_\infty^2}{8\pi} \sim 4 \times 10^{-14} \frac{\text{ergs}}{\text{cm}^3}$ . At large radii, the field may be of small magnitude that its influence would be negligible.

The magnetic energy in a given fluid element will scale as

$$E_{mag} \propto \frac{B^2}{8\pi} * r^{-\frac{5}{2}} \quad (6.41)$$

as the gas crosses the sonic point, the magnetic energy will increase as to become competitive with the thermal energy in the fluid element:

$$E_{thermal} = 2 * \left(\frac{3}{2}\right) \frac{kT}{m_p} * (\text{mass of element}) \propto r^{\left(-\frac{3}{2}\right)(\gamma-1)} \quad (6.42)$$

At this point, the magnetic pressure must affect the flow and it will deviate from the usual hydrodynamic laws (Novikov I. a., 1973).

The scale of interest for determining the accretion rate is the sonic radius:

$$r_s = \frac{5-3\gamma}{4} \frac{GM}{a_\infty^2} \cong (10^{13} \text{ cm}) \left(\frac{M}{M_\odot}\right) \left(\frac{T}{10^4 \text{ K}}\right)^{-1} \quad (6.43)$$

At the sonic radius,

$$\frac{\lambda_p(r_s)}{r_s} \sim 0.7 \left(\frac{M}{M_\odot}\right)^{-1} \left(\frac{\rho_\infty}{10^{-24} \frac{\text{g}}{\text{cm}^3}}\right)^{-1} \left(\frac{T_\infty}{10^4 \text{ K}}\right)^3 \quad (6.44)$$

The gas with no other external influences will not behave as a fluid near and beyond that point. The interstellar magnetic field can preserve the hydrodynamic approximation in that it deflects protons away from a direct path in a distance of the order of the Larmor radius:

$$\lambda_L = \frac{m_p c v}{e B} \cong (1 \times 10^8 \text{ cm}) \left( \frac{B}{10^{-6} \text{ G}} \right)^{-1} \left( \frac{T}{10^4 \text{ K}} \right)^{\frac{1}{2}} \quad (6.45)$$

This remains true even as the thermal pressure of the plasma overwhelms the magnetic pressure and the field gets dragged along with the spiraling gas. The Larmor radius is small in comparison to the sonic radius so the hydrodynamic approximation is a sufficient description for the gas.

As the gas nears the black hole, relativistic effects will modify the Newtonian scheme of accretion. Starting with the equation for free-fall from near rest for  $r \gg r_g$ :

$$\left( \frac{dr}{d\tau} \right)^2 = v^2 = \frac{2GM}{r} \quad (6.46)$$

and using the conservation of rest mass equation,

$$4\pi \sqrt{-g} \rho \left( \frac{dr}{d\tau} \right) = \dot{M}_0 \quad (6.47)$$

The density of rest mass varies as:

$$\rho = \frac{\dot{M}_0}{4\pi r^2} \left( \frac{r}{2GM} \right)^{\frac{1}{2}} \cong \left( 6 \times 10^{-12} \frac{\text{g}}{\text{cm}^3} \right) \left( \frac{r}{r_g} \right)^{-\frac{3}{2}} \quad (6.48a)$$

$$= \frac{6.0 \times 10^{-9} \frac{\text{kg}}{\text{m}^3}}{1.4 \times 10^3 \frac{\text{kg}}{\text{m}^3}} \left( \frac{r}{r_g} \right)^{-\frac{3}{2}} = (4.3 \times 10^{-12}) \left( \frac{M}{M_\odot} \right) \left( \frac{r}{r_g} \right)^{-\frac{3}{2}} \quad (6.48b)$$

The temperature approaches its Newtonian form as such:

$$T \cong (10^{12} \text{ K}) \left( \frac{r}{r_g} \right) \quad (6.49)$$

A rotating black hole will cause a dragging of the inertial frames that will pull the gas falling towards it in orbital rotation around the black hole. Its angular velocity to an observer at infinity will approach the angular velocity at the horizon (Novikov I. a., 1973):

$$\Omega \rightarrow \Omega_H = \frac{a}{r_H^2 + a^2} = \frac{c^3}{2GM} = \left(\frac{10^5}{s}\right) \left(\frac{M}{M_\odot}\right)^{-1} \quad \text{for } a = M \quad (6.50)$$

with  $a = J/M$ , where  $J$  is the angular momentum per unit mass.

The angular velocity scales as  $1/M$ , so frequencies of particles near the event horizon will be moving at the angular velocity near or approximately that of the black hole at its horizon, which would be scaled to the inverse mass of the black hole as well. The brightness of the accretion disk will be modulated with a period as this equation indicates:

$$P = \frac{4\pi}{\Omega} \geq (10^{-4} \text{ s}) \left(\frac{M}{M_\odot}\right) \quad (6.51)$$

due to the addition of the orbital period and the light travel time between the radius location of one spot at the start of a period to the new radius at the end of the period. I. D. Novikov and K. S. Thorne anticipated the existence of quasi-periodic oscillations in their 1973 publication (Novikov I. a., 1973).

### **Accretion onto a Kerr Black Hole**

At a radius  $r$  larger than  $r = \frac{2GM}{c^2}$ , the kinetic energy is larger than the potential energy  $\frac{GM}{r}$  so the gravity of the black hole does not affect the flow of the gas. At the radius  $r = \frac{2GM}{u_\infty^2}$ , the gravitational effect becomes significant. Due to the flow being supersonic, the gas will react to

the gravity like non-interacting particles--its pressure will have a negligible effect. Its enthalpy is negligible in comparison to its kinetic energy. The flow lines will be hyperbolae.

After passing around the black hole, the particles' trajectories will intersect, culminating in collisions. In the gas-dynamic case, increasing pressure will interfere with the collisions, which cause flow lines to stop intersecting. A shock front develops around the black hole where outside the shock front, the trajectories will be hyperbolae.

The shock front is located where the kinetic energy is equal to the potential energy (Novikov I. a., 1973):

$$\ell_s = \frac{GM}{u_\infty^2} \quad \text{with } \ell_s \text{ being the characteristic size of shock front} \quad (6.52)$$

Within the shock, the gas will have most of its sideways momentum dissipated and its forward momentum unaffected. Beyond the radius of the shock front, the gas will fall directly into the black hole. The dividing line between escape and capture is defined as the impact parameter,  $b_{capture}$ .

The shock is confined to the line of the impact parameter and the value of  $b_{capture}$  will correspond to an orbit where the following condition is met (Hoyle, 1939):

$$\frac{1}{2}v_x^2 = \frac{GM}{x} \quad \text{at } y = 0 \quad b_{capture} = \frac{2GM}{u_\infty^2} \quad (6.53a,b)$$

The mass flux at large radii is  $\rho_\infty u_\infty$ , so the accretion rate is:

$$\dot{M}_0 = (\pi b_{capture}^2) \rho_\infty u_\infty = \frac{4\pi G^2 M^2 \rho_\infty}{u_\infty^3} \quad (6.54)$$

According to Bondi and Hoyle, the accretion rate varies by a factor of 0.5 to 1.0 through careful calculations (Bondi H. H., 1944). With the rotating black hole, it differs from the

stationary black hole with the speed of flow  $u_\infty$  and a numerical coefficient of order unity.

Where sound speed  $a_\infty$  is approximately equal to speed of flow  $u$ , a hybrid formula is invoked

(Bondi H. , 1952):

$$\dot{M}_0 = \frac{4\pi G^2 M^2 \rho_\infty}{(u_\infty^2 + a_\infty^2)^{3/2}} \cong \frac{(1.1 \times 10^{11} \frac{g}{s}) \left(\frac{M}{M_\odot}\right)^2 \left(\frac{\rho_\infty}{10^{-24} \frac{g}{cm^3}}\right)}{\left[\left(\frac{u_\infty}{10 \frac{km}{s}}\right)^2 + \left(\frac{a_\infty}{10 \frac{km}{s}}\right)^2\right]^{3/2}} \quad (6.55)$$

Isolated black holes have low accretion rates ( $\sim 10^{-15} \frac{M_\odot}{yr}$ ), and low luminosities ( $\sim 10^{31} \frac{ergs}{s}$ ) from their accretion disks. Black holes in binary systems have a more steady mass accretion rate per unit time from a secondary star, ejecting mass at rates of  $10^{-5} \frac{M_\odot}{yr}$ , and as a consequence, have definitely higher luminosities ( $10^{37} \text{ ergs/s}$ ). An extreme example is a supermassive black hole that are found in the centers of galaxies, and due to its high mass and gas density in its proximity, will accrete at a much higher rate. Its accretion rate will be about  $10^{-3} \frac{M_\odot}{yr}$ , and its gas emitting a luminosity of  $10^{43} \text{ ergs/s}$ . Accreted mass will have higher angular momentum in binary systems and therefore depend on viscous processes to dissipate the angular momentum to veer away from Keplerian orbits. In those systems, the higher density of gas helps provide these viscous processes, which also causes the gas to heat up and emit radiation. Novikov and Zel'dovich and Shklovsky were among the first ones to propose that accretion onto black holes and neutron stars would produce x-rays (Novikov I. Z., 1966) (Shklovsky, 1967).

## Luminosity of an Accretion Disk

The luminosity also depends on the accretion rate. The Euler equation presents a qualitative picture of the deposition of gas into the disk and redistribution of angular momentum within the disk. The majority of the gravitational energy is released and the majority of the luminosity is emitted from the inner disk in contrast to the outer disk where angular momentum is dissipated. An understanding of the disk structure helps to clarify the events associated with the phenomenon.

Viscous stresses dissipate angular momentum from each gas element, enabling its path to turn into an inward spiral towards the compact object. The angular momentum is redistributed from the inner parts to the outer parts of the disk, its redistribution being mediated by the viscous stresses.

The shearing orbital motion of the inner disk gas, moving against the viscous stresses, heats up due to frictional heating. The heat reaches the point where the gas cannot contain it so the heat is radiated away through the broad sides of the disk.

The total energy emitted by an unit mass of a gas element moving through the disk must equal the gravitational binding energy of the unit mass at the point it reaches the inner edge of the disk, or the ISCO;

$$\begin{aligned} \check{E}_{bind} &\approx \frac{1}{2} \left( \frac{M_0}{R_0} \right) \approx 10^{-4} \text{ for a white dwarf} & (6.56) \\ &\approx 0.05 \text{ for a neutron star} \end{aligned}$$

With a black hole, the inner edge is the ISCO where the orbits remain Keplerian up until that point;



$$\begin{aligned}\tilde{E}_{bind} &\approx 0.057 \text{ for a Schwarzschild black hole} \\ &\approx 0.42 \text{ for a maximally rotating Kerr black hole}\end{aligned}$$

The total luminosity of the disk is:

$$L \sim 10^{-4} \dot{M}_0 \sim \left(10^{34} \frac{\text{ergs}}{\text{s}}\right) \left(\frac{\dot{M}_0}{\frac{10^{-9} M_\odot}{\text{yr}}}\right) \text{ for a white dwarf} \quad (6.57)$$

$$L \sim 0.1 \dot{M}_0 \sim \left(10^{38} \frac{\text{ergs}}{\text{s}}\right) \left(\frac{\dot{M}_0}{\frac{10^{-9} M_\odot}{\text{yr}}}\right) \text{ for a neutron star or black hole} \quad (6.58)$$

where  $\dot{M}_0$  is the accretion rate. For a star containing a magnetic field, the plasma hits the star's magnetic field with a kinetic energy equal to the gravitational binding energy  $\tilde{E}_{bind}$ .

The black hole absorbs all of the ensuing radiation so the disk is the only source of emission.

If the total luminosity approaches the Eddington limit,

$$L_{Edd} \cong \left(10^{38} \frac{\text{ergs}}{\text{s}}\right) \left(\frac{M}{M_\odot}\right). \quad (6.59)$$

The radiation pressure will distort the disk and disrupt the overall accretion. For  $L \ll L_{Edd} = L_{crit}$ , there exists an accretion rate of

$$\dot{M}_0 \ll \dot{M}_{0crit} \sim \begin{cases} 10^{-5} \frac{M_\odot}{\text{yr}} \text{ for a white dwarf} \\ 10^{-8} \frac{M_\odot}{\text{yr}} \text{ for a black hole or neutron star} \end{cases},$$

In the compact object's inertial frame and neglecting tidal gravitational forces of a secondary star, an accretion rate  $\dot{M}_0$  is given. The specific angular momentum of gas at radius  $r$  is:

$$\tilde{L} = \left(\frac{M}{r^3}\right)^{\frac{1}{2}} * r^2 = (Mr)^{\frac{1}{2}} \text{ with } M \text{ being the mass of the compact object} \quad (6.60)$$

A gas element must lose its angular momentum at the outer edge of the disk to reach the compact object so the rate at which its angular momentum is shed to passing gases within the disk is:

$$j = \dot{M}_0 \times \tilde{L} \text{ (at the outer edge of the disk } r_0) \quad (6.61a)$$

$$= \dot{M}_0 (Mr_0)^{\frac{1}{2}} \quad (6.61b)$$

The accretion rate and the outer edge of the disk will correct itself until this relation is satisfied, by any further dissipation by passing gas from the outer regions.

In the inner regions of the disk, the velocities of the gas are to be determined.  $\rho_0$  is the mass density, and  $2h$  is the disk thickness (height) and  $\Sigma = 2h\rho_0$ , (6.62)

where  $\Sigma$  is the surface density ( $\rho/cm^2$ ) at radius  $r$ .  $v^r$  is the radial velocity of the gas and negative in this case ( $v^r < 0$ ). The orbital velocity  $v^\phi$  and angular velocity  $\Omega$  is:

$$v^\phi = r\Omega = \left(\frac{M}{r}\right)^{\frac{1}{2}} \quad (6.63)$$

Due to viscous processes, the radial velocity will never surpass the orbital velocity ( $v^r < v^\phi$ ). The viscous stress (orthonormal to radius  $r$ ) is:

$$t_{\phi r} = -2\eta\sigma_{\phi r} \quad (6.64)$$

$$\sigma_{\phi r} = -\frac{3}{4}\Omega = -\frac{3}{4}\left(\frac{M}{r^3}\right)^{\frac{1}{2}} \quad (6.65)$$

where  $\eta$  is the coefficient of dynamic viscosity. The stress is related to the shear of the circular Keplerian orbits. Four conservation laws define the steady-state accretion disk structure, and, all depend on the accretion rate, which will be discussed now.

### Conservation of rest-mass

Mass flows through a cylinder of radius  $r$  at a rate equal to the accretion rate:

$$\dot{M}_0 = -2\pi r \Sigma v^r \quad (6.66)$$

### Angular momentum conservation

Angular momentum is carried inward across radius  $r$  by infalling gas at a rate equal to the rate viscous stresses transfer angular momentum out through same radius  $r$ , plus the rate  $\dot{J}_c$ , being the amount of angular momentum deposited into the compact object:

$$\dot{M}_0 (Mr)^{\frac{1}{2}} = 2\pi r * 2h * t_{\phi r} + \dot{J}_c \quad (6.67)$$

The angular momentum  $L_c$  deposited into the compact object cannot exceed the Keplerian angular momentum at the inner edge of the disk,  $r_I$ , so:

$$\dot{J}_c = \beta \dot{M}_0 (Mr_I)^{\frac{1}{2}} \text{ for some } |\beta| \ll 1 \quad (6.68)$$

Solving for stress and disk thickness (height):

$$\begin{aligned} 2ht_{\phi r} &= \frac{\dot{M}_0}{2\pi r^2} \left[ (Mr)^{\frac{1}{2}} - \beta (Mr_I)^{\frac{1}{2}} \right] \\ &\cong \frac{\dot{M}_0 (Mr)^{\frac{1}{2}}}{2\pi r^2} \quad \text{for } r \gg r_I \end{aligned} \quad (6.69)$$

The viscous stress product is determined by the accretion rate and mass of the compact object. If the viscous stress product is smaller than the equation above, the viscous stresses will not redistribute the mass flow fast enough, and the mass will accumulate in the region and inflate the

disk height and increase the viscous stresses in the region (Thorne, 1973).

### Energy conservation

Energy conservation is also dependent on the accretion rate. Heat is produced via viscosity at a rate per unit volume:

$$\epsilon = 2\eta\sigma^2 = 4\eta(\sigma_{\phi r})^2 = -2t_{\phi r}\sigma_{\phi r} \quad (6.70)$$

The heat generated per unit area as a result is:

$$2h\epsilon = (2ht_{\phi r})(-2\sigma_{\phi r}) = \frac{3\dot{M}}{4\pi r^2} \frac{M}{r} \left[ 1 - \beta \left( \frac{r_I}{r} \right)^{\frac{1}{2}} \right] \quad (6.71)$$

and the heat generated between the radii  $r_1$  and  $r_2$ :

$$\int_{r_1}^{r_2} 2h\epsilon \, 2\pi r \, dr = \frac{3}{2} \dot{M}_0 \left[ \frac{M}{r_1} \left( 1 - \frac{2}{3} \beta \left( \frac{r_I}{r} \right)^{\frac{1}{2}} \right) - \frac{M}{r_2} \left( 1 - \frac{2}{3} \beta \left( \frac{r_I}{r} \right)^{\frac{1}{2}} \right) \right] \quad (6.72)$$

$$\cong \frac{3}{2} \dot{M}_0 \left( \frac{M}{r_1} - \frac{M}{r_2} \right) \quad r_2 \gg r_1 \gg r_I$$

Half of the gravitational potential energy goes into heating and the remainder due to the virial theorem, goes into the orbital kinetic energy. The rate of conversion of gravitational energy into heat is:

$$E = \frac{1}{2} \dot{M}_0 \left( \frac{M}{r_1} - \frac{M}{r_2} \right) \quad (6.73)$$

The viscous stresses transfer the angular momentum and energy outward at radius  $r$ . The energy transfer rate through radius  $r$  is:

$$\dot{E} = \Omega j = \Omega(2\pi r * 2h * t_{\phi r} r) = \dot{M}_0 \left[ \frac{M}{r} \left( 1 - \frac{2}{3} \beta \left( \frac{r_I}{r} \right)^{\frac{1}{2}} \right) \right] \quad (6.74)$$

Energy through viscosity between  $r_1$  and  $r_2$  injected is:

$$\dot{M}_0 \left[ \frac{M}{r_1} \left( 1 - \frac{2}{3} \beta \left( \frac{r_I}{r} \right)^{\frac{1}{2}} \right) - \frac{M}{r_2} \left( 1 - \frac{2}{3} \beta \left( \frac{r_I}{r} \right)^{\frac{1}{2}} \right) \right] \quad (6.75)$$

The energy injection rate plus the gravitational potential deposition energy is equal to the total heating rate. As  $r \gg r_I$  (inner edge radius), gravity accounts for one-third of the heating. The remainder is redistributed via viscous stresses.

If all the heat were retained within the disk, the thermal energy would be 3/2 times the gravitational potential energy, which is unrealistically high. Thermal bremsstrahlung and radiative processes would radiate away the heat before it reached such heights and remove it altogether.

The total flux from the top and bottom sides of the disk must equal the heating rate per unit area:

$$F = \frac{3\dot{M}_0 M}{8\pi r^2 r} \left[ 1 - \beta \left( \frac{r_I}{r} \right)^{\frac{1}{2}} \right] \quad (6.76)$$

The total power radiated is:

$$L = \int_{r_I}^{\infty} 2F * 2\pi r dr = \left( \frac{3}{2} - \beta \right) \dot{M}_0 \frac{M}{r_I} \quad (6.77)$$

Gravity provides  $\frac{1}{2} \dot{M}_0 \frac{M}{r_I}$  and rotational energy provides  $(1 - \beta) \dot{M}_0 \frac{M}{r_I}$  of the total energy.

In terms of the blackbody radiation spectrum, the surface temperature of the disk at radius  $r$  is:

$$T_s = \left( \frac{4F}{b} \right)^{\frac{1}{4}} \cong (3 \times 10^7 K) \left( \frac{\dot{M}_0}{10^{-9} \frac{M_{\odot}}{yr}} \right)^{\frac{1}{4}} \left( \frac{M}{M_{\odot}} \right)^{-\frac{1}{2}} \left( \frac{M}{r} \right)^{\frac{3}{4}} \left[ 1 - \beta \left( \frac{r_I}{r} \right)^{\frac{1}{2}} \right] \quad (6.78)$$

Since most of the radiation is emitted from the radius  $r \sim 10 M$  for a black hole or neutron star,

and the blackbody spectrum peaks at  $h\nu_{MAX} \approx (2.44 \times 10^{-4} \text{ eV}) \left(\frac{T_s}{K}\right)$ . (6.79)

The spectrum of the disk should peak at:

$$h\nu_{MAX} \approx (1 \text{ keV}) \left(\frac{\dot{M}_0}{10^{-9} \frac{M_\odot}{\text{yr}}}\right)^{\frac{1}{4}} \left(\frac{M}{M_\odot}\right)^{-\frac{1}{2}} \quad (6.80)$$

which indicates a disk can emit x-rays (1 – 10 keV) for reasonable accretion rates although the x-ray spectrum should fall rapidly for increasing energy. The electron-scattering opacity interferes with the blackbody radiation emission, and as a result, the spectrum peaks at energies above the expected values.

### Thin Disks, Slim Disks and ADAFs

For thin and slim disk models, physical quantities are vertically integrated. Surface density can be defined as:

$$\Sigma(r) = \int_{-H(r)}^{H(r)} \rho(r, z) dz \quad (6.95)$$

where  $z = H(r)$  is the surface of the accretion disk.

A set of general relativistic equations govern the physics of thin disks, slim disks and ADAFs. They are the following equations:

For mass conservation (Sadowski, 2009):

$$\dot{M} = -2\pi\Sigma\Delta^{\frac{1}{2}}\frac{V}{(1-V^2)^{\frac{1}{2}}} \quad (6.96)$$

where  $V$  is the gas radial velocity measured by an observer at fixed  $r$ , co-rotating with the fluid

and

$$\Delta = r^2 - 2Mr - a^2 \quad (6.97)$$

For radial momentum conservation:

$$\frac{V}{(1-V^2)^{\frac{1}{2}}}\frac{dV}{dr} = \frac{\mathcal{A}}{r} - \frac{1}{\Sigma}\frac{dP}{dr} \quad (6.98)$$

where

$$\mathcal{A} = -\frac{MA}{r^3\Delta\Omega_k^+\Omega_k^-}\frac{(\Omega-\Omega_k^+)(\Omega-\Omega_k^-)}{1-\tilde{\Omega}^2\tilde{R}^2} \quad (6.99)$$

and  $\Omega = \frac{u^\phi}{u^t}$ , being the angular velocity with respect to the stationary observer,  $\tilde{\Omega} = \Omega - \omega$ , is

the angular velocity with respect to the inertial observer,  $\Omega_K$  is the Kelperian velocity,

$$(6.100a,b)$$

$$\Omega_K^\pm = \pm\left(\frac{M}{R^3}\right)^{\frac{1}{2}}\frac{1}{1\pm\left(\frac{M}{R^3}\right)^{\frac{1}{2}}} \quad (6.101)$$

and  $\tilde{R} = \frac{A}{r^2\Delta^{\frac{1}{2}}}$ , is the radius of gyration.

$$(6.102)$$

For angular momentum conservation:

$$\frac{M}{2\pi}(L - L_{in}) = \frac{A^{\frac{1}{2}}\Delta^{\frac{1}{2}}\gamma}{r}\alpha P \quad (6.103)$$

where  $L = u_\phi$ , is the specific angular momentum,  $\gamma$  the Lorentz factor,  $P = 2Hp$ , is the vertically integrated pressure,  $\alpha$  the standard alpha viscosity,  $L_{in}$ , the angular momentum at horizon.

$$(6.104a,b)$$

For vertical equilibrium:

$$\frac{P}{\Sigma H^2} = \frac{L^2 - a^2(\epsilon^2 - 1)}{2r^4} \quad (6.105)$$

with  $\epsilon = u^t$ , being the conserved energy associated with time symmetry.

For Energy conservation:

$$-\frac{\alpha P A \gamma^2}{r^3} \frac{d\Omega}{dr} - \frac{32}{3} \frac{\sigma T^4}{\kappa \Sigma} = -\frac{\dot{M}}{2\pi r \rho} \frac{1}{\Gamma^3 - 1} \left( \frac{dp}{dr} - \Gamma_1 \frac{p}{\rho} \frac{d\rho}{dr} \right) \quad (6.106)$$

where  $T$  is the temperature in the equatorial plane.

Through algebraic rearrangement, the thin disk equations can be reduced to two ordinary differential equations in terms of two dependent variables:

$$\text{Mach number: } M = -\frac{V}{c_s^2} = -\frac{V\Sigma}{P} \quad \text{angular momentum: } L = u_\phi \quad (6.107a,b)$$

$$\frac{d \ln M}{d \ln r} = \frac{N_1(r,M,L) d \ln L}{D(r,M,L) d \ln r} = \frac{N_2(r,M,L)}{D(r,M,L)} \quad (6.108)$$

The numerators must vanish at the same radius as the denominator, which it does at the sonic radius  $r_{sonic}$ , where the Mach number is equal to unity. The equation,

$$D(r, M, L) = 0 \quad (6.109)$$

determines the location of the sonic radius. The conditions at the sonic radius are satisfied only for one value of the angular momentum at the horizon ( $L_{in}$ ), which is the eigenvalue of the system.

For given  $\alpha$ , the sonic point relies on the mass accretion rate. With low accretion rates, the transonic transition happens near the ISCO and this has been determined for rates less than  $0.4 M_{Edd}$ . Around this point a change occurs reflecting a phase transition from that of the



Shakura-Sunyaev behavior to different slim disk behavior. For this accretion rate a double QPO frequency is made possible due to the vertical epicyclic frequency being coupled to the radial epicyclic frequency at the same time. If the accretion rate rises above this rate, the sonic point shifts into the plunging region and the vertical epicyclic frequency will be decoupled from the radial epicyclic frequency and suppressed due to the turmoil that occurs in that region.

As the accretion rate increases, the sonic point shifts away from the ISCO. For low  $\dot{m}$ , the sonic point moves closer to the horizon. For higher  $\alpha$  ( $\alpha > 0.2$ ), the sonic point moves further out for increasing accretion rates.

Four important quantities (temperature and mass density distribution, radius of influence, and the accretion rate) are loosely dependent on the adiabatic index of the gas and determining the value of the index can determine these quantities immediately. That would give us a larger picture of the accretion disk system in one single move.

## CHAPTER VII

### DISKSEISMOLOGY

I delve into this topic to provide more information and context in the kinds of waves and perturbations that occur in the gas of accretion disks. The perturbations can persist and form in specific patterns on the surface of any stellar body, including an accretion disk. It also focuses on the sources that can power the perturbations, including pressure and gravity.

Focusing on how gravity induces perturbations in the gas of accretion disks and how they travel over distances and pulsate in the body of the disk reveals information about the interior of the accretion disk. Pressure also becomes important in terms of how any radially directed motion can be translated into a lateral (or vertical) motion through coupled oscillations.

We start with focusing on the timescales of the dynamic processes.

Three timescales are necessary when it comes to non-stationary processes within accretion disks, which correspond to an instability for each:

$t_{dyn}$ : dynamical timescale for dynamical instabilities

$t_{th}$ : thermal timescale for thermal instabilities

$t_{vis}$ : viscous timescale for viscous instabilities

In the case of thin accretion disks, the timescales are estimated to have the following relationships:

$$t_{dyn} \sim \frac{1}{\Omega} \quad t_{ih} \sim \frac{t_{dyn}}{\alpha} \quad t_{vis} \sim \frac{t_{th}}{\left(\frac{H}{r}\right)^2} \quad (7.1a,b,c)$$

and  $t_{dyn} \ll t_{th} \ll t_{vis}$ .

The Eulerian perturbations can be used to express any and all physical quantities using a function:

$$\delta W \propto \frac{\delta p}{\rho} \quad (7.2)$$

Due to the stationary and axisymmetrical nature of the accretion disk, the angular and time dependence are factored out for

$$\delta W = W(r, z) e^{i(m\phi - \sigma t)} \quad (7.3)$$

with the eigenfrequency  $\sigma(r, z) = \omega - m\Omega$ , and  $m$  being the azimuthal wave number. (7.4)

A general assumption that the oscillation modes in the radial direction are greater than in the vertical direction,  $z = r \cos(\theta)$ , is usually used for most, if not all, cases. (7.5)

This creates two separable ordinary differential equations for the function's amplitude (Perez, *Relativistic Diskoseismology. I. Analytical Results for Gravity Modes*, 1997),

$$W(r, z) = W_r(r) W_y(r, y): \quad (7.6)$$

$$\frac{d^2 W_r}{dr^2} = \frac{1}{\omega^2 - \omega_r^2} \left[ \frac{d}{dr} (\omega^2 - \omega_r^2) \right] \frac{dW_r}{dr} + \frac{(u^t)^2 g_{rr}}{c_s} (\omega^2 - \omega_r^2) \left( 1 - \frac{\tilde{\Psi}}{\tilde{w}^2} \right) W_r = 0 \quad (7.7)$$

with  $y = (z/H)[\Gamma(\Gamma - 1)]^{\frac{1}{2}}$  being the rescaled vertical coordinate,  $\Gamma$  the adiabatic index,  $\tilde{w}(r)$  the ratio of epicyclic frequencies,  $g$  a function of  $\Gamma$ , and  $\tilde{\Psi}$  the eigenvalue of the WKB separation function.

$$(1 - y^2) \left( \frac{d^2 W_y}{dy^2} \right) - 2gy \frac{dW_y}{dy} + 2g[\tilde{w}^2 y^2 + \tilde{\Psi}(1 - y^2)] W_y = 0 \quad (7.8)$$

The eigenfunction  $w_r$  varies rapidly with  $r$ , while the eigenfunction  $w_y$  varies slowly. The

boundary conditions depend on the capture zone and type of mode involved.

Oscillations within the thin accretion disks are expressed in terms of  $\Psi(r, \theta)$ , including the angular, vertical, and radial mode numbers, involving the numbers of nodes in each mode, these being  $m, j$ , and  $n$ , respectively.

A radial mode oscillates in the range  $r > r_i$ , (outside the inner radius), where this condition is satisfied:

$$(\omega^2 - \omega_r^2) \left(1 - \frac{\Psi}{\omega^2}\right) > 0 \quad (7.9)$$

Two points where  $r = r_{\pm}(m, a, \sigma)$  are the locations of the ‘‘Lindblad resonances’’. They signify boundaries where different modes can exist, as we will see in the next section.

### **Vibration Modes**

Three modes exist within the accretion disks:

P-modes, which are inertial acoustic modes where  $\Psi < \tilde{w}^2$  and are trapped in two regions where  $w^2 > w_r^2$  within the inner and outer radii of the disk. The inner p-modes exist in the region between the inner disk edge and the radial epicyclic frequency at  $r_i < r < r_-$  where the gas accretes at a rapid rate. The outer p-modes exist in the region  $r_+ < r < r_o$ . These modes are responsible for stronger luminosity fluctuations, and appear at frequencies higher than the radial epicyclic frequency. Pressure is the driving force behind these modes.

G-modes are inertial gravity modes where  $\Psi > w_r^2$  and are trapped in the region  $r_- < r < r_+$  where  $w^2 < w_r^2$ . G-modes are trapped by gravity within the cavity of the radial epicyclic

frequency and tend to be the most prominent modes. This region also contains the maximum temperature of the disk. In a co-rotating frame, the modes correlate to low frequencies. Gravity is the driving force behind these modes.

C-modes are known as corrugation modes that occur in the region near the inner disk edge where  $\Psi = \tilde{w}^2$ . They are non-radial and precess at a slow rate around the rotation axis. The c-modes are moderated by a radial dependence of the vertical epicyclic frequency.

In the co-rotating frame, the c-mode manifests in the highest frequencies.

All the modes have frequencies that are inversely related to the mass of the central object. With a small viscosity ( $\nu \propto \alpha \ll 1$ ), the modes grow on a dynamical timescale, which means the disk will eventually become unstable as a result and disperse.

Geometrically thick accretion disks in all cases permit axisymmetric modes that correspond to oscillations of the disk at radial and vertical epicyclic frequencies. Solving the relativistic Papaloizou-Pringle equation yields modes, where  $m = 0$ , including p-, g-, and c-modes (Abramowicz M. B., 2006).

(7.10)

$$\begin{aligned} & \frac{1}{g^{\frac{1}{2}}} \left[ \partial_i \left[ (-g)^{\frac{1}{2}} g^{ij} f^n \partial_j W \right] \right] - (m^2 g^{\phi\phi} - 2mwg^{t\phi} + w^2 g^{tt}) f^n W \\ & = - \frac{(u^t)^2 (w - m\Omega)^2}{c_s^2} f^{n-1} W \end{aligned}$$

Which is incumbent on the boundary condition where the Lagrangian perturbations in pressure at the unperturbed incident surface ( $f = 0$ ) disappears:

$$\Delta p = \delta p + \xi^\alpha \nabla_\alpha p = 0 \quad (7.11)$$

the subscript zero relates to the pressure maximum  $r_1$ ,  $g$  is the determinant of the metric,  $\xi^\alpha$  is the Lagrangian displacement vector.

There are two equations in this eigenvalue problem that contains three frequencies: radial epicyclic frequency,  $\omega_r$ , vertical epicyclic frequency,  $\omega_\theta$ , and the characteristic frequency of modes,  $\kappa$ . A thick disk contains a zero co-rotating frequency mode and incompressible modes correlating to oscillations of the disk at the radial and vertical epicyclic frequencies as well as the inertial pressure and gravity waves.

An eigenfunction gives two modes with eigenfrequencies:

$$W = axy \quad (\text{x and y both odd}) \quad (7.12)$$

and the eigenfrequencies:

$$\bar{\sigma}_0^2 = \frac{1}{2} \left[ \omega_r^2 + \omega_\theta^2 \pm [(\omega_r^2 + \omega_\theta^2) + 4\kappa_0^2 \omega_\theta^2]^{\frac{1}{2}} \right] \quad (7.13)$$

Where  $\bar{\sigma}_0 = \frac{\sigma_\theta}{\Omega_0}$ .

The positive square root correlates to a surface gravity mode. The negative square root correlates to an incompressible c-mode, with a poloidal velocity field signifying a circulation about the pressure maximum.

Another eigenfunction containing three arbitrary constants yields two modes with eigenfrequencies:

$$W = a + bx^2 + cy^2 \quad (\text{x and y both even}) \quad (7.14)$$

and the eigenfrequencies:

$$\bar{\sigma}_0^2 = \frac{1}{2n} \left[ \left( (2n+1)(\omega_1^2 + \omega_2^2) - (n+1)\kappa_0^2 \pm \left[ ((2n+1)(\omega_z^2 - \omega_r^2)^2 + (n+1)\kappa_0^2)^2 + 4(\omega_r^2 - \kappa_0^2)\omega_\theta^2 \right]^{\frac{1}{2}} \right) \right] \quad (7.15)$$

The positive sign refers to an acoustic mode with the velocity field of an undulating mode. The negative sign refers to a gravity wave, with a velocity field that appears like a plus-mode.

### Basic oscillation properties

The oscillations are treated as small perturbations from a static equilibrium position and rotations as well as other perturbation from the spherical symmetry structure can be treated using a perturbation analysis.

Linearized perturbation equations describe the oscillations around a spherical equilibrium structure. Modes rely on co-latitude and longitude within the reference system invoked, namely  $\theta$  and  $\varphi$ , in spherical coordinates  $(r, \theta, \varphi)$  as using a spherical harmonic function  $Y_{lm}(\theta, \varphi)$ . The numbers  $l$ , signify the degree (which indicates the number of nodal surface lines and the complexity of the mode), and the azimuthal order  $m$ , (number of nodes around the equator), respectively. The modes are further characterized by the radial order number,  $n$ , which indicates the number of nodes along the radial direction (Scuflaire, 1974) (Osaki, 1975) (Takata, 2005).

## Properties of the nodes

The perturbations  $dp$  and  $d\rho$  (pressure and density, respectively) are related by:

$$\frac{dp}{p} = \Gamma_1 \frac{d\rho}{\rho}; \quad \Gamma_1 = \left( \frac{d \ln p}{d \ln \rho} \right) \quad (7.16)$$

which is the derivative corresponding to an adiabatic change. The frequencies of oscillation can be determined in the adiabatic approximation, following the motion (Lagrangian perturbations).

Using the equation, it is possible to derive precise frequencies. Gough has derived an approximation equation to find the frequency (Deubner, 1984) (Gough, EBK quantization of stellar waves., 1986) (Gough, Course 7. Linear adiabatic stellar pulsation., 1993):

$$\frac{d^2 X}{dr^2} = K(r) X \quad (7.17)$$

Where

$$K(r) = \frac{\omega^2}{c^2} \left[ 1 - \frac{\omega_p^2}{\omega^2} - \frac{S_l^2}{\omega^2} \left( 1 - \frac{N^2}{\omega^2} \right) \right] \quad (7.18)$$

$$X = c_s^2 \rho^{\frac{1}{2}} \text{div } dr \quad (7.19)$$

and  $c_s$  is the adiabatic sound speed, and  $dr$  is the displacement vector.

The behavior of the mode is determined by three characteristic frequencies:

Acoustic (Lamb) frequency  $S_l$ :

$$S_l^2 = \frac{l(l+1)c^2}{r^2} \quad (7.20)$$



Buoyancy (Brunt-Vaisala) frequency  $N$ :

$$N^2 = g \left( \frac{1}{\Gamma_1} \frac{d \ln p}{dr} - \frac{d \ln \rho}{dr} \right) \quad (7.21)$$

Acoustical cut-off frequency  $w_c$ :

$$w_c^2 = \frac{c^2}{4H^2} \left( 1 - 2 \frac{dH}{dr} \right) \quad H = - \left( \frac{d \ln \rho}{dr} \right) \quad (7.22)$$

where  $H$  is the density scale height.

With radiation pressure and degeneracy neglected, the adiabatic index for most stars is given as:

$$c_s^2 \approx \frac{5}{3} \frac{k_B T}{\mu m_H} \rightarrow \gamma = \frac{5}{3} \quad (7.23)$$

with  $k_B$  being Boltzmann's constant,  $T$  the temperature,  $\mu$  the mean molecular weight, and  $m_\mu$  the atomic mass unit.

The buoyancy frequency is further modified:

$$N^2 = g^2 \frac{\rho}{p} [\nabla_{ad} - \nabla + \nabla_\mu] \quad (7.24)$$

$$\nabla = \frac{d \ln T}{d \ln p} \quad \nabla_{ad} = \left( \frac{d \ln T}{d \ln p} \right)_{ad} \quad \nabla_\mu = \frac{d \ln \mu}{d \ln p} \quad (7.25a,b,c)$$

with  $g$  being the local gravitational acceleration.

In areas of ongoing nuclear fusion,  $\mu$  increases with depth and therefore pressure so  $\nabla_\mu$  leads to a positive contribution to  $N^2$ .

A mode oscillates as a function of  $r$  for  $K(r) > 0$  and varies on an exponential scale for  $K(r) < 0$ . For positive  $K(r)$ , the mode is a propagative mode, and for negative  $K(r)$ , the mode is an evanescent one.

Where the values of  $K(r)$  equals zero, those data points are described as turning points of the mode (Schmitz, 1998) (Gough, Course 7. Linear adiabatic stellar pulsation., 1993). The

mode, situated in a single region, has a large amplitude that its frequency is determined by the region is defined as a trapped mode.

Near the surface,  $S_l \ll w$  and  $w_c$  is the dominant factor in the mode behavior. Modes with frequencies below that of  $w_c$  decay exponentially in the atmosphere and are trapped inside the star itself.

In the remainder of the star,  $w_c$ 's role diminishes and  $S_l$  and  $N$  takes a re-dominating role in the mode behavior. For main sequence stars,  $N$  is low throughout the star so the default controlling influence reverts to  $S_l$ .

The eigenfunction oscillates as a function of  $r$  near the surface where  $w = w_c$  and a lower turning point at  $r = r_t$ , where:

$$\omega = S_l(r_t); \text{ or } \frac{c(r_t)^2}{r_t^2} = \frac{\omega^2}{l(l+1)} \quad (7.26)$$

This is indicative of a typical p-mode. For lower temperatures,  $r_t$  is small and the mode extends through most of the star, including the core. The radial p-mode extends to the center of the star. At the surface, where the radius is at the lower turning point,  $r_t$ , a total internal reflection occurs.

G-modes are characterized by the feature of  $w < N$ , and the mode being oscillatory in that region, especially for low frequency modes with  $w \ll S_l$  in most of the star.

$N$  may reach high value around the core of AGB stars.  $K$  can be positive at high frequencies in the outer regions where  $w$  overwhelms  $S_l$  and  $N$ , and the mode behaves as a p mode, and in the core where  $w$  is dominated by  $S_l$  and  $N$ , and the mode behaves as a g mode.

A particular property of the oscillation modes is the inertia:

$$E = \frac{\int_V |\delta r|^2 \rho dV}{M |\delta r|_{ph}^2} = \frac{M_{mode}}{M} \quad (7.27)$$

which defines the mode mass  $M_{mode}$ , and  $M$  being the mass of the star, and  $|\delta r|_{ph}$  being the norm of photospheric displacement.

Modes, trapped within the star with a large evanescent region between the trapping region and the surface, will have a large value of  $E$  (energy). The kinetic energy of the oscillation is indicated as:

$$E_{kin} = \frac{1}{2} M_{mode} V_{rms}^2 = \frac{1}{2} M E V_{rms}^2 \quad (7.28)$$

with  $V_{rms}$  being the photospheric rms velocity.

### Variations from Spherical Symmetry

With an spherically symmetric star, the properties of modes are independent of the integer  $m$ .

Departing from spherical symmetry causes  $m$  to come into play, especially with rotation. This would be important in a cylindrical reference frame. A rotating star has an angular velocity  $\Omega(r)$ , and while depending on  $r$ , also relates to  $m$  via this equation:

$$w_{nlm} = w_{nl0} + m \beta_{nl} \langle \Omega \rangle_{nl} \quad (7.29)$$

where  $\langle \Omega \rangle_{nl}$  is the average of  $\Omega$  that rely on properties of the eigenfunction in the non-rotating reference system (Ledoux, 1951) (Hansen, 1977) (Gough, A new measure of the solar rotation, 1981). The constant  $\beta_{nl}$  tends towards one for high order acoustic modes. For higher order g-modes (Wolff, 1974),

$$\beta_{nl} \simeq 1 - \frac{1}{l(l+1)} \quad (7.30)$$

In the scenario where the axis of rotation points towards the viewer, only  $m = 0$  modes are seen and no rotational splitting is observed. The opposite has the viewer looking upon the star on the equatorial plane and seeing only modes with  $|l-m|$  being even and the rotational splitting the largest for  $m = \pm l$ .

A particular dilemma exists with observing a rotating star: the difficulty of determining both the rotation rate and the inclination of the rotation axis from the splitting and the amplitudes of the split modes (Gizon, 2003). With a rotation rate twice that of the sun, it's possible to determine both inclination and rotation rate but with a rotation rate equal to that of the sun, it's significantly harder to determine inclination but not the rotation rate.

For increasing speeds, it becomes increasingly easier to determine latitudinal variation of rotation. The angular velocity equation holds for low rotational rates such those terms of  $\Omega^2$  and higher can be neglected. In most cases, the star rotates too fast for the equation to hold true. Higher-order effects veer from the uniform splitting and tend towards yet more complex frequency spectra. Due to higher-order effects, the surface behavior of modes diverges from a pure spherical harmonic.

Rotation is not the only factor that affects the oscillations in a non-spherical symmetrical way. Other factors such as magnetic fields and structural variations associated with stellar spots can affect the frequency of oscillations and geometry of the pulsations on the surface. The Lorentz force produced by an axisymmetric magnetic field and the Coriolis force both affect

the oscillations although only the latter is aligned with the axis of symmetry. In contrast to rotation, an axisymmetric magnetic field interacts and affects modes of the star with the same value of  $m$ . Stellar magnetic fields influence oscillations in a way not summarized easily by a perturbation analysis.

In the case that the magnetic field is force-free, the oscillations will be affected directly through the Lorentz force. The Lorentz force has its greatest effect in the outer regions of the star, being comparable to, or greater than, the pressure forces. A magnetic field of any magnitude will be able to affect the modes and their greatest amplitudes will be in those regions, such as high-frequency pressure waves.

The magnetic field influence has three consequences: the frequencies are offset from their non-magnetic values, and the oscillations on the surface are no longer summarily described by the spherical harmonic function  $Y_{lm}$ , but instead a sum of spherical harmonics with varying degrees of  $l$ . The coupling of the oscillations with the magnetic field in the outer layers incur shifting waves that drain away part of the pulsation energy, which manifest in the forms of slow-moving Alfvén waves that dissipate as they penetrate inward into the star and acoustic waves travelling outward along magnetic field lines (Saio H. , 2005) (Saio H. G., 2004) (Cunha M. , 2006) (Cunha M. G., 2000) (Bigot, 2000) (Dziembowski W. G., 1996)

## Oscillations and Instabilities in rotating fields

The Kelvin-Helmholtz instability comes in play when there are two different fluids of different densities. A fluid exists with the following characteristics:

$$\rho_o = \begin{cases} \rho_1; & z > 0 \\ \rho_2; & z < 0 \end{cases} \quad (7.31a)$$

$$v_o = \{\vec{v}_1 \hat{e}_x; z > 0, \vec{v}_2 \hat{e}_x, z < 0\} \quad (7.31b)$$

Where downward gravity exists, then for  $v_1 = v_2$ , at the  $z = 0$  interface, a Rayleigh-Taylor instability exists if  $\rho_1 > \rho_2$ . A shear ( $v_1 \neq v_2$ ) also produces instability. Neglecting gravity,

Assume that  $\delta x \propto e^{ikx-i\omega t}$ ,  $\delta v^y = 0 = \xi y$ ;

(7.32)

Focusing on incompressible perturbations (no sound waves) in play here:

$$\nabla(\delta v) = ik\delta v^x + \partial_z \delta v^z = 0 \quad (7.33)$$

The momentum equation is:

$$\partial_t \delta v + v_o \nabla \delta v = -\frac{\nabla P}{\rho} \quad (7.34a)$$

$$-i\omega \delta v^x + v_o^x ik\delta v^x = -ik \frac{\delta P}{\rho_o} \quad (7.34b)$$

$$-i\omega \delta v^z + v_o^z ik\delta v^z = -\partial_z \frac{\delta P}{\rho_o} \quad (7.34c)$$

Based on the previous equations (7.34a,b,c), we obtain:

$$\delta P = \rho_o \delta v^x \frac{(kv_o^x - \omega)}{k} \quad (7.35)$$

Due to incompressibility,  $\delta v^x = \frac{1}{ik} \partial_z \delta v^z$ . (7.36)

Solving for  $\delta v^z$  gives us:  $\partial_z^2 \delta v^z = k^2 \delta v^z \rightarrow \delta v^z = \delta v_0^z e^{\pm kz}$ , (7.37)

Since  $\delta v^z$  should revert to zero as  $z$  approaches infinity,

$$\delta v^z = \{\delta v_1^z e^{-kz}, z > 0; \delta v_2^z e^{kz}, z < 0\} \quad (7.38)$$

The boundary conditions at  $z = 0$  are such:

$$\xi_1^z = \delta v_1^z = \xi_2^z = \delta v_2^z \quad \frac{D\xi}{Dt} = \Delta \vec{v} \quad (7.39a,b)$$

$$\partial_t \vec{\xi} + (v_0 * \nabla) \vec{\xi} = \delta \vec{v} + (\xi * \nabla) \vec{v}_0 \quad (7.39c)$$

$$-iw\xi^z + v_0^x ik\xi^z = \delta v^z \quad (7.39d)$$

Let  $\xi_1^z = \xi_2^z = \Omega$ , then

$$dv_1^2 = i(-w + kv_1)l, \quad dv_2^2 = i(-w + kv_2)l \quad (7.40a,b)$$

Pressure continuity at the interface would be:  $\delta P|_{z=0+} = \delta P|_{z=0-}$ ;

(7.41)

Which leads to the following equation:

$$\left(\omega - k \frac{\rho_1 v_1 + \rho_2 v_2}{\rho_1 + \rho_2}\right)^2 = -\left(\frac{\rho_1 \rho_2 (v_1 - v_2)^2 k^2}{(\rho_1 + \rho_2)^2}\right) \quad (7.42)$$

The right-hand side is negative so the modes are unstable. So the shear layers are unstable: this is the case of the Kelvin-Helmholtz instability. Vortices form and break up the shears. The shears can be stabilized by stratification, surface tension, or magnetic tension.

## Rayleigh Criterion for Differential Rotation

There exists an axisymmetric fluid in a disk rotating about its axis with an angular speed  $\Omega(r)$  where  $r$  is the cylindrical radius.

At equilibrium, the radial force is zero:

0 = gravity + pressure + centrifugal forces;

$$0 = g - \frac{1}{\rho} \frac{dP}{dr} - r^2 \Omega \quad (7.43)$$

The specific angular momentum per unit mass is:  $l = r^2 \Omega$ ,  $F_{centrifugal} = \frac{l^2}{r^3}$  (7.44a,b)

So the combined forces can be expressed as:

$$F = 0 = g - \frac{1}{\rho} \frac{dP}{dr} + \frac{l^2}{r^3} \quad (7.45)$$

A ring expands from  $r = r_1$  to  $r = r_2$ , and viscosity is negligible. Angular momentum is conserved, which means  $l = l(r_1)$ . At  $r = r_2$ , a radial force is experienced: the equilibrium condition for  $r_2$ :

$$F = g(r_2) - \frac{1}{\rho} \frac{dP}{dr} + \frac{l(r_2)^2}{r_2^3} \quad (7.46a)$$

$$= \frac{1}{r_2^3} [l(r_1)^2 - l(r_2)^2] \quad (7.46b)$$

If  $|l(r_1)| < |l(r_2)|$ , the ring orbits more slowly than at equilibrium, and falls back (inward) as a result. The ring's equation of motion is:

$$\frac{d^2 \delta r}{dt^2} = F \approx -\frac{1}{r^3} \frac{d}{dr} (l^2) \delta r = -K^2 \delta r \quad (7.47)$$

where  $K$  is the epicyclic frequency, which is defined as the frequency of oscillations of perturbations from a circular orbit.



If  $|l(r_1)| > |l(r_2)|$ , the ring orbits more faster than at equilibrium, and moves out as a result.

Therefore, an instability exists- the instability condition is defined by the following equation:

$$\frac{d}{dr} [l^2] = \frac{d}{dr} [(r^2\Omega)^2] = \frac{d}{dr} [r^4\Omega^2] = 4r^3\Omega^2 \quad (7.48a)$$

$$= r^3K^2 < 0 \quad (7.48b)$$

This is the definition of the Rayleigh criterion.

Most astrophysical flows have  $\frac{d}{dr} [l^2] > 0$  so they would be assumed to be stable. Although it turns out that that may not be the case every time. Other factors come into play, such as the disk fluid being ionized, or magnetized by an innate magnetic field affects the instability criterion.

### **Magnetorotational (Balbus-Hawley) Instability**

We become concerned with the existence of a magnetorotational instability that gives rise to turbulence in the plasma. The following equations describe the physical action that occurs.

A stationary axisymmetric circular flow with  $\vec{v}_1 = v_0 \widehat{e}_\phi = \Omega(r)r \widehat{e}_\phi$ , exists. (7.49)

A magnetic field projected in the z direction,  $\vec{B} = B_0 \widehat{e}_z$ , is present. (7.50)

The momentum equation in cylindrical coordinates is:

$$d_t v^r + (v * \nabla) v^r - \frac{(v^\phi)^2}{r} = -\frac{1}{\rho} \frac{d}{dr} \left( P + \frac{B^2}{8\pi} \right) + \frac{1}{4\pi\rho} (B * \nabla) B^r \quad (7.51a)$$

$$d_t v^\phi + (v * \nabla) v^\phi - \frac{v^\phi v^r}{r} = -\frac{1}{\rho} \frac{d}{d\phi} \left( P + \frac{B^2}{8\pi} \right) + \frac{1}{4\pi\rho} (B * \nabla) B^\phi \quad (7.51b)$$

$$d_t v^z + (v * \nabla) v^z = -\frac{1}{\rho} \frac{d}{dz} \left( P + \frac{B^2}{8\pi} \right) + \frac{1}{4\pi\rho} (B * \nabla) B^z \quad (7.51c)$$

Axisymmetrical incompressible perturbations (no acoustic waves) exist ( $\delta p = \delta P = 0$ ) with

$$\xi^2 = dv^z = 0; \quad (7.52)$$

$$d_t \delta v^r - 2\Omega \delta v^\phi = B_0 d_z \delta B^r \quad (7.53a)$$

$$d_t \delta v^\phi + \delta v^r d_r (r\Omega) + \delta v^r \Omega = B_0 d_z \delta B^\phi \quad (7.53b)$$

An induction equation is:

$$d_t \delta B = -\nabla \times (\delta \vec{v} \times \vec{B}_0 + \vec{v}_0 \times \delta \vec{B}) \quad (7.54a)$$

$$d_t \delta B^r = B_0 d_z \delta v^r \quad (7.54b)$$

$$d_r \delta B^\phi = B_0 d_z \delta v^\phi + [d_r (r\Omega) + \Omega] \delta B^r \quad (7.54c)$$

Recasting in terms of Lagrangian perturbations  $\xi$ :

$$\Delta \vec{v} = \frac{D\xi}{Dt} \quad (7.55a)$$

$$\frac{D\xi}{Dt} = d_t \vec{\xi} + (v * \nabla) \vec{\xi}, \quad \Delta \vec{v} = \delta \vec{v} + (\xi * \nabla) \vec{v}_0 \quad (7.55b,c)$$

$$\delta \vec{v} = d_t \vec{\xi} + (v_0 * \nabla) \vec{\xi} - (\xi * \nabla) \vec{v}_0 \quad (7.55d)$$

$$\delta v_r = d_t \xi^r \quad \delta v_\phi = d_t \xi^\phi - r \xi^r d_r \Omega \quad (7.55e,f)$$

$$\text{This means that } \vec{B} = (B_0 * \nabla) \vec{\xi} = B_0 d_z \vec{\xi}. \quad (7.56)$$

This is the expression that shows that the field lines are frozen into the perturbed fluid, which is particularly relevant for the Blandford-Znajek mechanism commented on in Chapter II.

$$\text{Assuming } \xi^i \propto e^{i(\omega t + k z)}; \quad (7.57)$$

$$-w^2 \xi^r + 2\Omega i w \xi^\phi = - \left[ \frac{d(\Omega^2)}{d(\ln r)} + \frac{(k B_0)^2}{4\pi\rho} \right] \xi^r \quad (7.58a)$$

$$-w^2 \xi^\phi + 2\Omega i w \xi^r = - \left[ \frac{(k B_0)^2}{4\pi\rho} \right] \xi^\phi \quad (7.58b)$$

The dispersion relation is as follows:

$$w^4 - w^2 [k^2 + 2(k * v_A)^2] + (k * v_A)^2 \left[ (k * v_A)^2 + \frac{d(\Omega^2)}{d(\ln r)} \right] = 0 \quad (7.59)$$

An instability exists when the following condition is met:

$$(k * v_A)^2 = \frac{(k B_0)^2}{4\pi\rho} < - \frac{d(\Omega^2)}{d(\ln r)} \quad (7.60)$$

Which will be satisfied for some  $k$ , when  $\frac{d(\Omega^2)}{d(\ln r)} < 0$ , or  $\frac{d|\Omega|}{dr} < 0$ , which is the case for any

astrophysical fluid disk. The fastest growing mode has a wavelength  $\lambda_{MRI} \sim \frac{v_A}{\Omega}$  and growth rate

$$\tau_{MRI} \sim \frac{1}{\Omega}. \quad (7.61a,b) \quad (7.62a,b)$$

The evolution equations are similar to the equation of motion for the separation of point masses, orbiting a gravitational mass, connected by a spring. That spring-like tension is provided by the magnetic tension. The compression of the string exerts a torque on both connected particles and transfers angular momentum from the inner element to the outer element. The inner element falls further in and the outer element moves out.  $\xi$  grows and the instability

comes into effect. For a  $\alpha$ -disk, numerical simulations show that  $\alpha \sim 0.1$  can be achieved from MRI-induced turbulences, provided a non-negligible magnetic flux is present in the disk.

For a rotating disk with self-gravity, it would have to be a thin disk in equilibrium:

$$\rho = \Sigma(r)\delta(z) \quad (7.62)$$

The vertically integrated pressure is as follows:

$$P(r) = \int_{-\infty}^{\infty} c_s^2 \rho dz \quad (7.63)$$

The velocity is  $\vec{v} = r\Omega \hat{e}_\theta$ , and the gravitational field is: (7.64)

$$\nabla^2 \phi = 4\pi G\rho = 4\pi G[\Sigma\delta(r) + M\delta(r)] \quad (7.65)$$

With M being a central point mass and gravity from the disk is non-negligible.

A perturbation is provoked into existence, and the perturbed quantity  $\delta X$  is inputted into an amplitude and phase:

$$\delta X = Ae^{i\theta} = A(\cos(\theta) + i \sin(\theta)); \quad (7.66)$$

Assume  $\theta = \omega t - m\phi + \theta(r)$ ; a small perturbation manifests as: (7.67)

$$\lambda_{pert} \sim \frac{1}{\left|\frac{d\theta}{dr}\right|} \ll r \quad (7.68)$$

And invoking a WKB approximation:

The amplitude  $A$  approximately constant over the range of  $\lambda_{pert}$ ,  $\left|\frac{d\theta}{dr}\right| = k \approx \text{constant over}$

$\lambda_{pert}$ .

The maximum of  $\delta X$  occurs at peak phases where

$$\omega t - m\phi + \theta(r) = 2\pi n \quad (\text{n an integer}) \quad (7.69)$$

Each  $n$  is a spiral arm pattern signified by  $\phi = \frac{\theta(r)}{m}$ , and the next  $(n+1)$  spiral arm is the same, but rotated by  $\frac{2\pi p}{n}$  radians. There are then  $m$  equidistant spiral arms in the perturbation. The spiral arms rotate at a speed:

$$\Omega_p = \left( \frac{d\phi}{dt} \right)_{\theta,r} = \frac{\omega}{m} \quad (7.70)$$

$\Omega_p$  is a constant even though the speed at which the material flows,  $\Omega$ , is variable and decreases as a function of  $r$ .

$$\Omega_p < \Omega \quad (\text{for low } r) \qquad \Omega_p > \Omega \quad (\text{for high } r)$$

At a point,  $\Omega_p$  will equal  $\Omega$  and this location is defined as the co-rotation radius ( $r_{CR}$ ).

$$\Omega_p = \Omega(r_{CR}) \quad (7.71)$$

To find how tightly the spiral arms curve, we need to compute  $\frac{dr}{d\phi}$  on the perturbation peak, with

fixed  $t$ : 
$$m d\phi = \frac{d\phi}{dr} dr = k dr; \quad (7.72)$$

$$\left( \frac{d\phi}{dr} \right)_{peak} = \frac{m}{k} \quad (7.73)$$

The WKB approximation has  $k*r \gg 1$  so

$$\left( \frac{d(\ln r)}{d\phi} \right)_{peak} = \frac{m}{k} \ll 1 \quad (7.74)$$

The WKB approximation is a tight winding approximation as well. Finding the gravitational potential perturbation,  $\delta\phi$ , caused by the density perturbation,  $\delta\rho$ :

The Poisson equation is:

$$\nabla^2 \phi = 4\pi G \delta\rho \quad (7.75)$$

The perturbations are approximate to  $e^{ikr}$  and  $m/(kr) \ll 1$ , so the azimuthal derivatives can be

neglected.

$$\nabla^2 \delta\phi = -k^2 \delta\phi + \delta_z^2 \delta\phi = 4\pi G \delta\Sigma \delta(z) \quad (7.76)$$

Away from the equator:

$$\delta\phi = \begin{cases} Ae^{-|k|z}, & z > 0 \\ Ae^{|k|z}, & z < 0 \end{cases} \quad (7.77)$$

Integrating over the limit  $z = 0 - \epsilon$  to  $z = 0 + \epsilon$ ,

$$\left(\frac{d\delta\phi}{dz}\right)_{0-\epsilon}^{0+\epsilon} = A\pi G \delta\Sigma = A(-2|k|) \quad (7.78)$$

$$\text{Solving for } A, \quad \delta\phi = -\frac{2\pi G \delta\Sigma}{|k|} \text{ on the equator.} \quad (7.79)$$

This can be inserted into the perturbation wave equations and give us a dispersion relation:

$$(w - m\Omega)^2 = K^2 + k^2 c_s^2 - 2\pi G |k| \Sigma = w_s^2 \quad (7.80)$$

$K^2$  is the shear term, and being positive, serves as a stabilizing influence, and dominates at low  $k$ .  $k^2 c_s^2$  is the pressure (or acoustic) term and also acts as a stabilizer. Pressure dominates at high  $k$  (or small scales).

The term  $-2\pi G |k| \Sigma$  is the self-gravity term and is negative and serves to destabilize the overall action. The length scale at which shear and gravity are comparable is the Toomre wave number scale:

$$K_T = \frac{K^2}{2\pi G \Sigma} \quad (7.81)$$

$$\text{For axisymmetrical perturbations } (m = 0), \text{ there are unstable local modes if } Q = \frac{K c_s}{\pi G \Sigma} < 1. \quad (7.82)$$

$$Q \text{ is the Toomre stability parameter. With non-axisymmetrical waves, } \nu = \frac{(\omega - m\Omega)}{K}. \quad (7.83)$$

The dispersion relation is now:

$$\frac{|K|}{K_T} = \frac{2}{Q^2} \left( 1 \pm [1 + Q^2(1 - v^2)]^{\frac{1}{2}} \right) \quad (7.84)$$

With the plus solution, the short waves are pressure dominated. With the minus solution, the long waves are shear-dominated. The wave number  $k$  for long waves go to zero at the Lindblad resonances:

$$v^2 = 1 \rightarrow \Omega_p = \Omega(r_{LR}) \pm \frac{1}{m} K(r_{LR}) \quad (7.85)$$

Long waves can only propagate in the spaces between the two Lindblad resonances. At the resonances, the long waves are able to couple to the large-scale perturbations.

### Global Instabilities

Solving the dispersion relation, two modes come into play:

$$\Omega_{p+} = \frac{\omega_+}{m} = \Omega + \omega_s \quad \Omega_{p-} = \frac{\omega_-}{m} = \Omega - \omega_s \quad (7.86a,b)$$

where  $\frac{\omega}{m}$  sets the pattern speed. Two waves coexist with each other, with one moving with the flow (co-rotating), and one moving against it (counter-rotating). There is a co-rotation point ( $r_c$ ) at which  $\Omega(r_c) = \Omega_p$ . For a given  $m$ , there are two modes, (co-rotating and counter-rotating) with a distant co-rotation radius for each.

## Non-radial Stellar Pulsation

There is a non-radial motion in which some areas of the surface expand while others contract. They manifest in angular patterns for different non-radial modes. Scalar quantities like  $\delta p$  (pressure) follow the same pattern, varying from positive to negative from area to area. These patterns are described by two integers:  $l$  and  $m$ .

There are  $l$  local circles (where  $\delta r = 0$ ) with  $|m|$  of these circles passing through the poles of the star and the rest parallel to the equator of the body. If  $l = m = 0$ , the pulsation is purely radial.

The patterns for non-zero  $m$  correspond to travelling waves that move across the star parallel to its equator (latitude-wise). The time of the waves completing a full trip around the star is  $m$  times the star's pulsation period ( $\tau = 2\pi/\omega$ ).

Radial oscillations are attributed to standing waves in the stellar interior. For non-radial oscillations, the sound waves can move horizontally as well as radially to create waves that travel around the star.

Since pressure provides the impelling force, the non-radial oscillations are called p-modes. A p-mode description requires a specified radial and angular node.

The f-mode is the non-radial analog of the fundamental radial mode (f refers to fundamental).

The horizontal wavelength is given by the expression

$$\lambda_h = \frac{2\pi r}{\sqrt{l(l+1)}} \quad (7.87)$$

Where  $r$  is the distance from the center of the star.

For non-adiabatic oscillations, the time-dependence of the pulsation is usually the real part of



$e^{i\sigma t}$  where  $\sigma$  is the complex frequency,

$$\sigma = \omega + iK \quad (7.88)$$

Where  $\omega$  is the usual pulsation frequency and  $K$  is a stability coefficient.

The pulsation amplitude is proportional to  $e^{Kt}$  and  $1/K$  is the characteristic time of growth or decay for the oscillations.

The patterns correspond to the real parts of the spherical harmonic functions  $Y_m^l(\theta, \phi)$  where  $l$  is a non-negative integer and  $m$  is any integer between  $-l$  and  $l$ .

The acoustic frequency can be written as:

$$S_l = \frac{2\pi}{\text{time to travel } \lambda_h} = 2\pi \left[ \frac{v_s}{\frac{2\pi r}{\sqrt{l(l+1)}}} \right] \quad (7.89a)$$

$$= \sqrt{\frac{\gamma P}{\rho}} * \frac{\sqrt{l(l+1)}}{r} \quad (7.89b)$$

where  $v_s$  is the adiabatic speed of sound.

For no rotation, the pulsation period depends only on the number of radial modes and the value of  $l$  (independent of  $m$ ).

For rotation, the amount by which the pulsation frequencies are split depends on the angular rotation frequency of the star with the rotationally produced shift in frequency proportional to the product  $m*\Omega$ .

The pulsation frequencies for modes of varying values of  $m$  become separated or split as the waves move with or against the rotation. As pressure provides the impelling force for the

compression and expansion of the p-mode sound waves, gravity is the source of the restoring force for the non-radial oscillations called g-modes. (The prefixes preceding the modes indicate the force in play: g- for gravity and p- for pressure.)

### Oscillation motion for g-modes

A small bubble of stellar material is displaced from its equilibrium position by a distance  $\delta r$ . The motion is slow enough such that the pressure within the bubble,  $P^{(b)}$ , is equal to the pressure of the surrounding matter,  $P^{(s)}$ . And the motion also has to be fast enough that no heat is exchanged between the bubble and its surroundings.

The expansion and compression of the gas bubble is adiabatic. If the density of the bubble is greater than that of its surroundings, the bubble will revert back to its equilibrium position. The restoring force per unit volume on the bubble is the difference between the upward buoyant force and the downward gravitational force:

$$f_{net} = (\rho_f^s - \rho_f^b)g \quad g = \frac{GM}{r^2} \quad (7.90a,b)$$

Applying a Taylor expansion:

$$f_{net} = \left[ \left( \rho_i^s + \frac{d\rho^s}{dr} dr \right) - \left( \rho_i^b + \frac{d\rho^b}{dr} dr \right) \right] * g \quad (7.91a)$$

$$= \left( \frac{d\rho^s}{dr} - \frac{d\rho^b}{dr} \right) g dr \quad (\text{since } \rho_i^s = \rho_i^b) \quad (7.91b)$$

Since motion of the bubble is adiabatic,

$$f_{net} = \left( \frac{d\rho^s}{dr} - \frac{\rho_i^b}{\gamma P_i^b} \frac{dP^b}{dr} \right) g \, dr \quad (\text{now } b \rightarrow s) \quad (7.92a)$$

$$f_{net} = \left( \frac{1}{\rho} \frac{d\rho}{dr} - \frac{1}{\gamma P} \frac{dP}{dr} \right) \rho \, g \, dr \quad (7.92b)$$

$$f_{net} = A * \rho \, g \, dr \quad A = \frac{1}{\rho} \frac{d\rho}{dr} - \frac{1}{\gamma P} \frac{dP}{dr} \quad (7.92c,d)$$

$$a = -N^2 dr = A \, g \, dr \quad \rightarrow \quad -N^2 = A \, g \quad (7.92e,f)$$

The buoyancy frequency is:

$$N = \sqrt{-A \, g} = \sqrt{\left( \frac{1}{\gamma P} \frac{dP}{dr} - \frac{1}{\rho} \frac{d\rho}{dr} \right) g} \quad (7.93)$$

Accounting for the gravitational acceleration in the disk's reference frame:

$$g = \frac{GM}{r^2} \cos(\theta) = \frac{GM}{r^2} * \frac{z}{r} \approx \frac{GMz}{R^3} \quad (\text{when } z \ll R) \quad (7.94)$$

The gas within the disk is supported against gravity by a pressure gradient, and the pressure distribution gives:

$$\frac{dP}{dz} = -g\rho \quad \left( g = \frac{GM}{r^2} \cos(\theta) \right) \quad (7.95a,b)$$

Based on the assumption that the disk is isothermal in the vertical direction (z), the pressure becomes:

$$P = \rho \, c_s^2 \quad (7.96)$$

Where  $c_s$  is the speed of sound in the medium;

$$\frac{d}{dz} (\rho \, c_s^2) = c_s^2 \frac{d\rho}{dz} = -\frac{\rho GM}{R^3} z = -\Omega_K^2 \rho z \quad \Omega_K = \sqrt{\frac{GM}{R^3}} \quad (7.97a,b)$$

Where  $\Omega$  is the angular velocity in the disk.

$$\frac{d\rho}{\rho} = \frac{-\Omega_K^2}{v_s^2} z dz \quad (7.98)$$

$$\ln \rho = -\frac{\Omega_K^2}{2v_s^2} z^2 \quad \rightarrow \quad \rho(z) = \rho_0 e^{-\frac{\Omega_K^2}{2v_s^2} z^2} \quad (7.99)$$

Where  $\rho_0$  is the midplane density of the disk at ( $\theta = 0$ ) being the equatorial plane.

The equation can be rewritten as:

$$\rho(z) = \rho_0 e^{-\frac{\Omega_K^2}{h^2} z^2}; \quad h = -\frac{\Omega_K^2}{2v_s^2}; \quad (7.100a,b)$$

The latter equation also gives  $h$ , the vertical scale height of the disk. ‘ $h$ ’ can be recast in terms of the orbital velocity:

$$h^2 = \frac{2v_s^2}{\Omega_K^2} \quad v_K = R * \Omega_K \rightarrow \Omega_K = \frac{v_K}{R} \quad (7.101a,b)$$

$$h = \frac{2v_s^2 R^2}{v_K^2} \quad \rightarrow \quad \frac{h^2}{R^2} = \frac{2v_s^2}{v_K^2} \quad \frac{h}{R} \approx \frac{v_s}{v_K} \quad (7.102)$$

The thickness of the disk as a fraction of the radius is given by the ratio of the speed of sound (in that medium) to the orbital velocity. A ratio of  $h/R \ll 1$  would get the disk classified as geometrically thin. Thin disks are simple structures where radial pressure forces can be neglected; gas velocity is same as a particle orbiting at the same radius.

For a thin disk, the orbital velocity of the gas is Keplerian:

$$v_K = \sqrt{\frac{GM}{R}}; \quad (7.103)$$

The specific angular momentum per unit mass is expressed as:

$$l = R * v_K = \sqrt{GMR}; \quad (7.104)$$

At large  $R$ , gas has too much angular momentum to be accreted by the black hole. It has to lose some of it in order to fall inward towards the black hole, within the disk, so there must be a redistribution of the angular momentum from small  $R$  and large  $R$ . A torque would be necessary for such angular momentum transport.

### **Standing Wave Characteristics**

We focus on this because oscillating waves are ubiquitous phenomena in physical systems, including accretion disks. Those of stars have been studied in detail while accretion disks' have not been studied as extensively. Stellar oscillations and disk oscillations have many commonalities and some important differences. The most particular difference is the force balance. The geometry is different for either case. Stars are typically spherical and rotation serves as a minor factor in their structure. Disks are set in a cylindrical reference frame and rotation plays a larger factor in the structure.

A major restoring force against small perturbations is the pressure. In the case of disks, the centrifugal force due to rotation serves as the major force acting in opposition to the gravitational force and serves as the restoring force against small perturbations come from the disk rotation. The rotational effects take two forms: the characteristics of oscillation modes, and the excitation mechanisms of the oscillations. The rotational restoring force governs the oscillations and their frequencies are characterized by the epicyclic frequency,  $\kappa$ , defined by the following relation:

$$\kappa^2 = 2\Omega \left( 2\Omega + r \frac{d\Omega}{dr} \right) \quad (7.105)$$

with  $\Omega$  being the angular frequency of the disk. The radial distribution of  $\Omega$  determines the behavior of small oscillations. In terms of the perturbations, disks have no defined outer boundary in the radial direction, and the epicyclic frequency changes over the radial distance of the disk. The oscillations, to have observable features, have to be trapped in a specific region or manifest global features to take on information from their physical situation.

General relativity plays a large part in defining the oscillations. Another factor in disk rotational effects on the oscillations is the excitation mechanism. For disk oscillations, excitation processes are important as well as for stellar oscillations. In the disk case, these would be the viscous processes and they serve as the exciting influences by delivering heat to the disk and serves as mediator of angular momentum transport in the radial direction. Viscosity has two effects on the excitation of oscillations: thermal and dynamical. General Relativity figures in prominently for both effects.

For adiabatic motions the equation of state is:

$$\frac{dp}{dt} - \gamma \frac{p}{\rho} \frac{d\rho}{dt} = 0 \quad P = K\rho^\gamma \quad (7.106a,b)$$

with  $\gamma$  being the ratio of specific heats.

The energy equation for adiabatic perturbations is:

$$i\tilde{\omega}(p_1 - c_s^2 \rho_1) = \gamma p_0 (\vec{u} * \vec{A}) \quad (7.107)$$

with  $c_s$  being the sound speed, and  $A$  as the Schwarzschild discriminant vector, defined as:

$$\vec{A} = \ln \nabla \rho_0 - \frac{1}{\gamma} \nabla \ln \rho_0 = \nabla \left( \ln \frac{\rho_0}{p_0^{\frac{1}{\gamma}}} \right) \quad (7.108)$$

An effective gravitational acceleration is present:

$$g_{eff} = g + r\Omega^2 \hat{r} = \frac{1}{\rho_0} \nabla p_0 \quad (7.109)$$

$$N_r^2 = -(g_{eff})_r A_r \quad N_z^2 = -(g_{eff})_z A_z \quad (7.110a,b)$$

These are the Brunt-Vaisalia frequencies of the oscillations. When  $N_z^2 > 0$ , the entropy is confined to the vertical direction so the medium is convectively stable ( $A_z < 0$ ). If  $N_z^2 < 0$ , the medium is convectively unstable. It applies for  $N_r^2$ . The frequency is a measure of oscillations in either direction and a definitive characteristic of the system.

Starting with the assumption that the disk is isothermal:

$$\rho_0(r, z) = \rho_0(r) e^{-\frac{z^2}{2H^2}} \quad (7.111)$$

with H being the half-thickness of the disk, related to (7.111) via (7.101a):

$$P_0 = \rho_0 v_s^2 \rightarrow \Omega_K^2(r) H^2(r) = \frac{p_0}{\rho_0} \quad (7.112)$$

A dimensionless vertical coordinate is invoked:

$$\eta = \frac{z}{H(r)}; \text{ for separation of variables} \quad (7.113)$$

Two sets of equations were derived, by Nowak and Wagoner, to describe the oscillations (Nowak M. W., 1992):

$$v_s^2 \frac{d}{dr} \left( \frac{1}{\tilde{\omega}^2 - \kappa^2} \frac{dh_1^*}{dr} \right) + \left( 1 - \frac{\kappa c_s^2}{\tilde{\omega}^2 H^2} \right) h_1^* = 0 \quad (7.114)$$

with  $\kappa(r)$  slowly varying function of  $r$  to be determined by solving the separated equations with boundary conditions.

$$\frac{\partial}{\rho_0 \partial \eta} \left( \frac{\rho_0}{\tilde{\omega}^2 - N_z^2} \frac{\partial g}{\partial \eta} \right) + \frac{1}{p_0^\gamma} \frac{\partial}{\partial \eta} \left( p_0^{\frac{1}{2}} \frac{A_z H}{\tilde{\omega}^2 - N_z^2} \right) g + \frac{\kappa}{\tilde{\omega}^2} g = 0 \quad (7.115)$$

Assuming the disk is convectively neutral in the vertical direction, meaning  $N_z^2 = 0$ ,  $A_z = 0$ , and  $\gamma = 1$  (for vertically isothermal disks). The latter equation reduces to:

$$\frac{\partial^2 g}{d\eta^2} - \eta \frac{dg}{d\eta} + \kappa g = 0 \quad \text{Hermite equation} \quad (7.116)$$

A boundary condition on surface ( $\eta = \infty$ ) entails that  $\kappa$  be set equal to zero or a positive integer,  $n$  (Okazaki, 1987).  $g(\eta)$  becomes:  $g(\eta) = H_n(\eta)$ ;  $n = 1, 2, 3 \dots$  (7.117)

The  $n = 0$  mode is the fundamental mode in the vertical direction and the  $n = 1$  mode is the first overtone. Local perturbations with a radial wavelength  $\kappa_r$ , is defined by the earlier equation with  $\gamma = 1$  to a dispersion relation (Okazaki, 1987):

$$(\tilde{\omega}^2 - \kappa^2)(\tilde{\omega}^2 - n\Omega_K^2) = \tilde{\omega}^2 c_s^2 \kappa_r^2; \quad (7.118)$$

This dispersion relation contains basic properties of the disk oscillations (Nowak M. W., 1992) (Isper, Low-frequency modes and nonbarotropic effects in pseudo-Newtonian accretion disks, 1994) (Perez, Relativistic Diskoseismology. 1. Analytical results for gravity modes., 1997) (Silbergleit, 2001).



## Classification, and Coupling, of Radial and Vertical Oscillations

If  $n = 0$ , i.e. the oscillations have no node in the vertical direction, the dispersion relation becomes:

$$\tilde{\omega}^2 = \kappa^2 + k_r^2 c_s^2; \quad \tilde{\omega}^2 = 0; \quad (7.119a,b)$$

The former is the inertial-acoustic waves and the latter is a trivial mode.

A fluid element displaced in the radial direction returns to its original radius due to a restoring force from the rotation of the compact object. The oscillations from this action are inertial oscillations, and their frequencies are the epicyclic frequencies,  $\kappa(r)$ .

For compressible fluids, there is an extra restoring force due to a pressure variation, resulting in acoustic oscillations. The two combine to create inertial-acoustic waves. For the long wavelength limit in the radial direction,  $k_r = 0$ .

In the case that  $n \neq 0$ , the dispersion relation becomes:

$$\tilde{\omega}^2 = \kappa^2; \quad \tilde{\omega}^2 = n\Omega_K^2; \quad (7.120a,b)$$

The former represents the inertial oscillations. The latter represents an extra mode of oscillations and is the vertical oscillations of the disk and tied into the geometry of the disk itself.

For a perturbation of the disk plane in the vertical direction, a restoring force serves to bring it back to the equatorial plane. The restoring force is the vertical component of the gravitational force,

$$\left(\frac{GM}{r^2}\right)\left(\frac{z}{r}\right) = \left(\frac{GM}{r^3}\right)z = \Omega_K^2 * z; \quad (7.121)$$

This oscillation correlates to the  $n = 1$  mode and bears a similarity to surface gravity waves that happen at the interface between two distinct fluids.

If there exists any nodes in the vertical direction, meaning  $n \geq 2$ , the frequencies of the oscillations increase due to the pressure restoring force in addition to the gravitational restoring force. Ideally,  $k_r = 0$ , and the horizontal oscillations  $\tilde{\omega}^2 = \kappa^2$  and vertical oscillations  $\tilde{\omega}^2 = n\Omega_K^2$  would be separated. Due to the disk not being homogeneous, in the radial direction, the oscillations are coupled. Perturbations in the radial direction on the equatorial plane induce vertical motion due to the radial inhomogeneity. Vertical perturbations also induce radial motion. The coupling occurs through the pressure restoring force and is stronger with a shorter radial wavelength and higher acoustic speed.

The dispersion relation gives two frequency possibilities for a given positive  $k_r^2$ . Given  $\tilde{\omega}_1, \tilde{\omega}_2$  with  $\tilde{\omega}_2 > \tilde{\omega}_1 > 0$ . Modes with  $\tilde{\omega}_2$  are the p-modes and modes with  $\tilde{\omega}_1$  are the g-modes.

Axisymmetric wave modes ( $m = 0$ ) bear distinct characteristics that need to be understood. For modes of ( $m = 0, n = 0$ ), the dispersion relation comes out as:

$$\omega^2 = \kappa^2 + c_s^2 k_r^2, \quad \text{where } \omega > \kappa \quad (7.122)$$

taking  $\omega$  as a positive value. This indicates the propagation region of the wave is above the curve of  $\kappa(r)$ . If the disk touches the central object at a radius  $r_b$ , and  $\omega > \kappa(r_b)$  the waves can approach near the surface of the object and are reflected backward by the rotational barrier of the central object when  $\omega < \kappa(r_b)$ . In the context of a disk around a compact object in a general-relativistic field, the radius or effective surface would be at the ISCO as opposed to the literal

surface of a star.

For modes ( $m = 0, n = 1$ ), the structure of the propagation region changes to a degree. Since  $\kappa^2 < n\Omega_K^2$  (with  $n = 2$ ), the propagation region is set above and below the curves of  $\kappa$  and  $\sqrt{2}\Omega_K$ . The below region is the domain of the g-mode ( $\kappa(r)$  curve) and the above region is the domain of the p-mode ( $\sqrt{2}\Omega_K$  curve).

The differential equations describing the disk oscillations are comparable to those describing stellar oscillations, although their dispersion relations are different (Nowak M. W., 1992) (Perez, Relativistic Diskoseismology. 1. Analytical results for gravity modes., 1997) (Nowak M. L., 1998) (Hines, 1960).

The wave motions' characteristics as described by the dispersion relation are adjusted by the influence of General Relativity when a compact object is present. A deeper discussion is made by numerous theorists (Isper, Low-frequency modes and nonbarotropic effects in pseudo-Newtonian accretion disks, 1994) (Isper, 1995) (Perez, Relativistic Diskoseismology. 1. Analytical results for gravity modes., 1997) (Silbergleit, 2001).

The epicyclic frequencies are modified in a general-relativistic field, and vanish at  $r_{ms}$ . It differs from the Newtonian scheme in that the radial distribution is not monotonic and increases upward in the outer non-relativistic region as does  $\Omega_K$ , but approaches a maximum at a specific radius, then decreases from that point to  $r_{ms}$  where it disappears. The radial distribution of  $K(r)$  bears diagnostic characteristics in terms of wave trapping, particularly the g-modes (Okazaki, 1987) (Nowak M. W., 1992) (Perez, Relativistic Diskoseismology. 1. Analytical results for gravity modes., 1997) and the p-modes (Kato S. F., 1980).

The radial distribution of  $\kappa(r)$  in the Kerr metric is:

$$\kappa^2 = \left(\frac{GM}{r^3}\right) \left(1 + a \left(\frac{M}{r^3}\right)^{\frac{1}{2}}\right)^{-2} \left(1 - \frac{6M}{r} + 8a \left(\frac{M}{r^3}\right)^{\frac{1}{2}} - \frac{3a^2}{r^2}\right) \quad (7.123)$$

and the vertical distribution of the vertical epicyclic frequency  $\Omega_{\perp}$  is:

$$\kappa^2 = \Omega_K^2 \left(1 - 4a \left(\frac{M}{r^3}\right)^{\frac{1}{2}} + \frac{3a^2}{r^2}\right) \quad (7.124)$$

The dispersion relation is modified in the general-relativistic case:

$$(\tilde{\omega}^2 - \kappa^2)(\tilde{\omega}^2 - n\Omega_{\perp}^2) = \tilde{\omega}^2 c_s^2 k_r^2 \quad (7.125)$$

For thin disks, the strongest restoring force is the rotation of the compact object. The characteristic frequency of the restoring force is the radial epicyclic frequency  $\kappa$ . The radial distribution of  $\kappa(r)$  gives details on wave phenomena including trapping. If trapping is absent, the perturbation wavelength becomes short as the wave propagates outward. Short wavelength oscillations spread out through the disk and do not provide much information about the disk. A phenomena that entails further attention and provides information about the physical environment, are global oscillations and trapped oscillations. Two wave modes exist that can become global: ( $m = 1$ ) inertial-acoustic waves with  $n = 0$ , and inertial-acoustic waves with  $n = 1$ . The former is a deformation of the disk plane while the latter is a corrugation wave (c-mode).

In relativistic disks, the epicyclic frequencies do not come close to the Keplerian frequency,  $\Omega_K$ . If the rotation of the disk is low ( $a \ll 1$ ), low frequency oscillations manifest in the disk, these being of the ( $m = 1$ ) corrugation waves variety with  $n = 1$ .

The dispersion relation is:

$$((\omega - \Omega)^2 - \kappa^2)(\omega - \Omega)^2 - \Omega_{\perp}^2) = (\omega - \Omega)^2 c_s^2 k_r^2 \quad (7.126)$$

Due to the fact that  $\kappa^2 \ll \Omega^2$ , the conditions from the dispersion relation change.

The difference between  $\Omega_{\perp}$ , the vertical epicyclic frequency and  $\Omega$ , the disk angular frequency, is still valid if the rotation is low ( $a \ll l$ ). If we assume

$$(\omega - \Omega)^2 - \Omega_{\perp}^2 \rightarrow -2\omega\Omega + (\Omega^2 - \Omega_{\perp}^2) \quad (7.127a)$$

$$(\omega - \Omega)^2 - \kappa^2 \rightarrow \Omega^2 - \kappa^2 \quad (7.127b)$$

then the dispersion relation gives us:

$$\omega \sim -\frac{1}{2} \Omega \frac{\Omega^2}{\Omega^2 - \kappa^2} \frac{k_r^2 c_s^2}{\Omega^2} + \frac{1}{2} \Omega \frac{\Omega^2 - \Omega_{\perp}^2}{\Omega^2} \quad (7.128)$$

given that  $\frac{k_r^2 c_s^2}{\Omega^2} \ll 1$  and  $\frac{\Omega^2 - \Omega_{\perp}^2}{\Omega^2} \ll 1$ , the innermost region of rapid rotating disks will have low-frequency modes of oscillations with frequencies smaller than  $\Omega$ . (7.129a,b)

The pattern of oscillations slowly rotates in the opposite direction of the disk rotation. The frequency is smaller than by the order of  $(k_r * H)^2 \ll 1$ . (7.130)

Focusing on trapped oscillations in relativistic disks, they propagate away in the radial direction and will not grow to observable amplitudes unless there are reflection boundaries. Standing oscillations have to be trapped in a region to establish stable characteristics of a wave. Starting with a fundamental mode ( $n = 0$ ), particularly an axisymmetric oscillation ( $m = 0$ ) and  $\tilde{\omega}^2 = \omega^2$ , I can get a dispersion relation of  $\omega^2 = \kappa^2 + c_s^2 k_r^2$ ; (7.131)

The region the waves propagate in is defined by:  $\omega^2 < \kappa^2$ , since  $k_r^2$  has to be positive. The wave propagation region is divided in two areas: inner region ( $r < r_1$ ) and outer region ( $r > r_2$ ), where  $\omega < \kappa_{max}$ . The region is where the waves propagate. When  $\omega > \kappa_{max}$  and the

separation of the two areas for  $\omega < \kappa_{max}$  is due to general-relativistic effects.

Waves moving inward from the outer disk with frequency  $\omega < \kappa_{max}$  approaches  $r_2$  when its frequency,  $\omega = \kappa$ , occurs. The wavelength of the wave approaches infinity ( $k_r = 0$ ) at  $r = r_2$ , which means the waves are reflected back outward at that point. If  $\omega^2 > \kappa_{max}^2$ , the waves can propagate unhindered towards the inner edge of the disk, which isn't the case for non-relativistic disks where all the waves would be reflected back at  $r_b$  if  $\omega = \kappa^2$ . There exists a wave propagation region within the inner region of the disk for  $\omega < \kappa_{max}$ , and waves are trapped there (Kato S. F., 1980). An inertial-acoustic wave propagates outward in the region by the inner edge, or rms. If  $\omega < \kappa_{max}$ , the wave reflects back at the boundary  $r = r_l$ . A wave propagating inwards towards the inner edge would be partially reflected back at the inner edge as outgoing acoustic waves.

Outside the sonic radius, inward-propagating inertial-acoustic waves are linearly coupled with other perturbation modes such as outward propagating inertial-acoustic modes, thermal and viscous modes. An outward propagating inertial-acoustic mode is created and the wave is standing initially, with one end anchored near the sonic radius, and spreads outward after attaining maximum amplitude. This can be thought of as an inversion of the inward wave into an outward wave.

A thermal mode is also reflected back at the inner edge as an outward propagating acoustic wave, being linearly coupled with the other modes (Mammoto, 1996).

Perturbations are trapped between the inner edge and a radius that changes with parameters. A spectrum forms in the trapped oscillations that manifest as QPOs with frequencies close to  $\kappa_{max}$ .

This is a standard feature of oscillations in the inner region of thin relativistic disks (Kato S. F., 1998).

The first overtone ( $n = 1$ ) of the g-modes also is trapped with frequencies of  $\kappa_{max}$ . The axisymmetric first overtone ( $m = 0, n = 1$ ) wave has two modes: (g-mode) inertial-gravity waves,  $\omega^2 < \Omega_K^2$ , and (p-mode) inertial-acoustic waves, with  $\omega^2 > \Omega_K^2$ .

Focusing on the g-mode waves, at  $r_{max}$ , where  $\kappa$  has a maximum at the radius, and decreasing outward from there in both directions, the waves are trapped in a region  $r_1 < r < r_2$ , where their frequencies  $\omega < \kappa_{max}$  (Okazaki, 1987) (Nowak M. W., 1992) (Perez, Relativistic Diskoseismology. 1. Analytical results for gravity modes., 1997). The oscillations in that region will have frequencies around the value of  $\kappa_{max}$ , in the vicinity of  $r_{max}$ .

A notable feature of the oscillations is that their frequencies are independent of any changes in the disk structure provided the disk is geometrically thin. This is due to the fact  $K_{max}$  is dependent only on the mass of the central object.  $K_{max}$  scales to the inverse mass of the compact object since  $r_{max}$  scales to the mass of same object.

Calculations of the eigenfrequency for the g-mode oscillations were done using the Kerr geometry (Perez, Relativistic Diskoseismology. 1. Analytical results for gravity modes., 1997).

The oscillation frequency  $f$  is (Nowak M. W., 1997):

$$f = 700 \left( \frac{M}{M_{\odot}} \right)^{-1} F(a)(1 - \epsilon) \text{ Hz} \quad (7.132)$$

with  $\epsilon$  as the small correction factor pertaining to the disk thickness and the radial and vertical mode numbers.  $F(a)$  takes in the effects of the rotating compact object with  $a$  as a dimensionless spin parameter and  $F(a)$  monotonically increases from  $F(0)$  to  $F(0.998)$ . It was suggested the

trapped oscillations were the source of the 67 Hz QPO signal detected in GRS 1915+105 (Nowak M. W., 1997).

Other modes of oscillations are also trapped in the inner disk. One-armed corrugation waves ( $n = 1$ ) propagate in the region within the inner disk specified by the frequency combination:

$$(\omega - \Omega)^2 - \Omega_{\perp}^2 > 0; \quad \omega < \Omega - \Omega_{\perp}; \quad (7.133a,b)$$

when  $a \ll 1$ , are very close to each other.

Silbergleit discovered that one-armed corrugation waves are trapped in the inner region and the region is wide and the eigenfrequency low, for low values of  $a$ , and the region is narrow and the eigenfrequency high, for high  $a$ . The radial extent of the trapped region is a decreasing function of  $a$ , and the eigenfrequency increases monotonically for increasing  $a$  (Silbergleit, 2001). The eigenfrequency coincides with the Lense-Thirring frequency at its outer trapping boundary.

The Lense-Thirring frequency is the frequency of the vertical precession of a particle around a rotating compact object. The Lense-Thirring frequency at  $r$  is the difference between  $\Omega_K$  and  $\Omega_{\perp}$ :

$$\Omega_{LT}(r) = \Omega_K(r) - \Omega_{\perp}(r); \quad (7.134)$$

The condition,  $\omega = \Omega - \Omega_{\perp}$ , implies the outer boundary of the trapped region is the radius where the condition is satisfied, and since  $\Omega \sim \Omega_K$ , then becomes:

$$\omega \sim \Omega_{LT} \text{ at the outer boundary.} \quad (7.135)$$



## Trapped Oscillations

The trapped oscillations are a result of a non-monotonic spatial distribution of epicyclic frequencies in relativistic disks. This would be of particular interest to us, especially if a bounded region contained them. Another type of trapped oscillations exists along with the epicyclic frequencies, including in Newtonian disks. In a Newtonian disk, a type of instability occurs where outbursts occur in a non-relativistic disk and the disk undergo through limit-cycle oscillations due to the thermal instability. The instability creates a transition front that separates a hotter and cooler region from each other.

Consider a situation where an inner hotter disk touches an outer cooler disk at the transition radius  $r_{tr}$ , and an axisymmetric p-mode with ( $n = 0$ ) in the vertical direction exists in the area  $r < r_{tr}$ . The wave frequency is higher than the epicyclic frequency at  $r_{tr}$ . The wave propagates outward in the inner disk and is reflected back at  $r_{tr}$  due to an abrupt change in disk thickness and a dearth of gas outside  $r_{tr}$  except towards the equatorial plane. The reflected wave will reflect outward at  $r_{in}$  where the epicyclic frequency is equal to  $\omega$ , since the wave cannot propagate beyond that radius. Oscillations with  $\kappa(r) \sim \omega$  will be effectively trapped in that region between  $r_{in}$  and  $r_{tr}$ . These trapped oscillations' eigenfunctions were studied and invoked as an explanation for QPOs detected in white dwarf accretion disks (Yamasaki T. K., 1995). The analysis showed these oscillations could be simulated by the  $\kappa$ -mechanism (Yamasaki T. K., 1996).

Another type of oscillations is theorized to be contained in the transition region between

an ADAF (Advection Dominated Accretion Flow) disk and a Shakura-Sunyaev Disk (SSD). ADAFs are thought to explain the spectra of the hard state of x-ray stars. Accretion disks are thought to be ADAFs only in the inner regions and SSDs for the outer regions, so there must be a transition region between the SSD and the ADAF regions. There is no single established model for this transition region.

An important characteristic for the transition region is a super-Keplerian rotation occurring in the region (Honma, 1996) (Abramowicz M. I.-P., 1998). In the ADAF region, the rotation is sub-Keplerian, but becomes super-Keplerian in the transition region and the velocity plunges as the velocity distribution continues outward into the SSD region. Due to a super-Keplerian rotation reverting to a Keplerian rotation in the narrow transition region, the specific angular momentum also decreases sharply outward in this region.

This decrease in the specific angular momentum leads to the Rayleigh instability if the inhomogeneity of the transition region is negligible. Other physical variables, such as density, also change sharply, which serves to counteract any Rayleigh instability from occurring. If the physical variables' actions are stronger than the Rayleigh instability, perturbations manifest as oscillations rather than growing motions and the oscillations' frequencies would be low if the two opposing actions are close in magnitude to each other as to almost cancel each other out. The low frequency oscillations will be trapped in the transition region due to a number of reasons. The regions outside the transition region contain physical quantities which distributions are not sharp, so the propagation of the perturbations are moderated by the relation between the epicyclic frequency  $\kappa(r)$  and the wave frequency  $\omega$ .

Since the wave frequencies are smaller than  $\kappa$  in surrounding media, the waves cannot extend into the surrounding areas. So the waves are trapped in the narrow transition region. It has been considered these waves would explain the 1-15 Hz QPOs detected in GRS 1915+105 (Markwardt, 1999). It would be expected that the trapped oscillations would not cause observable luminosity variations, but the transition region emits considerable radiation with the whole luminosity emitted from the SSD region (Honma, 1996) (Kato S. N., 1998) (Manmoto, 2000).

The trapped oscillations' presence in the transition layer between the ADAF and SSD regions is based on an assumption that the transition region is a narrow region, which entails a large turbulent conductivity. This possibility stands as an unanswered question as of yet (Abramowicz M. G., 2000).

Viscosity induces an effect that leads to the excitation of oscillations. An increase of the viscosity in the compressed phase, or decrease of the viscosity in the expanded phase, serves as oscillation amplification. The viscous force is usually invoked using the  $\alpha$ -model of turbulent viscosity. A diffusive viscous force does not necessarily happen in reality due to the assumption that turbulence happens instantaneously as a physical response to any change in the surroundings, which would imply an infinite speed for the response. Others have sought to remedy this physical paradox (Popham, 1992) (Narayan R. , 1992) (Kato S. I., 1994) (Papaloizou, 1994).

This physical paradox can be worked around, though.

In considering the effects of viscous forces on oscillations, the time scale of the

turbulence is of the order of  $1/\Omega$ , so when the frequencies of oscillations are lower than  $\Omega$ , the invocation of a diffusive viscous force is appropriate in a description of the viscous stress force in steady disks. If the frequencies of oscillations are larger than  $\Omega$ , the turbulence cannot respond instantaneously to the change in the medium, which means a time lag in turbulence as a response to the oscillations. Studies show that the time lag in response of turbulence acts in a direction as to stabilize the oscillations (Kato S. , 1994) (Kato S. , Turbulent Stress Tensor in Accretion Disks Derived by Second-Order Closure Modeling, 1994) (Yamasaki T. K., 1996). Much remains to be discovered in this topic so there isn't an established full picture of this phenomenon of how the turbulent viscosity drives the oscillations.

The presence of viscosity creates large scale circulations as well as accretion flows in an unperturbed state. In the case of local oscillations, these effects only act to change the frequencies of the oscillations to a Doppler-shifted one and do not affect the growth rate (Ortega-Rodriguez, 2000). In ADAF disks, thermal energy via viscosity is not radiated away but transported inwardly as internal energy. The thermal imbalance, created by a radiative loss maintained by releasing of gravitational energy by contraction, renders the stellar pulsation unstable. The viscous processes are more important in disk oscillations in contrast to stellar oscillations and serve to drive the oscillations in disks through excitation by viscous processes of turbulence. More has to be discovered in studies of turbulence to expand on their contribution to oscillatory processes.

## CHAPTER VIII

### **RADIAL PULSATION (HELIOSEISMOLOGY)**

In this chapter we focus on radial pulsation so we can understand the phenomenon of oscillatory motion in the accretion disk. Diskoseismology pertains to the study of small perturbations of the geometrically thin, optically thick accretion disks around black holes. Perturbations can be compared to travelling disturbances in any medium, such as sound waves, and share such characteristic properties. Helioseismology is the study of same, applied to the surfaces of stars and diskoseismology extends these principles to the surfaces of the accretion disks in the extreme vicinity of the compact object (black hole for one). We use this as a starting point and extrapolate these features for the disk at its inner horizon where the QPO signal originates. We delved into the equations that describe helioseismology in the first chapter and now we expand on the topic for a cylindrical reference frame and find how the physical conditions change for that setting.

#### **Helioseismology in a Cylindrical Reference Frame**

Modifying the helioseismological approach to the disk scenario entails utilizing a cylindrical reference frame rather than a spherical one. Starting with the cylindrical coordinate,

$$r = \sqrt{R^2 + z^2}; \quad (8.1)$$

$R$  is the radial coordinate confined to the  $x$ - $y$  plane in the Cartesian reference frame while  $z$  is the vertical displacement from the equatorial plane.

Taking the derivative of  $r$  to find the velocity, then again to find the acceleration in terms of  $R$  and  $z$ :

$$v = \frac{dr}{dt} = \frac{1}{2}[R^2 + z^2]^{-\frac{1}{2}} * 2R \left(\frac{dR}{dt}\right) + \frac{1}{2}[R^2 + z^2]^{-\frac{1}{2}} * 2z \left(\frac{dz}{dt}\right) \quad (8.2a)$$

$$= \frac{R}{[R^2+z^2]^{\frac{1}{2}}} \frac{dR}{dt} + \frac{z}{[R^2+z^2]^{\frac{1}{2}}} \frac{dz}{dt} \quad (8.2b)$$

$$a = \frac{d^2r}{dt^2} = \frac{1}{[R^2+z^2]^{\frac{1}{2}}} \left(\frac{dR}{dt}\right)^2 - \frac{R^2}{[R^2+z^2]^{\frac{3}{2}}} \left(\frac{dR}{dt}\right)^2 + \frac{R}{[R^2+z^2]^{\frac{1}{2}}} \frac{d^2R}{dt^2} + \frac{1}{[R^2+z^2]^{\frac{1}{2}}} \left(\frac{dz}{dt}\right)^2 - \frac{z^2}{[R^2+z^2]^{\frac{3}{2}}} \left(\frac{dz}{dt}\right)^2 + \frac{z}{[R^2+z^2]^{\frac{1}{2}}} \frac{d^2z}{dt^2} \quad (8.3a)$$

$$= \frac{1}{r} v_R^2 \left(1 - \left(\frac{R}{r}\right)^2\right) + \frac{R}{r} \frac{d^2R}{dt^2} + \frac{1}{r} v_z^2 \left(1 - \left(\frac{z}{r}\right)^2\right) + \frac{z}{r} \frac{d^2z}{dt^2} \quad (8.3b)$$

The acceleration equation contains the individual acceleration terms for  $R$  and  $z$ , as well as the corresponding centrifugal forces in both the  $R$  and  $z$  directions.

Given that  $v_R$  is projected in the  $R$  direction only and  $v_z$  in the  $z$  direction only as well, the centrifugal force components of the equation (8.3) reduce to:

$$\frac{v_R^2}{r} \left(1 - \left(\frac{R}{r}\right)^2\right) \rightarrow \frac{v_R^2}{r} \left(1 - \left(\frac{R}{r}\right)^2\right) = \frac{v_R^2}{r} \left(1 - \left(\frac{R}{R}\right)^2\right) = 0, \quad r \rightarrow R \quad (8.4a)$$

$$\frac{v_z^2}{r} \left(1 - \left(\frac{z}{r}\right)^2\right) \rightarrow \frac{v_z^2}{r} \left(1 - \left(\frac{z}{r}\right)^2\right) = \frac{v_z^2}{r} \left(1 - \left(\frac{z}{z}\right)^2\right) = 0, \quad r \rightarrow z \quad (8.4b)$$

The acceleration equation is now simplified as:

$$a = \frac{d^2r}{dt^2} = \frac{R}{r} \frac{d^2R}{dt^2} + \frac{z}{r} \frac{d^2z}{dt^2} = \sin \theta \frac{d^2R}{dt^2} + \cos \theta \frac{d^2z}{dt^2} \quad (8.5)$$

For a disk in hydrostatic equilibrium, a model is utilized to determine the range of pulsation in the stellar matter. The interior of the disk is subject to a pressure  $P$  and the disk is comprised of thin cylindrical rings of mass  $m$ , radius  $R$ , and height  $z$ .

Newton's 2<sup>nd</sup> law (equation 1.3) as applied to this scenario is:

$$m \frac{d^2 r}{dt^2} = -\frac{GMm}{r^2} + 2\pi R z P, \quad M \text{ being the mass of the compact object.} \quad (8.6)$$

The equilibrium model requires the left hand of the equation to equal zero, which means that the following to be true:

$$-\frac{GMm}{R^2+z^2} = -\frac{GMm}{R^2\left(1-\left(\frac{z}{R}\right)^2\right)} = -\frac{GMm}{R^2}\left(1-\frac{2z}{R}\right) \rightarrow \frac{GMm}{R_0^2} - \frac{2GMmz_0}{R_0^3} = 2\pi R_0 z_0 P_0 \quad (8.7)$$

and for the vertical gravity component in the disk, with the disk self-gravity being negligible, the gravitational contribution comes from the cosine of the central object gravity:

$$\frac{GMm}{R^2} \cos \theta = \frac{GMm}{R^2} \left(\frac{z}{R}\right) \quad (8.8)$$

Linearizing the coordinates and pressure gives:

$$R = R_0 + \delta R; \quad z = z_0 + \delta z; \quad P = P_0 + \delta P; \quad (8.9a,b,c)$$

$$m \frac{d^2 r}{dt^2} = m \frac{d^2 R}{dt^2} + m \frac{d^2 z}{dt^2} \quad (8.10a)$$

$$= m \left( \frac{d^2 R_0}{dt^2} + \frac{d^2(\delta R)}{dt^2} \right) + m \left( \frac{d^2 z_0}{dt^2} + \frac{d^2(\delta z)}{dt^2} \right) \quad (8.10b)$$

$$m \frac{d^2 r}{dt^2} = -\frac{GMm}{(R_0+\delta R)^2+(z_0+\delta z)^2} + 2\pi(R_0 + \delta R)(z_0 + \delta z)(P_0 + \delta P) \quad (8.11a)$$

$$= \left[ -\frac{GMm}{R_0^2} \left( 1 - 2\frac{\delta R}{R_0} + 2\frac{z_0}{R_0} - 2\frac{\delta z}{R_0} \right) + 2\pi R_0 \left( 1 + \frac{\delta R}{R_0} \right) z_0 \left( 1 + \frac{\delta z}{z_0} \right) P_0 \left( 1 + \frac{\delta P}{P_0} \right) \right] \quad (8.11b)$$

$$= \left[ -\frac{GMm}{R_0^2} + \frac{2GMm}{R_0^3} \delta R + \frac{2GMmz_0}{R_0^3} + \frac{2GMm}{R_0^3} \delta z + 2\pi R_0 z_0 P_0 + 2\pi R_0 z_0 P_0 \left( \frac{\delta R}{R_0} \right) + 2\pi R_0 z_0 P_0 \left( \frac{\delta z}{R_0} \right) + 2\pi R_0 z_0 P_0 \left( \frac{\delta P}{R_0} \right) \right] \quad (8.12c)$$

Recall that the pressure relation can be substituted for another adiabatic relation:

$$\frac{\delta P}{P_0} = -3\gamma \frac{\delta R}{R_0} - 3\gamma \frac{\delta z}{z_0} \quad (8.13)$$

The force equation, with eq. (8.38) inserted in the pressure relations, becomes:

$$m \frac{d^2 r}{dt^2} = \frac{2GMm}{R_0^3} \delta R + \left( \frac{GMm}{R_0^3} \right) \delta R + \frac{2GMm}{R_0^3} \delta z + 2\pi R_0 z_0 P_0 \left( \frac{\delta R}{R_0} \right) + 2\pi R_0 z_0 P_0 \left( \frac{\delta z}{R_0} \right) + 2\pi R_0 z_0 P_0 \left( -3\gamma \frac{\delta R}{R_0} - 3\gamma \frac{\delta z}{z_0} \right)$$

(8.14)

$$= \left[ (3 - 3\gamma) \frac{GMm}{R_0^3} \delta R \right] + \left[ (3 - 3\gamma) \frac{GMm}{R_0^3} \delta z \right] \quad (8.15)$$

$$m \left[ \frac{d^2(\delta R)}{dt^2} + \frac{d^2(\delta z)}{dt^2} \right] = \left[ (3 - 3\gamma) \frac{GMm}{R_0^3} \delta R \right] + \left[ (3 - 3\gamma) \frac{GMm}{R_0^3} \delta z \right] \quad (8.16)$$

This is separable into two different equations in terms of  $\delta R$  and  $\delta z$ .

$$\frac{d^2(\delta R)}{dt^2} + \left[ (3\gamma - 3) \frac{GM}{R_0^3} \right] \delta R = 0 \quad (8.17a)$$

$$\frac{d^2(\delta z)}{dt^2} + \left[ (3\gamma - 3) \frac{GM}{R_0^3} \right] \delta z = 0 \quad (8.17b)$$

The corresponding angular frequencies of the oscillating models are as follows:

$$\omega_R^2 = (3 - 3\gamma) \frac{GM}{R_0^3} \quad (8.18a)$$



$$\omega_z^2 = (3 - 3\gamma) \frac{GM}{R_0^3} \quad (8.18b)$$

The disk scenario is hydrodynamically stable in the vertical direction and radial direction, since the adiabatic index of the matter would have to be below that of  $\gamma = 1$  to encounter a dynamical instability, which is a physical improbability. As the gas becomes increasingly ionized, the adiabatic index, due to the larger specific heats, would approach unity, or a value of one. So an dynamical instability in an accretion disk could be avoided in a cylindrical reference frame even as the gas became highly ionized and its adiabatic index approached unity.

### Adiabatic Index Relation for a Disk Distribution

The pressure follows a relation:

$$PV^\gamma = \text{constant} \quad (8.19)$$

with the volume of concern depending on the geometry and mass distribution of the situation of concern.

For a spherical mass density distribution:

$$V = \frac{4}{3}\pi R^3 \quad \rightarrow \quad P \left( \frac{4}{3}\pi R^3 \right)^\gamma = \text{constant} \quad (8.20a,b)$$

Which leads to the relation:

$$\frac{\delta P}{P_0} = -3\gamma \frac{\delta R}{R_0} \quad \text{for linearized pressure and radius} \quad (8.21)$$

$$P = P_0 + \delta P \quad R = R_0 + \delta R \quad (8.22)$$

$$P_0 \left( 1 + \frac{\delta P}{P_0} \right) \left( \frac{4}{3}\pi \right)^\gamma R_0^{3\gamma} \left( 1 + \frac{\delta R}{R_0} \right)^{3\gamma} = \text{constant} \quad (8.23)$$

$$\left(1 + \frac{\delta P}{P_0}\right) \left(1 + \frac{\delta R}{R_0}\right)^{3\gamma} = \frac{\text{constant}}{\frac{4}{3}\pi R_0^3 P_0} = 1 \quad (8.24)$$

$$1 + \frac{\delta P}{P_0} + 3\gamma \frac{\delta R}{R_0} = 1 \quad (8.25)$$

$$\frac{\delta P}{P_0} = -3\gamma \frac{\delta R}{R_0} \quad (8.26)$$

The geometry of a disk affects the mass distribution; the area of a cylindrical disk is:

$$A = 2\pi r^2 + 2\pi r h \quad r = \text{radius}, \quad z = \text{height} \quad (8.27)$$

$$\text{Let } h = \left(\frac{h}{R}\right) R = \frac{h}{R} (R_0 + \delta R) = \frac{h}{R} R_0 \left(1 + \frac{\delta R}{R_0}\right) \text{ and } \frac{z}{R} = \cos \theta,$$

(8.28a,b,c)

and  $\cos \theta$  sweeps from a vertical range of  $z = h$  above the equatorial plane, to  $z = -h$ , below the equatorial plane.

The volume of the disk becomes:

$$V = \frac{2}{3}\pi r^3 + \pi r^2 h = \frac{2}{3}\pi r^3 + \pi r^3 \left(\frac{h}{r}\right) \quad (8.29a)$$

$$= \pi r^3 \left[\frac{2}{3} + \frac{h}{r}\right] = \pi r^3 \left[\frac{2}{3} + \cos \theta\right], \quad z = h. \quad (8.29b)$$

Which is not much different from a spherical distribution.

$$PV^\gamma = \text{constant} \rightarrow P \left(\pi r^3 \left[\frac{2}{3} + \cos \theta\right]\right)^\gamma = \text{constant}; \quad (8.30)$$

Inserting the linearized terms yields the following expression:

$$(P_0 + \delta P)\pi^\gamma (R_0 + \delta R)^{3\gamma} \left(\frac{2}{3} + \cos \theta\right)^\gamma = (P_0 + \delta P) \left(\frac{2}{3}\pi\right)^\gamma (R_0 + \delta R)^{3\gamma} \left(1 + \frac{3}{2}\cos \theta\right)^\gamma = \text{constant}; \quad (8.31)$$

$$P_0 \left(\frac{2}{3}\pi\right)^\gamma R_0^{3\gamma} \left(1 + \frac{\delta P}{P_0}\right) \left(1 + \frac{\delta R}{R_0}\right)^{3\gamma} \left(1 + \frac{3}{2}\cos \theta\right)^\gamma = \text{constant}; \quad (8.32)$$

$$\left(1 + \frac{\delta P}{P_0}\right) \left(1 + \frac{\delta R}{R_0}\right)^{3\gamma} = \frac{\text{constant}}{P_0 \left(\frac{2}{3}\pi\right)^\gamma R_0^{3\gamma} \left(1 + \frac{3}{2}\cos\theta\right)^\gamma} = 1; \quad (8.33)$$

I obtain the relation for a cylindrical disk distribution:

$$\frac{\delta P}{P_0} = -3\gamma \frac{\delta R}{R_0} \quad (8.34)$$

The adiabatic relation is identical for a cylindrical distribution as it is to a spherical distribution. The pressure gradient is proportional to the gravitational force directed radially in the direction of the compact object so the equilibrium conditions will be in radial terms. The vertical equilibrium conditions will be taken as the cosine of the radial terms since the disk self-gravity is negligible and the compact object gravity is the dominant influence for the disk.

An interesting note is the correlation between the coefficients for both the cylindrical and spherical distributions:

$$\text{The spherical distribution coefficient is:} \quad \left(\frac{4}{3}\pi\right)^\gamma, \quad (8.35)$$

$$\text{while the cylindrical distribution coefficient is:} \quad \left(\frac{2}{3}\pi\right)^\gamma \left(1 + \frac{3}{2}\cos\theta\right)^\gamma. \quad (8.36)$$

Setting the two equivalent to each other, gives us a condition for  $\cos\theta$ :

$$\left(\frac{4}{3}\pi\right)^\gamma = \left(\frac{2}{3}\pi \left(1 + \frac{3}{2}\cos\theta\right)\right)^\gamma; \quad \cos\theta = \frac{z}{R} = \frac{h}{R} = \frac{2}{3}; \quad (8.37)$$

Since the QPO ratio of the vertical and radial epicyclic frequencies is 3:2, we look at the frequency ratio and compare it to the ratio of the height and radius:

$$\frac{\omega_z}{\omega_r} = \frac{3}{2} = \frac{\frac{v_s}{h}}{\frac{v_K}{R}} = \left(\frac{v_s}{h}\right) \left(\frac{R}{v_K}\right) = \left(\frac{v_s}{v_K}\right) \left(\frac{R}{h}\right); \quad (8.38)$$

The vertical angular frequency  $\omega_z$  is taken as the speed of sound,  $v_s$ , over the vertical coordinate at the top of the disk where  $z = h$ , and the radial angular frequency  $\omega_r$  is taken as the Keplerian velocity divided by the radial coordinate  $R$ , and the ratio of the two epicyclic frequencies give us the ratio of the sound speed to Keplerian velocity, times the ratio of the radius over the height. This relation holds true for any radius or height.

If we take the unifying geometric condition for the coefficients of both distributions, we get:

$$\frac{R}{h} = \frac{3}{2} \quad \frac{\omega_z}{\omega_r} = \frac{3}{2} = \left(\frac{3}{2}\right) \left(\frac{v_s}{v_K}\right) \rightarrow \left(\frac{v_s}{v_K}\right) = 1 \quad (8.39)$$

$$v_s = v_K \quad \text{for the QPO radius.} \quad (8.40)$$

There is only one location where the speed of sound matches the Keplerian speed at that location. The QPO signal would emanate from that radial location where the Keplerian velocity is greatest, and simultaneously induce a large sound speed in the vertical direction, creating a large amplitude in the signal. That location is also known as the sonic point where the speed of infalling material goes from subsonic to supersonic velocities. The sonic point is located at the sonic radius,  $r_{sonic}$ .

In the Shakura-Sunyaev and Novikov-Thorne models, the sonic radius is determined to coincide with the ISCO for sub-Eddington flows. As the accretion flow increases, the sonic radius migrates away from the ISCO. So it stands to reason the ISCO is the qualifying radius for the source phenomenon of the QPO signals for sufficiently low accretion rates. The relocation of the sonic point shifts the originating radius of the QPO further out from the compact object

through the accretion disk.

The geometric condition is useful in determining where the accretion turns from a disk-like flow scenario to a spherical (Bondi) flow one. The significance of the co-existence of the sonic point with the ISCO (also known as the marginally stable orbit,  $r_{ms}$ ) in the same location would explain the minority of cases of QPO candidates having a double QPO frequency. The location of the sonic point is dependent on the rate of accretion flow and as the accretion flow increases, the sonic point shifts below the ISCO into the plunging region. The speed of infalling matter becomes super-Keplerian in that region and the noise in the spectral signal emitted from that region due to the inbound turmoil of the falling matter would diminish the integrity of the QPO signal, as denoted by the quality factor, and any kind of coupling of radial and vertical oscillation modes would be inhibited. As the mass of the compact object increases, the mass accretion rate would increase so an upper bound on compact object candidate mass would be expected for a double QPO frequency signal.

## CHAPTER IX

### THE DISKOSEISMOLOGICAL APPROACH

Expanding on the diskoseismological equations from the last chapter, I go further in exploring the implications of the harmonic oscillation equation that describes the oscillation in the disk. The extended harmonic oscillation equation can be expanded in several powers for a better examination of the oscillation properties.

Starting with the following equation:

$$m \frac{d^2(\delta R)}{dt^2} = \frac{2GMm}{R_o^3} \delta R - \frac{3GMm}{R_o^3} \left(\frac{\delta R}{R_o}\right) \delta R + \frac{4GMm}{R_o^3} \left(\frac{\delta R}{R_o}\right)^2 \delta R + \frac{2GMm}{R_o^3} \delta R + \frac{(-3\gamma)GMm}{R_o^2} \left(\frac{\delta R}{R_o}\right) \quad (9.1)$$

This expression can be simplified as:

$$m \frac{d^2(\delta R)}{dt^2} = \frac{GMm}{R_o^3} (4 - 3\gamma - 3 \left(\frac{\delta R}{R_o}\right) + 4 \left(\frac{\delta R}{R_o}\right)^2 + \dots) \delta R \quad (9.2)$$

$$\frac{d^2(\delta R)}{dt^2} + \frac{GM}{R_o^3} \left(3\gamma - 4 + 3 \left(\frac{\delta R}{R_o}\right) - 4 \left(\frac{\delta R}{R_o}\right)^2 + \dots\right) \delta R = 0 \quad (9.3)$$

For the condition that the adiabatic index  $\gamma = 5/3$ , the expression is modified further:

$$\frac{d^2(\delta R)}{dt^2} + \frac{GM}{R_o^3} \left(1 + 3 \left(\frac{\delta R}{R_o}\right) - 4 \left(\frac{\delta R}{R_o}\right)^2 + \dots\right) \delta R = 0 \quad (9.4)$$

And the angular frequency becomes:

$$\omega^2 = \frac{GM}{R_0^3} \left( 1 + 3 \left( \frac{\delta R}{R_0} \right) - 4 \left( \frac{\delta R}{R_0} \right)^2 + \dots \right) \quad (9.5a)$$

$$\omega = \left( \frac{GM}{R_0^3} \right)^{\frac{1}{2}} \left( 1 + 3 \left( \frac{\delta R}{R_0} \right) - 4 \left( \frac{\delta R}{R_0} \right)^2 + \dots \right)^{\frac{1}{2}} \quad (9.5b)$$

The angular frequency yields the Keplerian frequency and the Keplerian velocity:

$$\omega = \left( \frac{GM}{R_0^3} \right)^{\frac{1}{2}} \rightarrow v = R_0 * \omega = R_0 \left( \frac{GM}{R_0^3} \right)^{\frac{1}{2}} = \left( \frac{GM}{R_0} \right)^{\frac{1}{2}} \quad (9.6)$$

Compare this to the orbital frequencies in Kerr space-time:

$$\omega = 2\pi\nu_K = \left( \frac{GM}{r^3} \right)^{\frac{1}{2}} \left( 1 + j \hat{r}^{-\frac{3}{2}} \right)^{-1}; \quad (9.7)$$

$$j = \frac{cJ}{GM^2} = \frac{a}{M} \quad \hat{r} = \frac{rc^2}{GM} = \frac{2r}{r_s} \quad (9.8a,b)$$

The radial epicyclic frequency is as follows:

$$\nu_r = |\nu_K| \left( 1 - \hat{r}^{-1} + 8j \hat{r}^{-\frac{3}{2}} - 3j^2 \hat{r}^{-2} \right)^{\frac{1}{2}} \quad (9.9)$$

The vertical epicyclic frequency is as follows:

$$\nu_\theta = |\nu_K| \left( 1 - 4j \hat{r}^{-\frac{3}{2}} + 3j^2 \hat{r}^{-2} \right)^{\frac{1}{2}} \quad (9.10)$$

If we revert back to Newton's second law expression with the linearized radial expression (equation 8.68), not stopping at the first power:

$$\frac{1}{(R_0 + \delta R)^2} = \frac{1}{R_0^2} \left( 1 - 2 \frac{\delta R}{R} + \frac{1}{2!} (-2)(-3) \left( \frac{\delta R}{R} \right)^2 + \frac{1}{3!} (-2)(-3)(-4) \left( \frac{\delta R}{R} \right)^3 + \dots \right) \quad (9.11)$$

$$\frac{1}{(R_o + \delta R)^2} = \frac{1}{R_o^2} \left( 1 - 2 \frac{\delta R}{R} + 3 \left( \frac{\delta R}{R} \right)^2 - 4 \left( \frac{\delta R}{R} \right)^3 + \dots \right) \quad (9.12)$$

$$m \frac{d^2(\delta R)}{dt^2} = -\frac{GMm}{R_o^2} + \frac{2GMm}{R_o^3} \delta R - \frac{3GMm}{R_o^4} (\delta R)^2 + \frac{4GMm}{R_o^5} (\delta R)^3 + 4\pi R_o^2 P_o + 8\pi R_o P_o \delta R + 4\pi R_o^2 \delta P \quad (9.13)$$

$$m \frac{d^2(\delta R)}{dt^2} = \frac{2GMm}{R_o^3} \delta R - \frac{3GMm}{R_o^4} (\delta R)^2 + \frac{4GMm}{R_o^5} (\delta R)^3 + 8\pi R_o^2 P_o \delta R + 4\pi R_o^2 \delta P \quad (9.14)$$

$$m \frac{d^2(\delta R)}{dt^2} = \frac{2GMm}{R_o^3} \delta R + \frac{2GMm}{R_o^3} \delta R - \frac{3GMm}{R_o^4} (\delta R)^2 + \frac{4GMm}{R_o^5} (\delta R)^3 + 4\pi R_o^2 \left( \frac{P_o}{P_o} \right) \delta P \quad (9.15a)$$

Inserting the hydrostatic equilibrium condition (equation 1.4) and the adiabatic relation (equation 8.34) into the above equation gives:

$$= \frac{4GMm}{R_o^3} \delta R - \frac{3GMm}{R_o^4} (\delta R)^2 + \frac{4GMm}{R_o^5} (\delta R)^3 + \left( \frac{GMm}{R_o^2} \right) \left( -3\gamma \frac{\delta R}{R_o} \right) \quad (9.15b)$$

$$m \frac{d^2(\delta R)}{dt^2} = \left( 4 - 3\gamma - 3 \left( \frac{\delta R}{R} \right) + 4 \left( \frac{\delta R}{R} \right)^2 - \dots \right) \left( \frac{GMm}{R_o^3} \delta R \right) \quad (9.15c)$$

If one neglects the powers of  $\frac{\delta R}{R}$ , a harmonic oscillation equation is yielded with a simple angular frequency:

$$\frac{d^2(\delta R)}{dt^2} + (3\gamma - 4) \left( \frac{GM}{R_o^3} \right) \delta R = 0 \quad (9.16a)$$

$$\omega = \left( \frac{GM}{R_o^3} \right)^{\frac{1}{2}} (4 - 3\gamma)^{\frac{1}{2}} \quad (9.16b)$$

With the powers of  $\frac{\delta R}{R}$  left in, one gets a harmonic oscillator equation in the following form:

$$\frac{d^2(\delta R)}{dt^2} + \left( 3\gamma - 4 + 3 \left( \frac{\delta R}{R} \right) - 4 \left( \frac{\delta R}{R} \right)^2 - \dots \right) \left( \frac{GM}{R_o^3} \right) \delta R = 0 \quad (9.17)$$

This gives us an elliptic equation. Let equation (8.82) be divided by  $\frac{1}{R_o}$ ;



$$\frac{1}{R_0} \left[ \frac{d^2(\delta R)}{dt^2} + \left( 3\gamma - 4 + 3 \left( \frac{\delta R}{R} \right) - 4 \left( \frac{\delta R}{R} \right)^2 - \dots \right) \left( \frac{GM}{R_0^3} \right) \delta R \right] = 0 \quad (9.18)$$

$$\left[ \frac{d^2 \left( \frac{\delta R}{R_0} \right)}{dt^2} + \left( 3\gamma - 4 + 3 \left( \frac{\delta R}{R} \right) - 4 \left( \frac{\delta R}{R} \right)^2 - \dots \right) \left( \frac{GM}{R_0^3} \right) \left( \frac{\delta R}{R_0} \right) \right] = 0, \quad \frac{\delta R}{R_0} = x. \quad (9.19a,b)$$

This can be rewritten as:

$$\frac{d^2 x}{dt^2} + \left( \frac{GM}{R_0^3} \right) (3\gamma - 4 + 3x - 4x^2 - \dots)x = 0, \quad \left( \frac{GM}{R_0^3} \right) = \sigma. \quad (9.20)$$

$$\frac{d^2 x}{dt^2} + \sigma[(3\gamma - 4)x + 3x^2 - 4x^3] = 0. \quad (9.21)$$

The  $\sigma$  factor can be scaled out: Let  $\tau = \sigma t$ , and

(9.22)

$$\frac{d^2 x}{d\tau^2} + [(3\gamma - 4)x + 3x^2 - 4x^3] = 0. \quad (9.23)$$

A mathematical approach can be taken here to simplify this equation further. Multiplying both sides by  $\frac{d}{dx}$ ,

$$\frac{d}{dx} \left( \frac{d^2 x}{d\tau^2} + [(3\gamma - 4)x + 3x^2 - 4x^3] \right) = 0, \quad (9.24)$$

$$\frac{d}{dt} \left( \frac{1}{2} \left( \frac{dx}{d\tau} \right)^2 + \frac{1}{2} (3\gamma - 4)x^2 + x^3 - x^4 \right) = 0, \quad (9.25)$$

$$\left( \frac{dx}{d\tau} \right)^2 + (3\gamma - 4)x^2 + 2x^3 - 2x^4 = 2c. \quad (9.26)$$

$$\left( \frac{dx}{d\tau} \right)^2 = 2x^4 - 2x^3 + (4 - 3\gamma)x^2 + q, \quad \text{where } q = \frac{2c}{\sigma}. \quad (9.27a,b)$$

We can get a modified angular frequency as a solution from this elliptic equation.

This equation can be solved numerically or analytically. The numerical method can be used to

find the characteristic frequency for the elliptic equation.

The perturbation model is scaled to this elliptic equation:

$$\left(\frac{dx}{d\tau}\right)^2 = 2x^4 - 2x^3 + (4 - 3\gamma)x^2 + q \quad (9.28)$$

A time integral is obtained this way:

$$t = \int_0^x \frac{dx'}{\sqrt{2x'^4 - 2x'^3 + (4 - 3\gamma)x'^2 + q}}, \quad \text{where } q = 1. \quad (9.29)$$

$$\text{For an initial displacement, } x_0 = -1, \text{ and } \left(\frac{dx}{d\tau}\right)_0 = 0, \quad (9.30a,b)$$

$$\text{so at } \left(\frac{dx}{d\tau}\right)_{x=x_0} = 0 = 1 + (4 - 3\gamma)x_0^2 - 2x_0^3 + 2x_0^4. \quad (9.31)$$

And solving numerically for the equation,

$$t(x_n) = \int_{x_0}^x \frac{d\tilde{x}}{\sqrt{2\tilde{x}^4 - 2\tilde{x}^3 + (4 - 3\gamma)\tilde{x}^2 + 1}}, \quad (9.32)$$

With the  $\{\{t(x_n), x_n\}, \dots\}$  data.

A curve should appear from a minimum at  $t_1$  and cross the x-axis in a sinusoidal manner to a maximum at  $t_2$ . The difference in the time interval is the half-period.

Since  $\left(\frac{dx}{d\tau}\right) = 0$  at maximal displacement, and  $x = x_{Max}$ , this indicates that

$$\left(\frac{dx}{d\tau}\right)^2 = 0 = 2x_{Max}^4 - 2x_{Max}^3 + (4 - 3\gamma)x_{Max}^2 + 1, \quad \text{for } x_{Max} \ll 1. \quad (9.33)$$

The higher power terms are smaller than the lower power terms, which indicate that this equation relates to small fluctuations and the requirement that  $q$  is larger than zero.

Obtaining the Fourier coefficients from the data and integrating numerically, then plotting them on a graph can recreate the curve of the fluctuation.

## Physical Context of the Radial Potential Energy Expression

We return to the elliptic equation, which describes the radial displacement, that is also an expression of the radial potential energy and is stated below:

$$p(x) = \left(\frac{dx}{d\tau}\right)^2 = 2x^4 - 2x^3 + (4 - 3\gamma)x^2 + q. \quad (9.34)$$

Close to  $x = 0$ , the value of the adiabatic index term dominates.

In the case where  $x = 0$ , there is no displacement, and

$$v_0^2 = \left(\frac{dx}{d\tau}\right)^2 = q. \quad (9.35)$$

This gives us a context of the constant  $q$ . Another context can be found at the location of the extrema, when  $x = x_{\max}$ , or  $x = x_{\min}$  (or  $x_m$ ):

$$0 = 2x_m^4 - 2x_m^3 + (4 - 3\gamma)x_m^2 + q. \quad (9.36)$$

To find the equilibrium points, I take the derivative of the equation:

$$8x^3 - 6x^2 + 2(4 - 3\gamma)x = 0. \quad (9.37)$$

So a root exists at  $x = 0$ , therefore an equilibrium point resides at that location.

To find more equilibrium points, other roots have to be found:

$$8x^2 - 6x + 2(4 - 3\gamma) = 0. \quad (9.38)$$

Two more roots are found:

$$x = \frac{6 \pm \sqrt{36 - 16(4 - 3\gamma)}}{16}, \quad x = \left(\frac{3}{8}\right) \pm \sqrt{\left(\frac{3}{8}\right)^2 - \left(\frac{1}{16}\right)(4 - 3\gamma)}. \quad (9.39)$$

Looking at the equation,

$$p(x) = 2x^4 - 2x^3 + 2(4 - 3\gamma)x^2, \quad (9.40)$$

Let the adiabatic index term equal a quantity,  $B$ :  $(n - 3\gamma) = B$ ,  $n = 4$  for spherical,  
 $n = 3$  for cylindrical,  
 $n = 2$ , for undetermined.

(9.41)

The value of 'n' is determined by the derived values multiplied with the Keplerian frequencies, in each case of the helioseismological approach, whether it is the spherical (classical) reference frame expressed by equation 9.16, or the cylindrical reference frame as taken for the accretion disk reference frame expressed by equation 8.18. The final value of  $n = 2$  is a lower value taken for an undetermined reference frame, presumably a flatter one, referring to accretion constrained to a two-dimensional plane.

The radial potential expression equation with the  $B$  term now is expressed as:

$$\left(\frac{\partial x}{\partial \tau}\right)^2 = 2x^4 - 2x^3 + Bx^2 + q. \quad (9.42)$$

Taking the case that  $\gamma = \frac{5}{3}$ , the adiabatic index term turns negative. The adiabatic index term remains negative for any value above the value of  $\gamma = \frac{4}{3}$ , for which the term becomes zero, and for all values less than  $4/3$ , the term becomes positive. The motion would be unstable for a positive adiabatic index term and stable for a negative one.

$$\gamma = \frac{5}{3} \quad \rightarrow \quad 4 - 3\gamma = -1, \quad (9.43)$$

$$\gamma < \frac{4}{3} \rightarrow 4 - 3\gamma > 0 \text{ (positive)} \quad (9.44)$$

At  $x = 0$ ,  $p(x) = 0$ , so in the case  $q > 0$ , the energy would be below what it would be at  $x = 0$ , so it never reaches the equilibrium point at  $x = 0$ . That value of  $x$  is an unstable equilibrium point and

any perturbation to either direction sends any particle towards the other equilibrium points at the bases of the curve, specifically, at the points  $x_1$  and  $x_2$ . There would be an oscillation motion about these points.

In the case  $q > 0$ , there are two ranges of motion that circulate about the two non-zero equilibrium points at  $x_1$  and  $x_2$ .

In the case  $q < 0$ , there is a distorted range of motion with a suppressed oscillation motion across the bottom of the curve.

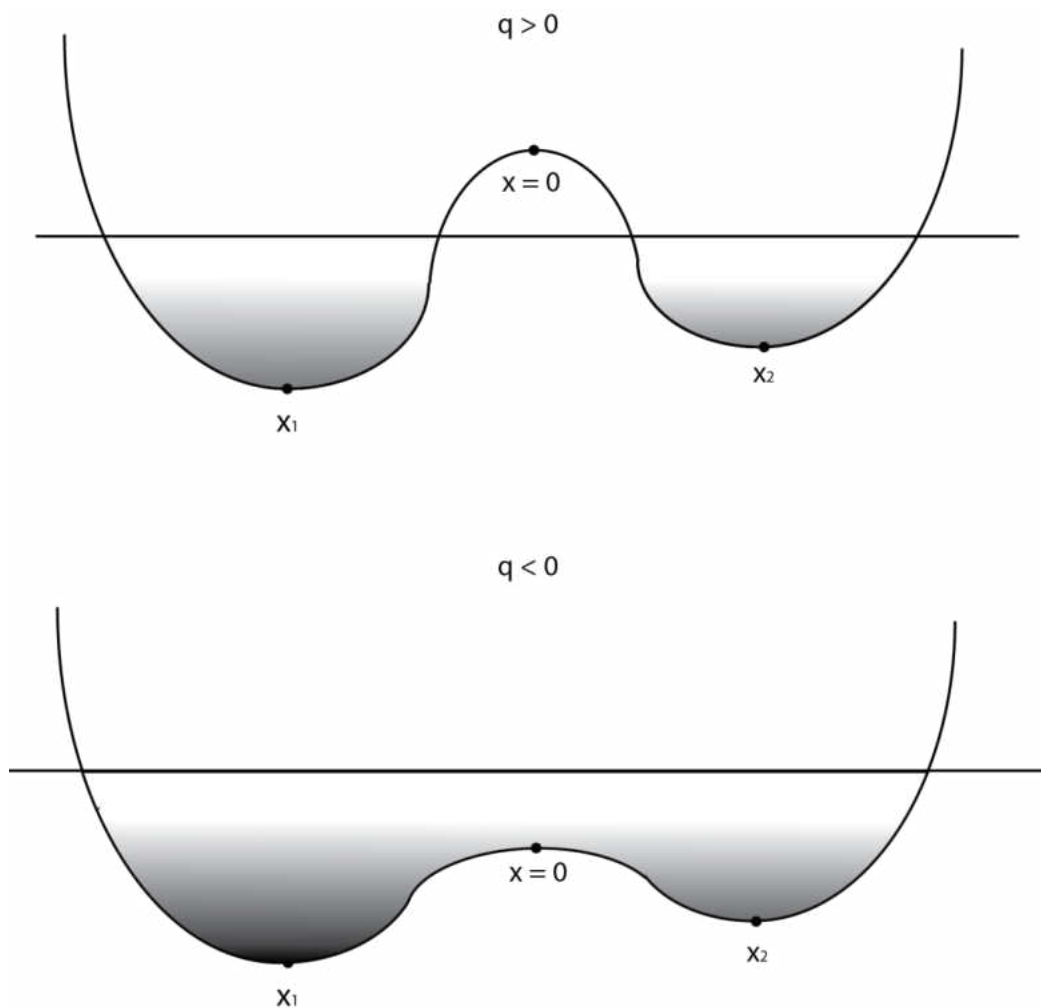


Figure 18. Diagram of the Radial Potential Energy curve with the roots shown for each case of  $q$ .

There are small oscillations about the equilibrium points  $x = x_1$ , and  $x = x_2$ , with a definite frequency ratio.

There would be spring constants corresponding to the oscillations such that:

$$k_1 = \left( \frac{\partial^2 p}{\partial x^2} \right)_{x=x_1}, \quad k_2 = \left( \frac{\partial^2 p}{\partial x^2} \right)_{x=x_2}. \quad (9.45a,b)$$

$$\frac{\partial^2 p}{\partial x^2} = 16x - 16, \quad k_1 = 16x_1 - 16, \quad k_2 = 16x_2 - 16. \quad (9.46a,b,c)$$

For  $\gamma = \frac{5}{3}$ ,  $x_1 = -0.076$ , and  $x_2 = 0.826$ .

The spring constants become:

$$k_1 = 7.211, \quad k_2 = -7.211.$$

In this case,  $k_1 = -k_2$ .

The angular frequencies can be found for each equilibrium point. Finding the roots for the equation for a given adiabatic index ( $\gamma = 5/3$ , for example) is the first step.

The next step is taking the second derivative, with respect to  $x$ , of the equation then inserting each value of the non-zero roots to yield an angular frequency for each root.

In the case of the adiabatic index term  $(4 - 3\gamma)$ , or  $B = -1$ , when taken with the adiabatic index of  $5/3$ , the first derivative of the equation, factored with respect to  $x$ , gives the roots:

$$8x^3 - 6x^2 + 2(4 - 3\gamma)x \rightarrow 8x^2 - 12x + 2(4 - 3\gamma) = 0. \quad (9.47)$$

$$\text{For } \gamma = \frac{5}{3}, \quad x = -\frac{1}{4}, 1. \quad (9.48)$$

The frequencies are found by inserting the root values into the second derivative of the equation with respect to  $x$ .

$$24\left(-\frac{1}{4}\right)^2 - 12\left(-\frac{1}{4}\right) - 2 = \frac{3}{2} + 3 - 2 = \frac{5}{2} = \omega_1^2 \quad (9.49)$$

$$24(1)^2 - 12(1) - 2 = 10 = \omega_2^2 \quad (9.50)$$

The ratio of angular frequencies is:

$$\frac{\omega_2}{\omega_1} = \sqrt{\frac{10}{2.5}} = 2. \quad \text{A ratio of } \frac{2}{1} \quad (9.51)$$

For the adiabatic index term derived for a spherical reference frame with an value of  $n = 4$  ( $4 - 3\gamma$ ), and the ideal gas adiabatic index of  $5/3$  inserted into the equation, which yields an value of  $B = -1$ , an integer ratio of 2 to 1 is found.

If the adiabatic index term is adjusted, like to  $(3 - 3\gamma)$ , the equation is modified further:

$$24x^2 - 12x - 2(3 - 3\gamma) = 24x^2 - 12x - 4 = 0. \quad (\text{for } \gamma = \frac{5}{3}) \quad (9.52)$$

The new roots are given:

$$x = \frac{1}{8}(3 \pm \sqrt{41}). \quad (9.53)$$

And the corresponding frequencies are:

$$24\left(\frac{1}{8}(3 + \sqrt{41})\right)^2 - 12\left(\frac{1}{8}(3 + \sqrt{41})\right) - 4 = 5.447 = \omega_1^2 \quad (9.54)$$

$$24\left(\frac{1}{8}(3 - \sqrt{41})\right)^2 - 12\left(\frac{1}{8}(3 - \sqrt{41})\right) - 4 = 15.0523 = \omega_2^2 \quad (9.55)$$

The ratio of angular frequencies is:

$$\frac{\omega_2}{\omega_1} = \sqrt{\frac{15.0523}{5.447}} = 1.66. \quad \text{A ratio of } \frac{5}{3}. \quad (9.56)$$

The adiabatic index term for a cylindrical reference frame with an value of  $n = 3$ ,  $(3 - 3\gamma)$ , in the case of ideal gas, which gives a value of  $B = -2$ , gives an integer ratio of 5 to 3 (~1.66).

Doing the same thing with a new adiabatic index term,  $(2 - 3\gamma)$ , the equation is modified further:

$$24x^2 - 12x - 2(2 - 3\gamma) = 24x^2 - 12x - 6 = 0. \quad (\text{for } \gamma = \frac{5}{3}) \quad (9.57)$$

The new roots are given:

$$x = \frac{1}{8}(3 \pm \sqrt{57}). \quad (9.58)$$

And the corresponding frequencies are:

$$24\left(\frac{1}{8}(3 + \sqrt{57})\right)^2 - 12\left(\frac{1}{8}(3 + \sqrt{57})\right) - 6 = 8.587 = \omega_1^2 \quad (9.59)$$

$$24\left(\frac{1}{8}(3 - \sqrt{57})\right)^2 - 12\left(\frac{1}{8}(3 - \sqrt{57})\right) - 6 = 19.9124 = \omega_2^2 \quad (9.60)$$

The ratio of angular frequencies is:

$$\frac{\omega_2}{\omega_1} = \sqrt{\frac{19.9124}{8.587}} \sim 1.5. \quad \text{A ratio of } \frac{3}{2} \quad (9.61)$$

The adiabatic index term with value of  $n = 2$  ( $2 - 3\gamma$ , and  $B = -3$ ), in the case of ideal gas, gives the magic ratio of 3 to 2 (3 : 2, or 1.5).

The adiabatic index ( $B$ ) term is the term that determines the ratio of the angular frequencies. It



implies for a higher adiabatic index and a lower value of  $n$ , a smaller integer ratio of frequencies occur. For double QPO frequencies that occur with those resonances, it'd reveal the situation the accretion was occurring in, and its reference frame.

### Context of the Orbital Frequencies

Going back to the orbital frequencies which are taken from equations (7.123 and 7124):

$$\omega_K = \left(\frac{GM}{r^3}\right)^{\frac{1}{2}} \left(1 + \frac{a}{M} \left(\frac{M}{r}\right)^{\frac{3}{2}}\right)^{-1} = \left(\frac{GM}{r^3}\right)^{\frac{1}{2}} \left(1 + a \left(\frac{M}{r^3}\right)^{\frac{1}{2}}\right)^{-1} \quad (9.62)$$

$$\omega_K = 2\pi\nu_K \quad (9.63)$$

$$\nu_r = |\nu_K| \left(1 - \frac{M}{r} + 8a \left(\frac{M}{r^3}\right)^{\frac{1}{2}} - 3\frac{a^2}{r^2}\right)^{\frac{1}{2}} \quad (9.64)$$

$$\nu_\theta = |\nu_K| \left(1 - 4a \left(\frac{M}{r^3}\right)^{\frac{1}{2}} + 3\frac{a^2}{r^2}\right)^{\frac{1}{2}} \quad (9.65)$$

Expanding the radial epicyclic frequency in full then as a Taylor series, from equation (7.123):

$$\nu_r = \left(\frac{GM}{r^3}\right)^{\frac{1}{2}} \left(\left(1 + a \left(\frac{M}{r^3}\right)^{\frac{1}{2}}\right)^{-2}\right)^{\frac{1}{2}} \left(1 - \frac{M}{r} + 8a \left(\frac{M}{r^3}\right)^{\frac{1}{2}} - 3\frac{a^2}{r^2}\right)^{\frac{1}{2}} \quad (9.66a)$$

$$\nu_r = \left(\frac{GM}{r^3}\right)^{\frac{1}{2}} \left(\left(1 - 2a \left(\frac{M}{r^3}\right)^{\frac{1}{2}}\right)\right)^{\frac{1}{2}} \left(1 - \frac{M}{r} + 8a \left(\frac{M}{r^3}\right)^{\frac{1}{2}} - 3\frac{a^2}{r^2}\right)^{\frac{1}{2}} \quad (9.66b)$$

$$\nu_r = \left(\frac{GM}{r^3}\right)^{\frac{1}{2}} \left(1 - \frac{M}{r} + 6a \left(\frac{M}{r^3}\right)^{\frac{1}{2}} + 6a \left(\frac{M}{r^3}\right)^{\frac{1}{2}} \left(\frac{a}{r}\right)^2 - \frac{3a^2}{r^2} - 16a^2 \left(\frac{M}{r^3}\right) + \dots\right)^{\frac{1}{2}} \quad (9.66c)$$

Taking the same approach for the vertical epicyclic frequency, as stated by equation (7.124):

$$\nu_{\theta} = \left(\frac{GM}{r^3}\right)^{\frac{1}{2}} \left( \left( 1 - 2a \left(\frac{M}{r^3}\right)^{\frac{1}{2}} \right) \right)^{\frac{1}{2}} \left( 1 - 4a \left(\frac{M}{r^3}\right)^{\frac{1}{2}} + 3\frac{a^2}{r^2} \right)^{\frac{1}{2}} \quad (9.67a)$$

$$\nu_{\theta} = \left(\frac{GM}{r^3}\right)^{\frac{1}{2}} \left( 1 - 6a \left(\frac{M}{r^3}\right)^{\frac{1}{2}} + 6a \left(\frac{M}{r^3}\right)^{\frac{1}{2}} \left(\frac{a}{r}\right)^2 + 3\frac{a^2}{r^2} + 8a^2 \left(\frac{M}{r^3}\right) + \dots \right)^{\frac{1}{2}} \quad (9.67b)$$

$$\nu_{\theta} = \left(\frac{GM}{r^3}\right)^{\frac{1}{2}} \left( 1 + 3 \left( -2a \left(\frac{M}{r^3}\right)^{\frac{1}{2}} - 2a \left(\frac{M}{r^3}\right)^{\frac{1}{2}} \left(\frac{a}{r}\right)^2 + \frac{a^2}{r^2} \right) - 4 \left( -2a \left(\frac{M}{r^3}\right)^{\frac{1}{2}} + \dots \right)^2 \right)^{\frac{1}{2}} \quad (9.67c)$$

The epicyclic frequencies can be regarded as a natural consequence of pulsations of matter moving along the general relativistic metric field. The gravitational field imparts a resonant influence that carries through to the natural frequencies of the emitted radiation.

Reconciling the radial epicyclic frequency expression with the classical helioseismological expression requires setting these two equations equal to each other:

$$\omega = \left(\frac{GM}{R_0^3}\right)^{\frac{1}{2}} (3\gamma - 4)^{\frac{1}{2}} \quad (9.68)$$

$$\omega = \left(\frac{GM}{R_0^3}\right)^{\frac{1}{2}} \left( 1 - \frac{M}{r} + 6a \left(\frac{M}{r^3}\right)^{\frac{1}{2}} + 6a \left(\frac{M}{r^3}\right)^{\frac{1}{2}} \left(\frac{a}{r}\right)^2 - \frac{3a^2}{r^2} - 16a^2 \left(\frac{M}{r^3}\right) + \dots \right)^{\frac{1}{2}} \quad (9.69)$$

and setting equations (9.68) and (9.69) equal to each other and scaling out the common

Keplerian angular frequency factor:

$$3\gamma - 4 = 1 - \frac{M}{r} + 6a \left(\frac{M}{r^3}\right)^{\frac{1}{2}} + 6a \left(\frac{M}{r^3}\right)^{\frac{1}{2}} \left(\frac{a}{r}\right)^2 - \frac{3a^2}{r^2} - 16a^2 \left(\frac{M}{r^3}\right) \quad (9.70a)$$

$$-3\gamma + 5 - \frac{M}{r} + 6a \left(\frac{M}{r^3}\right)^{\frac{1}{2}} + 6a \left(\frac{M}{r^3}\right)^{\frac{1}{2}} \left(\frac{a}{r}\right)^2 - \frac{3a^2}{r^2} - 16a^2 \left(\frac{M}{r^3}\right) = 0 \quad (9.70b)$$

I get a constraint for the adiabatic index in respect to the mass and spin parameter of the compact object. This equation can be solved for the adiabatic index in terms of  $M$ ,  $a$ , and  $r$ .

Taking the same approach for the vertical epicyclic frequency with equations (9.67) and (9.68) to find the vertical contribution to the constraint of the quantities between the two frequencies:

$$3\gamma - 4 = 1 - 6a \left(\frac{M}{r^3}\right)^{\frac{1}{2}} - 6a \left(\frac{M}{r^3}\right)^{\frac{1}{2}} \left(\frac{a}{r}\right)^2 + 3\frac{a^2}{r^2} + 8a^2 \left(\frac{M}{r^3}\right) \quad (9.71)$$

$$-3\gamma + 5 + 6a \left(\frac{M}{r^3}\right)^{\frac{1}{2}} + 6a \left(\frac{M}{r^3}\right)^{\frac{1}{2}} \left(\frac{a}{r}\right)^2 - 3\frac{a^2}{r^2} - 8a^2 \left(\frac{M}{r^3}\right) = 0 \quad (9.72)$$

We set the surface boundary at the ISCO as the location where the pulsations would occur and the inner disk begins, which entails inserting equation (8.136) into equation (8.135) for the value of  $r$ :

$$r_{ms} = M + \left(3 + z_2 - \left((3 - z_1)(3 + z_1 + 2z_2)\right)^{\frac{1}{2}}\right) \quad (9.73)$$

$$z_1 = \left(1 - \left(\frac{a}{M}\right)^2\right)^{\frac{1}{3}} \left(\left(1 + \frac{a}{M}\right)^{\frac{1}{3}} + \left(1 - \frac{a}{M}\right)^{\frac{1}{3}}\right) \quad z_2 = \left(3 \left(\frac{a}{M}\right)^2 + z_1^2\right)^{\frac{1}{2}} \quad (9.74a,b)$$

For the fractional displacements  $\left(\frac{\delta R}{R}\right)$  and  $\left(\frac{\delta z}{R}\right)$ , let  $r$  approach  $r_{ms}$  to determine the scope of the fluctuations of the surface of the disk at its location. Inserting equations (8.136a,b) into equation (8.135) gives the location of the ISCO in terms of the geometrized mass  $M$  and angular parameter  $a$ , which is converted into terms of distance.

When the radius is set for the ISCO, equation (9.72) can be solved for the adiabatic index alone, in terms of  $M$  and  $a$ , now. Or the equation can be solved for the angular momentum parameter  $a$ , if the adiabatic index is already determined and the mass known. Knowing two of the quantities will yield the third one, for the radius the QPO emerged from.

The fluctuations can be mapped out in terms of  $a^*$  (or the dimensionless ratio of  $a/M$ ) and be used as a qualifying criteria for the adiabatic index versus the spin and how the spin of the compact object affects the fluctuations. It can be used as a constraint with the mass and spin of the compact object since determining either quantity gives the other automatically. Using determined masses and spins of QPO candidates, these data can be applied to yield the value of the adiabatic index at the ISCO and yield an insight into the nature of the gas as it enters the plunging region below the ISCO.

The adiabatic index pertains to the presence of ionized gas and ideal gas and relativistic gas and what ratio of ideal to relativistic gas is present and is at play. It can serve as a diagnostic map of the distribution of the gases and the pertinent physical status. The radial and vertical epicyclic frequencies conform to the diskoseismological equation in this form and in order to maintain consistency, the adiabatic index has to accommodate the ratio of  $a/M$  to satisfy the equation and maintain the integrity of the equations. Thus the distribution of ionized gas versus relativistic gas can be mapped out using this as a criterion.

## Physical context of fractional displacements

To understand the meaning of the fractional displacements, we need to understand how the waves move in space. Sound waves involved with the radial modes of stellar pulsations are standing waves. Each standing wave for each mode has a node at one end (generally at the star's center, a fixed point with no moving gases), and an antinode set at the other end (at the star's surface, open for movement of the gases). The fractional displacement,  $\frac{\delta R}{R_0}$ , of the stellar gases from its equilibrium position is solved for unity at the stellar surface.

$$\frac{\delta R}{R_0} = 1; \quad (9.75)$$

Although in reality, for classical Cepheid stars, the fractional displacement is more in the range of 0.05 to 0.1 (Carroll B. O., 1996). To explore the pulsation mechanism and the implications for the adiabatic index, there needs to be a discussion of the events that transpire during the pulsation cycle.

Pulsating stars are essentially thermodynamic heat engines; the gases within the layers of the star do work as they expand and contract during the pulsation cycle. If a layer does positive work on its surroundings, it contributes to driving the oscillations. If a layer does negative work on its surroundings, it dampens the oscillations. If the total work of the layers is positive, the oscillations will grow in amplitude and if the total work is negative, the oscillations will decay as a result. So it continues until equilibrium is attained and the total work is zero.

A driving process entails heat flowing into a layer during a high-temperature part of the cycle and leaving during a low-temperature part of the cycle. The driving layers absorb heat at the time of their maximal compression, and maximal pressure will be attained after maximal compression. The oscillations will be amplified at this point. At the center of the star, the matter

is compressed and the temperature rises as a consequence and thermonuclear energy is generated. The displacement  $\frac{\delta R}{R}$  has a node near the center and the pulsation amplitude is very small. The energy mechanism ( $\epsilon$ -mechanism) operates in the core of the star although it is not enough to drive the pulsations.

If a layer became more opaque during compression, the energy flowing towards the surface gets stored up and dammed, pushing the surface layers up. When the expanding layer becomes more transparent, the trapped heat escapes and the layer collapses back to its original position. In the remainder of the star, the opacity decreases with compression.

The density and temperature increases while the layers compresses. Although the opacity is more sensitive to temperature changes, the opacity decreases with compression as a result. It requires special conditions for stellar pulsations.

Regions within a star where the valve mechanism can operate successfully are the partial ionization zones, where gases are partially ionized. Part of the work done on the gases while compressed gets directed into ionizing the matter rather than heating the gas itself. With a smaller temperature rise, the opacity increases with the increase in density. The ions recombine with electrons and release energy during expansion and the opacity decreases with the decrease in density.

This opacity mechanism is referred to as the  $\kappa$ -mechanism. In the partial ionization zone, the  $\kappa$ -mechanism is supported by the tendency of heat flow, during compression, into the zone (due to its temperature being lower than that of its surroundings). The heat flow effect is referred to as the  $\gamma$ -mechanism, due to the smaller ratio of specific heats,  $C_V$  and  $C_P$ , having larger values each. The partial ionization zones serve as the pistons that drive the pulsations of the star. Convection is the thermal process that determines the efficiency of the pulsation. Hence, the

adiabatic index tells us about the efficiency of the physical process driving the pulsations.

### Thermodynamics and Internal Energy Transport

Three energy mechanisms come in play within stellar interiors: Radiation, Conduction, and Convection. Radiation is energy transported purely through photon exchange between particles and enables energy released in nuclear reactions and gravitation to eventually reach the surface of stars and escape into space; Convection is a mode of energy transport within the layers of a star in which hot buoyant masses transporting excess heat as cooler masses subside inwardly within the star; and Conduction is the transportation of heat via collusive contact between particles. The latter generally is regarded as negligible and usually neglected in stellar modeling (Carroll B. W., An Introduction to Modern Astrophysics, 1996).

Exploring these energy mechanisms entails focusing on the equations that summarize the phenomenon. Starting with the radiation pressure gradient equation:

$$\frac{dP_{rad}}{dr} = -\bar{\kappa} \frac{\rho}{c} F_{rad} \quad (9.76)$$

$F_{rad}$  is the outward Radiative Flux;  $\bar{\kappa}$  is the Kramer's opacity,  $\rho$  the density, and  $c$  the speed of light.

The radiation pressure gradient equation is also expressed as:

$$\frac{dP_{rad}}{dr} = \frac{4}{3} aT^3 \frac{dT}{dr} \quad (9.77)$$

and merging the two equations (9.76) and (9.77), I get:

$$\frac{dT}{dr} = -\frac{3}{4ac} \frac{\kappa \rho}{T^3} F_{rad} \quad (9.78)$$

and inserting the relation for radiative flux into equation (9.78):

$$F_{rad} = \frac{L_{rad}}{4\pi r^2} \quad (9.79)$$

I get:

$$\frac{dT}{dr} = -\frac{3}{4ac} \frac{\kappa \rho}{T^3} \frac{L_{rad}}{4\pi r^2} \quad (9.80)$$

which gives us the temperature gradient for radiative transport. As the opacity or temperature increases, the temperature gradient becomes sharper (more negative) accordingly. The radiation is required to transfer all of the outward energy, and likewise for increases in density or temperature decreases.

If the temperature gradient becomes too sharp, convection comes into play where the hotter partitions of mass shift and rise as the cooler partitions sink inward. Convection is generally difficult to summarize via straightforward equations and require the utilization of fluid mechanics. Fluid mechanics invoke the Navier-Stokes equations, a three-dimensional set of equations describing the motion of gases and liquids (Carroll B. W., *An Introduction to Modern Astrophysics*, 1996).

Stellar computer programs invoke these equations in one dimension, the radial dimension only, due to limitations in computing power and reduce a 3-D process to a 1-D approach. It further requires a complex approach to deal with turbulent convection, especially in detailing the viscosity and heat dissipation within the star.



For convection, a characteristic length scale is invoked, referred to as the pressure scale height, particularly in terms of the star size. The timescale for convection is also comparable to that of the timescale for changes in the stellar structure, implying that the two are linked.

The pressure scale height is determined as such:

$$\frac{1}{H_p} = -\frac{1}{P} \frac{dP}{dr} = -\frac{d \ln P}{dr} \quad (9.81)$$

Assuming  $H_p$  is constant, the variation in pressure can be inferred:

$$P = P_0 e^{-\frac{r}{H_p}} \quad (9.82)$$

To derive a general expression for  $H_p$  specifically, we go back to the hydrostatic equilibrium equation:

$$\frac{dP}{dr} = -g\rho = -\frac{\rho GM}{r^2} \quad (9.83)$$

Invoking this relation gives us:

$$\frac{1}{H_p} = -\frac{1}{P} \frac{dP}{dr} = \frac{\rho g}{P}, \quad H_p = \frac{P}{g\rho} \quad (9.84)$$

To explore convection, we need to understand the thermodynamics at play. The first law of thermodynamics refers to the conservation of energy for heat transport:

$$dU = dQ - dW \quad (9.85)$$

in which the change in internal energy of a mass element,  $dU$ , is given by an amount of heat supplied to the element  $dQ$ , minus the work done by the element upon its surroundings,  $dW$ .

The total internal energy per unit mass is:

$$U = \frac{\bar{k}}{\bar{m}} \quad \bar{k} \text{ the average kinetic energy, } \bar{m} \text{ the average mass of particle in the gas}$$

$$(9.86a)$$

$$= \frac{3}{2} \left( \frac{k}{\mu m_H} \right) T = \frac{3}{2} nRT \quad (9.86b)$$

The internal energy is the kinetic energy per unit mass. The change in heat of mass element  $dQ$  is referred to in terms of the specific heat of the gas,  $C$ . The specific heat is the amount of heat required to raise the temperature by 1 K for a unit mass (Carroll B. W., An Introduction to Modern Astrophysics, 1996).

The equations for the specific heats are:

$$C_p = \left( \frac{dQ}{dT} \right)_p \quad C_v = \left( \frac{dQ}{dT} \right)_v \quad (9.87a,b)$$

(with  $C_p$  at constant pressure, and  $C_v$  at constant volume.)

The gas does a certain amount of work on its surroundings, expressed as  $dW$ . The gas exerts a force across a particular distance. The work can be compared to the action of a piston; the gas filling a cylinder, endowed with mass  $m$  and pressure  $P$ , can exert a force as expressed by the following equation:

$$F = P * A \quad (9.88)$$

and the work done per unit mass:

$$dW = \left( \frac{F}{m} \right) dr = \frac{P * A}{m} dr = P dV \quad (9.89)$$

$$dW = dQ - P dV \quad (9.90)$$

In the case of constant volume,  $dV = 0$ , so  $dU$  becomes:

(9.91)

$$dU = dQ|_v = \left. \frac{dQ}{dT} \right|_v dT = C_v dT \quad (9.92)$$

For a monatomic gas, 
$$dU = \frac{3}{2} nR dT \quad (9.93)$$

For relativistic gas, 
$$dU = 3 nR dT \quad (9.94)$$

so the specific heat becomes: (for constant volume)

$$C_v = \frac{3}{2} nR \quad \text{for ideal gas} \quad (9.95)$$

$$C_v = 3 nR \quad \text{for relativistic gas} \quad (9.96)$$

To find the specific heat (for constant pressure), for a monatomic gas (Carroll B. W., An Introduction to Modern Astrophysics, 1996):

$$dU = \left. \frac{dQ}{dT} \right|_P dT - P \left. \frac{dV}{dT} \right|_P dT \quad (9.97)$$

and the ideal gas law: 
$$PV = nR \quad (9.98)$$

using the following relation: 
$$P \frac{dV}{dT} = nR \quad (9.99)$$

and invoking the last three equations (9.97, 9.98, and 9.99) together gives us:

$$C_V dT = C_P dT + nR dT \quad (9.100a)$$

$$C_V = C_P + nR; \quad (9.101b)$$

The parameter  $\gamma$  is defined as the ratio of specific heats:

$$\gamma = \frac{C_V}{C_P} \quad (9.102)$$

For a monatomic gas,

$$\frac{C_V}{C_P} = \frac{C_V}{C_V} + \frac{nR}{C_V} = 1 + \frac{nR}{\frac{3}{2}(nR)} = 1 + \frac{2}{3} = \frac{5}{3} \quad (9.103)$$

This is the case whether the ideal gas is degenerate or not.

For relativistic gas,

$$\frac{C_V}{C_P} = \frac{C_V}{C_V} + \frac{nR}{C_V} = 1 + \frac{nR}{3(nR)} = 1 + \frac{1}{3} = \frac{4}{3} \quad (9.104)$$

The adiabatic index also applies for both the degenerate or non-degenerate cases of relativistic gas.

In the case of ionization, part of the heat that goes into increasing the kinetic energy of the matter gets redirected into ionizing the matter instead. As a consequence, the temperature doesn't rise as much, which indicates a larger value for the specific heats each in a partial ionization zone. For increasing  $C_p$  and  $C_v$ , the value of  $\gamma$  approaches unity (value of one). A lower value for  $\gamma$  implies increased ionization for the involved zone in question (Carroll B. W., *An Introduction to Modern Astrophysics*, 1996).

What occurs during convection is that a heated bubble of gas or plasma rises and expands (adiabatically, or without any heat exchange) and travels through the star's inner layers. At some point it loses its excess heat and thermalizes, dissolving into the surrounding gases. To understand the conditions for convection, we start with a relation for the pressure gradient:

$$P = \kappa \rho^\gamma \quad (6.126) \quad \frac{dP}{dr} = \frac{\kappa T}{\mu m_H} \frac{d\rho}{dr} + \frac{\rho \kappa}{\mu m_H} \frac{dT}{dr} - \frac{1}{\mu^2} \frac{\kappa T}{m_H} \frac{d\mu}{dr} \quad (9.105a)$$

$$= \frac{P}{\rho} \frac{d\rho}{dr} + \frac{P}{T} \frac{dT}{dr} - \frac{P}{\mu} \frac{d\mu}{dr} \quad (9.105b)$$

Setting  $\mu$  as a constant and invoking another pressure relation:

$$\frac{dP}{dr} = \kappa \gamma \rho^{\gamma-1} \frac{d\rho}{dr} \quad (9.106)$$

$$\frac{d\rho}{dr} = \frac{1}{\kappa \gamma} \rho^{1-\gamma} \frac{dP}{dr} \quad (9.107)$$

Inserting (9.106) into the above equation (9.107) and isolating the pressure gradient term gives

us:

$$\frac{dP}{dr} \left( 1 - \frac{1}{\kappa\gamma} \rho^{1-\gamma} \frac{P}{\rho} \right) = \frac{P}{T} \frac{dT}{dr} \quad (9.108)$$

$$\frac{dP}{dr} \left( 1 - \frac{\kappa\rho^{\gamma-1}}{\kappa\gamma} \rho^{1-\gamma} \right) = \frac{P}{T} \frac{dT}{dr} \quad (9.109)$$

$$\frac{dP}{dr} \left( 1 - \frac{1}{\gamma} \right) = \frac{P}{T} \frac{dT}{dr} \rightarrow \left( 1 - \frac{1}{\gamma} \right) = \frac{P}{T} \frac{dT}{dP} = \frac{d \ln T}{d \ln P} \quad (9.110)$$

For convection to occur, the following condition must be satisfied:

$$\frac{d \ln T}{d \ln P} < \frac{\gamma-1}{\gamma} \quad (9.111)$$

Convection and radiation both transport energy simultaneously so conditions exist in the case one can dominate over the other. Advection also transports energy in the case of accretion disks due to gravity.

The temperature gradient determines which mechanism prevails in its operation. To understand the events that occur with convection, the physical event must be discussed in more detail. A bubble of gas rises towards the surface, traveling a distance  $dr$ .

If the bubble's density is less than that of its surroundings, it will rise accordingly. The buoyant force acting on the bubble can be expressed by the following equation:

$$f_B = \rho_i^s g \quad (9.112)$$

where  $\rho_i^s$  = fluid density,  $g$  is the local acceleration and  $f_B$  is the buoyant force per unit volume.

Another force acts in opposition to the buoyant force: the gravitational force:

$$f_g = \rho_i^b g \quad (9.113)$$

and a net force acting upon the bubble can be expressed as:

$$f_{NET} = -g \delta\rho \quad \delta\rho = \rho_i^b - \rho_i^s \quad (9.114a,b)$$

If the bubble increases its density in relation to its surroundings after traveling a distance, the bubble will sink and convection will stop.

In the case that  $\rho_i^b < \rho_i^s$  (bubble density less than surrounding density), (9.115)

the bubble will continue its rise and convection ensues (Carroll B. W., An Introduction to Modern Astrophysics, 1996). To determine the condition for convection, we start with the premise that the bubble is in near thermal equilibrium ( $T_i^b \approx T_i^s$ ) and  $\rho_i^b \approx \rho_i^s$ . (9.116a,b)

The bubble expands adiabatically and the pressures involved remain equal throughout the event;

$$P_f^b = P_f^s. \quad (9.117)$$

The bubble moves over a certain distance:

$$\text{(Bubble)} \quad \rho_f^b \approx \rho_i^b + \left. \frac{d\rho}{dr} \right|^b dr \quad (9.118)$$

$$\text{(Surroundings)} \quad \rho_f^s \approx \rho_i^s + \left. \frac{d\rho}{dr} \right|^s dr \quad (9.119)$$

Assuming the densities of the bubble and surroundings remain nearly equal, the condition gives us:

$$\left. \frac{d\rho}{dr} \right|^b < \left. \frac{d\rho}{dr} \right|^s \quad (9.120)$$

Focusing on the adiabatic relationship between pressure and density:

$$P = \kappa \rho^\gamma \quad (9.121)$$

$$\frac{dP}{dr} = \kappa \gamma \rho^{\gamma-1} \frac{d\rho}{dr} = \frac{\gamma P}{\rho} \frac{d\rho}{dr} \quad (9.122)$$

Inserting this into the condition (8.184) gives us:

$$\left. \frac{1}{\gamma} \frac{\rho_i^b}{P_i^b} \frac{dP}{dr} \right|^b < \left. \frac{1}{\gamma} \frac{\rho_i^s}{P_i^s} \left[ \frac{dP}{dr} \right]^s - \frac{P_i^s}{T_i^s} \left. \frac{dT}{dr} \right|^s \right] \quad (9.123)$$

Since  $P^b = P^s$ , (8.146)  $\left. \frac{dP}{dr} \right|^b = \left. \frac{dP}{dr} \right|^s = \frac{dP}{dr}$  (9.124)

The equation becomes:

$$\frac{1}{\gamma} \frac{dP}{dr} < \frac{dP}{dr} - \frac{P_i^s}{T_i^s} \left. \frac{dT}{dr} \right|^s \quad (9.125)$$

$$\left(1 - \frac{1}{\gamma}\right) \frac{dT}{dr} < - \left. \frac{P}{T} \frac{dT}{dr} \right|_{act} \quad (9.126)$$

$$\left(\frac{1}{\gamma} - 1\right) \frac{\ln P}{\ln T} > \left. \frac{dT}{dr} \right|_{act} \quad (9.127)$$

$$\left. \frac{dT}{dr} \right|_{ad} > \left. \frac{dT}{dr} \right|_{act} \quad (9.128)$$

The condition for convection to occur is that the adiabatic temperature gradient be greater than the actual temperature gradient. As temperature decreases inside the star with increasing radius, the temperature gradient is negative:

$$\frac{dT}{dr} < 0 \quad (9.129)$$

The inequality is written then as:

$$\left. \frac{dT}{dr} \right|_{act} > \left. \frac{dT}{dr} \right|_{ad} \quad (9.130)$$

In the case the actual temperature gradient is superadiabatic (larger than the adiabatic temperature gradient), convection occurs. Convection will only occur when the following four

conditions are met: (1) the stellar opacity is large, which indicates an extremely sharp temperature gradient enabling radiative transport; (2) an area where ionization is happening, creating a higher specific heat and lowered adiabatic temperature gradient; (3) the gravitational acceleration is low (meaning lower adiabatic gradient), and (4) the nuclear energy generation rate temperature dependence is large, incurring a sharp radiative flux gradient and large temperature gradient.

The first three conditions occur readily in most stars while the fourth tends to occur deep within stellar interiors, and tends to occur at a later stage in the star's evolution, when temperature-dependent CNO cycle or triple-alpha processes are happening within the star (Carroll B. W., *An Introduction to Modern Astrophysics*, 1996).

### **Determining the Adiabatic Index in the Outermost Layer of a Star**

We are interested in determining the adiabatic index in an outermost layer of an oscillating body. A method for detecting it was developed recently. The effective adiabatic index can be determined for the outermost layer of a star, using observations of a slow-moving magnetohydrodynamical wave in the corona (Van Doorselaere, 2011). One such observation was made for the Sun using the Extreme-ultraviolet Imaging Spectrometer on Hinode. The spectrometer was used to detect oscillations in the electron density using the CHIANTI atomic database for the spectroscopy.



A relationship between the relative density and temperature perturbations was determined from the time-dependent wave signals from multiple spectra lines, which found an effective adiabatic index of  $1.10 \pm 0.02$ . This indicates the gas is highly ionized since the ratio of specific heats approach unity. The adiabatic index plays an important part in solar and stellar models, as well as natural plasma systems where it regulates the energetics of monatomic plasma. An adiabatic index of  $\gamma = 5/3$  is often invoked in most cases, and determining the precise value of  $\gamma$  also enables more complicated physics (thermal conduction and radiative cooling) to be explored. The measurement was made of the temperature and density dynamics in a coronal loop. The comparison of the two quantities yielded the effective adiabatic index in the corona. The effective adiabatic index bears information about the thermal properties of the corona. Coronal seismology techniques were used to get results, which combined with the magnetohydrodynamical theory of waves in structured plasmas enables measurement of the intrinsic physical quantities (Roberts, 1983).

It was recently shown that the corona and chromosphere of the sun manifested transverse waves (Tomczyk, 2007) (De Pontieu, 2007). Slow magneto-acoustic waves can be detected as periodic variations in intensity and Doppler shifts, given that the observations are made along the line of sight. Perturbations in velocity and intensity were observed using SOHO to single out hot corona lines containing Fe XIX and Fe XXI (Wang T. S., 2002) (Wang T. S., 2003). Accretion disks also typically exhibit iron lines in their spectra.

The perturbations were taken as standing magneto-acoustic waves due to the quarter-period phase shift between the velocity and intensity oscillations. Other observations confirmed

the assessment of the disturbances being slow magneto-acoustic modes with periods of approximately 5 minutes (De Moortel L. H., 2002) (King, 2003) (Robbrecht, 2001). The perturbations were taken for slow-moving magneto-acoustic modes due to their propagation speeds being less than the local sound speed, moving along magnetic field lines. The CHIANTI software was used to determine the density from the line ratio of FE XII and FE XIII spectral lines while taking the density variations in account. The electron density is expected to be oscillating in phase with the intensity and the temperature variations mirror the trend.

Linearized MHD theory gives us the following equation (Goosens, 2003):

$$\frac{\rho'}{\rho_0} = \frac{1}{\gamma_{eff}} \frac{P'}{P_0} = \frac{1}{\gamma_{eff}-1} \frac{T'}{T_0}; \quad (9.131)$$

with  $\rho$  being the mass density,  $P$  the gas pressure, and  $T$  the temperature. The ' subscript denotes perturbed quantities and the  $0$  subscript denotes the equilibrium quantities.

For this equation, the equation of state follows a polytropic relation  $P = \kappa \rho^{\gamma_{eff}}$ ; (9.132)

with the effective adiabatic index  $\gamma_{eff}$ .

The observable quantities bear a linear relationship summarized by the equation. The implication of the effective adiabatic index veering from a value of 5/3 means the energy equation in the MHD equations cannot be invoked with an adiabatic form using small correction terms for energy losses and gains. Certain factors must serve to lower the adiabatic index (such as thermal conduction, radiative losses, and turbulence). For the corona, the low amplitude of the temperature variations indicates that thermal conduction is very efficient, which was predicted by others (De Moortel L. H., 2003). Thermal conduction introduces a phase shift

between the density and temperature perturbations. The phase shift is defined by the equation as:

$$\tan \phi = \frac{\kappa(\gamma-1)\kappa_{II}T_0}{P_0\omega}; \quad (9.133)$$

$$\text{with } \kappa_{II} = \kappa_0 T_0^{-5/2}, \quad (9.134)$$

being the parallel thermal conduction, and the density and temperature variations following the equation  $e^{i(\omega t - kz)}$  with frequency  $\omega$ , the wave number  $k$ , time  $t$ , and  $z$  as the direction of the magnetic field.

De Moortel and Hood (De Moortel L. H., 2003) found a relation for the adiabatic index that can be determined from the phase shift between perturbations:

$$A_T = \cos \phi (\gamma - 1)A_\rho; \quad (9.135)$$

for cases when thermal conduction is not negligible.  $A_T$  is the relative oscillation amplitude of the temperature and  $A_\rho$  is the relative oscillation amplitude for the density.

The adiabatic index given for the corona is 1.17, which is higher than the given value of the earlier equation. This approach can be applied in observations of accretion disks' spectra, especially focused on the area of inner edges of the disks, where the QPO signals originate from. The reflection edge is one of several qualifying candidates for the inner edge of an accretion disk, where it is defined as the smallest radius capable of producing a fluorescent iron line.

The iron  $K_\alpha$  fluorescent line is a characteristic feature observed in numerous accretion disks and its intensity and shape is dependent on the conditions near the inner edge. Doppler shifts and intensity variations can be used to determine the adiabatic index using the correct approach with the observation data and singling out the diagnostic features in the power spectrum. The adiabatic index being determined through this method can be used as a criterion to isolate the ratio of  $a/M$  from the helioseismological approach applied to the QPO frequency expression.

This along with a high resolution observation and measurement of the event horizon as well as determining the location of the ISCO through a drop-off in the quality factor measurement in the power spectrum of any observations of the same candidate will give a more precise measurement of both the compact object's mass and angular momentum.

CHAPTER X  
PULSATION ACTIVITY

We now look at the implications that come from the pulsations within the accretion disk gas. Pulsations can reveal details of the interior of a stellar object. The radial oscillations of a pulsating star are a result of sound waves resonating through the stellar interior. The sound waves involved in the radial modes of stellar pulsation are standing waves, akin to these that happen in an organ pipe capable of several modes of oscillation. The wave of each mode has one node (fixed point) where the gases do not move, and one anti-node (moving point) at the star's surfaces where the gases can undulate. The fundamental mode has the gas moving in the same direction at every point along the pipe or the radial direction within the star. The first overtone has a node between the center and the surface with the gases moving in opposite directions of each side of the node, and the second overtone has two nodes. The fractional displacement,  $\frac{\delta R}{R}$ , is the amount of displacement of the stellar material from its equilibrium position relative to the radial extent of the star. The radial modes have the motion of the stellar material confined to the surface. The majority of the Cepheids pulsate in the fundamental mode.

The displacement  $\frac{\delta R}{R}$  also follows an exponential equation:

$$\delta R = R_0 e^{\pm i\omega t}; \quad (10.1)$$

$$\text{where } \omega = \sqrt{(3\gamma - 4)\left(\frac{GM}{R^3}\right)}; \quad (10.2)$$

for values of  $\gamma > 4/3$ , the exponent is positive and the displacement moves in a pulsation (sinsoidal) pattern. If  $\gamma < 4/3$ , the exponent is negative and the displacement is of the form  $\delta R = A e^{-\kappa t}$ ; where the displacement approaches a floor value of zero. The value of  $\gamma$  determines the dynamical stability of a star and when  $\gamma < 4/3$ , the star is doomed to gravitational collapse.

In terms of the accretion disk, as the value of  $\gamma$  approaches  $4/3$ , and drops beyond that value near the compact object, the stellar material will undergo gravitational collapse. This is also the criterion that occurs with white dwarfs when electron degeneracy pressure fails as the adiabatic index  $\gamma$  approaches the relativistic value of  $4/3$  and they succumb to gravitational collapse. The increase in gas pressure cannot overcome the inward pull of gravity and cause the mass shell to rebound outward.

The range in space where matter obeys a polytropic equation of state with an adiabatic index  $\gamma > 4/3$  is dynamically stable. At the place where  $\gamma = 4/3$ , gravitational collapse is the fate for matter in that region. The equation of state that matter obeys in an accretion disk obey a polytrope with an adiabatic index higher than  $4/3$ , especially at the accretion disk inner edge. The QPO signal lends an insight into what happens at the inner edge with increased spin. As the spin value  $a$  approaches the maximum value  $a = M$ , the ISCO ( $r_{ms}$ ) approaches the same radius as the event horizon at the same value and the accretion disk inner edge meets the edge of the black hole.

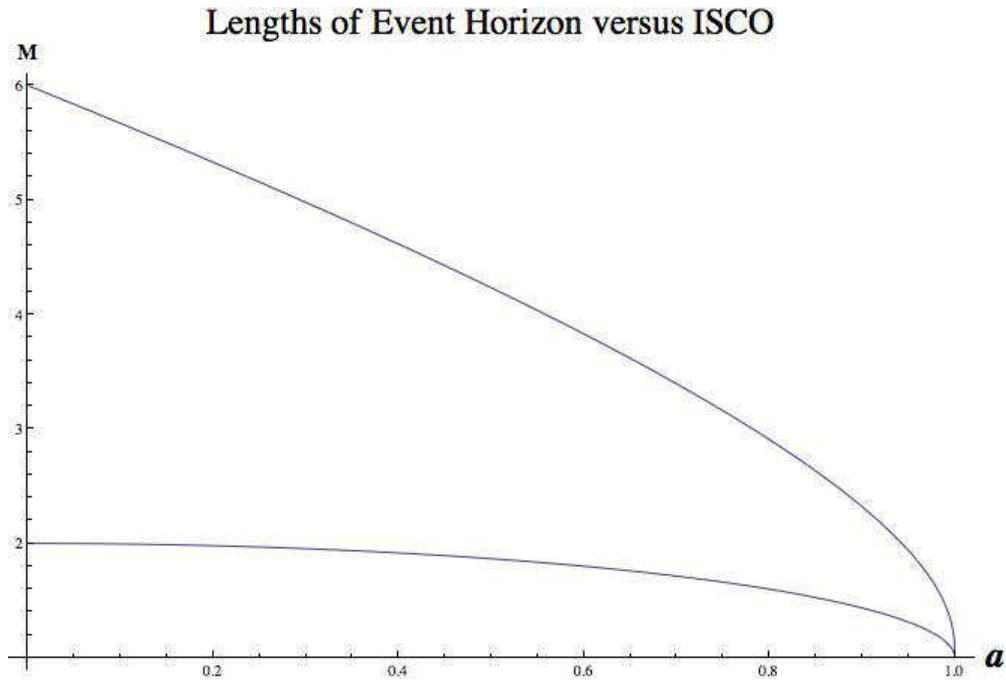


Figure 19. Lengths of Event Horizon versus ISCO (Marginally Stable Circular Orbit) versus Spin.

The upper line is the curve representing the length of the ISCO or  $r_{ms}$ , and the lower line is the curve representing the length of the event horizon of the compact object (also denoted as  $r_H$ ). At maximal spin, the ISCO and the event horizon coincide at the same radius.

Using the QPO frequency equation along with the helioseismological expression, it yields two expressions for the fractional displacement (range of pulsation along the radial extent of the stellar body, provided  $\gamma > 4/3$ ) for each epicyclic frequency expression.

The radial fractional displacement and vertical fractional displacement are calculated at the fixed radius  $r = r_{ms}$ , and then plotted for varying values of  $\gamma$  versus varying values of  $a$ . The significance of the radial fractional displacement is linked to the net work done within the gaseous atmosphere of the astronomical body. Positive values indicate a positive work done, and negative values indicate a negative work done.

If the work is positive, the gas does work on the surroundings, and if negative, the surroundings do work on the gas instead (Carroll B. W., An Introduction to Modern Astrophysics, 1996). According to the first law of thermodynamics, in a reversible process, an increment of heat  $\delta Q$  absorbed by an element of gas during an incremental change of state, must equal a sum of incremental change of internal energy  $dU$  of the sample, and the incremental work  $\delta W$  done on the surroundings:

$$dQ = dU + \delta W; \quad (10.3)$$

The quantity  $\delta W$  is positive if the gas element absorbs heat as is the latter when it does work on the surroundings. The net work done by the gas over a cycle equals the total heat absorbed:

$$W = \oint dQ; \quad (10.4)$$

The work must be positive for pulsations to occur. If heat is released ( $\delta Q < 0$ ), the work is negative. Regions that do positive work drive the pulsations in the atmosphere, and regions that do negative work are dissipative.

The radial fractional displacement has a solution for a fixed radius, set at the ISCO. The first has a smaller range of pulsation (for  $\gamma = 5/3$ ); a negative (inward  $\sim -0.05$ ) pulsation range for both low and high values of  $a$ . For all values of  $a$ , the pulsation is positive. As the spin approaches  $a = M$ , the displacement turns upward again and grows larger in magnitude, approaching infinity, which meets expectations when one considers the inner edge approaching the event horizon at that spin value. It would be taken as a drastic response to the approaching contraction of the marginally stable circular orbit (ISCO) towards the event horizon of the compact object.



## The Fractional Displacement Solutions of the Simple Harmonic Oscillator Equation

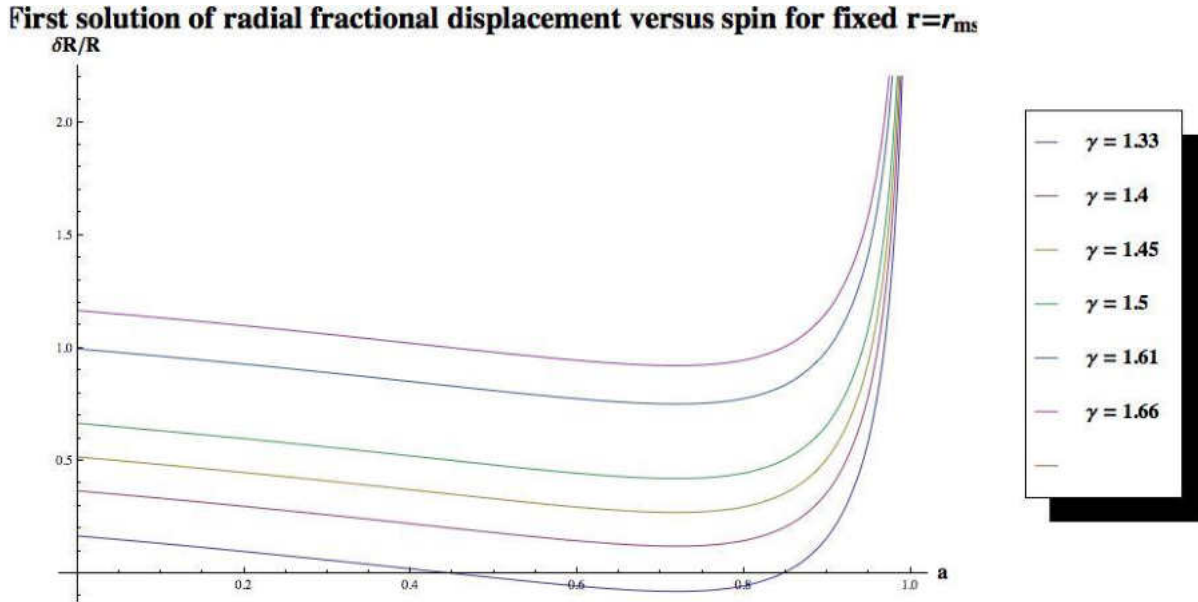


Figure 20. First solution of the radial fractional displacement versus spin.

For the radial fractional displacement, the values are positive for the majority of values of spin parameter  $a$  (in Figure 20), for all adiabatic index values, when the displacement remains positive and dips for increasing spin, and jumps towards positive infinity with near maximal spin, suggesting a dynamic instability incurring for that spin value (resulting in an explosive expansion in the gas), even with a high adiabatic index. The lower the value of the adiabatic index, the sooner the dynamic instability in the inner disk occurs, and occurs for that of relativistic gas the soonest.

Even with adiabatic index  $\gamma = 5/3$ , the spin of the black hole modifies gravity such that it causes a dynamical instability even for non-relativistic gas, meaning the value of  $a = 1.0$  turns into an asymptote that all curves for all values of  $\gamma$  turn sharply to avoid, towards infinity. As

depicted in Figure 19, for the vast majority of spin values, with varying values of the adiabatic index, the radial displacement is positive.

For decreasing values of  $\gamma$ , the radial fractional displacement diminishes in magnitude and then increases slowly, finally approaching the asymptote at the maximal value of  $a = M$ , indicating an explosive expansion.

The first solution for the vertical fractional displacement (Figure 21) are all positive (for all values of  $\gamma$ ) and starts from a floor value that varies for each adiabatic index, then increases for increasing values of  $\gamma$  and reaches a ceiling of 2.0 at  $a = M$  for non-relativistic gas, and 0.7 for relativistic gas. Pulsation occurs in the vertical direction, for all values of  $a$ , and most strongly for ideal gas for maximal spin.

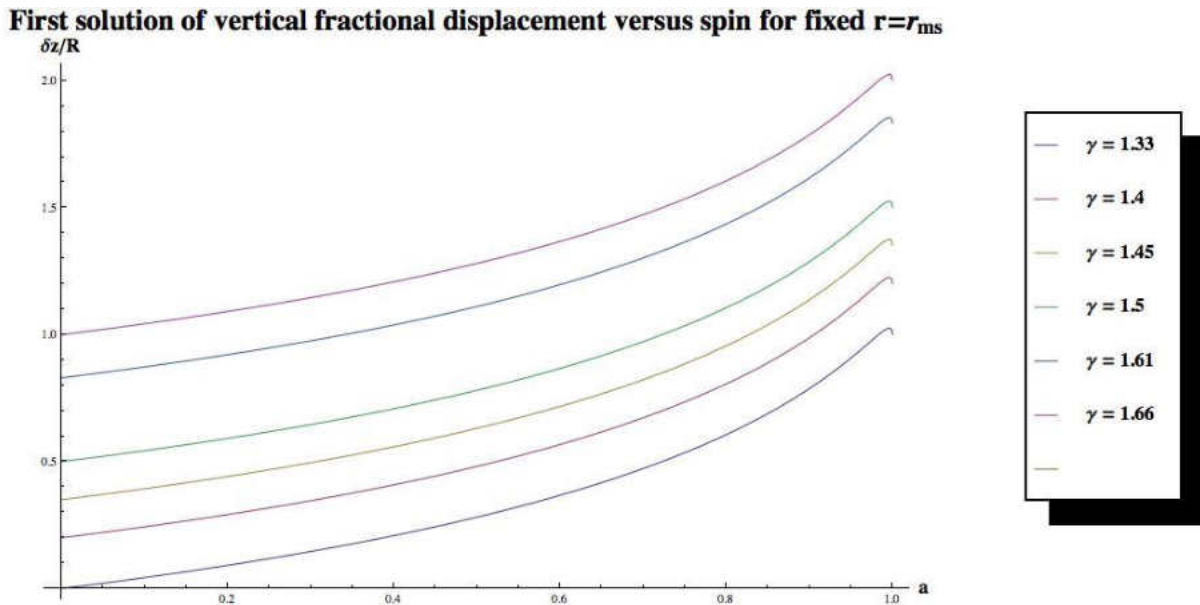


Figure 21. First solution of the vertical fractional displacement versus spin.

The other adiabatic indices show positive work for increasing spin, and the index of relativistic gas shows positive work even only near maximal spin for the first solution. This is the first solution to the vertical fractional displacement at a fixed radius, the ISCO, plotted versus spin parameter  $a$  (Figure 21). For ideal gas, the displacement is positive and increases with spin until it reaches a maximal value then takes a slight turn. Even with a slight decrease in the adiabatic index, the displacement turns negative and the work done becomes negative although for all adiabatic index values, the displacement and by inference, the work becomes positive, eventually with increasing spin.

With relativistic gas, the work does not become positive until near maximal spin. There are pulsations in the gas atmosphere of the disk for positive displacements, and none for negative displacements due to the dissipative energy that inhibit such pulsation activity. This would indicate the QPO frequency versus the pulsations is not dependent on the nature of the gas as it is advected past the ISCO.

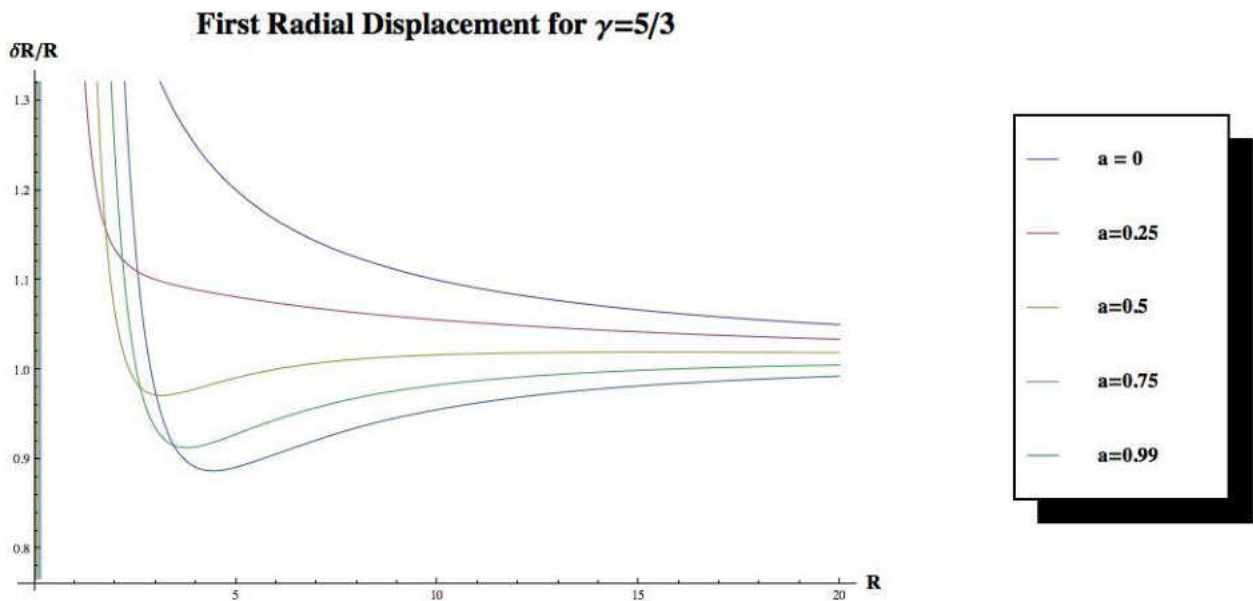


Figure 22. First Radial Displacement for fixed index = 5/3.

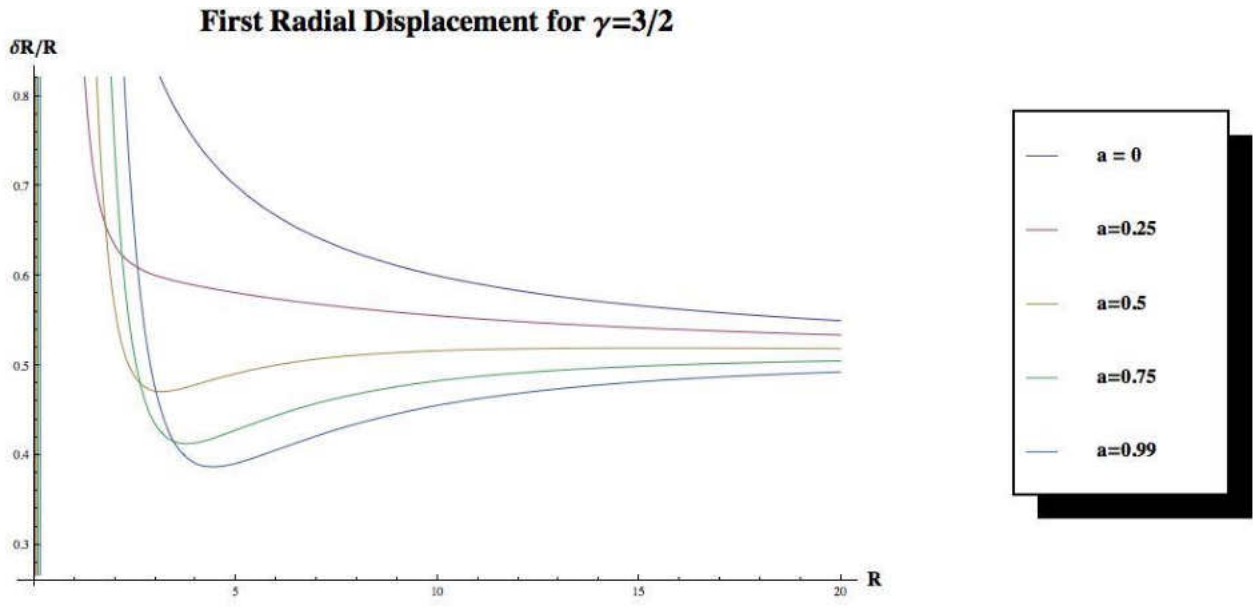


Figure 23. First Radial Displacement for fixed index = 3/2.

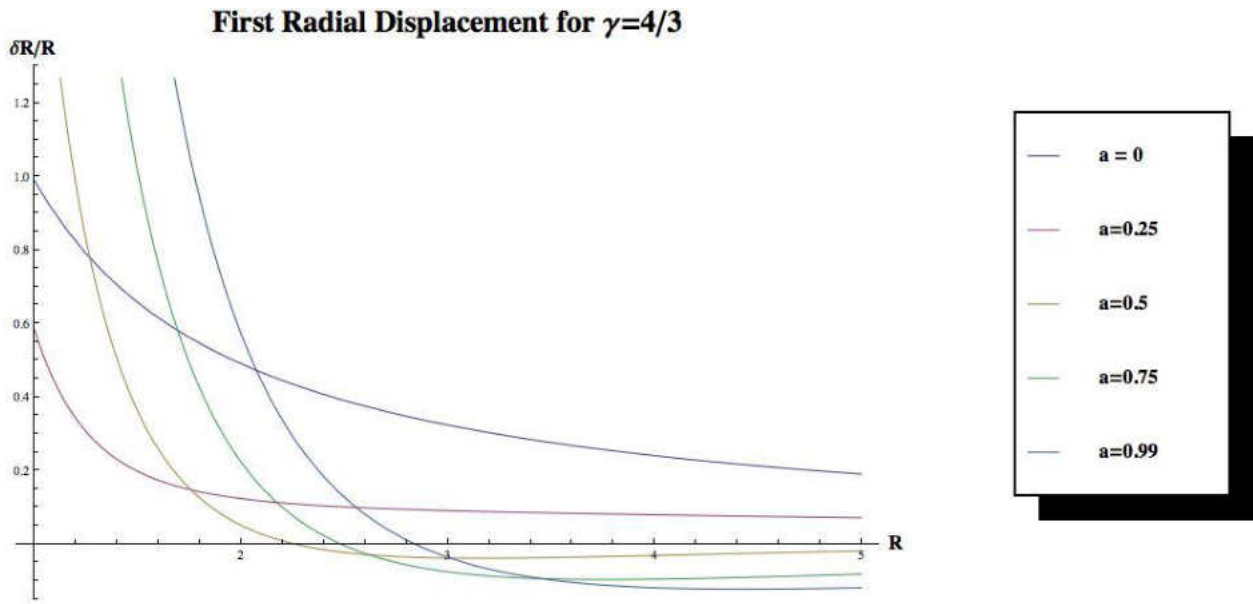


Figure 24. First Radial Displacement for fixed index = 4/3.

The real values of the radial displacement for varying values of the adiabatic index, from 5/3 (ideal gas) to 4/3 (relativistic gas), are plotted over a radial range in terms of Schwarzschild radii (in Figures 22, 23, and 24). For non-relativistic gas, the radial displacement is in the form

of a steep peak that rises to a high amplitude near the inner disk edge then drops from there to a smooth curve that approaches a horizontal asymptote of 1.0, for radial values beyond the ISCO. As the spin decreases, the peak gets shallower and wider, indicating a wider dispersal in the work being done within the inner disk in a widening ring that extends outward. The increased spin would have the opposite effect, with the work becoming increased localized within a narrowing ring set at the ISCO and radiating outward.

As the adiabatic index drops towards a mix of relativistic and ideal gases, the radial displacement culminates in a shallower peak that also is shallower and wider for low spin, then the displacement curve becomes narrower and the peak shifts to a higher amplitude. The radial displacement is of a lower magnitude than that of non-relativistic gas, indicating a decrease in the adiabatic index shows an inhibition in the work driving the pulsations. Maximal spin shows a steeper peak with a narrower width and a more depressed distribution in the radial displacement with increasing radial distance. In the case of non-relativistic gas, and an even mix of ideal and relativistic gas, pulsation activity is supported at all radial ranges outward from the ISCO. Even with increasing spin, the pulsation becomes more concentrated towards the inner disk edge, especially with decreasing adiabatic index values.

With relativistic gas, for zero spin, the radial displacement starts out from a value of 1.0 and then decreases gradually from that value outward over increasing radial values. A peculiar trend occurs when the spin increases and the amplitude of the displacement decreases but the displacement also decreases gradually over all outward radii, and then at some point, as the spin further increases, the displacement increases in magnitude at the inner disk edge and the curve

drops more sharply and plunges beneath the x-axis into negative territory. With increasing spin, the curve reaches negative values at higher radial values but the displacement is even more negative. This indicates the presence of negative work being done within the inner disk and suppressing pulsations in the region. For relativistic gas, the spin of the compact object acts to suppress pulsation activity in the inner disk, which indicates there would be no expected QPO signals for a high enough spin, in the case of relativistic gas at the ISCO.

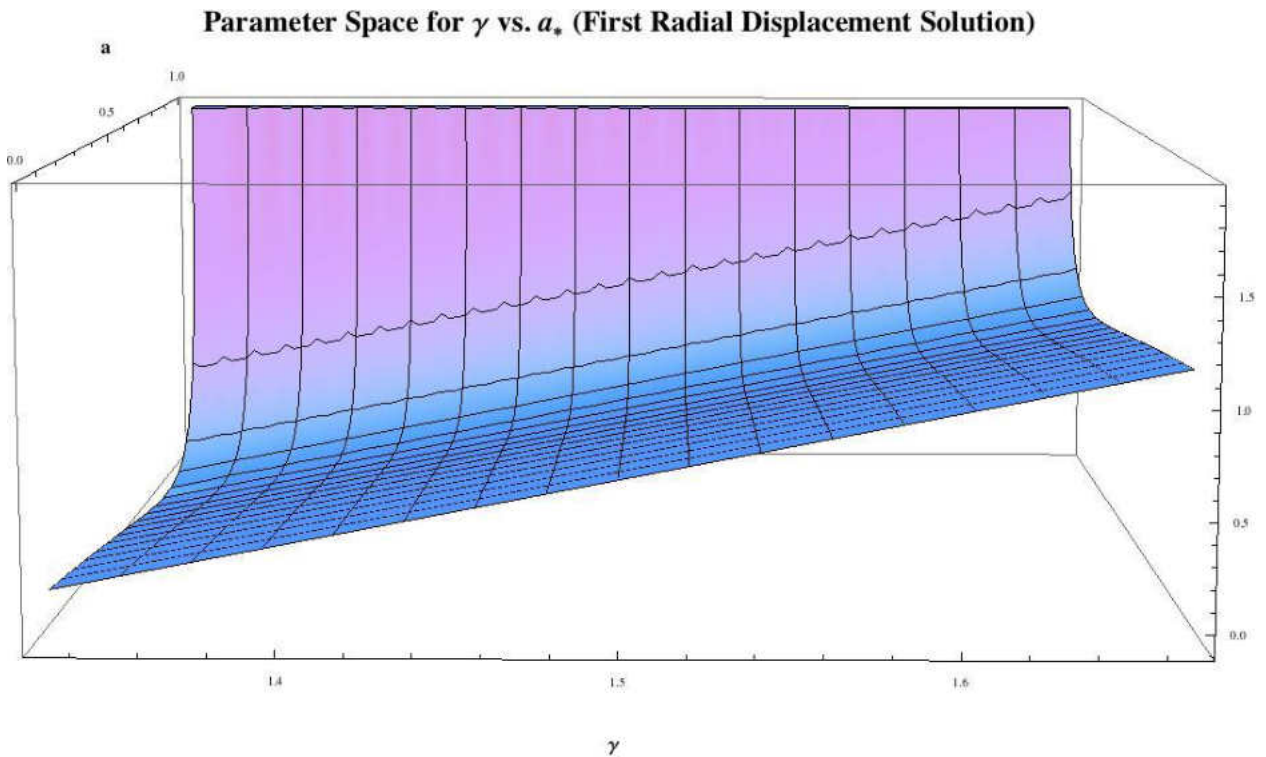


Figure 25. Parameter space for adiabatic index versus  $a$  (First Radial Displacement Solution).

The plotted parameter  $\gamma$  versus  $a_*$  (Figure 25) shows the constraint of  $\gamma$  versus the dimensionless ratio for  $a_*$  ( $a_* = a/M$ ), so it satisfies the epicyclic frequency expressions (equations 8.129 and 8.130) as plotted on a two-dimensional curve in three-dimensional space ( $\gamma$  vs.  $a_*$  vs.  $\frac{\delta R}{R_0}$ ).

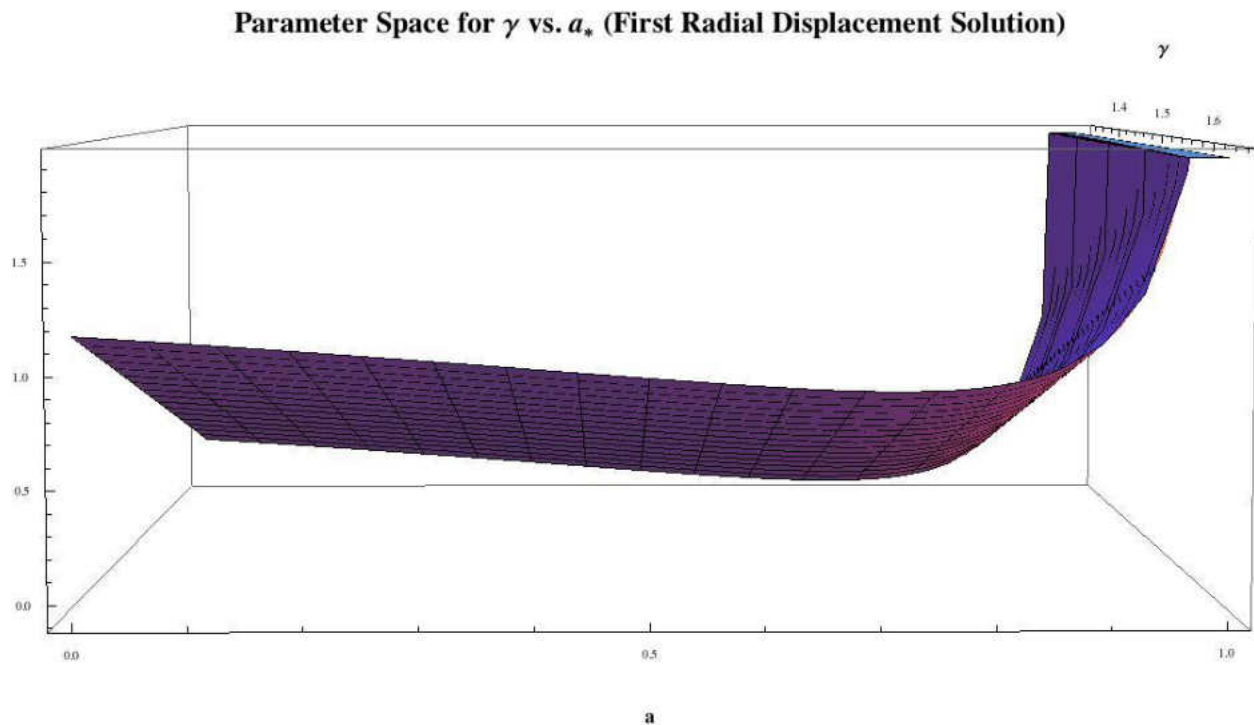


Figure 26. Parameter space for adiabatic index versus  $a$  (First Radial Displacement Solution).

The fractional displacement is positive for all values of the adiabatic index and all spin values. Since the displacement is positive, it indicates positive work being done for any spin. Near maximal spin, the adiabatic index affects the displacement significantly. For non-relativistic gas, it increases to about 50 percent of the value for zero spin. For relativistic gas, there is an extreme response to the spin in such that the displacement shoots up from a floor value for median to near maximal spin values, to 2.0. The value for the same index in the case of zero spin is approximately 0.25, indicating an eight-fold increase in the displacement.

A lower displacement indicates less work being done and less heat gain for median to near maximal spin, for relativistic gas, than for zero spin or maximal spin. A similar trend occurs for non-relativistic gas although the trend is not as extreme as in the relativistic gas case.

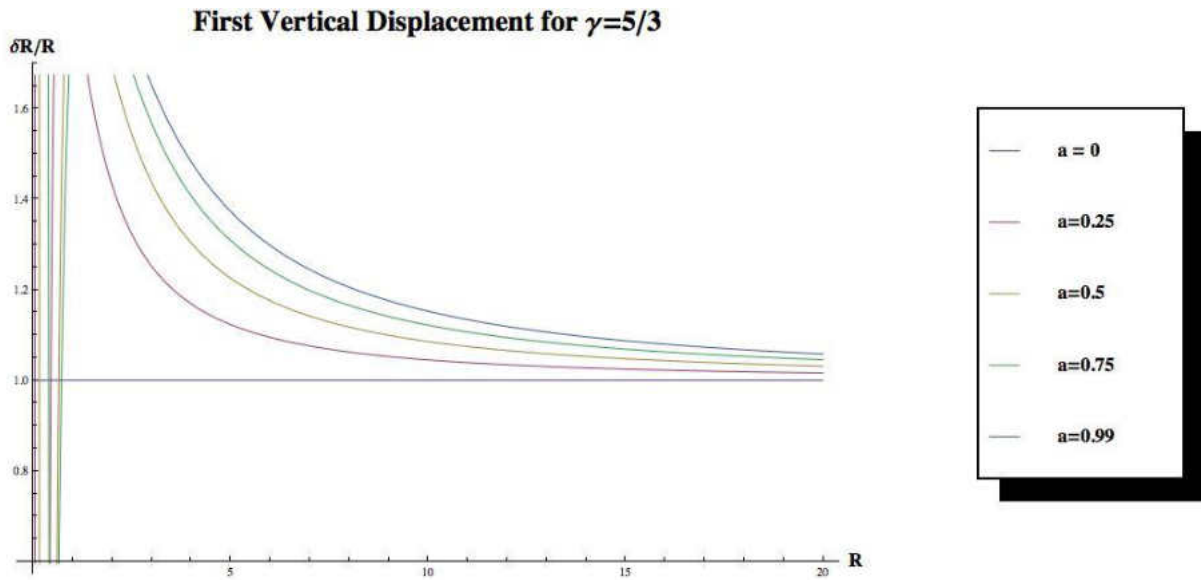


Figure 27. First Vertical Displacement for fixed index = 5/3.

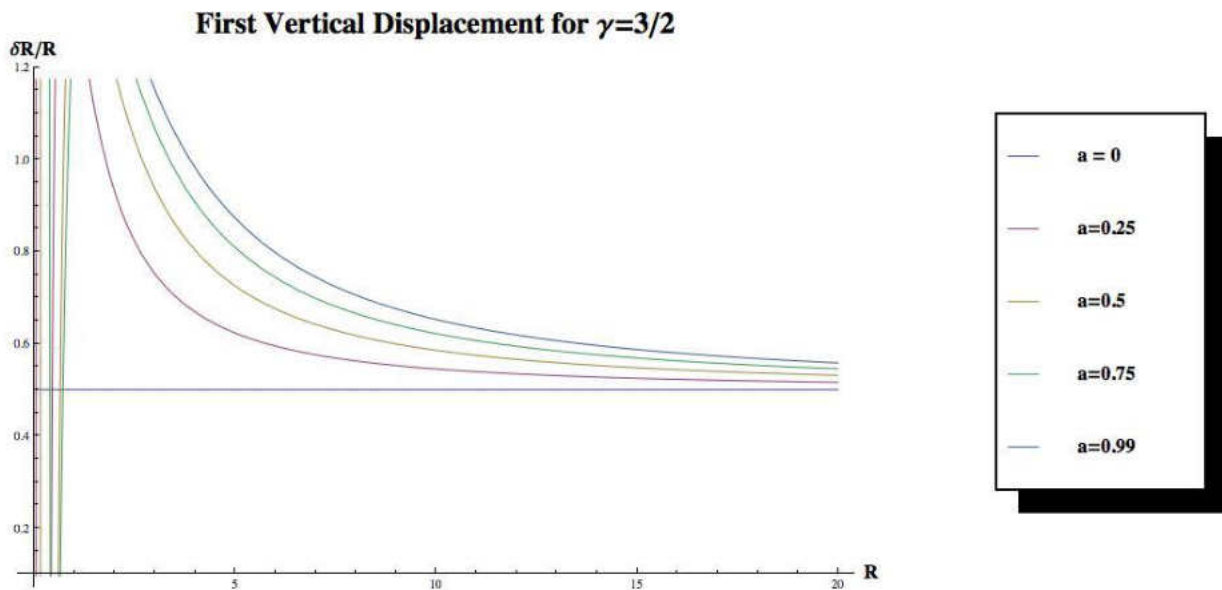


Figure 28. First Vertical Displacement for fixed index = 3/2.



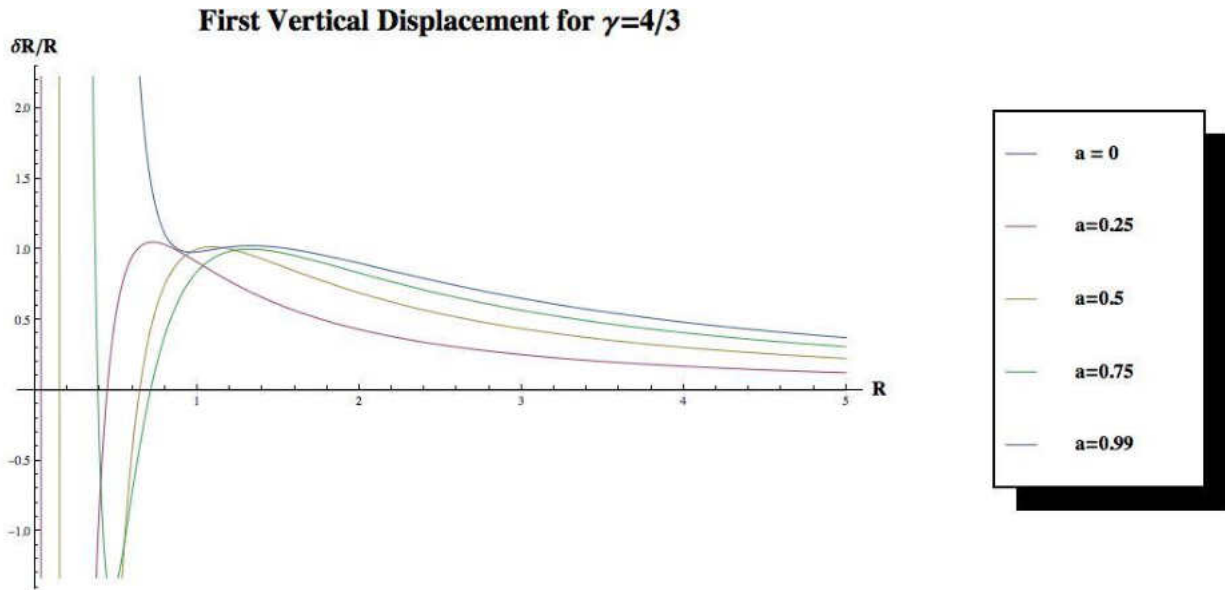


Figure 29. First Vertical Displacement for fixed index = 4/3.

The solution to the vertical fractional displacement is positive for all values of spin parameter  $a$  for all radii outside a particular extent, and approaches zero with increasing radial value, for non-relativistic ideal gas (Figure 27). As the adiabatic index goes to an even mix of ideal and relativistic gases (Figure 28), the vertical fractional displacement drops in magnitude. For zero spin, the displacement is a consistent flat value at 0.5 at all radii and for increasing spin, becomes a curve with a peak just outside the ISCO. As the spin increases, the curve shifts outward and widens. This would indicate positive work being done and heat being retained in an annular region that would widen and shift outward with increased spin.

As the adiabatic index approaches the value of relativistic gas (Figure 29), the fractional displacement for each spin value drops in magnitude and manifests as a curve that extends out and decreases in value over a radial range. Zero spin shows no curve for relativistic gas indicating that there would be no displacement for a stationary black hole with relativistic gas at

the ISCO. This would indicate that the gas would not likely be relativistic at the ISCO in such a case and there would be no QPO signal apparent. The increased spin causes the displacement curve to shift outward and widen as well. But the displacement reaches a lower amplitude with the highest value for near maximal spin. Positive work is done in this case as well and the heat is retained in a small annular region just outside the inner disk edge that broadens slowly with increasing spin. In the immediate vicinity of the black hole, there is negative pulsation meaning there is a loss in the heat, which would be consistent with the heat being rapidly absorbed through the event horizon.

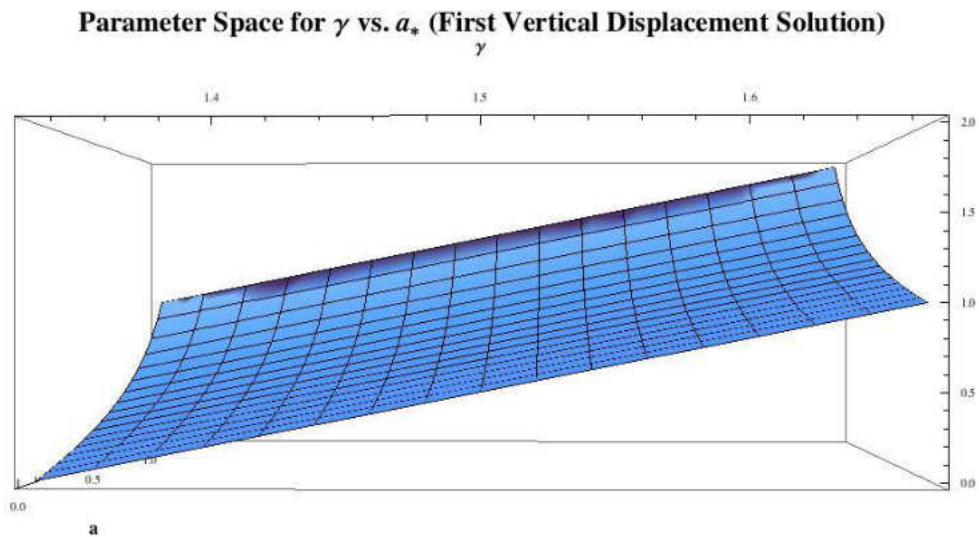


Figure 30. Parameter space for adiabatic index versus  $a_*$  (Vertical displacement solution).

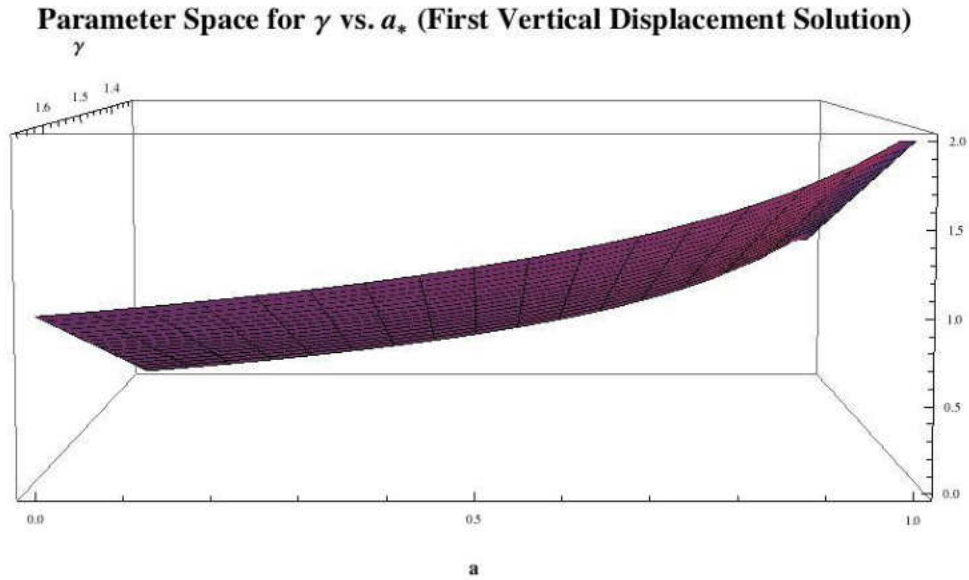


Figure 31. Parameter Space for the adiabatic index versus  $a_*$  (Vertical Displacement Solution)

The parameter space as defined by the solution for the vertical fractional displacement (Figure 31) is positive for all spin values and all adiabatic indexes. A higher spin induces a larger vertical displacement for non-relativistic gas, indicating a higher range in pulsation in the vertical direction. The opposite trend shows the opposite behavior: zero spin with relativistic gas shows a minimal vertical displacement. Even with zero spin, ideal gas shows a vertical displacement of 1.0, and it increases from there as the spin increases. The relativistic gas climbs to approximately the same vertical displacement as non-relativistic gas (at zero spin) with high spin values and the displacement builds to a maximum for maximal spin (in either the ideal or relativistic gas case).

## The Radial Displacement Solutions of the Elliptic Equation

The solution to the elliptic equation was calculated numerically and plotted for different values of the adiabatic index. For each varying value of the adiabatic index, there was a corresponding frequency and change in the range of the radial fractional displacement. A general trend was discovered in the changes in the frequencies and the radial displacements. This implies the nature of the gas affects the periodicity and range of pulsation in the gas. This can be used as a diagnostic into the inner disk and determine how the gas behaves as determined by the measured frequency from that region.

The first figure (Figure 32) is a graph of the radial displacement for ideal gas, with an index of  $5/3$ . The radial displacement oscillates from a low negative value ( $-0.05$ ) to a higher value of ( $+0.5$ ). The period is 2.18267 seconds, which can be detected and approximated from a visual observation of the graph.

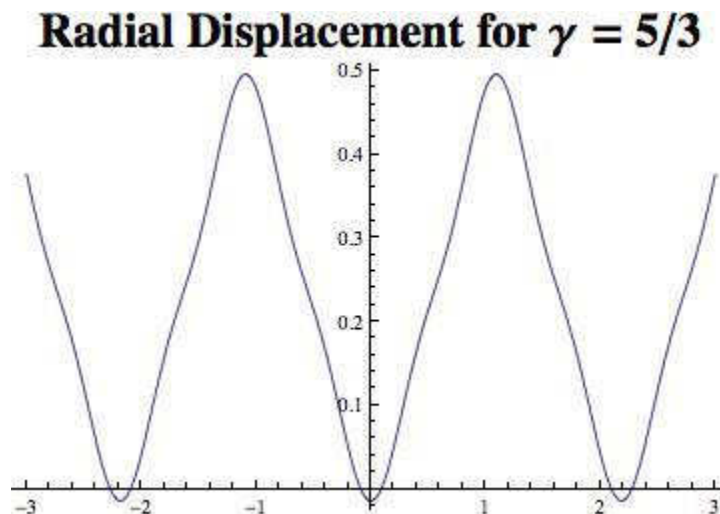


Figure 32. The Radial Displacement for  $\gamma = 5/3$  for the elliptic equation solution for the radial displacement calculated numerically.

### Radial Displacement for $\gamma = 1.6$

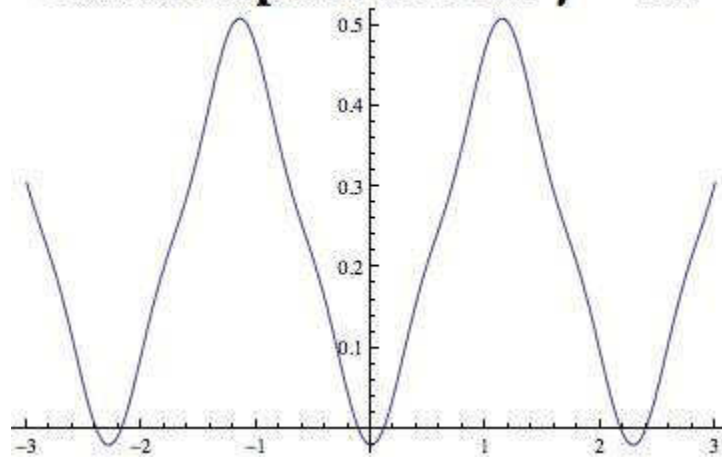


Figure 33. The Radial Displacement for  $\gamma = 1.6$  for the elliptic equation solution for the radial displacement calculated numerically.

The radial displacement is identical to that for  $\gamma = 5/3$ . The displacement increases slightly in both directions. The period is 2.284 seconds for  $\gamma = 1.6$ .

### Radial Displacement for $\gamma = 3/2$

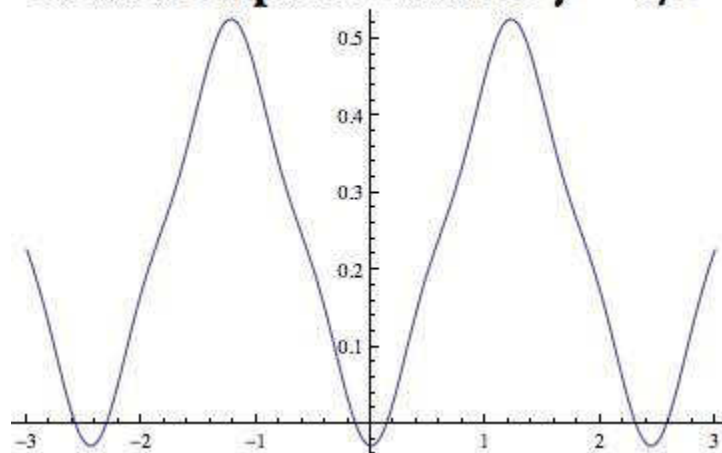


Figure 34. The Radial Displacement for  $\gamma = \frac{3}{2}$  for the elliptic equation solution for the radial displacement calculated numerically.

The radial displacement continues to increase in both directions and the period is also increasing in duration. The period in this case is 2.44 seconds. As the adiabatic index drops, the pulsation grows stronger in magnitude and the period increases in time.

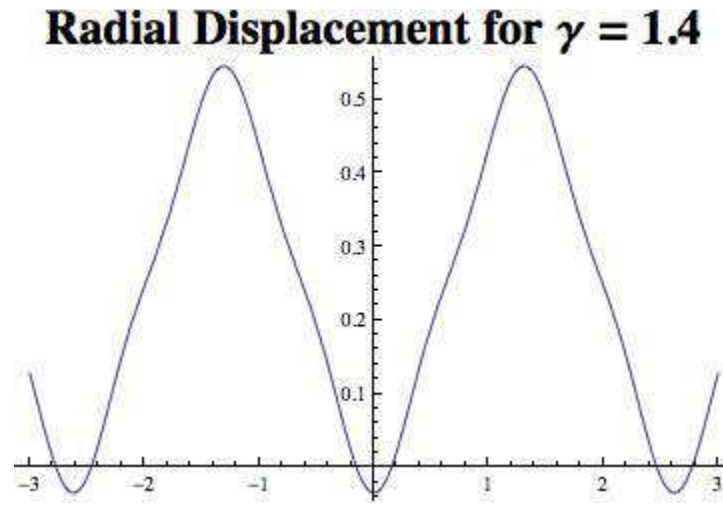


Figure 35. The Radial Displacement for  $\gamma = 1.4$  for the elliptic equation solution for the radial displacement calculated numerically.

The displacement also continue to grow larger in both directions and the minimum occur near  $(-0.10)$  and the maximum near  $(0.60)$  for near-relativistic gas. The period for this case is 2.617 seconds. The behavior from this graph confirms a continued trend in the pulsation and period changes.

## Radial Displacement for $\gamma = 4/3$

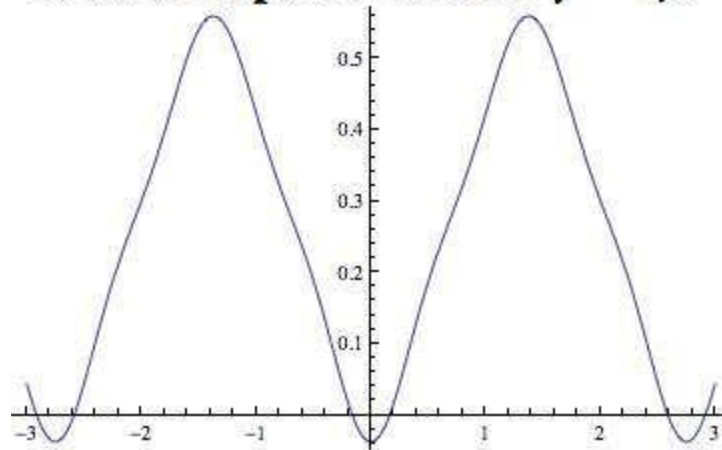


Figure 36. The Radial Displacement for  $\gamma = \frac{4}{3}$  for the elliptic equation solution for the radial displacement calculated numerically.

For relativistic gas as depicted by Figure 36, the radial displacements are the largest and reach both the highest and lowest values of any adiabatic index. They approach a maximum of (+0.65) and a minimum of (-0.10). The strongest fluctuations occur in this case and the period also is the longest for any adiabatic index case. The period in this case is 2.749 seconds.

As the adiabatic index decreases, it changes the coefficient value of the adiabatic index term in the elliptic equation and yields different roots for the equation (and hence, equilibrium points for the physical actions of the pulsations). This would have an effect on the overall frequency solution to the elliptic solution, causing it to get larger (or longer) in the time domain.

Finding the adiabatic index through observations of the accretion disk, particularly the inner region, of a source similar to the way the adiabatic index was found for the corona of the sun, would serve as a way to constrain the ratio of spin over mass, and together with a high

resolution observation of the event horizon with a large telescope and using the equation:

$$r_H = M + \sqrt{M^2 - a^2}; \quad (10.5)$$

The dimensionless ratio of  $a$  to  $M$  can be determined by comparing the measurement of the event horizon to the ISCO, which can be determined by finding where the drop-off in the quality factor is in radial terms from the center of the accretion disk. For example, the ratio of the event horizon radius to the ISCO (Figure 40) for zero spin is  $6 r_S$  to  $2 r_S$ , or 3 to 1. For maximal spin, the ratio of  $r_H$  to  $r_{ms}$  (or ISCO) is  $1 r_S$  to  $1 r_S$ , or 1 to 1.

But it's difficult to glean the approximate mass or spin independently of each other. The adiabatic index  $\gamma$  can be used independently as a way to pinpoint both the mass and spin of the compact object source in question by using the epicyclic frequency relationship between the adiabatic index and the ratio of spin to mass, to determine the adiabatic index at  $r_{ms}$ .

The epicyclic frequencies give a predictable relationship between the adiabatic index and the ratio of black hole or neutron star spin to mass so it can serve as an identification tool to determine the approximate mass of the compact object to a higher degree of accuracy and infer the spin of same object.

The relativistic resonance model serves to provide a situational context for the phenomenon of accretion and how the QPO signals emerge as a natural consequence of a vibrating region situated along the inner edge of the accretion disk. The QPOs show up as prominent peaks in the spectrum for each source and particularly sharper than any peaks that would emerge from pulsations for any other ordinary star. The intense gravity of the compact



object has an amplifying effect that enhances the peak to prominent amplitude that is hard to miss in observations.

The thermal state of the accretion disk gives a disk spectrum that is close to that of a sum of blackbody contributions from different radial locations. Its shape is determined by the radial distribution of temperature, given by the Novikov-Thorne model, which is dependent on the spin, given by the relation:

$$T = T(r, a^*); \quad (10.6)$$

The total radiative power  $L$  is determined by the averaged temperature,  $T_0 = T_0(a^*)$ , and the surface area  $A = A(a^*)$  of the radiative region. The total radiative power is given as:

$$L = \sigma T_0^4 A; \quad (10.7)$$

By calculating different spectral shapes and the power of different  $a^*$  in the Novikov-Thorne model, we can get a best-fit estimate for the temperature and area. Inconsistencies due to assumed flow rates lead to error ranges in the determined mass estimates for the black holes in question.

By using the diskoseismological approach to bring in the independent factor of adiabatic index  $\gamma$ , it can be used to narrow the error margin on mass and spin estimates for the compact object in question and the approach puts the phenomenon of the QPO signal generation in a physical context that points towards the relativistic resonance model as the salient cause and explanation for the QPO. It can help clarify any assumptions about the conditions of the accretion within the inner disk and make it possible to refine our understanding of the inner workings of accretion disks.

## CHAPTER XI

### CONCLUSIONS

QPO signals emanate from compact objects that are situated in a general relativistic gravitational field. A double frequency signal detected from the same source are explained as the radial and vertical epicyclic frequencies in a relativistic resonance model, emanating from infalling matter moving through a curved space-time field that imparts a distinctive beat to its oscillating motion.

I applied a helioseismological model that describes surface and interior oscillations in the sun and yields a characteristic Keplerian frequency for the oscillations of its solar matter at the surface. In the Newtonian setting, the linearization part that yields the expression  $\frac{\delta R}{R_0}$  is generally equal to one in a flat space-time. Following that I applied the method to a general relativistic case in a cylindrical reference frame.

In the general relativistic setting some differences were found. The difference in this model with the Newtonian expression served as a general relativistic correction and my model was amended with the epicyclic frequencies. Since Helioseismology hinges on one equation found following from the hydrostatic equilibrium condition and linearized relations of R and P (radius and pressure, respectively) to yield an eigenfrequency, this approach was applied to the two eigenfrequencies of the QPO operating in two different dynamic directions (radial and vertical) from a specific region (inner edge) of the disk and serves as a diagnostic probe into the

area to indicate the driving phenomena behind the generation of the signal. In contrast to helioseismology, diskoseismology introduces an additional degree of freedom, which provides movement in the vertical direction as opposed to only in the radial direction.

In this work two expressions are found for  $\frac{\delta R}{R_0}$  and  $\frac{\delta Z}{R_0}$  to determine the general relativistic corrections in either direction within the disk. Using these newly derived expressions I explored the range and nature of the pulsations in the inner disk. I assume a relativistic resonance model for the disk, with the QPO signals emerging from the inner edge or the ISCO (Innermost Stable Circular Orbit), the last radius where the orbits can remain Keplerian (space-time is sufficiently quasi-Newtonian and flat) and typically regarded as the inner edge in all cases of accretion disks. Any further inward, the particles' orbits begin to precess (as a result of the curvature of the Kerr space-time) and overlap, resulting into increased rates of collision and all lateral momentum is dissipated as heat and radiated away and results into a fatal free-fall for the advecting plasma into the event horizon of the black hole or surface of the neutron star. It is for this reason that the region below or within the ISCO is called the "plunging region". This is important because it shows that the QPO signal cannot come from material below the ISCO. The signal would be suppressed and vanish in the noise in the x-ray light curve due to the turmoil that occur in the plunging region. I argue that the disk must behave according to the relativistic resonance model such that that the inner disk edge vibrates due to matter moving along the edge of the plunging region and the QPO signal emerge as a result of the vibration.

In Chapter II, the boundary layer is defined by requiring  $R_*$  to be at the ISCO because it contributes and controls a significant amount of the luminosity of the accretion disk that contains the QPO signal in its overall power spectrum. The same region set at the inner disk edge would

contain standing perturbations in the region. This region is treated as a boundary layer that modulates the luminosity and controls the scaling of the frequencies in both the radial and vertical directions. The width of the boundary layer is calculated, invoking the physics of the environment and the dimensions of the boundary layer reveal the physical parameters behind the oscillations, i.e., the magnitude of the vertical oscillations versus that of the radial oscillations being coupled to the size of the containing region and the ratio of the height to the radial width.

The boundary layer model was adapted into a cusp layer model where the radius was extended outward to a selected radius (specifically, the ISCO) and the physical parameters invoked for an annular region containing a significant luminosity that would be controlled by the region. The boundary layer imparted its scaling onto the frequencies of the radiation emanating from the controlling region. An equation was derived to give the dimensions of the boundary layer and the ratio of the Keplerian angular frequencies derived from the equation that gives the two locations of the ends of the cusp layer comes out to a rational ratio of 3 : 2. This mirrors the ratio of the double QPO frequencies detected in observations for a number of QPO candidates. In the calculation done here the two QPO frequencies emerge from two different radii.

In the relativistic resonance model, a coupling factor is invoked to relate the vertical and radial epicyclic frequencies. Using the boundary layer calculations, the coupled resonance equations by Abramowicz in a 2005 paper were explored and yielded a relation for the coupling constant  $\chi$  in terms of the pressure. The coupling constant is strongest where the pressure is the highest, which would be at the inner edge. Coincidentally, the sonic edge also is situated at the ISCO.

We find that the vertical and radial oscillations would be the most strongly coupled at the

ISCO. They also would be the most strongly coupled at the equatorial plane and their signal would emerge most strongly where the flow was the thinnest. In that thin region the signal could emerge without being scattered or re-absorbed by the heated, infalling matter.

For higher accretion rates, the sonic radius (the point where the speed of sound goes from subsonic to transonic) shifts to a radius below the ISCO, which would explain why there are no double QPO frequencies for higher mass compact objects since compact objects with higher mass tend towards higher accretion rates which cause an increased separation, or dislocation, of the sonic radius from the ISCO, which would lead to a decoupling of vertical and radial epicyclic frequencies. Only one QPO frequency would emerge since the sonic radius would fall within the plunging region, with the second signal lost in the noise due to the turmoil of the chaotic collisions of the gas particles.

In Chapter IV, I discuss the heated gas as it spirals in towards the central object and above a specific temperature ( $\sim 10^4$  K), the magnetic field flux lines become frozen into the plasma. In terms of the Blandford-Znajek mechanism, I first use the Li-Xin model to compare the comparative strengths of the magnetic field of the disk and the compact object (black hole ergosphere to be specific). The black hole would likely be rotating and if contained an electric charge, would create its own magnetic field. However, in nature, black holes do not have charge so whatever ambient magnetic field would come from the plasma trapped within the ergosphere of the black hole. The ergosphere is a region that extends from the event horizon to the static surface. The static surface is where matter would appear to be moving at the speed of light to an observer far away from the black hole as opposed to actually travelling at the speed of light. The plasma trapped within this region would be outside the black hole and be rotating with the black

hole. The Li-Xin model was used to find that the black hole magnetic field was weaker than that of the disk magnetic field, except in the case of near maximal spin. So the disk magnetic field is the primary source for the magnetic field in the accretion disk system. I then utilized the Li-Xin model to model the magnetospheric radius due to the disk's magnetic field, where the flow of the ionized matter would be diverted by the innate magnetic field of the disk to a significant degree. As far as the model goes, no significant disruption in the flow of the gas occurs to affect the shape or dimension of the trapping region to a significant degree, even for high spin.

As stated in the earlier discussion on the Alfvén radius, the ISCO remains the effective edge of the inner disk so the pulsations will reflect off that radius as if it was a closed boundary. For any electric current configuration (dipole, quadrupole, multipole), the Alfvén radius remains close to the ISCO as far as to be indistinguishable from the ISCO, for any mass measure. The inner disk would remain thin without the advection-hindering effects of the disk's magnetic field that serves to dam the incoming material and divert it vertically within the disk or upward and towards the poles for the purposes of providing jet material.

The inner edge of the disk also serves as a closed boundary which supports standing waves along the circumference of the orbit and can retain integer multiples of wavelengths along the length of the circumference. The lowest value integer wavelengths would have higher amplitudes and would be more discernible than higher-valued integer wavelengths. This would explain the higher prevalence of the parametric resonance (ratio of 3 : 2) of the epicyclic frequencies in contrast to higher integer ratios. Multiple double QPO frequencies have been found with the 3 : 2 resonance, most of them in neutron star binaries, but a small number have been found for black hole binaries with this persistent feature. All other cases entail only one

QPO frequency.

The inner edge of the disk can be treated as a membrane with boundary conditions of both the compact object and the disk material on either side of the membrane, set equal at that radius. The compact object's gravity is the dominant influence and imparts its effect onto the surface of the inner disk to a prominent degree. It also serves as the informing source for the ISCO orbit that contains the standing waves. The orbit radius of the ISCO also serves as an equipotential boundary between the disk self-gravity and the compact object's Kerr gravity.

In Chapter VI, the accretion rate is discussed at length and is significant because several variables as derived by Novikov and Thorne in 1973 (Novikov I. a., 1973), depend on the adiabatic index: the mass accretion rate, the radius of influence, the density of the infalling matter, and the temperature distribution. This underscores the significance of the adiabatic index when it comes to accretion disks. The diskoseismological expressions from Chapter IX link the adiabatic index to the mass and angular momentum parameter of the compact object as dictated by the QPO frequency. The mass and angular momentum of a compact object can be determined independently through other methods, such as measuring the event horizon (by the methods of Event Horizon Telescope) and detecting the location of the QPO by finding the radius where the quality factor of the x-ray emissions drop off to zero. We can then compare the ratio of the radial lengths of the two quantities. Because the event horizon and the ISCO both simultaneously shrink inward with increasing spin, at a predictable rate for each, it could be used to give the dimensionless ratio of the angular momentum parameter to the mass, or  $a/M$ . That ratio can be used to refine the mass estimates for the compact object under observation, and when those quantities are inserted into the diskoseismological expressions, it will yield the value of the

adiabatic index at the ISCO. Determining that value yields more information about the accretion disk from which the QPO signal originates. That information can be used to refine accretion disk models. Chapter VII explored the phenomenon of diskoseismology and how the disk oscillations travel and translate into other forms of motion and energy within the accretion disk.

In Chapter VIII, radial pulsation equations are explored for any unique properties inherent in the phenomenon and what information it can yield about the infalling gas. The classical case of helioseismology, when it comes to radial pulsations, is set in a spherical reference frame. I used the same methods and applied them to diskoseismology, taking the same radial pulsation equations and adapting them for a cylindrical reference frame. In deriving the adiabatic relation for a disk distribution, the geometry of a cylindrical disk yielded an expression for the ratio of height to radius for a geometric condition. When applied to the ratio of vertical to radial epicyclic frequencies, it gives a requirement that the speed of sound be equivalent to the Keplerian speed at a particular location. It also yields a particular resonance of 3 to 2 between the epicyclic frequencies at that point. In this case, the two QPO frequencies emanate from the same radius.

In Chapter IX, we explored the radial pulsation equations, which are harmonic oscillator equations extended in terms of a fractional displacement,  $\frac{\partial R}{R}$ , and can yield, depending on how many powers in that term one can truncate, more than one solution. Since  $\frac{\partial R}{R}$  typically is less than one, any ascending powers of the term can be neglected (usually the first and higher) and a simple harmonic oscillator equation is obtained. It also has a characteristic angular frequency in terms of the Keplerian angular frequency multiplied by an adiabatic index term.

When further powers of the displacement term are examined, up to the first term, one gets



an Abel ordinary differential equation. If further powers are included up to the second term, an elliptic equation is obtained. In this case, the elliptic equation is numerically evaluated to get the frequency solution for each case of the adiabatic index. For different values of the adiabatic index, starting from that of an ideal gas, a period and displacement range is obtained. As the adiabatic index value decreases with each computation of the frequency value, the period grows longer in time and the perturbations slowly increase in magnitude. The largest perturbation values are obtained for the adiabatic index of a relativistic gas, indicating a relativistic environment is needed. As the adiabatic index value decreases towards unity, the period would grow even longer.

The elliptic equation, when handled with a numerical fitting treatment, also gives a radial potential equation yielding information about the pulsating matter. I found that for each root of the equation, there exists an equilibrium point where matter would tend to settle in a potential field and with a particular condition (value of  $q$ ), the range of motion is revealed. The value of  $q$  is indicated by initial conditions, or the square of the initial velocity at the start of the perturbation action. With a positive  $q$ , the range of motion is divided into two oscillatory regions, while with a negative  $q$ , a single range of distorted motion exists over a single region.

Taking the second derivative of the radial potential expression with respect to  $x$  and then inserting each root of the same equation, can give us the angular frequency for each root. The ratio of the angular frequencies is found by dividing the square root of the larger value (positive root of the potential expression) by the square root of the smaller value (negative root of the potential expression). This was the result that gave a general solution to the ratio of the

frequencies and dependent on the  $B$  term in the solution.

The adiabatic index term ( $B$ ) controls the value of the integer ratio. For decreasing values of  $n$ , the value of  $B$  decreases as well and becomes more negative. For the adiabatic index term derived for a spherical reference frame with a value of  $n = 4$  ( $4 - 3\gamma$ ), and the ideal gas adiabatic index of  $5/3$  inserted into the equation, which yields a value of  $B = -1$ , an integer ratio of 2 to 1 is found.

The adiabatic index term for a cylindrical reference frame with a value of  $n = 3$ , ( $3 - 3\gamma$ ), in the case of an ideal gas, which gives a value of  $B = -2$ , gives an integer ratio of 5 to 3 ( $\sim 1.66$ ).

The next adiabatic index term with value of  $n = 2$  ( $2 - 3\gamma$ , and  $B = -3$ ), in the case of ideal gas, gives the magic ratio of 3 to 2 ( $3 : 2$ , or  $1.5$ ). For that integer ratio, as far as the radial potential expression is concerned, a different reference frame is effective in terms of explaining the pulsations of the matter.

A more conflated reference frame is responsible for generating the integer ratio of the angular frequencies, in the case of ideal gas. When the index for relativistic gas ( $4/3$ ) is inserted into the second derivative of the radial potential expression with respect to  $x$ , it also yields an integer ratio of 5 to 3 ( $5 : 3$ ) for  $n = 2$ . The integer ratio of the frequencies due to the adiabatic index for relativistic gas (in the cylindrical reference frame) is the same as that for the adiabatic index of ideal gas in the spherical reference frame. The integer ratio of the frequencies for the

relativistic gas index for one reference frame with a value of  $n$ , will equal that of the integer ratio due to the index for ideal gas in a reference frame with a value of  $n - 1$ .

So based on this trend, a lower  $n$  (specifically,  $n = 1$ ) will yield a 3 : 2 resonance in the case of relativistic gas. This scenario is unlikely since the gas would only become relativistic near the event horizon and the QPO signal with that integer ratio would only emerge from the ISCO in the case that the compact object was near or at maximal spin. In that case, the ISCO would have retreated all the way down to near or at the same radius as the event horizon itself.

The implication of the 3 : 2 ratio in the QPO frequencies in this context is that the gas would tend to have a higher adiabatic index, and the inner disk in the double QPO frequency case, would operate in a different reference frame, one distinct from that of the cylindrical or spherical ones.

I found implications of the fractional displacements and pulsation ranges, for each case of the adiabatic index, for each value of the spin parameter  $a$ . The elliptic equation solution is found and numerically evaluated and plotted for each value of the adiabatic index.

I found that the radial fractional displacement at a fixed radius, set at the ISCO, is more sensitive to the spin of the compact object than the vertical fractional displacement at the same radius. As spin reaches its maximum possible value, the radial displacement moves towards infinity, implying an explosive expansion outward from the ISCO. The vertical fractional displacement is more stable, only increasing steadily to a value, which is twice that of zero spin, at maximum spin. The pulsations are more stable in the vertical direction (in the cylindrical reference frame), than in the radial direction (parallel to the equatorial plane). The radial displacement turns negative for median values of spin for the relativistic gas index, which

implies negative work is being done and heat was being released instead of gained and supporting the pulsation activity. For median values of spin, all other index values also showed decreased displacements but they all increased again as the spin increased towards the maximum.

The displacements are plotted across a radial range for different values of spin (for each individual value of the adiabatic index), and in the case of ideal gas, the pulsations are most pronounced within a few Schwarzschild radii of the inner disk edge and as the spin increases, the distribution of the displacement peak changes, with the peak shifting to a lower value and the peak broadening outward. This indicates the pulsations occurring in a broadening annular ring that widens as the spin of the compact object increases. The same thing occurs with decreasing adiabatic index value, although the displacements drop in value across all radii. For relativistic gas, the displacement turn negative at a radius, starting at a radius of about  $2.0 r_s$ , for a spin value of 0.5 and increasing from there. This implies no pulsation activity is supported for relativistic gas with a spinning compact object spinning at half the maximum possible speed or above that, at extended radii within the accretion disk. The negative work indicates a dissipation of heat beyond that radius and the positive work indicates a retaining of heat within a close annular region within the inner disk.

It indicates the nature of the gas responsible for the QPO signal will be likely confined to a region that is filled with gas that is likely to be ideal, rather than relativistic. Although a lower adiabatic index (adjusted mix of ideal and relativistic gas) will still support pulsation activity for any spin of the compact object, up to a point. The lowered adiabatic index will indicate an increasingly concentrated annular region of heat that closes inward to the inner disk edge and

contain the pulsation activity.

The vertical displacements show a similar trend to the radial displacements over a radial range but reaches lower maximum peak values compared to that of the radial displacements. They also decrease in amplitude for lower adiabatic index values. The vertical displacements do differ from the radial displacement in that they all reach floor values that remain constant for all radii outward, indicating steady heat retention over a distance from the equatorial plane.

With zero spin for any adiabatic index value, there is a flat constant value for all radii (1.0 for  $\gamma = 5/3$ , 0.5 for  $\gamma = 3/2$ , and 0 for  $\gamma = 4/3$ ). As the spin increases, the displacement starts to gather up into peaks that shoot up then drop in amplitude and broaden with increasing spin. In the relativistic gas case, the amplitude drops to around 1.0 for a variety of spin values and slowly spreads out with increased spin. This indicates retention of heat for all radii in the vertical direction although to a diminished extent.

The solution to the elliptic equation for the radial displacement was numerically evaluated and yielded different periods and radial displacements for each adiabatic index value (1.66, 1.6, 1.5, 1.4, and 1.33). The smallest radial displacements were found for that of ideal gas, and as the adiabatic index dropped, the displacements increased, until they reached their largest values for that of relativistic gas. The periods also became longer as the adiabatic index decreased, from that of 2.18 seconds for  $\gamma = 5/3$ , to 2.75 seconds for  $\gamma = 4/3$ . As the adiabatic index drops further, the period will get even longer.

A number of models have been considered here and explored to find characteristics that can explain the emergence of the quasi-periodic oscillation signals that manifest in x-ray

radiation from numerous binary systems. The QPO signals can either occur in one single peak in the frequency spectrum derived from an x-ray light curve, or a double peak, in some cases. The interesting feature for double QPO peaks is that they always occur with a rational resonance ratio. The most prominent ratio is that of 3 : 2, and a number of models have arrived at that resonance ratio as a feature. The boundary layer model, extended to the inner disk edge, recreates the characteristics and the scaling of the epicyclic frequencies.

A geometric condition (equation 8.63) due to reconciling the coefficients of the cylindrical and spherical reference frames where the accretion would become Bondi (or free-fall) accretion also yields a specific ratio between the radius and height. When this condition is invoked, with the ratio of Keplerian velocity and speed of sound, it yields the 3 : 2 resonance of the vertical and radial frequencies, due to equation (8.64).

The elliptic equation also yields a radial potential equation that also creates the conditions for a 3 : 2 resonance in the case of ideal gas that requires a particular reference frame for the accretion disk scenario.

Ultimately results of my dissertation could be used to explore testable implications that can be resolved with the LOFT satellite mission. Large Observatory for X-ray Timing (LOFT) is a proposed ESA space mission slated to launch around 2022, and is dedicated to the study of neutron stars, black holes, and compact objects by means of their rapid x-ray variability.

The source of the QPO origin can be resolved with more observations, like LOFT, and more extensive knowledge of the conditions within accretion disks. Such knowledge would help refine our understanding of accretion disks and binary systems in general. Most stars are found in binary systems and understanding these systems would help us understand a major component

of the universe. We would reinforce and expand our understanding and comprehension of the astronomical fundamentals that operate in these systems. A QPO signal embodies more information and can serve as an incisive probe into the mechanics of an accretion disk and binary systems in general and reveal a lot. By using diskoseismology to connect the QPO signal to the adiabatic index, which is connected to a lot of quantities within the disk, it can be turned into an observational tool by itself. It would resolve a number of questions, particularly the density and temperature distributions, among other quantities involved when it comes to the composition and internal anatomy of accretion disks. By confirming the adiabatic index, it yields these quantities in one single swoop and gives us a lot of information about the accretion disk. This information can be used to further refine accretion disk models. So QPOs shed more light on the subject matter than just the nature of the x-ray radiation in which they manifest.

## REFERENCES



- Abramowicz, M. A. (2002). Holonomy invariance, orbital resonances and kilohertz QPOs. *Classical and Quantum Gravity* 19 , L57.
- Abramowicz, M. B. (2006). Epicyclic oscillations of fluid bodies: II. strong gravity. *Classical and Quantum Gravity*, 23 , 1689-1696.
- Abramowicz, M. G. (2000). Accretion Disks Phase Transition: 2-D or Not 2-D. *Pub. Astron. Soc. Japan*, 52 , 295.
- Abramowicz, M. I.-P. (1998). A note on the conditions for SSD-ADAF transitions. *Mon. Not. R. Astron. Soc.*, 293 , 443.
- Abramowicz, M. J. (1978). Relativistic, accreting disks. *Astron. and Astrophys.*, 63 , 221.
- Abramowicz, M. K. (2001). A precise determination of black hole spin in GRO J1655-40. *Astron. Astrophys.*, 374 , L19.
- Abramowicz, M. K. (2004). Twinpeak QPOs frequencies in microquasars and Sgr A\*. The resonance and other orbital models. *Hledik and Stuckhlik* , 1-23.
- Alpar, M. S. (1985). Is GX5-1 a millisecond pulsar. *Nature*, 316 , 239.
- Balbus, S. a. (1991). A powerful local shear instability in weakly magnetized disks. I-Linear analysis. II-Nonlinear evolution. *Astrophys. J.*, 376 , 214-233.
- Balbus, S. A. (2003). Enhanced Angular Momentum Transport in Accretion Disks. *Annu. Rev. Astron. Astrophys.* 41 , 555-597.
- Bardeen, J. P. (1972). Rotating Black Holes: Locally Nonrotating Frames, Energy Extraction, and Scalar Synchrotron Radiation. *Astrophys. J.*, 178 , 347.
- Barret, D. K. (2005). *MNRAS*, 327 , 1288.
- Biehle, G. B. (1993). Hard apex transition in quasi-periodic oscillators- Closing of the accretion gap. *Astrophys. J.*, 411 , 302.
- Bigot, L. P. (2000). Non-axisymmetric oscillations of roAp stars. *Astron. Astrophys.*, 356 , 218-233.
- Blandford, R. Z. (1977). Electromagnetic extraction of energy from Kerr black holes. *Mon. Not. R. Astron. Soc.*, 179 , 433-456.
- Bondi, H. H. (1944). On the Mechanism of Accretion by stars. *Mon. Not. R. Astr. Soc.*, 112 , 195.
- Bondi, H. (1952). On spherically symmetric accretion. *Mon. Not. R. Astr. Soc.*, 112 , 195.
- Carroll, B. O. (1996). *An Introduction to Modern Astrophysics*. New York: Addison and Wesley Publishing Co, Inc.
- Carroll, B. W. (1996). *An Introduction to Modern Astrophysics*. New York: Addison-Wesley Publishing Co, Inc.
- Carroll, B. W. (1996). *An Introduction to Modern Astrophysics*. New York: Addison-Wesley Publishing Co., Inc.
- Christen-Dalsgaard, J. G. (1982). On the Interpretation of 5-minute oscillations in solar spectrum line shifts. *Mon. Not. R. Astr. Soc.*, 198 , 141-171.
- Corbet, R. (2004, June 6). *RXTE TOO observations of GRS 1915+105 on day 152 of 1996*. Retrieved from RXTE Guest Observer Facility:  
[http://heasarc.gsfc.nasa.gov/docs/xte/SOF/TOO/GRS1915/GRS1915\\_d152.html](http://heasarc.gsfc.nasa.gov/docs/xte/SOF/TOO/GRS1915/GRS1915_d152.html)
- Cunha, M. G. (2000). Magnetic perturbations to the acoustic modes of roAp stars. *Mon. Not. R. Astr. Soc.*, 319 , 1020-1038.
- Cunha, M. (2006). Improved pulsating models of magnetic Ap stars-I. Exploring different magnetic field configurations. *Mon. Not. R. Astr. Soc.*, 365 , 153-164.
- De Moortel, L. H. (2002). Longitudinal intensity oscillations in coronal loops observed with TRACE II. Discussion of Measured Parameters. *Sol. Phys.* 209 , 89.

- De Moortel, L. H. (2003). The damping of slow MHD waves in solar coronal magnetic fields. *Astron. and Astrophys.*, 408 , 755.
- De Pontieu, B. (2007). Chromospheric Alfvénic waves Strong Enough to Power the Solar Wind. *Science*, 318 , 1574.
- Deubner, F.-L. G. (1984). Helioseismology: Oscillations as a diagnostic of the solar interior. *Annu. Rev. Astron. Astrophys.*, 22 , 593-619.
- Domiciano de Souza, A. K. (2003). The spinning-toy Be star Acleamar from VLTI-VINCI. *Astron. Astrophys.* 407 , L47-L50.
- Dziembowski, W. G. (1996). Magnetic Effects on Oscillations in roAp stars. *Astrophys. J.*, 458 , 338-346.
- Dziembowski, W. (1977). Light and radial velocity variables in a nonradially oscillating star. *Acta Astron.* 27 , 203-211.
- Esin, A. N. (1996). Hot One-Temperature Accretion Flows around black holes. *Astrophys. J.*, 465 , 312-+.
- EventHorizonTelescope*. (2014, August 1). Retrieved from <http://www.eventhorizontelescope.org/science/index.html>
- Gizon, L. S. (2003). Determining the inclination of the rotational axis of a Sun-like star. *Astrophys. J.*, 589 , 1009-1019.
- Goossens, M. (2003). *An Introduction to Plasma Astrophysics and Magnetohydrodynamics*. Dordrecht: Kluwer.
- Gough, D. (1981). A new measure of the solar rotation. *Mon. Not. R. Astr. Soc.*, 196 , 731-745.
- Gough, D. (1993). Course 7. Linear adiabatic stellar pulsation. In D. Gough, *Astrophysical Fluid dynamics, Les Houches Session XLVII eds.* (pp. 399-560). Amsterdam: Zahn, J.P., and Zinn-Justin, J., Elsevier.
- Gough, D. (1986). EBK quantization of stellar waves. *Hydrodynamical and Magnetodynamical problems in the sun and stars, ed.* , 117-143.
- Gruzinov, A. (1999). *Spin 3/5 Black Hole in GRO J1655-40*. Retrieved from astro-ph/9910335
- Hansen, C. C. (1977). The effects of differential rotation on the splitting of nonradial modes of stellar oscillation. *Astrophys. J.*, 217 , 151-159.
- Hartle, J. a. (1968). Slowly Rotating Relativistic Stars. II. Models for Neutron Stars and Supermassive Stars. *Astrophys. J.*, 153 , 807.
- Hartle, J. T. (1968). Slowly Rotating Relativistic Stars. II. Models for Neutron Stars and Supermassive Stars. *Astrophys. J.*, 153 , 807.
- Hines, C. (1960). Internal atmospheric gravity waves at ionospheric heights. *Can. J. Phys.*, 38 , 1441.
- Hoffleit, D. (1977). History of the discovery of Mira stars. *JAVSO*, 25 , 115-136.
- Homan, J. v. (2002). RXTE Observations of the Neutron Star Low-Mass X-Ray Binary GX 17+2: Correlated X-Ray Spectral and Timing Behavior. *Astrophys. J.*, 568 , 878.
- Honma, F. (1996). Global Structure of Bimodal Accretion Disks around a Black Hole. *Pub. Soc. Astron. Japan*, 48 , 77.
- Hoyle, F. L. (1939). The Effect of Interstellar Matter on Climatic Variation. *Proc. Camb. Phil. Soc.*, 35 , 405.
- Hubeny, I. (1990). Vertical Structure of accretion disks-A simplified analytical model. *Astrophys. J.*, 351 , 632-641.
- Isper, J. (1995). *Astrophys. J.*, 458 , 508.
- Isper, J. (1994). Low-frequency modes and nonbarotropic effects in pseudo-Newtonian accretion

- disks. *Astrophys. J.*, 435 , 767.
- Karas, V. (1999). Twin Peak Separation in Sources with kHz QPOs. *Astrophys. J.*, 526 , 953.
- Kato, S. (1994). *Pub. Astron. Soc. Japan*, 46 , 415.
- Kato, S. F. (1998). *Black Hole Accretion Disks*. Kyoto: Kyoto Univ. Press.
- Kato, S. F. (1980). Trapped Radial Oscillations of Gaseous Disks around a Black Hole. *Pub. Astron. Soc. Japan*, 32 , 377.
- Kato, S. I. (1994). A non-local description of turbulent stress tensor in accretion disks. *Pub. Astron. Soc. Japan*, 46 , 289.
- Kato, S. N. (1998). Transition Radius from Cooling-Dominated to Advection-Dominated Regimes in Two Temperature Disks. *Pub. Astron. Soc. Japan*, 50 , 559.
- Kato, S. (1994). Turbulent Stress Tensor in Accretion Disks Derived by Second-Order Closure Modeling. *Pub. Astron. Soc. Japan*, 46 , 589.
- King, D. N. (2003). *Astron. and Astrophys.*, 404 , L1.
- Kluźniak, W. A. (2004). Nonlinear Resonance in the Accretion Disk of a Millisecond Pulsar. *Astrophys. J.*, 603 , L89.
- Kluźniak, W. M. (1990). Determining the properties of accretion-gap neutron stars. *Astrophys. J.*, 358 , 538.
- Kluźniak, W. W. (1985). Evolution of the innermost stable orbits around accreting neutron stars. *Astrophys. J.*, 297 , 548.
- Komissarov, S. S. (2009). Blandford-Znajek Mechanism versus Penrose Process. *J. Korean Phys. Soc.* 54:2503-2512,2009 .
- Krolik, J. H. (2002). Where is the Inner Edge of an Accretion Disk around a Black Hole? *Astrophys. J.*, 573 , 754.
- Lai, D. (1998). Transonic magnetic slim accretion disks and kilohertz quasi-periodic oscillations in low-mass x-ray binaries. *Astrophys. J.*, 502 , 721.
- Lamb, F. a. (2001). Changing Frequency Separation of Kilohertz Quasi-Periodic Oscillations in the Sonic-Point Beat-Frequency Model. *Astrophys. J.*, 554 , 1210.
- Lamb, F. S. (1985). Quasi-periodic oscillations in bright galactic-bulge X-ray sources. *Nature*, 317 , 681.
- Landau, L. a. (1959). *Fluid Mechanics*. Oxford, U.K.: Pergamon Press.
- Leavitt, H. S. (1908). Variables in the Magellanic Clouds. *Annals of Harvard College Observatory*, 60 , 87-108.
- Ledoux, P. (1951). The nonradial oscillations of gaseous stars and the problem of beta Canis Majoris. *Astrophys. J.*, 114 , 373-384.
- Lee, W. A. (2004). Resonance in Forced Oscillations of an Accretion Disk and Kilohertz Quasi-Periodic Oscillations. *Astrophys. J.*, 603 , L93.
- Lense, J. T. (1918). *Phys. Z* 19 , 156.
- Li, L.-X. (2000). A Toy Model for Blandford-Znajek Mechanism. *Phys. Rev. D* 61 .
- Liang, E. T. (1980). Transonic disk accretion onto black holes. *Astrophys. J.*, 240 , 271.
- M.A. Abramowicz, M. J.-P. (2010). Leaving the ISCO: the inner edge of a black hole accretion disk at various luminosities. *Astron. Astrophys. vol 521* .
- Mammoto, T. T. (1996). *Physics of Accretion Disks*. Amsterdam: Gordon and Breach.
- Manmoto, T. K. (2000). Dynamics of the Transition from a Thin Accretion Disk to an Advection-dominated Accretion Flow. *Astrophys. J.*, 538 , 295.
- Markovic, D. L. (n.d.). Retrieved from <http://arxiv.org/abs/astro-ph/0009169>
- Markwardt, C. S. (1999). Variable-Frequency Quasi-periodic Oscillations from the Galactic

- Microquasar GRS 1915+105. *Astrophys. J.*, 513 , L37.
- McClintock, J. a. (2006). *Black Hole Binaries, Compact Stellar X-ray Sources*, Lewin, W. and van der Klis, M. eds. Cambridge, UK, New York City, USA: Cambridge Press.
- Meringa, J. (2013, July 19). [www.since.uva.nl](http://www.since.uva.nl). Retrieved from <http://www.science.uva.nl/onderwijs/thesis/centraal/files/f2138922945.pdf>
- Merloni, A. V. (1999). On gravitomagnetic precession around black holes. *Mon. Not. R. Astron. Soc.*, 304 , 155.
- Miller, M. L. (1998). Effects of Rapid Stellar Rotation on Equation-of-State Constraints Derived from Quasi-periodic Brightness Oscillations. *Astrophys. J.*, 509 , 793.
- Miller, M. L. (1998). Sonic Point Model of KiloHertz Quasi-periodic Brightness Oscillations in Low Mass X-ray Binaries. *Astrophys. J.*, 508 , 791.
- Miller, M. L. (1998). Sonic-Point Model of KiloHertz Quasi-periodic Brightness Oscillations in Low-Mass X-ray Binaries. *Astrophys. J.*, 508 , 791.
- Morsink, S. S. (1999). Relativistic precession around rotating neutron stars: Effects due to frame-dragging and stellar oblateness. *Astrophys. J.*, 513 , 827.
- Narayan, R. (1992). A flux-limited model of particle diffusion and viscosity. *Astrophys. J.*, 394 , 261.
- Narayan, R. a. (1995). Advection-dominated Accretion. Underfed black holes and neutron stars. *Astrophys. J.*, 452 , 710-+.
- Narayan, R. a. (1994). Advection-dominated accretion: A self-similar solution. *Astrophys. J. Lett.* 444 , L13-L16.
- Narayan, R. a. (1995). Advection-dominated accretion: Self-similarity and bipolar outflows. *Astrophys. J.* 444 , 231-243.
- Narayan, R. a. (1995). Advection-dominated accretion: Underfed Black Holes and Neutron Stars. *Astrophys. J.* 452 , 710+.
- Novikov, I. a. (1973). Astrophysics of black holes. *Black holes (Les astres occlus)* , 343-450.
- Novikov, I. a. (1973). Astrophysics of Black Holes. In C. D. DeWitt, *Black Holes* (pp. 343-450). Paris: Gordon and Breach.
- Novikov, I. Z. (1966). *Nuovo Cim. Suppl.* 4 , 810, addendum 2.
- Nowak, M. L. (1998). *Theory of Black Hole Accretion Disks*. Cambridge: Cambridge Univ. Press.
- Nowak, M. W. (1992). Diskoseismology: Probing accretion disks. II-G-modes, gravitational radiation reaction, and viscosity. *Astrophys. J.*, 393 , 697.
- Nowak, M. W. (1997). The 67 Hz feature in the Black Hole Candidate GRS 1915+105 as a Possible "Diskoseismic" Mode. *Astrophys. J.*, 477 , L91.
- Okazaki, A. K. (1987). Global trapped oscillations of relativistic accretion disks. *Pub. Astron. Soc. Japan*, 39 , 457.
- Ortega-Rodriguez, M. W. (2000). On the Perturbations of Viscous Rotating Newtonian Fluids. *Astrophys. J.*, 537 , 922.
- Osaki, Y. (1975). Nonradial Oscillations of a 10 solar mass star in the main-sequence stage. *Publ. Astron. Soc. Japan*, 27 , 237-258.
- Paczynski, B. (1987). Possible relation between the X-ray QPO phenomenon and general relativity. *Nature*, 327 , 303.
- Papaloizou, J. S. (1994). A Comparison of One-Dimensional and Two-Dimensional Models of Transonic Accretion Discs around Collapsed Objects. *Mon. Not. R. Astron. Soc.*, 268 , 29.
- Perepelitsa, D. V. (2007). Spinning Black Hole Energetics.

- Perez, C. S. (1997). Relativistic Diskoseismology. I. Analytical results for gravity modes. *Astrophys. J.*, 476 , 589.
- Perez, C. S. (1997). Relativistic Diskoseismology. I. Analytical Results for "Gravity Modes". *Astrophys. J.*, 476 , 589.
- Popham, R. N. (1992). Supersonic infall and causality in accretion disk boundary layers. *Astrophys. J.*, 394 , 255.
- Press, W. a. (1972). Rotating Black Holes: Locally Nonrotating Frames, Energy Extraction, and Scalar Synchrotron Radiation. *Astrophys. J.* 178 , 347-370.
- Psaltis, D. (2001). Models of quasi-periodic variability in neutron stars and black holes. *Advances in Space Research*, 28 , 481.
- Robbrecht, E. V. (2001). Slow magnetoacoustic waves in coronal loops: EIT and TRACE. *Astron. and Astrophys.*, 370 , 591.
- Roberts, B. E. (1983). Fast Pulsations in the Solar Corona. *Nature*, 305 , 688.
- RXTE Guest Observer Facility*. (2001, June 27). Retrieved from NASA RXTE Site: [http://heasarc.gsfc.nasa.gov/docs/xte/Greatest\\_Hits/khz.qpo.html](http://heasarc.gsfc.nasa.gov/docs/xte/Greatest_Hits/khz.qpo.html)
- Ryden, B. (n.d.). Retrieved from <http://ftp.astronomy.ohio-state.edu/~ryden/ast825/ch10.pdf>
- Saio, H. (2005). A non-adiabatic analysis for axisymmetric pulsations of magnetic stars. *Mon. Not. R. Astr. Soc.*, 360 , 1022-1032.
- Saio, H. G. (2004). Axisymmetric p-mode pulsations of stars with dipole magnetic fields. *Mon. Not. R. Astr. Soc.*, 350 , 485-505.
- Schmitz, F. F. (1998). On wave equations and cut-off frequencies of plane atmospheres. *Astron. Astrophys.* 337 , 487-494.
- Schnittman, J. B. (2004). The Harmonic Structure of High-Frequency Quasi-Periodic Oscillations in Accreting Black Holes. *Astrophys. J.*, 606 , 1098.
- Schwarzenberg-Czerny, A. (1997). The Correct Probability Distribution for the Phase Dispersion Minimization Periodogram. *Astrophys. J.*, 489 , 941-945.
- Scuflaire, R. (1974). The non radial oscillations of condensed polytropes. *Astron. Astrophys.*, 36 , 107-111.
- Shakura, N. a. (1973). Black holes in binary systems. Observational appearance. *Astronomy and Astrophysics*, Vol. 24 , 337-355.
- Shibata, M. S. (1998). Innermost Stable Circular Orbits around Relativistic Rotating Stars. *Phys. Rev. D*, 58 , 104011.
- Shklovsky, I. (1967). On the Nature of the Source of X-Ray Emission of SCO XR-1. *Ap. J. Letters*, 148 , L1.
- Sibgatullin, N. (2002). Nodal and Periastron Precession of Inclined Orbits in the Field of a Rapidly Rotating Neutron Star. *Astronomy Letters*, 28 , 83.
- Silbergleit, A. W.-R. (2001). Relativistic diskoseismology. II. Analytical results for c-modes. *Astrophys. J.*, 548 , 335.
- Stella, L. a. (1998). Lense-Thirring Precession and Quasi-Periodic Oscillations in Low Mass X-ray Binaries. *Astrophys. J.*, 492 , L59.
- Stella, L. V. (1999). kHz Quasiperiodic Oscillations in Low-Mass X-Ray Binaries as Probes of General Relativity in the Strong Field Regime. *Physical Review Letters*, 82 , 17.
- Stella, L. V. (1998). Lense-Thirring Precession and Quasi-Periodic Oscillations in Low-Mass X-Ray Binaries. *Astrophys. J.*, 492 , L59.
- Stepney, S. a. (1997). Numerical FITS to important rates in high temperature astrophysical plasmas. *Mon. R. Astron. Soc.*, 288 , 333-342.

- Sunyaev, R. (1973). Variability of X-Rays from Black Holes with Accretion Disks. *Soviet Astronomy* , 941.
- Svenson, R. (1982). Electron-Positron Pair Equilibria in Relativistic Plasmas. *Astrophys. J.*, 238 , 335+.
- Takata, M. (2005). Momentum conservation and model classification of the dipolar oscillations in stars. *Publ. Astron. Soc. Japan*, 57 , 375-389.
- Thorne, K. I. (1973). Nonradial Pulsation of General Relativistic Stellar Models. VI. Corrections. *Astrophys. J.*, 181 , 181-182.
- Tomczyk, S. M. (2007). Alfvén Waves in the Solar Corona. *Science*, 317 , 1192.
- van der Klis, M. (2002). *XEUS-studying the evolution of the hot universe*, MPE rep. 281 , 354.
- van der Klis, M. (2000). Millisecond oscillations in X-ray Binaries. *Annual Review of Astronomy and Astrophysics*, vol 38 , 717.
- van der Klis, M. (1989). Quasi-periodic oscillations and noise in low mass x-ray binaries. *Annual Review of Astronomy and Astrophysics*, vol. 27 , 517.
- Van Doorselaere, T. W. (2011). The First Measurement of the Adiabatic Index in the Solar Corona Using Time-Dependent Spectroscopy of HINODE/EIS Observations. *Astrophys. J.*, 727 , L32.
- van Straaten, S. v. (2005). Relations between Timing Features and Colors in Accreting Millisecond Pulsars. *Astrophys. J.*, 619 , 455.
- Wang, T. S. (2002). Doppler Shift Oscillations of Hot Solar Coronal Plasma Seen by SUMER: A Signature of Loop Oscillations? *Astrophys. J.*, 574 , L101.
- Wang, T. S. (2003). Hot coronal loop oscillations observed with SUMER: Examples and statistics. *Astron. and Astrophys.*, 406 , 1105.
- Watarai, K. M. (2003). Where is a Marginally Stable Last Circular Orbit in Super-Critical Accretion Flow? *Pub. Astron. Soc. Japan*, 55 , 959.
- Weizsacker, C. (1948). Die Rotation Kosmischer Gasmassen. *Z. Naturforsch.* , 524-539.
- Wijnands, R. v. (2003). Quasi-periodic x-ray brightness fluctuations in an accreting millisecond pulsar. *Nature*, 424 , 44.
- Wolff, C. (1974). Distinctive patterns on the surface of slowly rotating stars whose oscillations are nonlinearly coupled. *Astrophys. J.*, 193 , 721-727.
- Yamasaki, T. K. (1996). *Pub. Astron. Soc. Japan*, 48 , 99.
- Yamasaki, T. K. (1996). *Pub. Astron. Soc. Japan*, 48 , 99.
- Yamasaki, T. K. (1995). Excitation of Trapped Oscillations in Dwarf-Nova Accretion Disks. *Pub. Astron. Soc. Japan*, 47 , 59.
- Yi, W. (2007). Coupling between the 45 Hz Horizontal-Branch Oscillation and the Normal-Branch Oscillation in Scorpius X-1. *Astrophys. J.*, 659 , 145.